Polycyclic evolution of the Eastern Central-Asia orogenic belt : microtectonic analysis, geochronology and tectonics in central Inner Mongolia

Guanzhong Shi

ÉCOLE DOCTORALE [SCIENCE ET TECHNOLOGIE]

INSTITUT DES SCIENCES DE LA TERRE D'ORLEANS
SCHOOL OF EARTH AND SPACES SCIENCES, PEKING UNIVERSITY

THÈSE EN COTUTELLE INTERNATIONALE présentée par :
Guanzhong SHI
soutenue le : 29 septembre 2013

pour obtenir le grade de :
Docteur de l'Université d'Orléans
et Peking Université

Discipline : Sciences de la Terre et del'Univers

Polycyclic evolution of the Eastern Central-Asia Orogenic Belt

Microtectonic analysis, geochronology and tectonics in Central Inner Mongolia

THÈSE dirigée par :
M.Michel FAURE Professeur, ISTO, Université d'Orléans
M.Bei XU Professeur, Université de Pékin
M. Yan CHEN Professeur, Université d'Orléans

RAPPORTEURS :
M. Liangshu SHU Professeur, Nanjing University
M. Wei LIN Professeur, Chinese Academy of Sciences IGG

JURY:
M. Michel FAURE Professeur, Université d'Orléans – Directeur de thèse
M. Yan CHEN Professeur, Université d'Orléans
M. Bruno SCAILLET Directeur de Recherche, CNRS ISTO
M. Bei XU Professeur, Peking University
M. Liangshu SHU Professeur, Nanjing University
M. Wei LIN Professeur, Chinese Academy of Sciences IGG
M. Shihong ZHANG Professeur, China University of Geosciences
M. Hongrui ZHOU Professeur, China University of Geosciences

Polycyclic evolution of the Eastern Central-Asia Orogenic Belt

Microtectonic analysis, geochronology and tectonics in Central Inner Mongolia

Guanzhong Shi (Major in Structural geology)

Directed by:
Prof. Faure Michel (University of Orléans, France)
Prof. Bei Xu (Peking University, China)
Prof. Yan Chen (University of Orléans, France)

Abstracts

The study region located at the southeast of Central Asian Orogenic Belt (CAOB) is the ideal area to research ancient accretionary orogen. It is hotly debated about the final closural time and position of the Paleo Asian Ocean. Some geologists advocated the “Solonker” suture marks the final closural zone. However, the basal geological materials are few reported. The tectonic evolution of our three study areas, the Hongqi, the Ondor Sum and the Mandula is essential and important to solve those controversies. The Mandula area as part of the “Solonker” suture plays a curial role for us to understand the Permian tectonic setting.

We recognize several litho-tectonic units in the light of the theory of accretionary orogen belt in the Hongqi, the Ondor Sum and the Mandula areas. A multidisciplinary research including structural geology, sedimentology and geochronology make us propose a new possible Paleozoic tectonic evolutional model for the three study areas. This model reinterprets the available lithological and geochemical data. Combined with the precursors’ research data, we reevaluate the central Inner Mongolia regional tectonic evolutionary history.

The litho-tectonic units recognized in the Hongqi-Ondor Sum area include the Hongqi-Ondor Sum mélange belt, the Bainaimiao arc belt, North China Craton and some post-orogenic unconformably sedimentary rocks. The matrix of the Hongqi-Ondor Sum mélange belt mainly consists of sericite-chlorite schists, chlorite-quartz schists, sericite-quartz schists, chlorite-epidote schists and tuffaceous

sandstones. Various sized of blocks, for example, marble, sandstones, pillow basalt and blueschist are imbedded in the matrix. The Bainaimiao arc is composed of the Bulongshan Formation and the Hala Formation in Hongqi area, granitic plutons in the Bater Obo, and amphibolitic intrusions, plagiogranite, gabbro in the Tulinkai area.

The Hongqi-Ondor Sum mélange belt experienced two phases' ductile deformations and one phase ductile-brittle deformation. D_1 is responsible for the regional greenschist foliation S_1, elongated mineral lineation L_1, and intrafolial fold F_1. The kinematic criteria, such as sigmoidal object, oblique fabric, mica fish, shear band etc. indicates a top-to-the-NW shearing sense. D_2 is characterized by various sized of unsymmetrical folds with nearly NE axis corresponding to the NW thrust shearing. D_3 formed the regional framework in the Hongqi and the Ondor Sum areas. It developed typical SE trending upright fold in the Hongqi area whereas formed an E-W strike antiform structure in the Ondor Sum. The Devonian sediments are involved in the D_3 deformation, confining a lower deforming time limit.

We present a U-Pb zircon concordia age of 485±14Ma for a metavolcanic block in the mélange, suggesting it from the upper plate volcanic arc. The mélange belt contains Silurian fossiliferous limestone blocks, which is the youngest blocks in the mélange for current knowledge. The Early Devonian clastic sediments and fossiliferous carbonate rocks unconformably covering the Hongqi-Ondor Sum mélange belt and the Bainaimiao arc belt suggest a coastal sedimentary environment. All those geological data support that a broad ocean has disappeared; Oceanic crust subduction terminated by the arrival of a potential microcontinent during Late Silurian and Early Devonian.

The Mandula area contains olistostrome sediments, turbiditic sediments and volcano-sedimentary rocks. The olistoliths including limestone, sandstone, volcanic blocks and siliceous mudstone are imbedded in the matrix of disordered or semi-continuous sandy and argillitic sedimentary beds. Turbidite developing typical Bouma sedimentary sequence is divided as coarse turbiditic sedimentary subunit and fine turbiditic sedimentary subunits. The Dashizhai Formation consisting of several

sequences of volcano erupting, effusive sediments and intermittent sediments presents a littoral environment. The Zhesi Formation interpreted as alluvial environment features by upperward fining and thinning conglomerate, coarse grain sandstone and fine grain sandstone association.

The basaltic lavas in Mandula give a U-Pb concordia age of 289 ± 4Ma. A group of zircon xenocrysts are detected with U-Pb average age of 434 ± 4 Ma. Those xenocrysts are well proved the Permian magmatism is contaminated or metasomatized by Early Paleozoic arc magmatic materials. Therefore the Permian magmatic rocks present some arc-like features geochemically. A gabbro vein with U-Pb concordia age of 257 ± 1Ma intrudes into the turbiditic sediments implying it not typical ophiolitic fragments. The xenocrysts of ca.1850Ma, 1600Ma，1000Ma in the gabbro suggest a potential Precambrian crystalline basement in deep.

The limestone olistolith possibly came from the southern the Amushan Formation in the Hongqi area due to similar fossil associations. Detrital zircon grains in sedimentary samples have two notable age peaks of ca.270-280Ma and ca.420-440Ma, and several grains of 700-1000Ma、1800-2200Ma and 2300-2500Ma. These two grain peaks argue the Mandula study area received the southern Bainaimiao arc materials and coeval Permian volcanic erupting materials nearby. The 1800-2200Ma and 2300-2500Ma grains probably are related to the North China Craton whereas the grains of 700-1000Ma are common in the southern Mongolia. Therefore a microcontinent is deduced existing to the north of study area.

The regional lithological and structural features, temporal and spacial distribution of these litho-tectonic units and available geochemical data lead us to conclude a rifting setting in Permian. The paleogeography features a deep water environment in the southern Mandula while shallow or littoral environment in the north on the basis of sedimentary facies analysis. The so called “Solonker” ophiolitic fragments indeed are olistostrome. Typical ophiolite components, for example, ultramafic blocks and cherts are not observed in the Mandula area.

The sediments and volcanic rocks in Mandula area subject a nearly NW-SE or N-S compressional shortening, which is named D_4 following the order in the study region. D_4 presents various types of folds in the turbiditic sediments with well developed cleavage, such as isoclinal folds, recumbent fold and overturned folds. The volcanic rocks and coarse grains deposits in the northern Mandula are characterized by E-W or ENE-WSW trending open folds. We argue that the folding in the Late Permian to Early Triassic finally leads to the rift closure.

Key words: Central Inner Mongolia; Central Asian Orogenic Belt; Polyphase deformation; Sedimentary facies analysis; Tectonic evolution

Contents

Chapter 1 Introduction

Section 1.1 Research background

1.1.1 Accretionary orogens

Currently three end-member types of orogens are recognized namely, collisional, accretionary and intra-cartonic (Cawood et al., 2009, Fig.1-1-1). Collisional orogens related to continent-continent collision imply that the mountian building occupy the internal location among the assembled continents (Wilson, 1966; Dewey, 1969). However, this model can not explain the orogenic belts that lie at the plate margin characterized by continuing subduction and accretion. These belts are termed accretionary orogens, also refers as non-collisional or exterior orogens, Cordilleran-, Pacific-, Andean-, Miyashiro- and Altaid-type orogens, or zones of type B subduction (Matsuda and Uyeda 1971; Crook 1974; Bally 1981; Murphy and Nance 1991; Windley 1992; Sengor 1993; Sengor and Natal'in 1996; Maruyama 1997; Ernst 2005; Cawood; 2009).

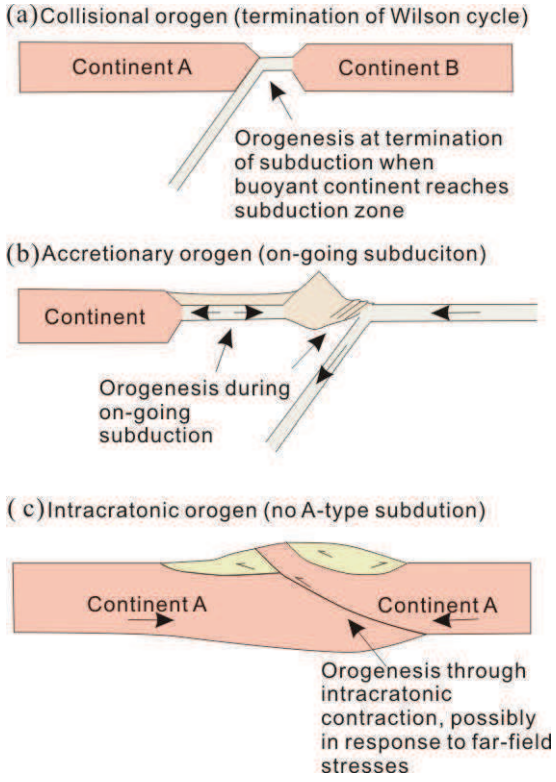

Fig.1-1-1 Schematic cross-sections through (a) collisional, (b) accretionary and (c) intracratonic orogens (after Cawood et al., 2009)

Our understanding of the evolutional process for accretionary orogens is moderately well established in modern orogens such as the Andes, Japan, Indonesia and Alaska. The western and northern Pacific extending from Indonesia via the Philippines and Japan to Alaska, and the North and South American Cordillera are archetypical modern examples. The ancient examples, taking the Phanerozoic Terra Australis and Central Asian orogens for example, also contribute to the understanding of accretionary orogens (Windley 1992; Kroner et al., 2008; Cawood et al., 2009). Accretionary orogens include accretionary prism, island arcs, back-arcs, dismembered ophiolites, oceanic plateaux, old contienntal blocks, post-accretion granitic rocks, syn-deformation metamorphic rocks and clastic sedimentary basins (Cawood, 2009).

The accretionary prism is usually associated with the offscraping and underplating of matrial from the downgoing plate to the upper plate in intraoceanic or continental subduction zones. High fluid pressure and shearing lead to a spectrum of strucutre within the prism ranging from discrete thrust imbrication of relatively coherent sedimentary packages to chaotic melange formation. Locally, the sequence displays a distinctive ocean plate stratigraphy consisting, from bottom to top, of a succession of mid-ocean ridge basalt (MORB), chert, hemipelagic mudstone, turbidite or sandstone and conglomerate. All these materials preserve a record of deformation and metamorphism during the burial in the lower plate, the accretion process at maximum depth, and exhumation in the upper plate (Kimura et al., 1996; Agard et al., 2001, 2009; Lister and Forster, 1996; Stanek et al., 2006). The high-P/Low-T metamorphism may occurred at both the wedge and/or in the subduction channel (Platt, 1993; Ring et al., 1999; Jolivet et al., 2003; Agard et al., 2009; Guillot et al., 2009). The downward migration of subducting materials creates a serieous of faults, including subduction thrust, later reverse faults, or out of sequence thrust, high-angle and detachment normal faults, and strike-slip fault systems which alter substantially their original architecture(Ring and Brandon, 1994; Ring et al., 1999; Ring and Layer, 2003; Mann, 2007). The arrive of the low-density continental material in the subduction channel is generally thought to be responsible for the choking of subduction and linking to ocean closure, which then stops or jumps outboard of the

continental block (Ernst, 2005; Chopin, 2003; Stern, 2004). When a large buoyancy mass (e.g. continental plate, large sea mount) enters the subduction zone, after a restricted period of time of being dragged into subduction belt, the collision develops.

Accretionary orogens usually are divided into two types, namely retreating and advancing based on the relative velocity of two plate and contrasting geological character(Royden 1993). Accretionary plate margins and orogenic systems can switch between phases of advance and retreat (e.g. the Lachlan segment of the Terra Australis orogen; Collins 2002), Also the accretionary orogen can undergo multiple cycles of tectonic mode switching that the dock of microcontinent at a convergent plate margin was followed by a stepping out of the subduction zone beyond the accreted terrane (Lister et al., 2001; Beltrando et al., 2007).

Island arc accretion in the accretionary orogen is important, for example, Japan (Isozaki 1996; Maruyama 1997) and Alaska (Sisson et al., 2003). The magmatism of Accretionary orogens can range from mafic to silicic. Magmatic arc activity is characteristically calc-alkaline in composition but also contain components ranging from low-K tholeiite to shoshonitic which partly depends on the nature of the interaction of the magma with the arc substrate (Tatsumi and Eggins 1995). Arc magmatism within accretionary orogens is invoked as the major source of continental growth. Geochemical and isotopic data have shown that the composition of continental crust resembles subduction-related igneous rocks and suggest a progressive growth modle of continental crust through time (Taylor 1967; Taylor and McClennan 1985; McCullonch and Bennett 1994; Arculus 1999). Thus, research the accretionary orogen belt is critical to clarity plate tectonics and to understand the significant crustal growth process (Sasmon and Patchett 1991; Sengor and Natal'in 1996; Jahn et al., 2000; Wu et al., 2000; Jahn 2004).

1.1.2 A brief introduction of Central Asian Orogenic Belt (CAOB)

The Central Asian Orogenic Belt (CAOB), also called Altaids (Altaid Tectonic Collage, Sengor et al., 1993; Sengor and Natal'in, 1996) is a complex collage of island arcs, micro-continental fragments and remnants of oceanic crust as well as

small forearc and backarc basins. It situated between the Siberian craton to the north and the Kazakhstan, North China and Tarim cratons in the south. To the east, the western margin of the Precambrian silvers of Mongolia and northeast China is a suggested border of the CAOB. To the south, the boundary follows the northern margin of the Karakum, Alai-Tarim, and North China cratonic blocks. In the west, the boundary starts near the Caspian Sea and then follows the Main Urals faults as a principal boundary between the non-oceanic and oceanic complexes (Fig.1-1-2, Sengor et al., 1993, Mossakovsky et al., 1994; Sengor and Natal'in, 1996; Yakubchuk et al., 2002; Jahn et al, 2000; Badarch et al., 2002; Jahn, 2004; Xiao et al., 2003, 2008; Windley et al., 2007).

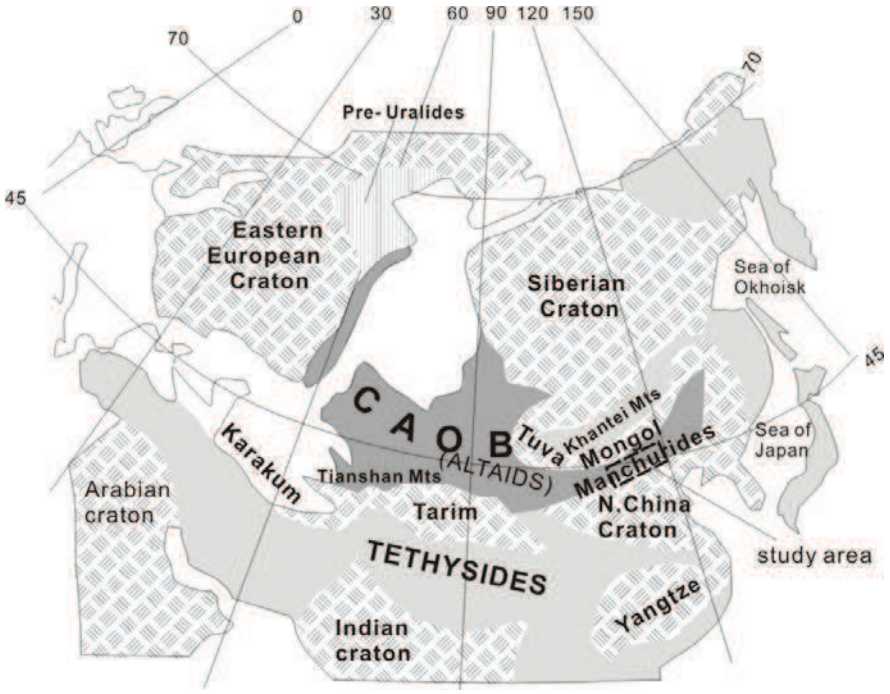

Fig.1-1-2 the Central Asian Orogenic Belt and adjacent structures (modified after Alexander Yakubchuk, 2004)

Sengor et al. (1993) and Sengor and Natal'in (1996) synthesize that the Central Asian Orogenic Belt formed from c.542Ma to 250Ma involving one main island arc (Kipchak-Tuva-Mongol arc) along the outboard marin of the Baikalides and Ore-Uralides orogen. This arc collaged to Siberia and Baltica by differential rotation, causing the arc duplication and oroclinal bending by the late Carboniferous. Some researchers enlightened by the geology and tectonics of the modern western Pacific

suggested that island arcs, oceanic islands, seamounts, accretionary wedges formed in the Palaeo-Asian ocean and accreted to the margins of Siberia and Baltica. Simultaneously several Precambrian blocks were rifted off the margins of Gondwana and/or Siberia and drifted to dock with the growing accretionary margins (Zonenshain et al., 1990; Mossakovsky et al., 1993; Badarch et al., 2002; Khain et al., 2003).

1.1.3 Paleozoic tectonic evolution controversy and problems in Inner Mongolia

The vast territory of Central Inner Mongolia lies in the eastern part of the CAOB, also called Manchurides (Sengor and Natal'in, 1996; Fig.1-1-2). Numerous research have been carried out around the tectonic division and evolution, sedimentology, magmatism, structural deformation, paleobiogeography, and paleomagnetism of Inner Mongolia since several decades. However, there are markedly conflicting interpretations on some questions, such as the tectonic affiliation of the Permian marine basin in the eastern Paleo-Asian orogens, the postion and timing of the collision between the Sino-Korean and Siberian Paleoplates (Wang and liu 1986; Shao et al., 1991; Xiao et al., 2003; Zhang et al., 2008, 2011; Jian et al., 2008, 2010; Xu et al., 2012). The Solonker (also called Solon Obo) suture is considered by most of geologists as the major structure that delineates the final location of the Paleo-Asian Ocean (Sengör and Natal'in, 1996; Xiao et al., 2003; Windly et al., 2007; Chen et al., 2009; Jian et al., 2010). However, the exact position of the Solonker suture is still in controversy. Some geologists advocated that the suture line extends from Solon Obo to the Hegenshan (Shao 1991; Nozaka and Liu 2002). On the contrary, some believes that the suture extends from Solon Obo eastwards through the region of Linxi and XarMoron river (Wang and Liu 1986; Tang 1990, 1992; Sengor and Natal'in 1996; Xiao et al.2003).

Several different models have been proposed to explain the tectonic evolution of Inner Mongolia involving closure of ocean basins by multiple/doule-opposite subduction, accretion and collision of island arcs and microcontinents, and formation of multiple suture zones. Here list the main models:

1) Xiao et al.(2003) proposed a model for the evolution of the CAOB with three

main stages that are related to progressive two-way subduction of the Paleo-Asian Ocean (Fig.1-3): 1) early to mid-Paleozoic Japanese-type subduction-accretion, 2) a Permian Andean-stage when the two opposing margins became sufficiently consolidated, and 3) continent-continent collision, leading to the formation of the Solonker suture zone at the end of the Permian during the final closure of the Paleo-Asian Ocean due to its coeval southward and northward subduction beneath the Tarim and North China cartons and Siberia, respectively. This process was accompanied by emplacement of immense volumes of mafic and granitic magmas (Chen et al., 2000; Jahn et al., 2000, 2004; Wu et al., 2002).

2) Jian et al. (2008, 2010) proposed two phases of orogenic cycles with a timporal gap of ca. 120Ma. The southeastern CAOB evloved in a progression from oceanic subduction/arc formation (ca.500-438Ma), to ridge subduction (ca.451-434Ma), and microcontinent accretion/collision (ca.430-415Ma). The Permian-Triassic orogenic cycle is associated with pre-subduction extension (ca.299-290Ma), subduction initiation (ca.294-280), ridge-trench collision (ca.281-271Ma) and slab break-off (ca.255-248Ma).

3) Recently, Xu et al., (2012) recognized several litho-tectonic units in Inner Mongolia on the basis of regional lithological correlation and geochronology. It argued that during early Palezoic, a south-directed oceanic subduction below the North China Craton coeval with a north-directed oceanic subduction. Finally, the two opposite subduction systems ended around 420-380Ma.

These numerous differing models are mostly based on various types of geological data such as regional stratigraphic correlation, paleomagnetism, paleontology, geochronology and geochemistry (Zhang and Tang, 1989; Tang, 1990; 1992; Shao, 1991; Ren et al., 1999; Nozaka and Liu, 2002, Chen et al., 2000, 2008;

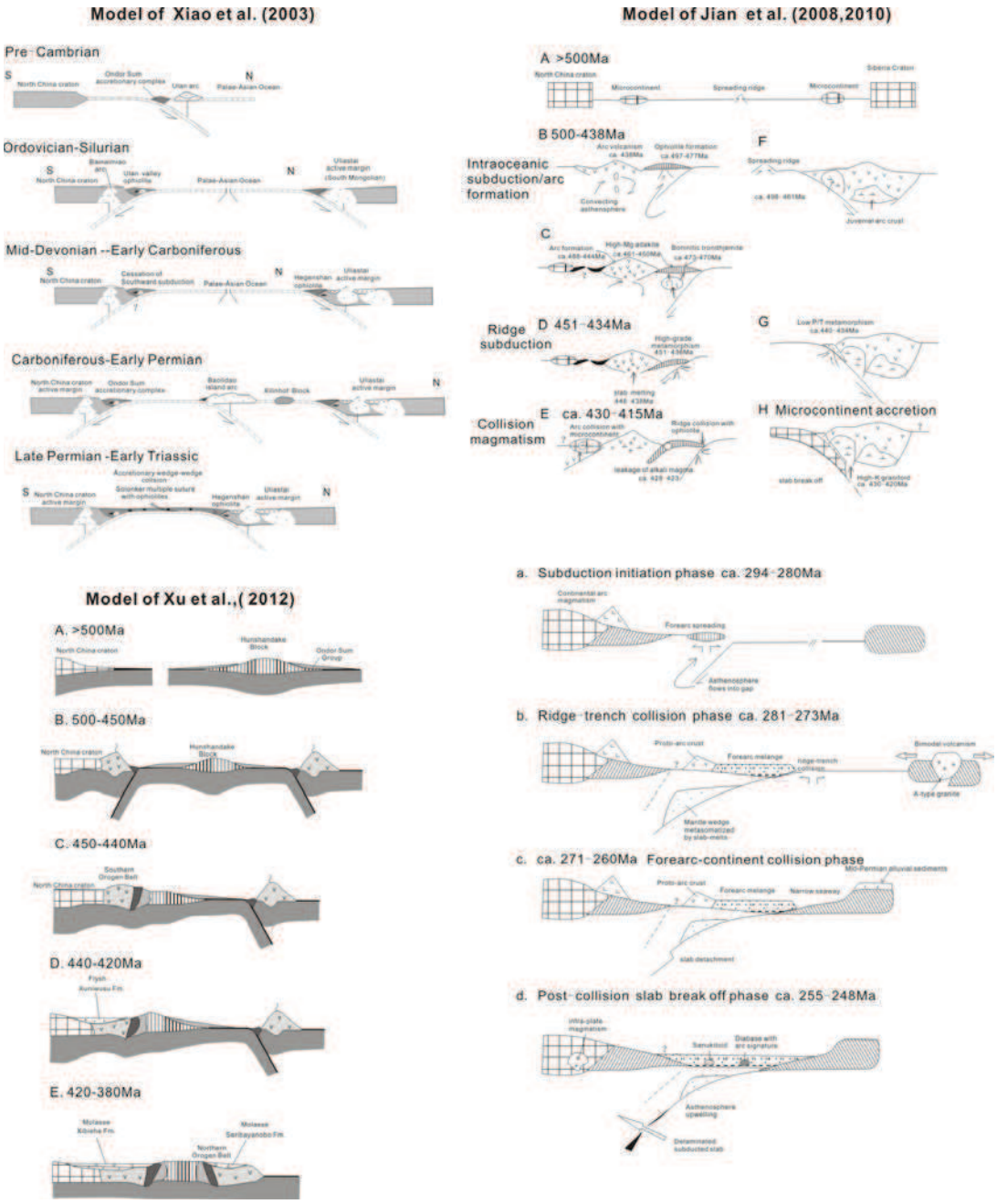

Fig.1-1-3 the exiting modles about the tectonic evolution of Inner Mongolia

Jian et al., 2008, 2010). However, none appears to account for all the geological data. Here we synthsis all these problems about several geodynamic scenarios:

A) Although there were several models, the structure of this zone is poorly constrained, so that it is difficult to evaluate these models.

B) It is widely regarded that the Solonker suture represents the final closure positon of CAOB. However, there is rare geological data are documented about the Solon Obo ophiolite and surrounding geology.

C) The Permian tectonic affinity in Inner Mongolia is arc or rifting setting. It is still debated problem, even though plenty of geochemical data were reported.

D) The feaures of microcontinent that involved in the evolution of CAOB is another problem. Rare existing evidences are reported, even though plenty of models mentioned the existence of a microcontinents titled the South Gobi microcontinent (Sengör and Natal'in, 1996;), South Mongolia microcontinent (Xu et al., 2012) and Hutag Uul terrane (Badarch et al., 2002).

Thus, the structural deformation data, new geological observation about the Solonker ophiolite and new age dating data are important and will be critical constraints about the eastern segment of the CAOB.

1.2 Research contents and methods

To solve the problems mentioned above, three research areas, Hongqi area, Onder Sum area and Mandula area respectively, are seleted to carry out detailed geological mapping about Paleozoic lithological and structural feasures. A multidisciplinary research was carried into execution in this project, including:

1) Differentiating the litho-tectonic units concerning the accretionary orogenic process on the basis of regional geological survey, lithological correlation and deformation features. Recognizing the relationship between the differing the litho-tectonic units.

2) Structral analysis: recording the geometric and kinematic characteristics, especially the mélange belt. Differentiating the successive deforming phases to discuss the relationship with the subduction-collision process.

3) Sedimentary facies analysis: analyzing the sedimentary facies and sedimentary environment on the basis of sedimentary stratigraphy geometry, thickness and distribution, sedimentary structure etc. Discussing the relationship between stratigraphic development and the collision and/or rifting phases.

4) Geochronology and provenace analysis: with the help of the detrital zircon dating method, creating the litho-geochronlogical framwork in the study area. comparing the age distribution with the regional particular tecotnic event to anaylize the sediementart provenace.

Finally, synthesizing our geological survey data and precursors' research results, a tentative geodynamic evolution model was proposed about the Central Inner Mongolia to solve the problems mentioned above and to evaluate the existing geodynamic modles.

第二章　区域地质背景（Regional Geological Setting)

第一节　研究区的地理与构造位置 (Geographic and Tectonic position)

研究区处于我国内蒙古自治区，濒临中蒙边界（图 2-1-1），南起于呼和浩特以北，约北纬 41°，以北至中蒙边界。东西跨度较大，跨越了 E108°－E115°广大地区。地貌上属于蒙古高原丘陵地带，其次为山地和平原，平均海拔在 1000 米左右。大兴安岭、阴山、贺兰山蜿蜒相连，呈 S 形贯穿全区。横亘内蒙古中部的阴山山脉，由大青山、乌拉山、色尔腾山和狼山组成，绵延 1000km，海拔 1500-2000m。研究区地表多被植被覆盖，地貌相对高差较小，露头出露较差，给地质调查工作带来困难。

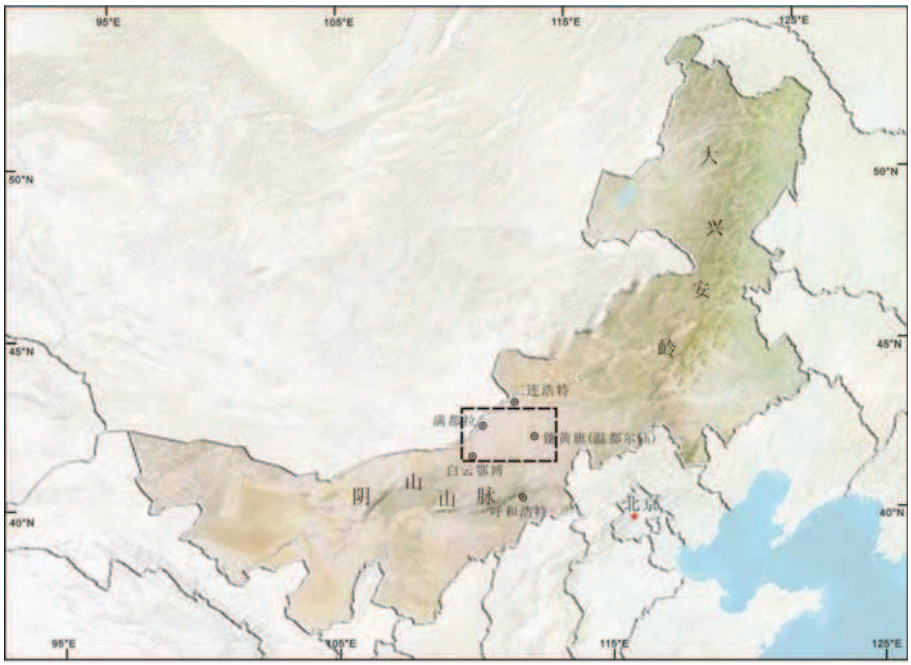

图 2-1-1 内蒙古地区区域位置图 （据 http://www.masterfile.com 修改）

大地构造位置上，研究区属于中亚造山带在中国境内的部分，向西与蒙古境内的造山带对应。该区是古亚洲构造域的重要组成部分，北与蒙古—鄂霍茨克造山带相邻，南接华北克拉通（图 2-1-2）。我国地质学家称其为兴蒙造山带，其南侧的华北板块是吕梁运动后已基本固结的稳定块体，两者以高家窑-乌拉特后旗-化德-赤峰深大断裂为界。内蒙古中亚造山带主要包括加里东和海西等不同时

期岩石地层单元，后被中新生代盆地覆盖（内蒙古区域地质志，1991）。由于该区涉及古亚洲洋构造域最终拼合的位置及时代等基础地质问题，是研究中亚造山带古生代构造演化、深部动力学背景的理想之地，因此受到国内外地质学家所关注。

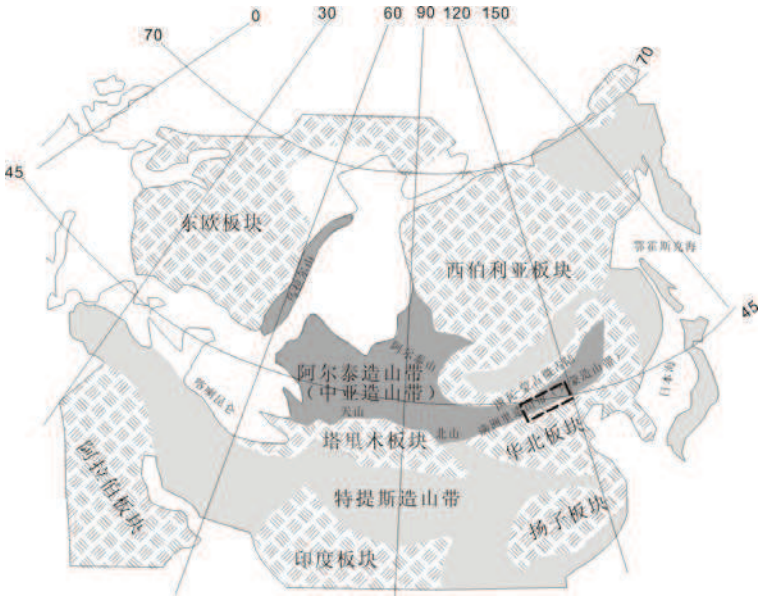

图 2-1-2 中亚造山带大地构造带划分（据 Alexander Yakubchuk，2004 修改）

第二节　研究区地质背景 (Geological background)

红旗牧场-温都尔庙-满都拉地区跨越了华北板块和兴蒙造山带两大构造单元。前人根据区域上的构造岩石特征以及接触关系，将中亚造山带内蒙古段分为南北两个造山带（图 2-2-1，Wang and Liu et al.，1986； Xiao et al.，2003；Jian et al.，2008，2010；Xu et al.，1997，2012）。北造山带分布于苏尼特左旗-锡林浩特一线，由一系列的向南仰冲的带组成，包含低 P/T 变质杂岩、俯冲增生杂岩和侵入岩（胡骁，1990；Xiao，2003；Xu et al.，1997，2012）。南造山带位于温都尔庙-白云鄂博一线，主要包括 5 个构造岩石单元，从南向北依次为：华北板块（克拉通）、白乃庙岛弧带、温都尔庙俯冲增生杂岩、

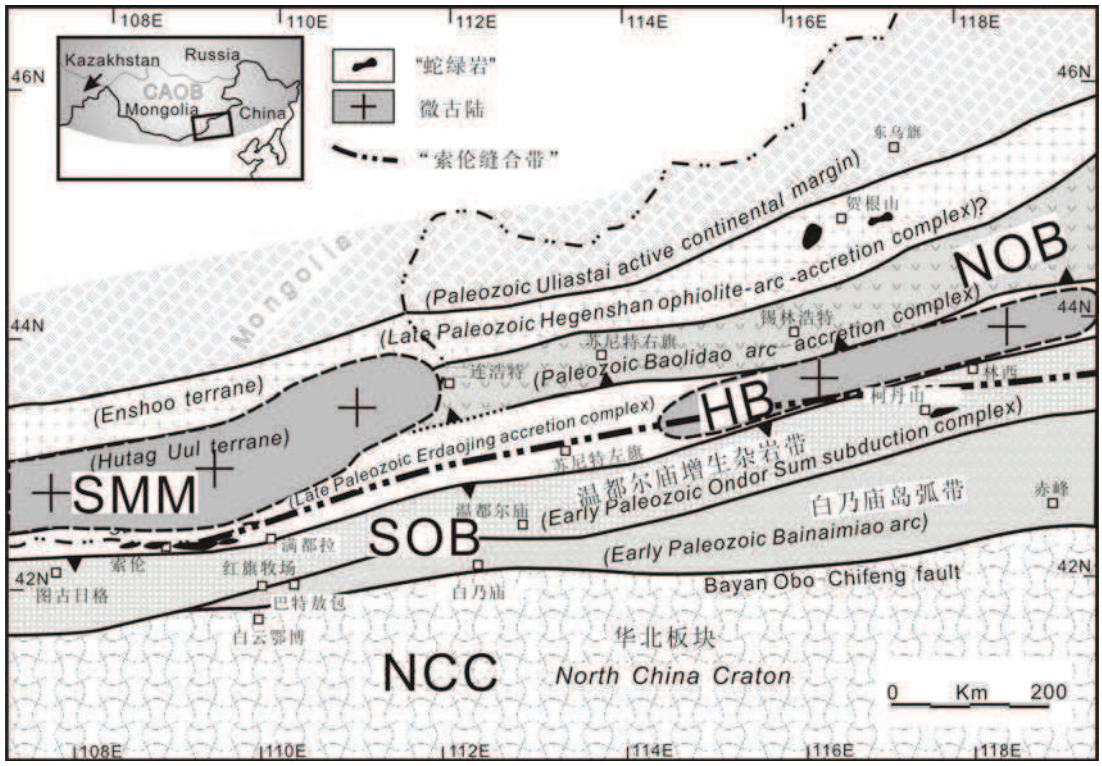

图 2-2-1 内蒙古古生代主要构造岩石单元划分 （据 Badarch et al., 2002; Xiao et al., 2003; Xu et al., 2012, 修改）NCC=华北克拉通，SOB=南造山带，HB=浑善达克陆块，SMM=南蒙古微陆块，NOB=北造山带 。

“索伦缝合带”以及北部可能存在的微陆块。在造山带的研究中，通过分析地层的物质组成、时空分布规律、成因环境以及与岩浆活动关系，能够对造山带的形成演化进行约束。本文研究区主要跨域了南造山带构造单元，下面根据主要地层的时代和分布特征，将前人划分的岩石结构单元分别进行简要的介绍。

2.2.1 华北板块（the North China Craton)

华北克拉通主要由太古代结晶基底和沉积盖层组成（肖荣阁等，2000；内蒙古自治区区域地质志 1991）。结晶基底由古太古界兴和岩群、中太古界乌拉山岩群和新太古界色尔腾山岩群组成，另外还分布有大量太古代的 TTG 岩系，变质程度达低角闪岩相－麻粒岩相。此外在乌拉特后旗-白云鄂博一带分布有古元古界宝音图群，岩性为片岩、石英岩和大理岩等，为一套角闪岩相变质地层，时代为 2.45-2.50Ga（徐备，2001；张臣等，2001；张玉清和苏宏伟，2002，张玉清，2002，2004；沈存利等，2004）。中新元古界白云鄂博群和渣尔泰山群，为华北地台形成后的第一个（准）盖层沉积，它们属于两个近平行的裂谷型沉积（王楫

等，1992)。白云鄂博群为一套碎屑岩、碳酸盐岩建造，夹有板岩及少量火山岩，浅变质或未变质。其中基性火山岩层单颗粒锆石 U-Pb 年龄 1728±5Ma（王楫等，1991；Chao et al.,1997；张宗清等，2003)。渣尔泰山群是一套碎屑岩、碳酸盐岩及黑色页岩建造，沉积始于 1750Ma 左右（王楫，1992；陈从云，1993)。在华北克拉通北缘，白云鄂博地区分布震旦系腮林呼洞组和寒武系阿牙登组，为一套碳酸盐岩夹碎屑岩建造含有藻类等微体化石，底部与白云鄂博群呈断层接触，部分呈飞来峰形式出现（白云鄂博幅 1/25 万区调，2002)。下二叠统苏吉组，呈北西向、近东西向带状展布于白云鄂博断裂以南，岩性为陆相中酸性火山碎屑岩、火山熔岩，底部不整合在白云鄂博群和阿牙登组之上，被白垩系李三沟组不整合覆盖。这些沉积地层普遍被早中二叠世、三叠纪花岗岩侵入(内蒙古区域地质志，1991； Hsu et al., 1991； Zhao et al., 2005)。沿着东-西向展布的白云鄂博-赤峰断层被认为华北克板块和白乃庙岛弧的边界线(邵济安，1991；唐克东，1992；Tang et al., 1993；Xiao et al., 2003)。

2.2.2 白乃庙岛弧单元区 (The Bainaimiao Arc Belt)

白乃庙岛弧单元呈条带状近东西向展布，从西部的图古日格至东部赤峰延伸近千公里（图 2-2-1)，主要由奥陶系和志留系火山岩、碎屑岩和碳酸盐组成。在白云鄂博东北至达茂旗以北广泛分布奥陶系包尔汉图群和志留系西别河组。包尔汗图群分两个岩组，下部为布龙山组，上部为哈拉组。布龙山组主要为早期喷出拉板玄武岩，后期喷出钙碱性系列的安山岩、英安岩及火山角砾岩等，以及含粉砂硅泥质板岩、含砾砂岩、大理岩、含铁石英岩薄层，厚度 1359m（内蒙古区域地质志，1991)。在布龙山组顶部的凝灰质粉砂岩中采到笔石：Callogaptus sp., Desmograptus sp. 和 Dictyonema sp., Aspidograptus sp. Dicranograptus?sp., 时代属于奥陶纪（唐克东等，1992)。哈拉组则主要是一套中基性火山熔岩、火山碎屑岩，整合或逆冲覆盖于布龙山组之上。与火山岩同时产出大量的花岗岩，花岗闪长岩和石英闪长岩,分布于巴特敖包一带。闪长岩和石英闪长岩属于高钾-中钾钙碱性系列，地化特征显示强烈的 LILE 富集和突出的 Nb-Ta 和 Ti 负异常，高 Sr、Ba 低 Y、Yb 特征具有 adakite 特性，La/Yb 变化较大并伴随着低 Yb 特征，可能与长石和角闪石的分异作用有关（许立权等，2003；陶继雄等，2005；Jian et al.,2008)。该地区的花岗质岩石获得锆石年代多在 440-460Ma 之间（Jian et

al.,2008；李建锋等，2010)。巴特敖包地区西别河组不整合覆盖奥陶纪花岗岩之上，沉积年代为晚志留纪（Johnson et al., 2001)。

在白乃庙和温都尔庙地区，奥陶系地层由白乃庙群组成。白乃庙群可分为三个火山-沉积岩组。下部乌鲁乌苏组主要由基性火山岩及火山沉积岩组成，下部以沉积岩为主，向上为基性熔岩，更上出现安山质火山岩，该岩组厚度大于744m；其上的榆树沟组为另一火山喷发旋回产物，该组下部沉积岩中偶夹大理岩透镜体，岩组厚约1236m。最上部的徐尼乌苏组与其下的火山岩层整合产出，主要由硬砂岩和粉砂岩组成，厚 1520m（内蒙古区域地质志，1991)。白乃庙岛弧与华北板块断层接触，胡骁等（1990）在白乃庙岛弧相关沉积中发现笔石化石，时代定为早-中奥陶纪。Zhang et al.(2012)在白乃庙群火山岩中获得SHRIMP锆石年龄为474-436Ma。白乃庙群火山岩同位素显示高Sr和Nd低值（$^{87}Sr/^{86}Sr$=0.7146, εNd=2.4±1.7)，说明有地壳元素的混入，被解释为大陆边缘弧环境(Shao, 1989; Nie and *Bjørlykke*, 1999; Xiao et al., 2003)。

2.2.3 温都尔庙增生杂岩区 (The Ondor Sum Subduction/Accretion Belt)

温都尔庙增生杂岩带东西延伸约700km，横跨西部的白云鄂博至东部的西拉木伦河广阔区域（Wang and Liu, 1986; Xiao et al., 2003)。在内蒙古中部集二线两侧有较好的出露，被命名为温都尔庙群（内蒙古区域地质志，1991)，主要由一套海相火山-沉积的变质岩系组成，包含有蓝片岩和超基性岩块体。唐克东等人 （1983）将温都尔庙群划分为6种岩石组合：即石英片岩-石英岩组合、绿片岩-拉斑玄武岩组合、大理岩组合、辉长-辉绿岩组合，超基性岩组合及片麻状斜长花岗岩组合。温都尔庙群总的特点是一套以绿片岩为主的火山碎屑岩夹中基性熔岩和正常碎屑沉积，属于海底喷发的产物。胡骁等（1990）应用方解绿泥石片岩、含铁层和条带状石英岩等标志，重建了温都尔庙群的层序，主要由桑达来音组细碧角斑岩、哈尔哈达组铁硅质岩和混杂体组成。下部桑达来音组主要由中基性喷发岩、熔岩组成，大部分为块状或者片理化的绿泥细碧岩、细碧质凝灰岩和玄武岩、安山玄武岩、安山玢岩和辉绿岩及凝灰岩组成，常夹粗粒大理岩或大理岩化灰岩。岩石常见强烈的绿泥石化、碳酸盐化和硅化。上部哈尔哈达组岩性单一，主要为石英岩、含铁石英岩和绿泥绢云石英片岩，原岩以深海相硅质化学沉积为主。在绿片岩系中普遍发育蓝闪石片岩，含蓝闪石的岩石类型有钠长蓝

闪石片岩、钠长绿泥蓝闪片岩、绿帘绿泥蓝闪片岩、蓝闪绿帘大理岩等，蓝片岩呈透镜状和团块状断续出露。前人对温都尔庙的混杂岩进行了详细的变质岩石学研究（Wang and Liu, 1986；Yan et al., 1989； Tang and Yan, 1993；De Jong et al., 2006），蓝片岩共生的矿物组合有：蓝闪石+多硅白云母+黑硬绿泥石+文石+钠长石+石英，蓝闪石+羟硅锰铁石+铁滑石。变质基性熔岩中出现蓝片岩相矿物组合为硬柱石+绿泥石+钠长石+石英，硬柱石+绿帘石+绿泥石+榍石。温都尔庙地区分布着近百个超基性岩体，呈东西向展布，个体规模小，岩相简单，蚀变强烈，多呈透镜状、束状或不规则的块状、片状产出。

Xiao et al.（2003）报道了乌兰沟地区地质组成，包括三个结构单元。：其中混杂岩由含金云母石英糜棱岩、石英绢云片岩、云母石英片岩、绿泥绿帘片岩等构成，混有大小不等的变质玄武岩、硅质岩、大理岩和蓝片岩等块体。在乌兰沟一带发现的蓝片岩新获得的 Ar/Ar 年龄为 453.2±1.8Ma 和 449.4±1.8Ma（De Jong et al., 2006）,442±12 Ma（邵济安等，2007）。图林凯地区蛇绿混杂岩带由一系列向南仰冲的席状体构成，东西延伸 200km，宽 25km 左右。该混杂岩底部为 5km 的角闪岩相变质单元，上部被志留纪砾岩、硬砂岩和碳酸盐建造覆盖（胡骁等，1990；王荃等，1991），其中所含岩浆岩块体获得 425-490Ma 锆石年龄（刘敦一等，2003；Jian et al.,2008）。

2.2.4“索伦缝合线”单元区 (The “Solonker Suture” Suture)

2.2.4.1 晚古生代地层

该单元横穿了索伦敖包至西拉木伦河的广阔区域，一些地质学者认为索伦缝合线为古亚洲洋最终的拼合位置（图 2-2-1；Xiao et al., 2003；Chen et al.,2000,2008；Jian et al.,2008,2010）。该单元主要出露晚石炭系本巴图组、阿木山组和二叠系地层(内蒙古自治区区域地质志，1991；李文国等，1996)。本巴图组主要分布在苏尼特左旗、达尔罕茂明安联合旗一带，为一套浅海相碎屑岩系，岩石组合为杂砂岩、长石砂岩、石英砂岩、变质粉砂岩及灰色板岩，夹有灰岩透镜体和火山碎屑岩。从岩性组合来看，本巴图组形成于较为动荡的沉积环境（李文国等，1996；鲍庆中等，2006）。本巴图组包含 2 个化石组合带，*Eostaffella-Millerella* 组合带和 *Triticites-Pseudoschwagerina* 组合带，时代为石炭纪威宁世（满都拉地区 1/25 万区调，2003）。阿木山组分布范围与本

巴图组一致，横向上与本巴图组呈锯齿状递变关系，为一套以海相碳酸盐岩为主的岩石地层序列，岩石组合为生物灰岩、白云质灰岩、角砾状灰岩夹钙质砂岩、粉砂岩等，含丰富的海相动物化石，有腕足类、腹足类、双壳类、苔藓虫等化石(李文国等，1996；鲍庆中等，2006；满都拉地区 1/25 万区调，2003)。

研究区二叠纪地层分布广泛，自下而上依次发育大石寨组、哲斯组，在内蒙古林西地区主要发育晚二叠世林西组等地层单元（内蒙古自治区岩石地层，1996)。大石寨组火山岩分布于西部的满都拉，二连浩特、锡林浩特以及东部的林西等地,喷发环境为浅海相和滨海相,含有 *Derbyia* sp.，*Streptorhynchus* sp. 等腕足类化石（李文国等，1996)。在满都拉地区主要出露中酸性熔岩夹火山碎屑岩及正常沉积碎屑岩（苏新旭等，2000)。在锡林浩特一带，由流纹-英安岩和玄武质安山岩，具有双峰火山岩的特征，时代为 280Ma（Zhang et al.,2008)。在林西地区该火山序列主要为玄武岩、玄武质安山岩、粗面安山岩和相关的凝灰岩及火山碎屑沉积(Zhu et al.2001)。苏尼特左旗地区，大石寨组自下而上由巨厚层安山质玻屑-晶屑-岩屑凝灰岩夹安山岩和少量玄武质熔岩过渡到安山岩-英安岩-流纹岩为主的中酸性喷出岩系（李述靖等，1998；张晓晖等，2010)。黄岗梁-林西地区，则由下部的角斑岩-石英角斑岩-流纹岩组合，中部枕状细碧岩-玄武岩组合，上部玄武岩-安山玄武岩为主的中基性熔岩组成（邵济安，1991；吕志成等，2002；Zhu et al.,2001)。哲斯组是研究区在大石寨组火山岩之后发育的最为广泛的沉积地层，它是一套浅海相砂岩、页岩和碳酸盐组合，部分地区发育有火山碎屑岩和硅质岩，产非常丰富的海相生物化石（王成源等，2006)。对于哲斯组所代表的大地构造环境研究，前人多认为其代表了浅水的沉积环境（内蒙古自治区区域地质志，1991；高德臻等，1998；王惠等，2002)。但最近的研究在泥页岩沉积中获得了放射虫等化石，指示较深水沉积环境，(尚庆华，2004)。上二叠统林西组主要由一套黑色板岩、粉砂岩、砂岩组,含丰富的淡水瓣鳃类和植物化石。李福来等（2009）应用地球化学方法,对内蒙古上二叠统林西组的沉积环境进行了研究，通过沉积环境判别指标的分析,确定林西组为开阔的淡水环境,主要为陆相沉积体系,在其沉积初期为海陆交互环境。

2.2.4.2 镁铁-超镁铁质岩

索伦地区：索伦山蛇绿岩沿中蒙边界分布，在我国境内出露长约 100km，宽小于 5km。包括数百个蛇绿岩块，大者达上百平方公里，小者数平方米，呈扁豆

状和透镜状的块体或狭长的断片产出于中上石炭统和下二叠统地层中。块体主要由变质橄榄岩、辉长岩、斜长花岗岩和辉绿岩岩墙群四部分组成。野外见到蛇绿岩块体性脆而破裂，节理发育。钻探和物探资料证明它们是无根的，索伦岩体向下延续 500-600m 后，便逐渐尖灭（邵济安等，1991）。地表残留的超镁铁质岩石表面往往可以见到风化散落的红色铁碧玉岩岩块或者赭色的硅质风化壳（唐克东等，1992；邵济安等，1991）。

满都拉地区：在达茂旗北部的满都拉地区，超基性—基性岩块呈构造侵位（苏新旭等，2000）或飞来峰（陶继雄等，2004）形式产于石炭系本巴图组中。岩块主要为大小不等的形态各异的超镁铁质岩、辉长质岩、镁铁质火山岩、硅质岩等岩块，在基质中的含量约占 30-50%，蛇绿岩以构造碎块形式出现，产出状态和构造特征均表明它们是异地残留的古洋壳碎块（苏新旭等，2000；陶继雄等，2003，2004）。一些地质学家研究认为，早石炭世后由上述基性—超基性岩代表的洋壳向北俯冲，形成晚石炭世—早二叠世岛弧带和构造混杂带，因此满都拉地区蛇绿岩带代表晚古生代缝合带（苏新旭等，2000；Jian et al.，2010）。在硅质岩中新发现的中二叠纪放射虫（王惠等 2005；尚庆华，2004），该蛇绿岩带被认为代表中二叠世早期的古洋盆。 陶继雄等（2004）根据变质辉长岩的单颗粒锆石年龄（433.6±3.6Ma）和附近有古老地块的特征认为该蛇绿岩带可能代表中古生代的陆间小洋盆。

二道井杂岩：在二道井地区以北东东-南西西向延伸约 150km，宽约 1-5km，由变形不均一的基质和各类岩块组成。岩块的类型以白云岩最多，其次为石英岩和石英片岩、超镁铁质和镁铁质岩石、大理岩、灰岩、砾岩和蓝片岩。基质由变质砂岩、变质火山岩和云母石英片岩组成，遭受绿片岩相变质作用（徐备和陈斌，1997；张臣和吴泰然，1999）。蛇绿混杂岩被晚泥盆世色日巴彦敖包组碎屑岩不整合覆盖（徐备等， 1997），其中所含蓝片岩岩块的 Ar/Ar 年代为 383±13Ma（徐备等，2001）。根据蓝片岩年龄和不整合关系，这条混杂岩带被认为属中古生代造山带的混杂堆积带。但 Xiao et al.(2003）认为该带属于晚古生代混杂堆积的下部组合，上述蓝片岩年龄仅代表俯冲带高压岩石冷却和上升年龄。

西拉木伦河地区：西拉木伦河北侧，断续出露一些蛇绿岩碎块。柯单山蛇绿岩构造侵位于二叠系地层中，与围岩呈断层接触关系，被中侏罗统火山沉积岩覆

盖。包含块体有斜辉辉橄岩，辉橄岩等，强烈蛇纹岩化和碳酸盐化，呈土黄色（邵济安等，1991）。在杏树洼一带，蛇绿岩构造侵位于上志留统，岩石蚀变和破碎强烈，强烈片理化（邵济安等，1991；王荃等，1991）。

2.2.5 微陆块 (Microcontinents)

研究区涉及到的古老块体只要有南蒙微大陆（SMM）和浑善达克陆块（HB）。南蒙古微陆块又称为 Hutag Uul 或者 Totoshan Ulanul（Badarch et al.,2002; Demoux et al., 2009），沿东西向延伸近 600km，在中国境内以艾力格庙群为代表。艾力格庙群分布在二连浩特西南艾力格庙地区，主要由一套中等变质的大理岩、结晶灰岩、石英岩及绢云石英片岩组成。厚度大于 778 米。在该群所采藻类化石有 *Vermiculitescf. tortuosus Reitllinger* 及 *Vermiculites irregularis Reitlinger, Osagia cf.libidinosa Zhuravleva*， *Radiosus* cf. *badius Zhuravleva* 等其时代相当于晚元古代（600-1000Ma）（艾力格庙 1/20 万区调，1981）。

在托托尚山东部，南蒙古微陆块由托雷努力斯群组成，下部为大理石化灰岩，往往具有钙泥质胶结的角砾状灰岩，上部为淡灰色、玫瑰灰色和灰绿色流纹质斑岩，有时为霏细斑岩；顶部为碳酸盐岩至碎屑岩层。在托雷乌拉山东 8km 处的该群上部层位中采到藻类化石：Vesicularites concretus Zhur,V.congermaus Zhur, Nubecularites abustus Zhur.含化石层位时代归属于文德阶（约 600-700Ma）（艾力格庙 1/20 万区调，1981）。

大量的片麻岩锆石定年显示中、南蒙古前寒武纪地体的存在（Antoine Demoux，2009; Hargrove et al. 2006; Kroner et al., 2007)。A.Demoux 在 Baga Bogd（南蒙古）花岗质片麻岩中获得锆石 SHRIMP 年代 1519±11Ma 和继承锆石年代 1700Ma，说明南蒙古 Baga Bogd 地区古元古代-中元古代地壳的存在，侵入该片麻质岩石的花岗岩体获得锆石 SHRIMP 年龄为 983±6，956±3 和 954±8Ma，而在托托尚山 (totoshan-Ulanul)块体，花岗质片麻岩获得 952±8Ma 年龄值（U-Pb 单颗粒锆石法）(Yarmolyuk et al. 2005)。

Xu et al.(2012)通过研究温都尔庙群的碎屑锆石年龄分布，分析其含有的 1300-900Ma 和 700-500Ma 的年龄谱峰与华北克拉通物源和北部蒙古地区不一致，推断在浑善达克沙漠下面存在微小陆块。

第三章 早古生代大地构造特征 (The Early Paleozoic Tectonics)

本文选择白云鄂博地区红旗牧场研究区和镶黄旗温都尔庙研究区进行重点分析，通过野外地质考察，对研究区进行了造山带次级构造单元划分和构造变形分析。

第一节 红旗牧场研究区（The Hongqi area）

红旗牧场研究区位于白云鄂博北部，其东侧的巴特敖包地区出露大量的花岗岩、花岗闪长岩，是南造山带主要组成部分。根据地质组成特征、将红旗牧场研究区从南向北划分为四个次级构造带，分别为华北板块（前寒武系）、白乃庙岛弧带、红旗牧场混杂岩带和晚泥盆系-石炭纪滨浅海相的碳酸盐岩和陆缘碎屑岩沉积。下面分别进行论述：

3.1.1 岩石构造单元划分 (The Litho-tectonic framwork)

3.1.1.1 华北板块 (The North China Craton)

本次研究将古元古界宝音图岩群和中-新元古代白云鄂博群作为华北板块的基底，主要分布在乌拉特后旗-白云鄂博一带。宝音图岩群为一套高绿片岩—低角闪岩相的变质岩，下部主要为石英岩、大理岩组合，上部主要为一套石英片岩夹石英岩、薄层状大理岩透镜体和阳起片岩透镜体，时代为 2.45-2.50Ga（徐备，2001；张臣等，2001；张玉清等，2002，张玉清，2004；沈存利等，2004）。白云鄂博群呈近东西向展布,主要分布在乌拉特中旗、白云鄂博、达茂旗、四子王旗等地,是中—新元古代华北地台北缘被动大陆边缘沉积产物（Chao et al.,1997；张宗清等，2003）。白云鄂博群下部由砂砾岩段、石英岩段、黑色板岩、白云岩或灰岩所组成；上部为滨浅海碳酸盐台地至较深水陆坡滑塌堆积与浊积岩（内蒙古自治区区域地质志，1991），其中基性火山岩单颗粒锆石 U-Pb 年龄 1729±5Ma（王楫等，1991）。

3.1.1.2 白乃庙岛弧带 (The Bainaimiao Arc Belt in Hongqi area)

野外特征

火山岛弧主要由中下奥陶统包尔汗图群火山岩、火山碎屑岩及深成岩组成。火山岩构成岛弧主体,岛弧岩浆岩侵入其中。在白云鄂博地区，包尔汉图群主要分布

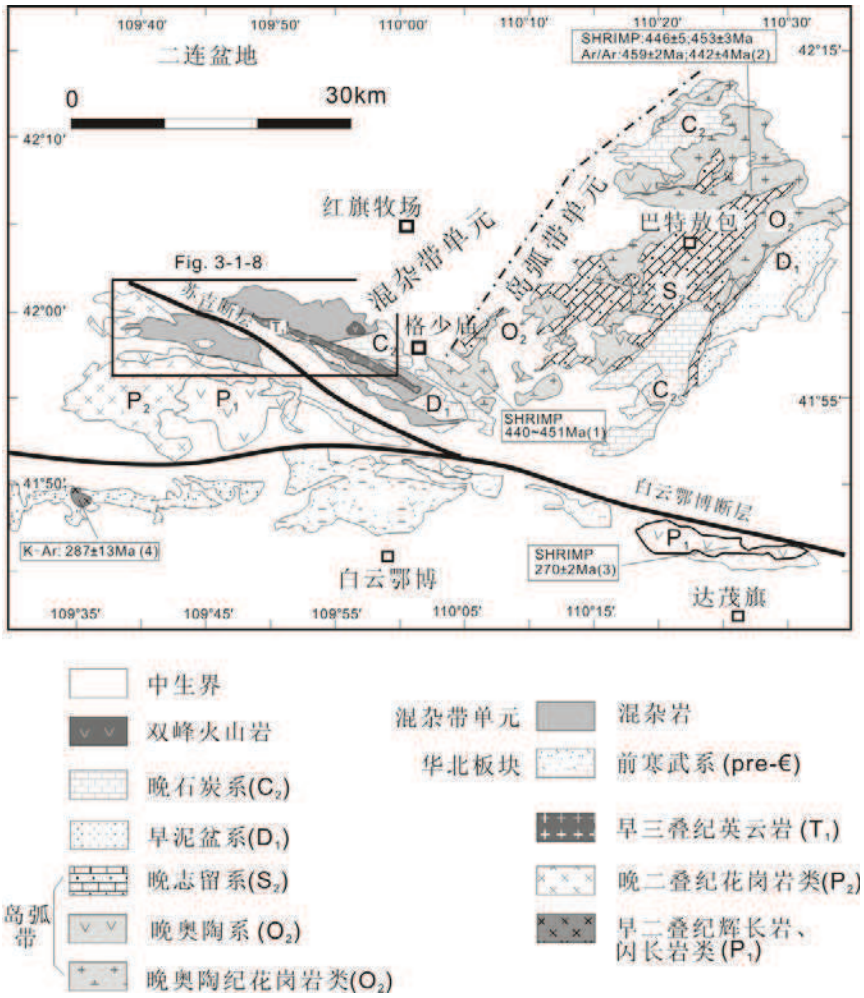

图 3-1-1 红旗牧场地区造山带岩石构造单元划分（年代数据及来源见附件 1）

在白云鄂博北 25 公里格少庙一带，可分两个岩组，下部为布龙山组，上部为哈拉组。布龙山组主要为凝灰质粉砂岩、含砾砂岩，其中夹数层火山岩层，从拉斑玄武岩逐渐过渡到安山岩和少量英安岩，同时产出有大量火山角砾岩和凝灰岩。哈拉组为一套中基性火山熔岩、火山碎屑岩。为了更好地描述布龙山组的地质组成和层序特征，我们在格少庙以东约 8km 处测定了精细的剖面，描述如下：

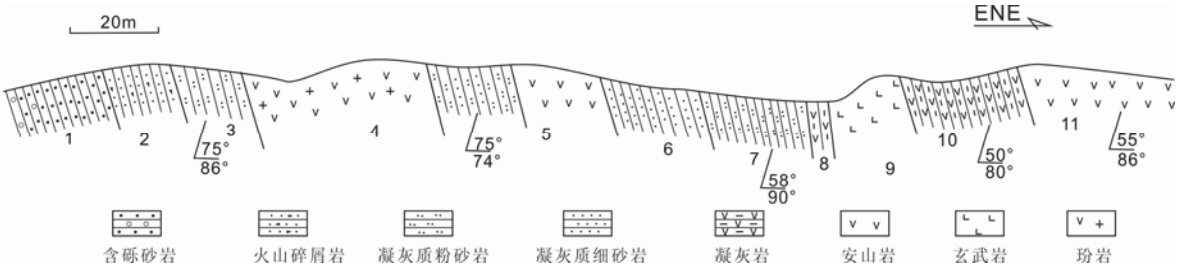

图 3-1-2 格少庙地区布龙山组实测剖面 I

-----未见顶----

11 灰绿色安山岩 68.2m

10 紫红色薄层状韵律凝灰岩 30.4m

9 灰绿色玄武岩 气孔构造和杏仁构造较发育 18.6m

8 青灰色薄层状凝灰岩 9.8m

7 紫红色薄层状韵律砂岩 31m

6 紫红色-灰白色薄层状韵律细砂岩，顶部含一层灰白-紫红色厚层粗砂岩 27.8m

5 灰白色薄层状凝灰质砂岩，顶部为灰绿色气孔状安山岩 47.6m

4 灰白色安山玢岩，顶部为紫红色粗砂岩和薄层凝灰岩 58.9m

3 薄层状韵律粉砂砂岩 18.5m

2 灰白色火山碎屑岩和灰绿色含砾砂岩，砾石成分以火山砾、凝灰岩为主，大小约 2-5mm 含量约 10% 18.4m

1 紫红色砂砾岩，含灰白色砂岩透镜体 37.6m

---未见底------

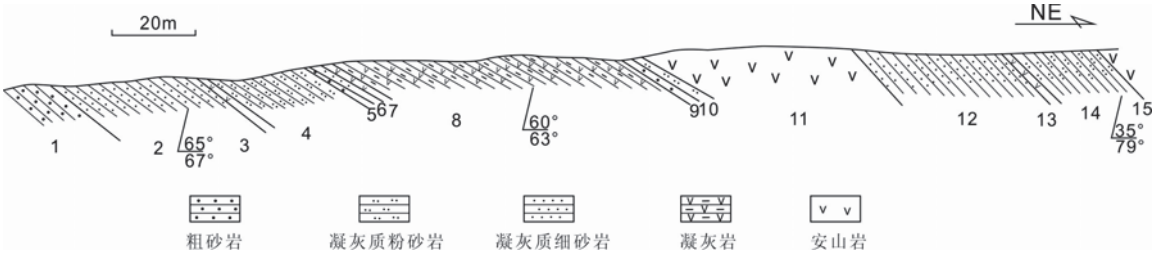

图 3-1-3 格少庙地区布龙山组实测剖面 II

-----未见顶----

15 安山岩 1m

14 薄层状韵律凝灰质粉砂岩 12.3m

13 安山岩夹层 0.5m

12 紫红色韵律凝灰质砂岩 17.9m

11 灰绿色安山岩 23.6m

10 紫红色韵律状凝灰质粉砂岩 2.8m

9 紫红色厚层状粗砂岩 2.3m

8 青灰色薄层状韵律凝灰岩，局部含安山岩夹层 30.4m

7 土黄色安山岩 3.2m

6 青灰色厚层状细砂岩，顶部为薄层韵律凝灰质粉砂岩 3.8m

5 灰白色粗砂岩与薄层状韵律凝灰质粉砂岩互层 0.7m

4 紫红色韵律凝灰质粉砂岩 10.8m

3 黄色-土黄色安山岩夹层 0.5m

2 紫红-灰白色韵律凝灰质砂岩-粉砂岩 16.4m

1 紫红色粗砂岩，含凝灰岩砾石 砾径约 3-5mm 2.5m

---未见底------

本研究区布龙山组主要为含砾砂岩、凝灰质砂岩、粉砂岩和凝灰岩薄层，其中夹数层火山岩层（图 3-1-4A），局部出露安山玢岩，总体上可分为数个安山质或玄武质火山岩和细碎屑沉积旋回，代表了多次火山喷发-间歇沉积作用。火山喷发-沉积旋回。剖面底部玄武岩主要为块状熔岩，发育大量的杏仁体，被方解石充填。玄武岩之上的火山碎屑岩主要为火山角砾岩，熔结凝灰岩等，紫红色，块状构造，角砾大小不等，成分以气孔或杏仁状玄武岩为主，基质为棱角状长石晶屑和绿泥石化火山灰，顶部可见少量的凝灰岩(图 3-1-4B)。该旋回之上出露安山岩，代表着又一次火山喷发活动开始。火山岩中大量的杏仁体存在可能与火山喷发时水体较浅有关。剖面上部层位出现子紫红色-青灰色凝灰砂岩，砂岩中含青灰色凝灰质粉砂岩薄层透镜体，砂岩成份以长石、火山碎屑为主，发生绿泥石蚀变，胶结物为凝灰质或泥质。向上变为较细的紫红色凝灰质粉砂岩砂岩韵律（图 3-1-4C），发育水平层理，指示了相对较深，水动力较弱的沉积环境。在本研究区相当于布龙山组凝灰质粉砂岩中（剖面 II 层 10）发现笔石化石 *Callogratus* sp.， *Desmograptus* sp 和 *Dictyonema* sp.,时代定为奥陶纪（内蒙古区域地质志，1991）。

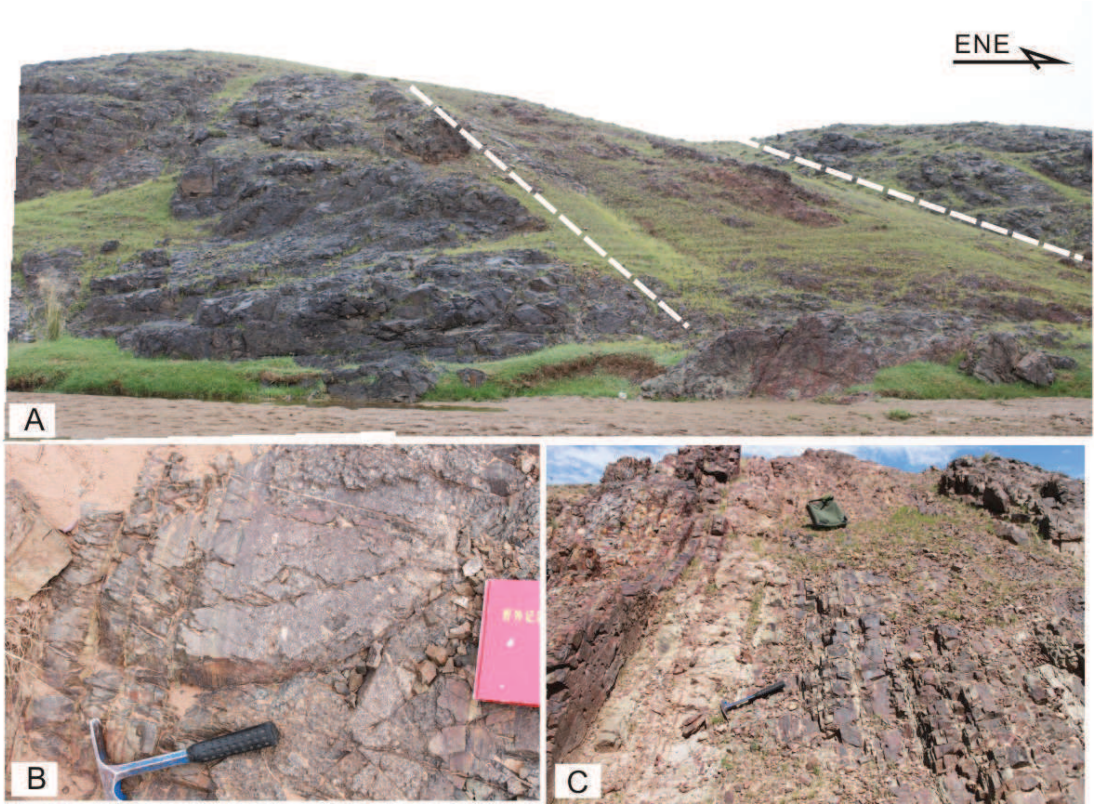

图 3-1-4 格少庙地区布龙山组火山岩野外露头特征图片

A：玄武质火山岩层与凝灰质砂岩、粉砂岩沉积互层；B：火山岩碎屑岩顶部的凝灰岩夹层；C：薄层泥质粉砂岩与泥岩形成的韵律层

哈拉组在格少庙东南一带出露较好，岩石类型主要为安山岩、流纹岩、火山碎屑岩和砂岩，这些岩石均遭受不同程度的蚀变。由于露头连续性较差（图 3-1-6A），本文仅通过 GPS 定位，划分了其火山岩层序，描述如下：

-----未见顶-----

8 灰白色块状结构安山岩

7 灰黄色蚀变火山岩

6 灰绿色致密块状蚀变安山岩火山岩

5 灰绿色碳酸盐化杏仁状安山岩，局部夹安山质集块熔岩

4 深灰绿色蚀变杏仁状安山岩，杏仁体主要为长英质矿物

3 浅灰色安山岩，气孔构造发育

2 紫红-青灰色薄层状凝灰质砂岩，发生绢云母蚀变

1 灰白色致密块状结构流纹岩

-----未见底-----

哈拉组中熔岩以安山岩为主，另有少量玄武岩。杏仁构造是本剖面安山岩的

一个特点，气孔直径一般 2-4mm，多被方解石或长英质矿物填充（图 3-1-6B）。安山质集块熔岩由大小不等的火山块体组成，形态多为棱角状、椭球状，发生较强的塑性变形，胶结物为褐绿色物质，发生绿泥石化蚀变（图 3-1-6C）。该剖面底部以流纹岩为主，向上出现砂岩沉积；之后是出露大量的安山岩，代表了另一期的火山活动。

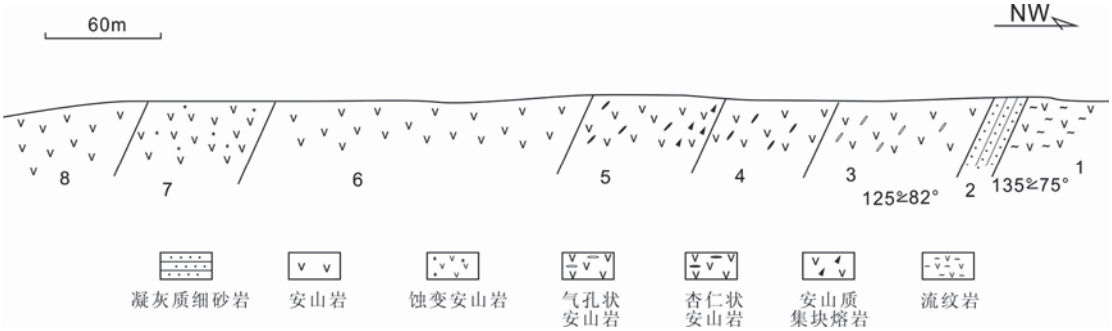

图 3-1-5 格少庙地区哈拉组火山岩层序实测剖面

岛弧深成岩在巴特敖包地区大面积出露，主要由闪长岩、 石英闪长岩、 英云闪长岩、花岗闪长岩四个岩石单元组成,相对时序由早到晚分别为：中细粒闪长岩、细粒黑云石英闪长岩、中细粒英云闪长岩、花岗闪长岩（陶继雄等，2005）。前人对其进行了详细的岩石学、地球化学和年代学研究，岩石地球化学特征与典型的火山岛弧相似，其年龄在 440-460Ma 之间（许立权等，2003；陶继雄等，2005；Jian et al., 2008；李剑锋等，2010）。

火山岩石学特征

包尔汗图群火山岩以熔岩类为主,主要为杏仁状玄武岩、致密块状安山岩、杏仁状蚀变安山岩、蚀变角闪安山岩、安山玢岩等。火山碎屑岩类有安山质凝灰岩,火山集块岩，安山质晶屑凝灰岩等,多为中性火山碎屑岩类。

杏仁状玄武岩（图 3-1-7A）：灰绿色，斑状结构、基质间粒结构或间隐结构，杏仁状构造。斑晶主要由斜长石和辉石组成，含量约 15-25%。斜长石为 0.5-3mm，自形-半自形板状。辉石斑晶大小约 0.5-3mm，常被次闪石、绿泥石、绿帘石蚀变。基质由微晶板条状斜长石（约 25%）和纤状或玻璃质物质组成，含少量磁铁矿，粒度小于 0.2mm。气孔、杏仁体发育，镜下常见 0.1-0.3mm 的球粒构造，球粒被玻璃质或长英质微晶组成外壳，球粒内部由纤维状的绿泥石放射集合体组成，杏仁体内部多被方解石填充。

致密块状安山岩（图 3-1-7B）：灰绿色，斑状结构，基质具交织结构或间粒

-间隐结构，块状构造。斑晶主要为斜长石，含量约 15%左右，大小在 0.3-2mm 之间，自行板状结构，常发生绢云母和粘土蚀变。基质主要由玻璃质或斜长石雏晶组成。含少量磁铁矿。

图 3-1-6 格少庙地区布哈拉组火山岩野外露头特征图片

A：哈拉组火山岩野外宏观露头特征，多被植被覆盖不连续；B：气孔状安山岩，有的被方解石或长英质矿物填充；C：安山质集块熔岩，形态多为棱角状、椭球状发生绿泥石化蚀变

杏仁状安山岩（图 3-1-7C）：浅灰绿色，具斑状结构、杏仁状构造。斑晶中斜长石 15%，粒度 0.2-1mm，自形-半自形结构，强烈绢云母化；基质具隐晶质结构，少量斜长石雏晶弱定向排列。杏仁体多数为 0.3-4mm，浑圆状、椭圆状及不规则状，成份为方解石、石英等。

安山质玢岩是浅侵火山岩，具有斑状结构或似斑状结构，斑晶主要为斜长石，自形-半自形结构，斜长石往往蚀变为绿泥石、绿帘石、高岭石等。

流纹岩（图 3-1-7D）：褐灰色-土黄色，少斑状结构、流纹构造。斑晶含量约 8%，成份主要为斜长石，粒度 0.2-1mm 不等，呈板条状，半自形结构，偶见聚片双晶；石英约 5%，粒度 0.2-0.5mm，它形粒状结构；基质含量约 80%，隐晶质，霏细结构，由石英、长石及玻璃质组成。

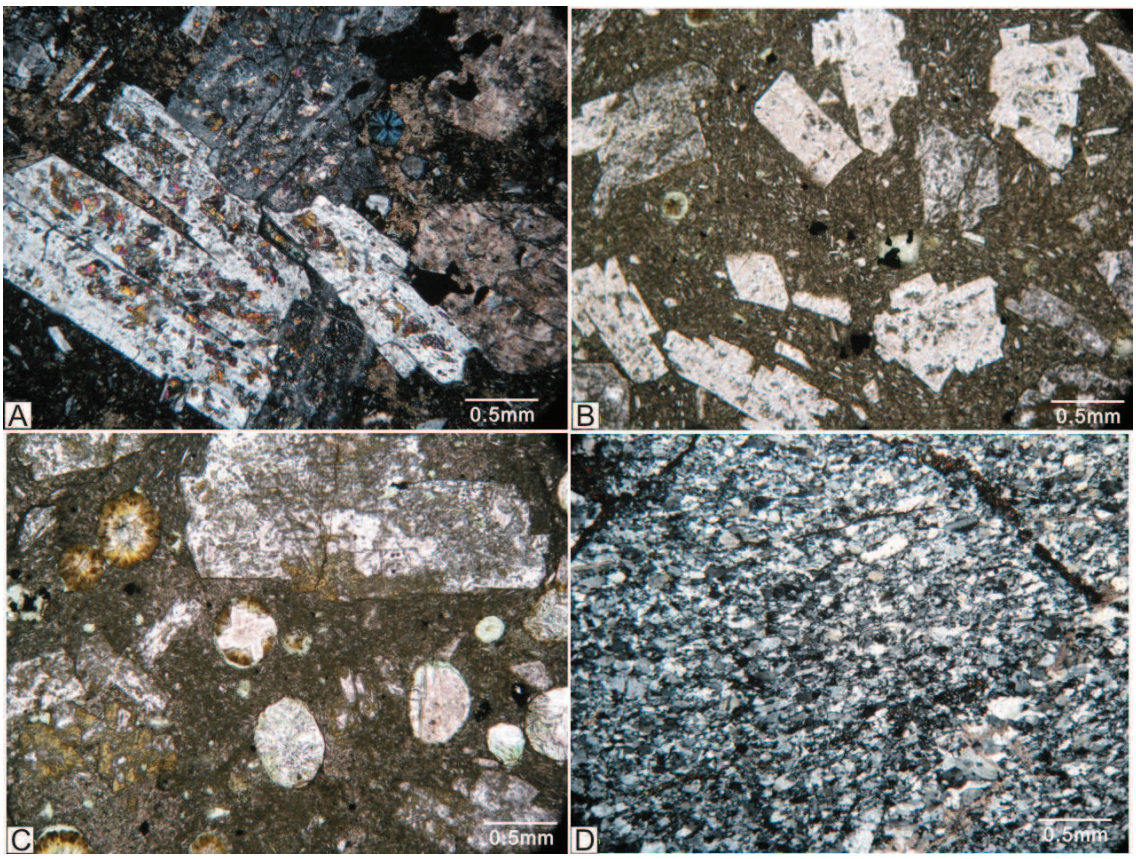

图 3-1-7 红旗牧场地区包尔汉图群火山岩镜下特征图

A：杏仁状玄武岩，斑状结构，基质间隐结构。斑晶含量约 20-30%，基质由微晶板条状斜长石和纤状或玻璃质物质组成，含少量磁铁矿。气孔、杏仁体被玻璃质或纤维状的绿泥石放射集合体填充；正交镜下；B：块状安山岩斑状结构，基质具间粒-间隐结构，斑晶含量约 15%左右，发生绢云母和粘土蚀变。基质由玻璃质或斜长石雏晶组成,含少量磁铁矿；单偏光镜下；C：杏仁状安山岩，斑状结构、杏仁状构造。斑晶含量 15%，绢云母化蚀变；杏仁体浑圆状、椭圆状，内部成份为方解石、石英等；单偏光镜下；D：流纹岩，少斑结构、流纹构造。基质隐晶质、霏细结构，由石英、长石微晶及玻璃质组成；单偏光镜下。

凝灰岩：深灰、灰绿色，氧化色为紫红色，火山凝灰结构、块状构造。岩石由晶屑 20%、岩屑 60%，及少量玻屑组成。岩屑成分多为安山岩、粒度 0.5-2mm。晶屑主要为斜长石，偶见石英，形状呈锯齿状、不规则状，粒度＜0.5mm。玻屑呈撕裂状，多已脱玻化为粘土矿物及霏细状长英质。胶结物为火山灰 25%，已重结晶为粘土矿物。

小结

布龙山组由喷出岩和凝灰质沉积岩组成，早期喷出拉斑玄武岩，后期喷出钙碱性系列的安山岩、英安岩及火山角砾岩，凝灰质沉积岩占较大比例（本剖面约 65%），这些反映了典型岛弧火山岩喷发建造特点。玄武岩中火山碎屑岩和集块岩发育，说明经历了较强烈的爆发阶段，细碎屑岩和凝灰质粉砂岩水平纹层十分发

育，含有门类单调的笔石化石，指示静水低能环境，陆源供给不充分。哈拉组出露大量的安山岩和流纹岩。布龙山组至哈拉组火山岩经历了玄武质火山岩至中上部的中-中酸性火山岩，构成一个完整的岛弧火山岩演化序列。前人进行了详细的地球化学研究，认为包尔汉图群火山岩从低钾到高钾玄武岩、安山岩都有出露，属于钙碱性系列，富集大离子亲石元素 Rb、Ba、Th、K 等，相对亏损 Nb、Zr、Ti 等高场强元素，显示为岛弧火山岩特征（邵济安 1991；尚恒胜等，2003；许立权等，2003）。

3.1.1.3 混杂带 (The Hongqi melange belt)

混杂带位于岛弧带西北侧，分布于乌德一带，沿北东-南西展布，宽处可达 2 km，窄处有百余米。北部被中生代二连盆地沉积物覆盖，南部被二叠纪岩浆岩侵入。混杂带被下泥盆统查干哈布组不整合覆盖，东西总长度约 20 km（图 3-1-8A）。混杂带被苏吉断层分为东北、西南两部分，西南部主要由石英岩、云母片岩、绢云母板岩、千枚岩、含铁石英岩、变质砂岩等组成，含有少量灰岩块体。局部可见细粒石英砂岩和变泥质韵律互层，保留原始层理，可能与弧前浊流沉积构造残片有关。苏吉断层东北部混杂带具有典型的杂乱堆积结构，主要由云母绿泥片岩、绿泥石英片岩、钙质板岩、硅质岩、凝灰质粉砂岩、以及少量杂砂岩等组成。混杂岩块大小各异，大者可达数公里，镶嵌在上述基质中（图 3-1-9A）。岩块类型可以分为异地岩块和原地岩块。异地岩块主要为具结晶基底性质的古元古界宝音图岩群的大理岩、斜长角闪岩和具洋壳性质的蛇纹岩，蛇纹石化橄榄岩，枕状玄武岩、硅质岩。出露蛇纹岩、蛇纹岩化橄榄岩和变质辉长岩，但是它们不具有典型的蛇绿岩层序，表现为被肢解的碎块（图 3-1-9B）。原地块体主要为火山岛弧相关的火山岩块体、含化石灰岩等。这些岩块经历了强烈的动力改造，发生韧性变形，它们以柔流的形式呈不规则状、透镜状、条带状镶嵌基质中。有时在十几平方米的范围内可见到几种不同时代的岩石(块)混杂在一起。

枕状玄武岩块体呈墨绿色，单枕规模在 0.3-0.5m 左右，岩枕的形态不规则，有遭压扁变形现象（图 3-1-9C），部分熔岩具气孔、杏仁构造，气孔、杏仁中充填后期石英集合体、方解石脉。镜下为鳞片粒状变晶结构，由微晶黑云母、阳起石、绿泥石等暗色矿物和浅色长英条带状集合体所组成。岩枕之间填充物主要为绿泥片岩。

石英角闪片岩块体，石英、斜长石构成浅色条带与片理化角闪石构成的暗色条带相间排列（图 3-1-9D），角闪石含量 80%，石英含量 10%，斜长石 10%，还有少量磁铁矿。

变流纹岩块体为灰白-浅灰绿色，野外常常呈巨大的山丘产出，由于受到动力挤压作用石英颗粒（集合体）定向拉长（图 3-1-9E）。镜下鉴定，其组成矿物主要为细粒长英质集合体（65%）和斑状斜长石（15%），显示定向构造，显微粒状变晶结构。

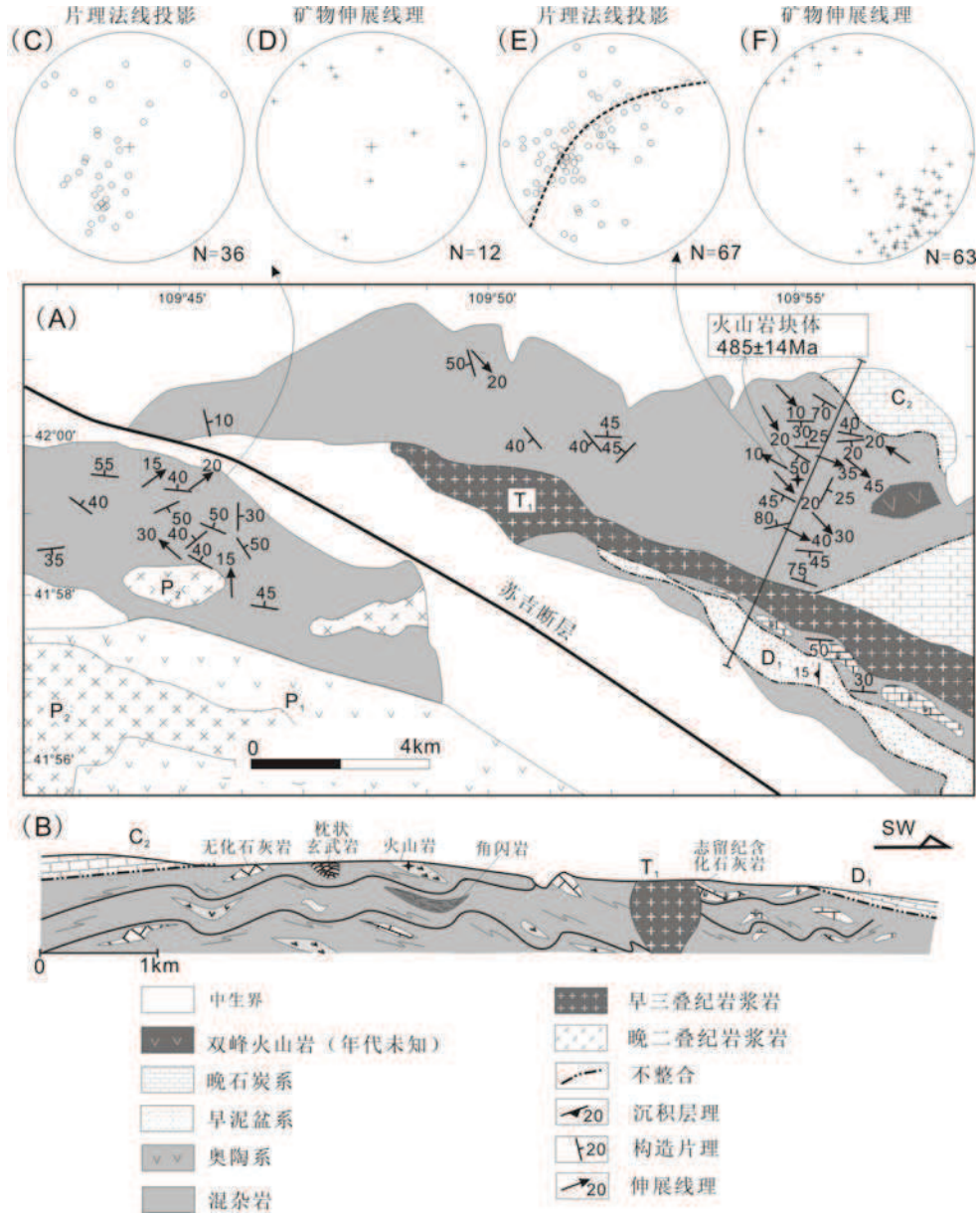

图 3-1-8 红旗牧场地区混杂带地质简图（A）、剖面（B）、和构造数据分析（D-F）

硅质岩和大理岩块体常常呈层状镶嵌于基质中，层理与基质片理平行，延伸

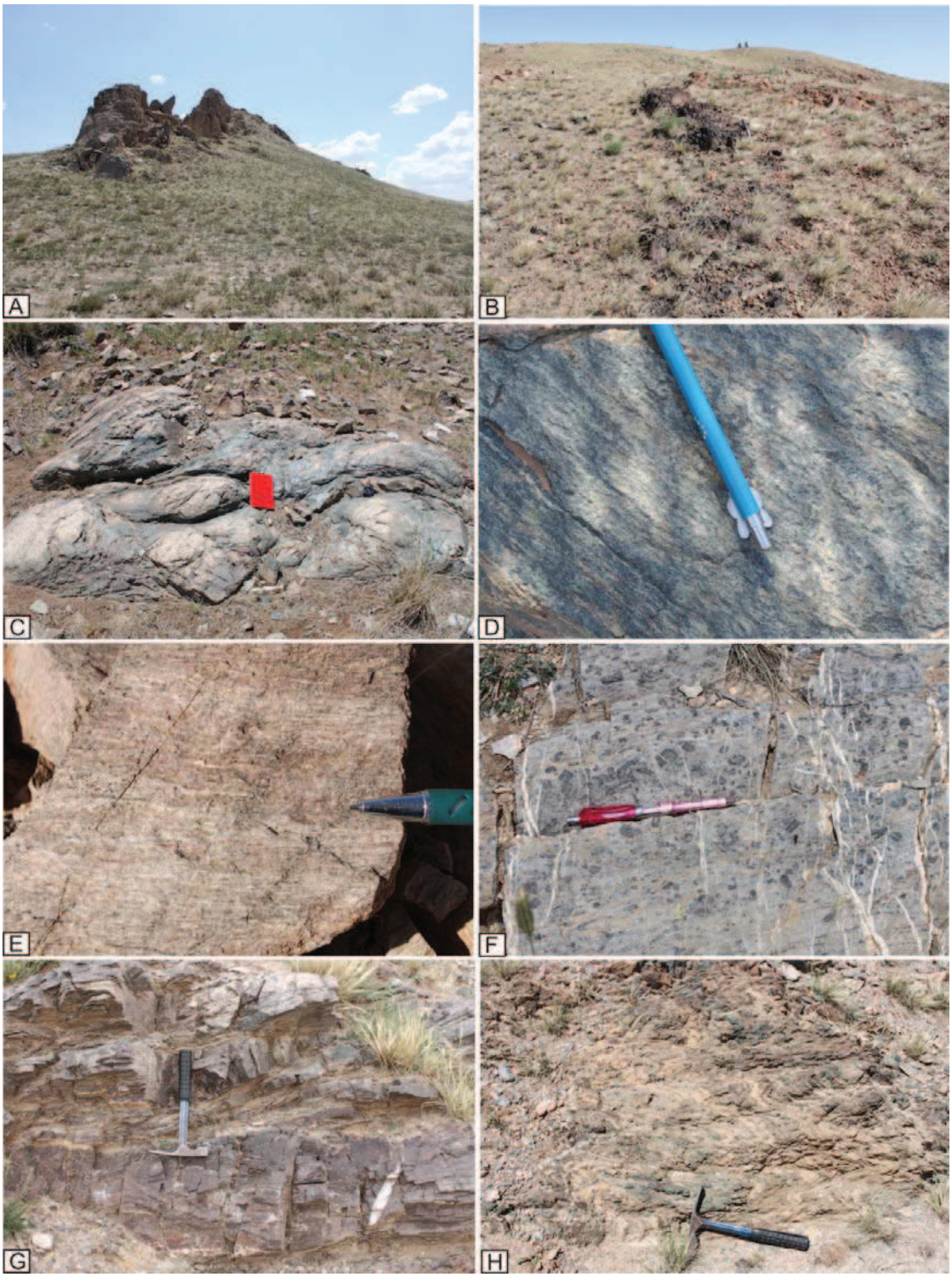

图 3-1-9 红旗牧场地区混杂带野外特征图片

A：数公里规模的灰岩块体“掩埋”在基质中，灰岩块体侧向不连续；B：被肢解的蛇纹岩、蛇纹岩化橄榄岩和变质辉长岩碎块，由于蚀变呈土黄色和深绿色；C：枕状玄武岩块体岩枕的形态遭压扁变形；D：石英角闪岩块体，石英、斜长石构成浅色条带与角闪石构成的暗色条带相间排列；E：变质火山岩块体，石英等颗粒受剪切作用定向拉长；F：含化石灰岩块体，珊瑚，海百合茎化石定向拉长或扯断；G：变质石英砂岩和千枚岩互层，原岩为浊流沉积；H：硅质条带灰岩，强烈剪切使具 S-C 组构特征

较远，可达数百米。有时可见大理岩中含黑色硅质条带，变形强烈，局部可见无根褶皱。在混杂带南部，志留纪含化石灰岩和砂岩块体珊瑚化石定向拉长或扯断（图 3-1-9F）。这些含灰岩块体代表了混杂带的最年轻年龄。

苏吉断层西南部局部出露变浊积岩（图 3-1-9G），厚度较大。岩性主要以千枚岩、砂质千枚岩为主，局部夹有含铁石英岩条带。砂质单元主要为变余石英砂岩，变余长石石英砂岩，发育块状层理。千枚岩单元内发育薄层粉砂质千枚岩与泥质千枚岩组成的薄互层水平层理。砂质千枚岩灰绿色，变余砂状结构，千枚状构造，镜下呈纤状变晶结构，由砂屑长石和绢一白云母、石英组成，长石已绿帘石化、云母化蚀变。在砂岩中有时可见灰岩块体，由于强烈剪切作用呈 S-C 组构（图 3-1-9H）。整个混杂带以绿片岩变质为主，变泥质岩主要矿物组合为绿泥石、白云母、黑云母、斜长石和石英。夹杂其中的角闪岩块体主要矿物组合为角闪石、斜长石、绿帘石和石英。

3.1.1.4 后造山沉积单元 (The overlying sedimentary succession)

红旗牧场地区的沉积地层主要包括上志留统西别河组、下泥盆统查干哈布组和上石炭统阿木山组。这些沉积地层不整合覆盖在上述岩石地层单元之上，除少数西别河组含化石灰岩块体经历韧性变形外，其它地层未显示经历强烈的韧性变形和变质。

上志留统西别河组

西别河组在巴特敖包地区出露较好，主要由三部分组成：下部砾岩、砂砾岩、含砾粗砂岩、中细粒砂岩、粉砂岩夹灰岩薄层或透镜体；中部为深灰色薄层状生物碎屑泥晶灰岩，浅灰色中厚层状含砾屑生物灰岩及砂屑灰岩，局部成礁。灰岩中富含珊瑚、层孔虫和苔藓等造礁生物,赋礁生物为海百合茎、腕足等；上部为灰色粉砂岩夹厘米级灰岩和砂岩透镜体，局部为含砾中粗粒岩屑长石砂岩。

本次研究分别在格少庙地区测绘了大比例剖面（图 3-1-10），描述如下：

9 薄层生物化石灰岩

8 土黄色薄层状钙质细砂岩 14.5m

7 薄层状生物化石灰岩，局部夹土黄色薄层钙质砂岩 26.2m

6 土黄色钙质石英砂岩和薄层钙质细砂岩，发育大量斜层理 17.1m

5 灰白色中薄层状生物化石灰岩，夹钙质生物碎屑砂岩，发育小型斜层理 14.5m

4 灰白色-紫红色中厚层状石英长石砂岩，局部含化石灰岩透镜体，顶部为灰白色厚层石英粗砂岩 16.7m

3 灰色-灰白色薄层状生物化石灰岩，中间夹土黄色钙质细砂岩薄层和泥质粉砂岩，粉砂岩中含灰岩透镜体；顶部为薄层化石灰岩和钙质细砂岩互层，含珊瑚类等化石 26.4m

2 底部为砾岩、含砾石英粗砂岩岩，向上变为土黄色中层状钙质砂岩夹薄层状钙质细砂岩、粉砂岩；钙质砂岩成分主要为石英，分选较差，夹少量灰岩透镜体 16.3m

——不整合覆盖——

1 安山岩

——未见顶——

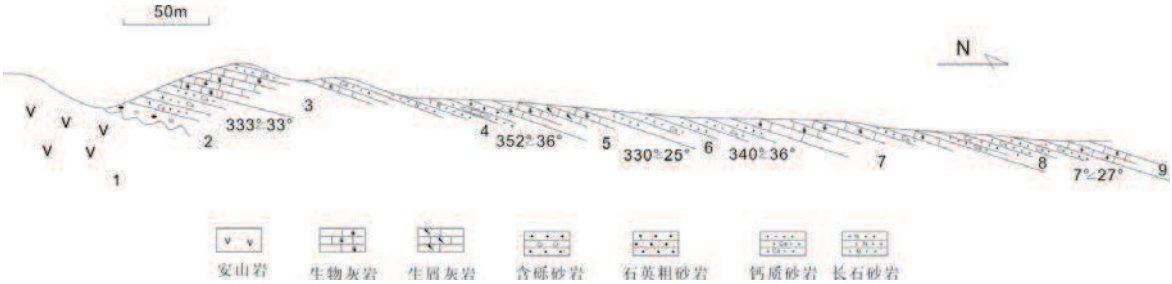

图 3-1-10 红旗牧场格少庙地区上志留统西别河组沉积层序实测剖面 I

该剖面代表西别河组底部层序，不整合该在于奥陶纪安山岩之上（图 3-1-12A），底部砾岩厚约 2m，砾石含量约 15-30%，成份主要为火山岩、砂岩和石英岩（图 3-1-12B），大小在 2-10cm 之间，大小混杂。向上渐变为为薄层状石英粗砂岩、钙质砂岩、生物化石灰岩和生屑灰岩。中部的石英粗砂岩，发育大量水平层理和斜层理（图 3-1-12C），其内夹有少量灰岩透镜体，代表水动力较强的潮间带环境。灰岩主要为灰色、深灰色厚层结晶灰岩和生物碎屑灰岩,灰岩中富含珊瑚、层孔虫等化石，其间夹紫红色粗粒长石石英砂岩、泥质粉砂岩等，厚度在 15-20cm 之间，成层性较好，侧向延伸较远。砂泥岩夹层成层性好,为开阔台地相的产物,说明水体较深,海平面相对稳定,为潮下低能环境。

我们同时在在巴特敖包地区绘制了西别河组沉积剖面（图 3-1-11），描述如下：

——未见顶——

10 黄绿色厚层状含砾粗砂岩，夹少量薄层粉砂岩 ＞42m

9 灰色中薄层状生物碎屑灰岩，局部可见泥质团块 16.8m

——断层——

8 生物碎屑灰岩，含珊瑚、腕足类化石，顶部为灰白色厚层状化石灰岩

7 灰白色厚层状粗砂岩，砂质成份主要为石英和长石，可见黄铁矿；顶部变为细砂岩 47.4m

6 灰白色中层状生物碎屑灰岩　19.4m

5 黄绿色含砾粗砂岩，砾石含量约 10%，大小约 2mm，分选和磨圆均较好，成份主要为石英和火山岩，发育平行层理，顶部变为粗砂岩 22.5m

4 青灰色厚层状中砂岩 49.6m

3 青灰色含砾砂岩，顶部为泥质粉砂岩，发育水平层理 8.7m

2 青灰色厚层状细-中砂岩，砂质成份主要为石英和长石，发育脉状层理 12.3m

1 下部为薄层钙质粉砂岩，夹少量中薄层状化石灰岩或化石灰岩透镜体，化石为珊瑚和腹足类 17.4m

——未见底——

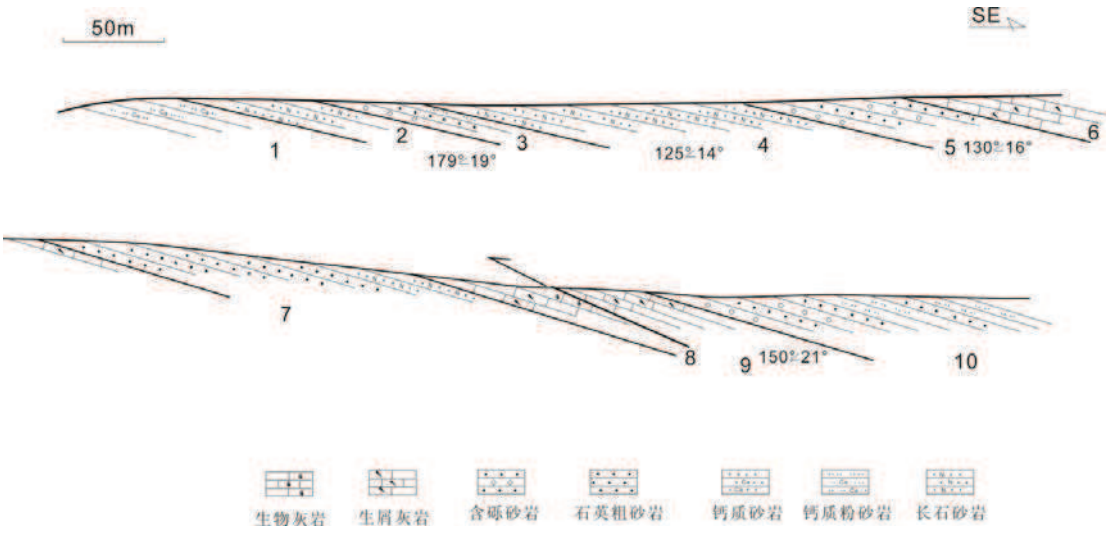

图 3-1-11 红旗牧场巴特敖包地区上志留统西别河组沉积层序实测剖面 II

该剖面代表西别河组中上部层序，碎屑岩与碳酸盐岩交互出现。该剖面主要由生物化石灰岩、生物碎屑灰岩、砂砾岩、钙质砂岩和薄层状粉砂岩组成。剖面下部粗粒长石砂岩和钙质粉砂岩组成，局部可见脉状层理，反应水动力中等。砂砾岩层之间常发育断续成层的毫米级泥质条带和条纹，向上泥岩逐渐增厚至数厘米，发育水平层理和透镜状层理（图 3-1-12D），其内常夹有砂砾岩透镜体。上部生物碎屑灰岩中含生物碎片，未见完整化石，反映水动力较强。砂质成分主要为长石和石英，分选和磨圆较好，成分成熟度较低，结构成熟度较高，这反映陆源

碎屑供应充分，为中等-强烈动荡水环境。综上分析，西别河组中上部代表了为水体动荡的潮间-潮下带沉积环境。

下泥盆统查干哈布组

查干哈布组分布研究区东部和南部，在乌德一带不整合覆盖在混杂带单元之上，在巴特敖包一带，以角度不整合覆盖在西别河组之上（张玉清等，2004）。

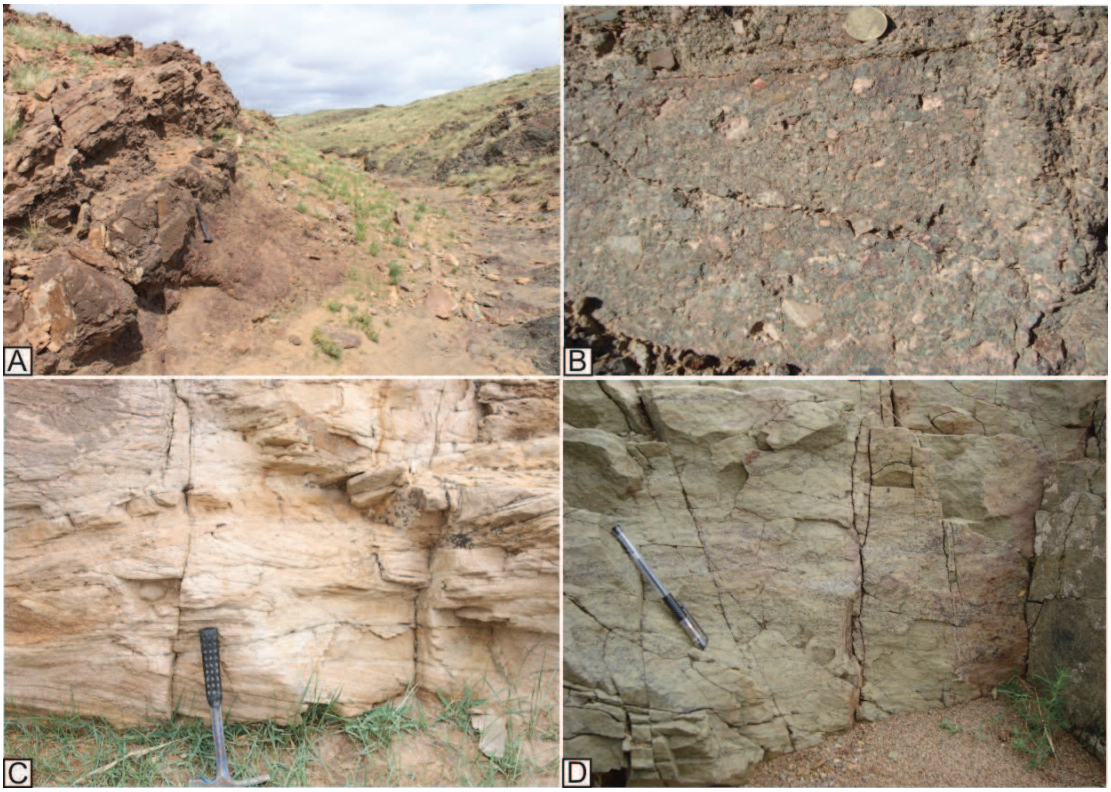

图 3-1-12 红旗牧场地区上志留统西别河组沉积特征野外图片

A：西别河组沉积岩与奥陶纪火山岩不整合接触图片；B：西别河组底部砾岩，含大量下伏火山岩角砾状砾石；C：西别河组底部沉积层序中发育的槽状斜层理；D：西别河组顶部层序中发育透镜状层理

查干哈布组包含紫红色底砾岩、紫红色砂岩、灰白色长石石英砂岩以及生物礁灰岩，生物碎屑泥晶灰岩和粉砂岩,沉积厚度大于 2km，含有大量腕足、珊瑚、苔藓虫和层孔虫等生物化石。野外调查表明，在乌德地区查干哈布组主要包括两个沉积组合，下部组合为由底部紫红色砾岩、砂岩和碳酸盐岩组成，含生物化石（图 3-1-13）。上部组合为紫红色陆源碎屑岩组成（图 3-1-14），发育大量原生沉积构造（图 3-1-15）。在乌德一带实测剖面如下：

13 灰色生物碎屑灰岩

12 紫红色中层状细砂岩

11 灰白色薄层状泥质粉砂岩夹薄层泥质灰岩

10 灰色灰岩，顶部为紫红色粗砂岩

9 灰白色泥质灰岩

8 灰色生物碎屑灰岩

7 灰色中-薄层状生物碎屑灰岩和厚层状含砾粗砂岩互层

——断层——

6 紫红色厚层状含化石灰岩

5 灰色中厚层状化石灰岩，顶部为含硅质条带灰岩，硅质条带宽约 1cm 左右

4 紫红色含化石灰岩

3 灰黑色中薄层状亮晶灰岩

2 砾岩层，砾石含量约 30%，分布在杂砂岩基质中。砾石成份复杂，主要为硅质岩、石英岩、火山岩和灰岩，分选较差（4-7cm），磨圆较好，略具定向性，顶部为粗砂岩

——不整合——

1 灰白色片理化灰岩，由于成份分异而形成浅黄色和灰白色相间分布

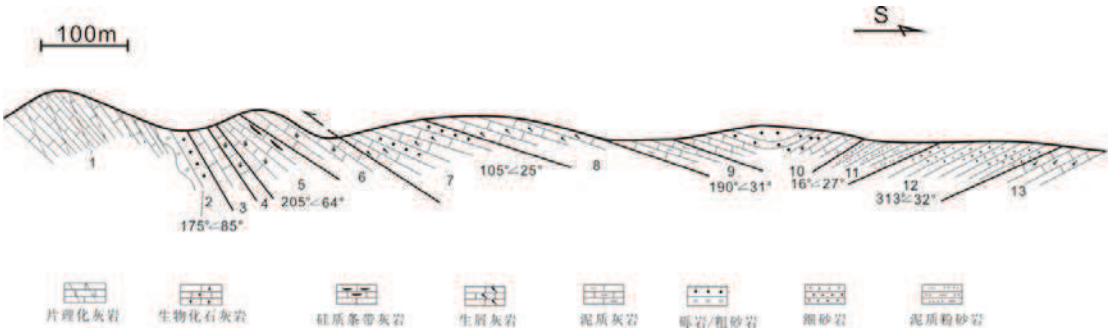

图 3-1-13 红旗牧场乌德地区下泥盆统查干哈布组底部沉积层序实测剖面 I

由于露头出露连续，在改剖面西南约 5km 处，我们连续观测了查干哈布组沉积地层，其沉积层序描述如下：

——未见顶——

13 紫红色中薄层砂岩，少量含砾，发育水平层理

12 紫红色-浅黄色中薄层状细砂岩，分选较好，顶部变为厚约 1m 的粗粒杂砂岩

11 紫红色中薄层状含砾砂岩、杂砂岩，砾石成份主要为石英、长石、火山碎屑，砾径大小约 3cm

10 紫红色薄层状粗砂岩

9 紫红色-黄色中薄层细砂岩，块状构造

8 紫红色中薄层状含云母砂岩，发育少量水平层理

7 紫红色粗砂岩

6 紫红色含云母砂岩

5 紫红色中薄层细砂岩，发育水平层理

4 紫红色中薄层状细砂岩，分选较好， 顶部粒度变粗

3 紫红色中薄层状细-粗砂岩，成份主要为石英和长石，含少量云母，发育水平层理

2 紫红色中薄层状细砂岩，块状构造，分选和磨圆均较好

1 紫红色中薄层细砂岩，发育水平层理

——未见底——

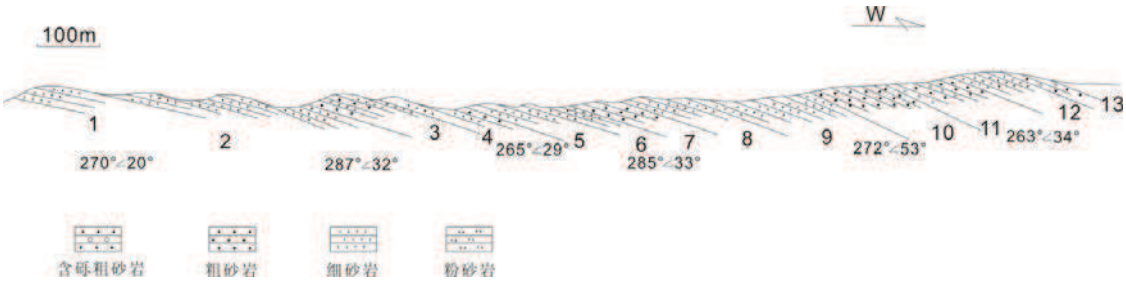

图 3-1-14 红旗牧场乌德地区下泥盆统查干哈布组中上部沉积层序实测剖面 II

我们的野外观察与前人结论一致，在乌德地区下泥盆统查干哈布组不整合覆盖在混杂岩带之上（图 3-1-15A），在剖面底部为混杂带岩块—强烈片理化灰岩（图 3-1-15B），向上为查干哈布组底砾岩，岩石成份复杂，如硅质岩、火山岩等（图 3-1-15C），说明来源于下伏岩石构造单元，向上渐变为化石灰岩，薄层状生物碎屑泥晶灰岩和毫米级泥灰岩层对（图 3-1-15D），含珊瑚生物化石组合 *Favosites-Squameofavosites*, 腕足 *Cyrtia* sp. 层孔虫 *parallelostroma* cf. *Pseudotuberculatum*（白云鄂博地区 1:25 万区调，2002），化石体型完好，非异地产物，这些特征指示浅海碳酸盐台地相关的环境。另一条剖面代表了查干哈布组中-上部沉积特征，主要为紫红色碎屑岩，含砾中粗粒岩屑长石砂岩、中细粒长石砂岩、泥质粉细砂岩或绢云母砂（板）岩，粗碎屑物结构成熟度高，成分成熟度低，岩屑、长石含量较高，说明其物源区较近。粗砂岩中常见大量的原生沉积构造，如水平层理、小型交错层理等（图 3-1-15E），属前滨碎屑沉积物。细砂岩、粉砂岩沉积常发育水平层理（图 3-1-15F），指示近滨带低能沉积物。

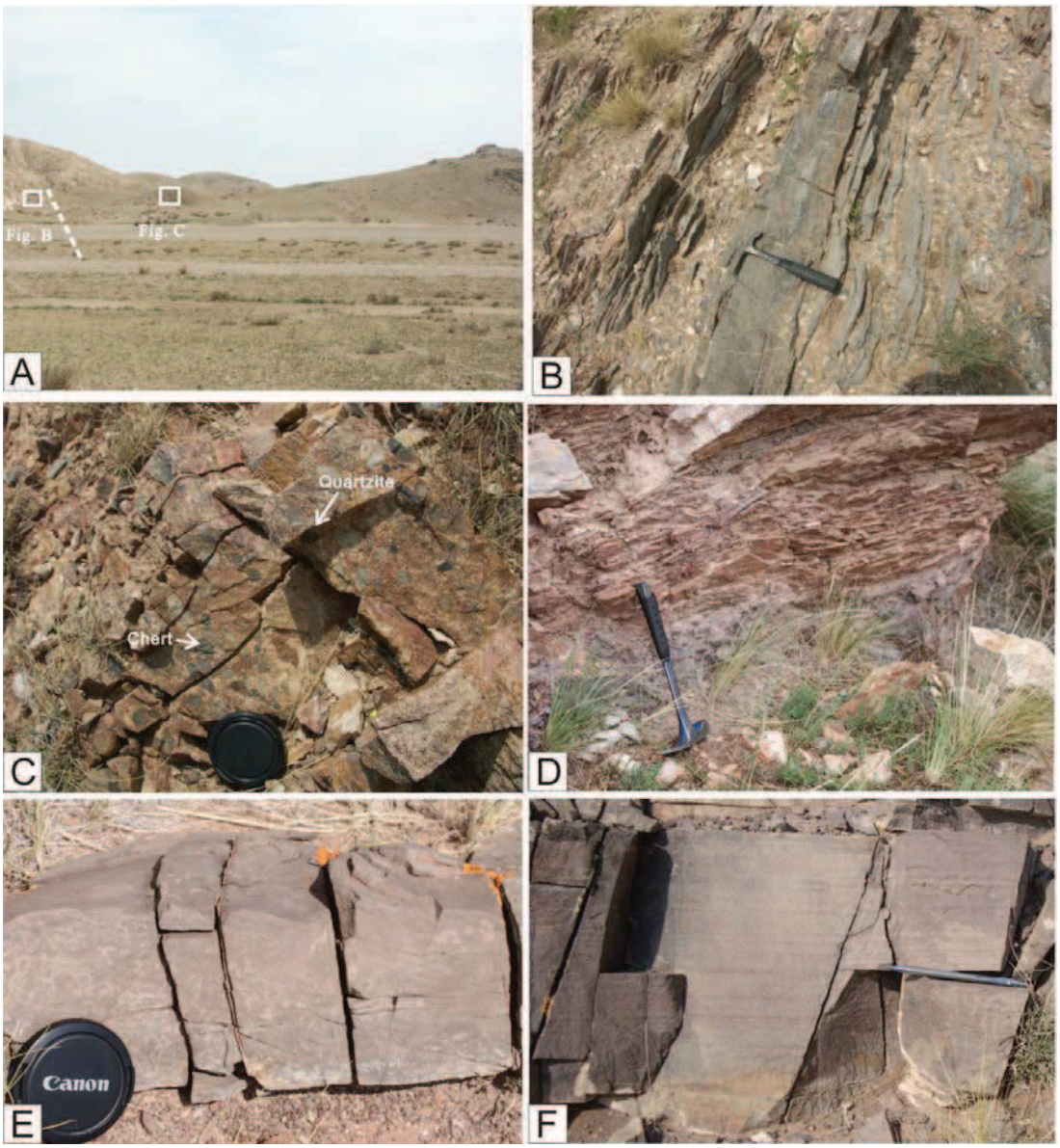

图 3-1-15　红旗牧场乌德地区下泥盆统查干哈布组野外沉积特征图片

A：下泥盆统查干哈布组与底部混杂带堆积不整合接触关系宏观图像；B：不整合下伏滑塌堆积单元的韧性变形的生物灰岩块体；C：不整合之上的底部砾岩沉积，含石英岩、硅质岩砾石；D：查干哈布组沉积薄层状生物碎屑泥晶灰岩和毫米级泥灰岩层对；E：查干哈布组中上部紫红色砂岩中发育的小型交错层理；F：查干哈布组中上部紫红色砂岩中发育的水平层理

阿木山组

阿木山组在研究区分布较为广泛，不整合覆盖于上述地层单元之上，岩性主要为生物灰岩、白云质灰岩、角砾状灰岩夹钙质砂岩、砂岩、灰岩、砾岩、粉砂岩等，含丰富的海相动物化石，有腕足类、腹足类、双壳类、苔藓虫等化石，为晚石炭世顶部 *Triticites* 带化石和早二叠世下部 *Pseudoschwagerina* 带化石(内

蒙古自治区区域地质志，1991；白云鄂博地区 1:25 万区调，2002）。我们的野外调查发现，在研究区北部阿木山组地层中存在大量生物礁丘灰岩，在灰岩地层中夹有少量的安山岩、凝灰岩夹层。该生物礁丘在地形上呈局部隆起，规模大小各异，大的可长达数公里，小的直径约数十米，有的呈条带状延伸（图 3-1-16A），有的呈圆环状分布（图 3-1-16B），它们具块状构造，岩性为灰白色含生物碎屑微晶灰岩，内部含有丰富的造礁生物化石（图 3-1-16C）。在灰岩地层当中可见黄褐色凝灰岩夹层（图 3-1-16D）。

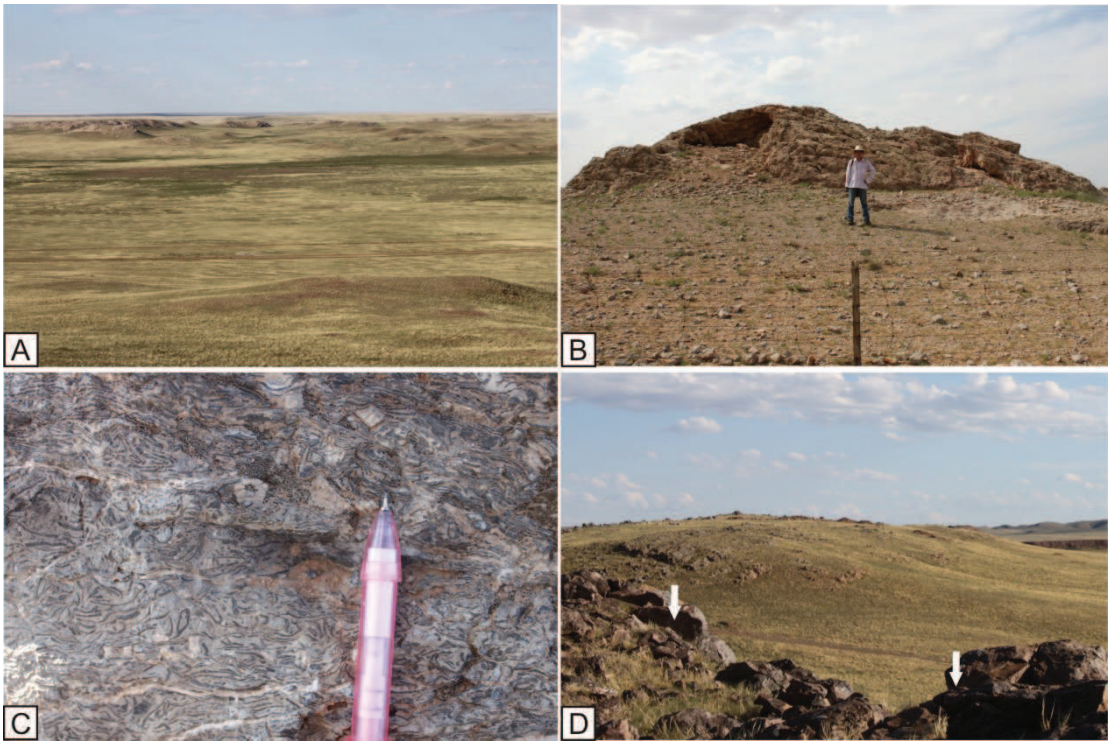

图 3-1-16 红旗牧场地区上石炭统阿木山组沉积特征野外图片

A：生物礁丘灰岩宏观图片，呈堤岸状或堡状分布；B：圆环状生物礁丘灰岩；C：生物灰岩所含大量造礁生物化石；D：灰岩地层夹薄层状黄褐色凝灰岩层（箭头处）

石炭纪阿木山组被认为不整合覆盖在泥盆系沉积地层之上（内蒙古区域地质志，1991；李文国，1996；苏养正，1996；鲍庆中等，2006），陆源碎屑岩中含有大量的岩屑和长石成份。同时发育大量的含生物化石灰岩，生物礁丘灰岩等，指示稳定的开阔碳酸盐台地沉积。但是值得注意的是，碳酸盐沉积中含凝灰岩夹层，说明在晚石炭纪该地区附近存在火山喷发活动，该岩浆岩活动可能与同时期的裂谷作用相关（见后文）。

小结

整个红旗牧场地区，主要发育上志留统西别河组、下泥盆统查干哈布组和上石炭统阿木山组，其沉积厚度在 4-5km（白云鄂博地区 1:25 万区调，2002）。上志留统西别河组不整合覆盖在晚奥陶世石英闪长岩和哈拉组之上，底部为砾岩、砂砾岩等陆源碎屑沉积，向上变为中厚层状含砾屑生物灰岩及生屑灰岩，局部成礁，碎屑岩与碳酸盐岩互层，指示碳酸盐台坪或混合坪沉积环境，代表了较稳定的滨浅海沉积环境。砂岩和砾岩层分选较差，砂屑主要为长石、石英和岩屑，砾岩中含大量火山岩颗粒，结构成熟度和成分成熟度均低,说明其物源区较近，可能接受了岛弧火山岩的剥蚀。

下泥盆统查干哈布组不整合覆盖在西别河组和混杂带之上。岩性为砂岩、长石石英砂岩、粉细砂岩以及生物礁灰岩，生物碎屑灰岩，含有大量腕足类、珊瑚类、苔藓虫和层孔虫等生物化石，碎屑岩分选磨圆较好，结构成熟度高，发育大量原生沉积构造，属于滨岸带沉积物。在碎屑成分上，长石和岩屑含量较高，成分成熟度低,暗示物源区较近。

上石炭统阿木山组不整合覆盖在上述沉积单元之上（白云鄂博地区 1:25 万区调，2002），包括碎屑岩、碳酸盐岩及火山岩夹层，火山岩的出现意味着研究区构造体制可能发生变化。值得注意的是，我们在混杂带单元中发现晚志留纪灰岩块体发生韧性变形，并作为块体夹在混杂带单元中，说明该造山带活动应该志留纪晚期之后。下泥盆统查干哈布组不整合覆盖在上志留统西别河组和混杂带之上，其沉积环境为稳定的滨浅海沉积，标志在此之前造山活动已经结束。

3.1.2 红旗牧场混杂岩变形分析 (the structual and kinematic analysis)

3.1.2.1 宏观构造

混杂带岩石遭受了强烈的韧性变形，显示出强烈的揉皱、混合和破碎作用，不同岩块的变形样式各异。本文综合野外露头调查，根据片理、拉伸线理、小褶皱、断层等小构造特征，并结合显微镜下定向薄片中的微构造特征，将混杂带从韧性变形到浅表层次脆-韧性变形划分为三期变形序列(期次)，从老到新依次为：D_1，形成区域片理；D_2，以非对称褶皱为特征；D_3,发育直立褶皱，形成区域构造格架（图 3-1-8B 和 D-F）。

D_1变形以区域上广泛分布的绿片岩片理 S_1为特征，与绿片岩变质同期。在野外，S_1以绿泥石英片岩和绢云绿泥片岩互层为标志。绿片岩中多硅白云母、绿泥

石等矿物定向排列构成的片理，是绿片岩的主期构造形迹，虽然遭后期褶皱作用叠加和改造，产状有所变化，但消除后期叠加变形的影响，片理面走向与区域构造线延伸一致，总体倾向 SE，代表产状为 140°/60°。片理面的形成与绿片岩中主期矿物组合代表的绿片岩相变质作用是同时的，形成片理面的变形作用与中构造层次的压扁作用有关。

D_1期形成的褶皱以紧密同斜褶皱为主 F_1，塑性流动变形特征明显，两翼夹角均小于 30 °，转折端窄而略微加厚，有时可见层（片）内无根钩状褶皱形式残留在后期褶皱的转折部位。野外露头可见绿片岩中发育大量同斜层内褶皱，轴面平行区域片理，倾向 SE（图 3-1-17A）。局部原始地层层理保存较好，以变泥岩和变质砂岩互层为特征。紧闭同斜和平卧褶皱导致大多数地区的 S_1面理和局部原始层理（S_0）接近一致，即 $S_0 \approx S_1$。沿着 S_1片理面，局部发育韧性剪切变形，沿着剪切面理，矿物定西排列，发育剪切石英脉及强烈变形形成的无根褶皱。S_1片理遭受后期 D_3变形的影响，倾向 NE 或 SW。

本期不同级别的褶皱的枢纽 F_1和矿物拉伸线理 L_1是区内广泛发育的线理。L_1矿物拉伸线理主要由拉伸的岩屑、石英条带、绿泥石和云母集合体构成（图 3-1-17B）。在石英片岩中，石英脉沿着 S_1定向拉长或扯断，发育涨缩构造或石英布丁构造（图 3-1-17C）。在角闪岩块体中，L_1线理表现为定向拉长的角闪石和重结晶的长英质条带。枕状熔岩块体同时也收到挤压作用，沿 NW-SE 方向定向拉长（图 3-1-9C）。 杂砂岩块体中，砂岩碎屑，如硅质砾石也沿着 NW-SE 方向定向拉长，含珊瑚化石灰岩中，珊瑚化石遭受挤压破碎变形，沿着 NW-SW 方向定向拉长，形成 L_1拉伸线理。

混杂岩块体常常镶嵌在 S_1片理中，它们之间多以断裂或剪切面为界，表现为宽数厘米或数十厘米的糜棱岩带，同一岩块在走向上具有不连续性。这些块体遭受变形方式以剪切破裂为主，形成一系列菱形块体。在苏吉断层西部的变浊积岩中，其变形显的比较复杂，形成一系列 B 型杆状构造（窗棂构造）、塑性流变褶皱等（图 3-1-17D）。闪长岩和酸性火山岩岩块的变形表现为整个岩块发育透入性的片理，矿物和残斑沿片理面定向拉长。

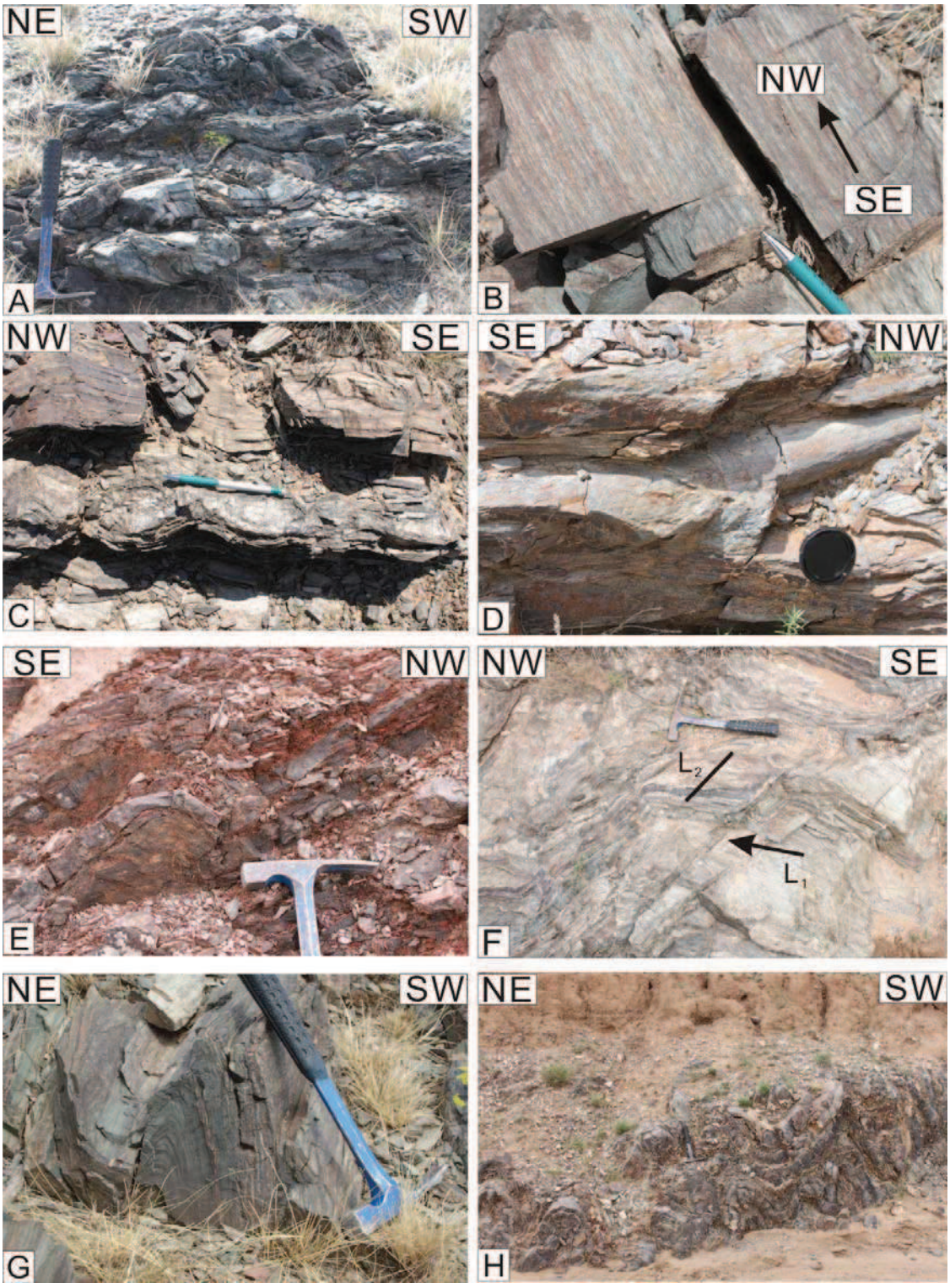

图 3-1-17　红旗牧场混杂岩带变形特征野外图片

A：绿片岩中发育同斜层内褶皱，轴面和枢纽倾向 SE；B：绿片岩中普遍发育的矿物拉伸线理，主要由拉伸的岩屑、石英条带、绿泥石和云母集合体构成；C：在石英片岩中发育涨缩构造；D：在绢云石英片岩中形成的窗棂构造；E：混杂岩中片理发生褶皱，轴面 SE 陡倾；F：石英绢云片岩发育的膝折构造，改造 S_1 片理和 L_1 线理；G、H：在绿泥片和能干层石英岩形成的直立褶皱

D_2期变形是以 D_1绿片岩片理 S_1作参考面发生的再褶皱，以发育非对称褶皱为主要特征。在野外露头可见大量的米级尺度的非对称褶皱，轴面走向 NE-SW，南翼缓，北翼陡，多数 NW 向倒倾（图 3-1-17E）。膝折构造在石英绢云片岩中较为发育（图 3-1-17F），改造 D_1期片理 S_1和拉伸线理 L_1。需要强调的是，红旗牧场混杂岩 D_2期褶皱变形与 D_1变形相比，明显地表现为共轴叠加关系或两期褶皱的枢纽以小角度斜交，可以认为与 D_1期挤压-剪切变形进一步发展相关。

D_3期变形塑造研究区区域性的构造格架，主要表现为轴面近于直立的开阔褶皱。绿片岩主期片理发生弯曲，形成褶皱 F_3，褶皱轴面倾向 NW 或 SE，轴面陡倾，一般在 65-80 度左右枢纽近水平 NW-SE 向延伸。相似褶皱在能干性较差的绿泥片岩中较为发育（图 3-1-17G），而在能干层石英岩可见较多的平行褶皱（图 3-1-17H）。虽然在野外露头可见大量直立褶皱，但是本期大型褶皱的枢纽 F_3主要是通过大范围内对片理 S_1的测量统计而确定的（图 3-1-8B 和 E）。D_3期直立褶皱变形构成了整个区域的构造格架，泥盆系沉积地层也卷入其中，表现为波长约上百米的开阔至中常直立褶皱(图 3-1-13)。在苏吉断层以东，该褶皱轴向 NW-SE，但是在苏吉断层西部，褶皱轴向变化较大（图 3-1-8C 和 D），可能和后期断层活动和岩浆侵入相关。

3.1.2.2 显微组构特征

在 XZ 切面的薄片中，可以观察到明显的岩石显微特征。在绿泥云母片岩中，可见片理面上的绿泥石、云母发育，并且强烈的置换了 S_0；在变质砂岩中，S_1以难溶的暗色物质与定向排列的重结晶硅酸盐矿物互层为特征，而有一些则 $S_0 \wedge S_1$，交角 10-60 度（图 3-1-18A），劈理和片理产状走向 NE，倾角 30-45 度之间，近东西向延伸。L_1拉伸线理则由拉长的石英单晶、重结晶的石英亚颗粒集合体等构成。

在显微尺度上，我们主要通过岩石的旋转残斑、云母鱼和剪切条带等构造特征判断构造变形的运动学。在角闪岩块体中，其旋转碎斑以角闪石等为主，均发生后期的绿泥石化，重结晶的石英集合体构成石英的拔丝构造，指示其顶部向 WNW 向的剪切的运动学特点（图 3-1-18B），而条带状石英亚颗粒的锯齿状边缘和波状消光，并斜向排列。在变质绿片岩和糜棱岩化火山岩碎屑岩中，发现大量的

旋转碎斑、斜列长石阶步、云母鱼等构造，它们均指示顶部向 NW 的剪切运动特征。如在糜棱岩化火山碎屑岩中，沿着长石残斑发育不对称的绿泥石压力影，指示顶部 NW 的剪切方向（图 3-1-18C 和 D）。碳酸盐颗粒和长石颗粒遭受碎裂形成的“多股诺”构造，同样指示其顶部 NW 的运动方向（图 3-1-18E）。薄片中一些拉断的碎屑颗粒中发育重结晶的绿泥石颗粒，其拉伸方向为 NW-SE（图 3-1-18F）。在变泥质岩中，可见云母鱼和剪切条带构造，指示顶部 NW 向的剪切运动方向。在变砂岩中，石英碎屑颗粒被绿泥石和云母围绕，并且在剪切应力作用下形成了压力影构造，同时在基质中还生成了剪切条带（图 3-1-18G）。在苏吉断层西部，发现同样的运动学证据，如 σ 碎斑，指示其顶部向 N 的运动学方向（图 3-1-18H）。综上微观证据，可以断定这个混杂带遭受了顶部向 NW 的韧性挤压-剪切作用。

3.1.2.3 小结：

整个混杂带被苏吉断层分为两部分，西南部分出露浊积岩沉积，包含少量灰岩块和火山岩块体，经历后期变质叠加作用；东北部分包含了大量的灰岩、火山岩和少量角闪岩块体，具有典型的混杂结构。混杂带无论基质或岩块均经受了不同程度变形变质作用的改造，主要表现为绿片岩相变质作用。　野外调查发现，其变形期次可以划分为 3 期：D_1 期变形伴随绿片岩相变质过程，形成第一期片理 S_1 和矿物拉伸线理 L_1，通过镜下旋转碎斑的鉴定，拉伸线理由拉长石英单晶、长石石英集合体等构成。眼球状、透镜状旋转长石残斑、斜列长石阶步、云母鱼等均指示顶部向 NW 的推覆运动。由于受到 D_3 期变形的影响，片理倾向 SE 或 NW；D_2 期变形以大量发育的不对称褶皱为特征。这些褶皱枢纽 NE，轴面多数 NW 向倒倾，形成北翼短，南翼缓倾的不对称褶皱或膝折构造。D_3 期变形以 S_1 为主要参考面，形成两翼开阔至中常的直立褶皱，枢纽水平，走向近 NW-SE，推断挤压应力主要为近 NE-SW 向，是中浅层次挤压应力下弯流-弯滑作用的结果。D_3 期变形塑造了红旗牧场区域构造格局，早泥盆纪地层也卷入其中，说明变形时代至少在泥盆纪之后。消除 D_3 期变形的影响，D_1 期片理倾向 SE，运动学标志显示上部向 NW 的剪切作用，与由 SE 向 NW 的逆冲剪切运动有关。我们推断可能是洋壳 SE 向俯冲过程造成的。

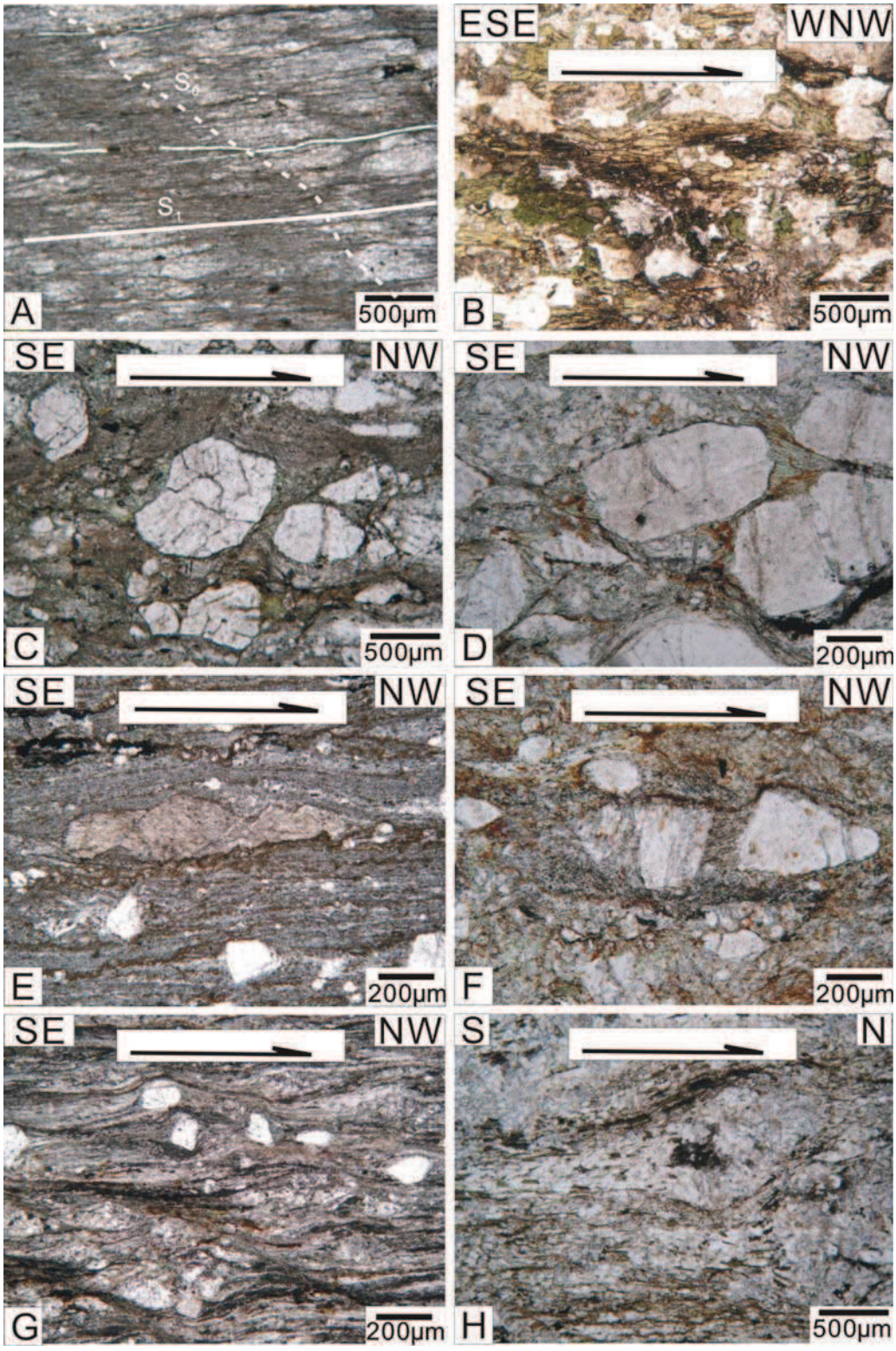

图 3-1-18　红旗牧场混杂岩带微观变形特征镜下图片

A：S_0∧S_1角度切割关系，S_0以石英和泥质物质交替为标志，S_1以难溶的暗色物质为特征；B：角闪岩块体中角闪石形成 σ 形指示 WNW 向的剪切；C、D：火山碎屑岩中，沿着长石残斑发育不对称的绿泥石压力影；E:。碳酸盐颗粒破碎形成的多股诺构造；F：长石颗粒被拉断，间隙中发育重结晶的绿泥石和云母颗粒；G：变泥质岩中剪切条带构造；H：变泥质岩中 σ 碎斑指示顶部向 N 的运动学方向。

第二节 温都尔庙研究区 (The Ondor Sum area)

温都尔庙研究区位于内蒙古镶黄旗地区，主要出露绿片岩相变质火山岩和沉积岩，其中夹杂蛇绿岩块、蓝片岩块体，前人将其命名为温都尔庙群。其西南侧白乃庙地区出露大量的变质火山岩和火山沉积岩，时代为早-中奥陶纪，具有岛弧火山岩性质，前人命名为白乃庙群。由于温都尔庙群和白乃庙群蕴含了重要的铁、铜等重要矿产，我国地质学家对温都尔庙群和白乃庙群很早就进行了研究，获得了比较丰富的基础地质资料。本小节在前人的研究基础上，侧重于构造单元划分和构造学解析。

3.2.1.岩石构造单元划分 (The litho-tectonic framwork)

根据野外地质组成特征，本次研究将温都尔庙地区从北向南划分为三个次级构造单元，分别为白乃庙岛弧带、温都尔庙混杂岩带和石炭纪碳酸盐岩沉积盖层（图 3-2-1）。下面分别进行论述：

3.2.1.1 白乃庙岛弧带 (The Bainaimiao arc in the Ondor Sum area)

多数地质学家将白乃庙地区出露的火山岩及相关的碎屑沉积岩作为奥陶纪火山岛弧，而将图林凯地区出露的一套变质角闪岩作为温度尔庙群中的蛇绿岩组份（胡骁等，1990；唐克东等，1992；Xiao et al., 2003；Jian et al., 2008；Zhang et al., 2012）。本次野外调查发现，图林凯地区岩浆岩主要由角闪岩类岩石、斜长花岗岩、辉长岩等组成，典型的蛇纹岩、变质橄榄岩、辉长岩以及硅质岩等蛇绿岩组份没有观察到。这些岩石沿东西向分布于南部的图林凯一带，延伸长达约 20km，南北宽约 3-4km，其北侧与温都尔庙群以断层分开，被上石炭统生物灰岩覆盖（图 3-2-1）。

角闪岩类岩石包括斜长角闪岩、角闪岩、角闪斜长片岩。这些岩石一般呈层状和条带状，条带宽 0.2-10cm 不等（图 3-2-2A 和 B），主要由普通角闪石、斜长石和少量石英组成。局部斜长角闪岩中发生强烈的揉皱（图 3-2-2C），并混合岩化，浅色脉体由斜长石和石英组成，暗色脉体由角闪岩组成。斜长花岗岩常呈不连续的不规则体产出，它们有的作为岩脉呈大角度切穿斜长角闪岩片理，有的平行片理穿插其中（图 3-2-2D）。斜长花岗岩岩石呈灰白色，中粒花岗结构，主要由斜长石（65%）和石英(30%）组成。在斜长角闪岩带以南，可见石英闪长岩、

闪长岩和花岗闪长岩块以及基性岩块，它们呈数十平方米的小岩体，以长条带状、椭圆状或不规则状分布。石英闪长岩岩石为深灰色，中粗粒，近等粒结构，略具片理化，主要由斜长石(50%)、角闪石 (25%)和石英 (20%) 组成。

前人对这些花岗岩类和角闪岩类岩石进行了地球化学和年代学研究，它们具有埃达克岩的大部分岩石地球化学特点。这些岩石富集大离子亲石元素、Nb-Ta 和 Zr-Hf 负异常显著，轻稀土元素稍微亏损，同时显示类似 IAT 岛弧的 V-Ti 特征；锆石 U-Pb 年代分析在 ca.430-470Ma 之间（刘敦一等；2003；Jian et al.，2008）。

这套斜长角闪岩类和花岗岩类岩石所属的构造环境，有研究认为其原岩为大洋拉斑玄武岩，发生角闪岩相变质作用(胡骁等，1990)；有的研究则认为其具有埃达克岩浆岛弧性质，被解释为 SSZ 俯冲带中的蛇绿岩残块（刘敦一等，2003；Jian et al., 2008）。我们的野外观察，典型的蛇绿岩组份如蛇纹岩化的橄榄岩、枕状熔岩以及硅质岩等没有被观察到。与北侧的温都尔庙群相比，图林凯岩浆岩类具有明显不同的变形特征（见下文）。地球化学数据显示类似岛弧的特征（Jian et al., 2008），因此我们认为这些岩石代表了岛弧岩浆岩深部组份。

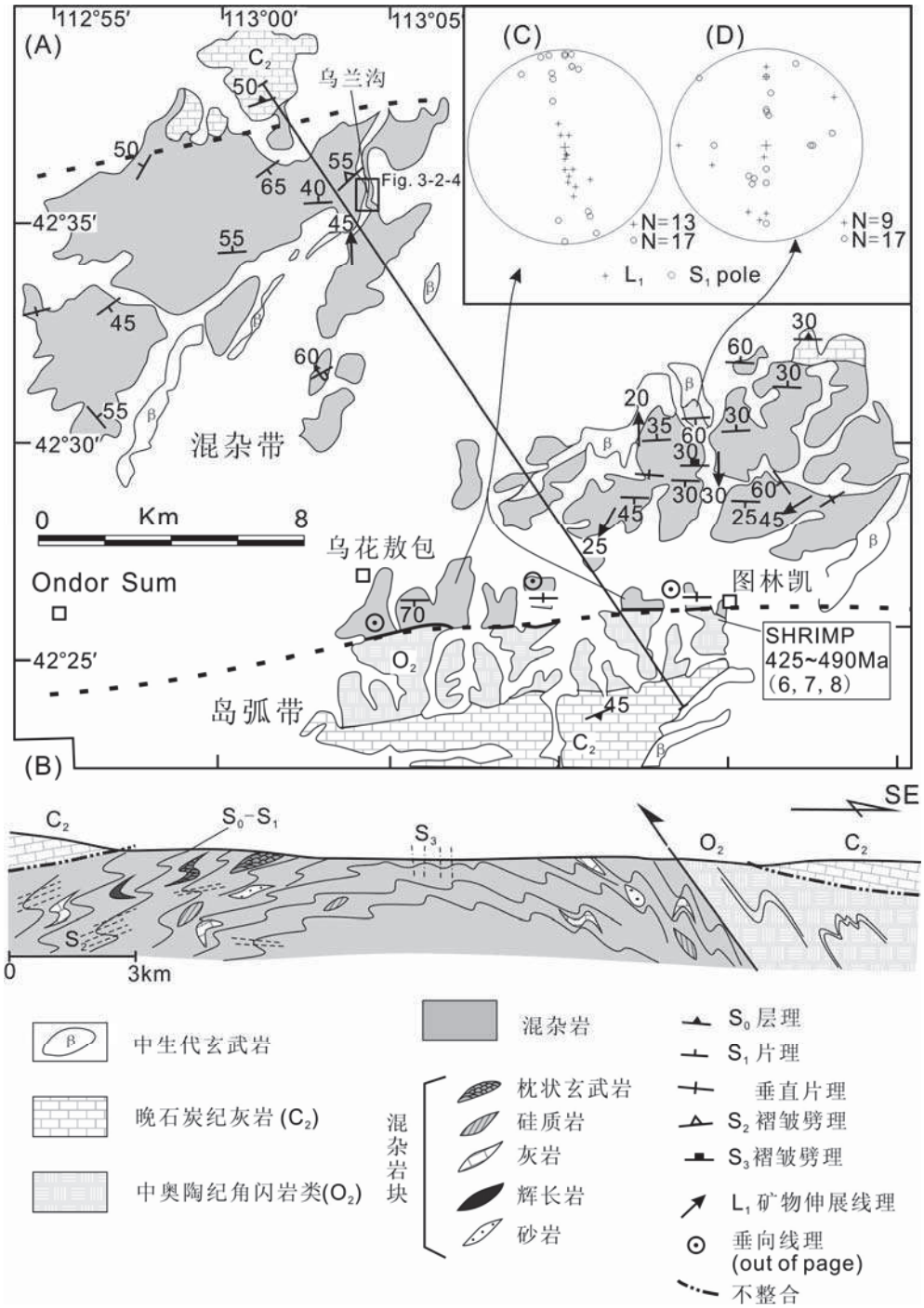

图 3-2-1 温都尔庙地区造山带岩石构造单元划分 （年龄数据及文献见附件 1）

3.2.1.2 混杂岩带 (The Mélange Belt)

温都尔庙混杂带在乌花敖包和乌兰沟一带出露较好，东西延伸约 50km，南北宽约 20km。向东和向西被中生界和新生界沉积物覆盖，与南部的岛弧带呈断层接触（图 3-2-1）。根据出露岩石组合特征和变形特点，本文将其分为南、中和北三部分进行描述和研究。

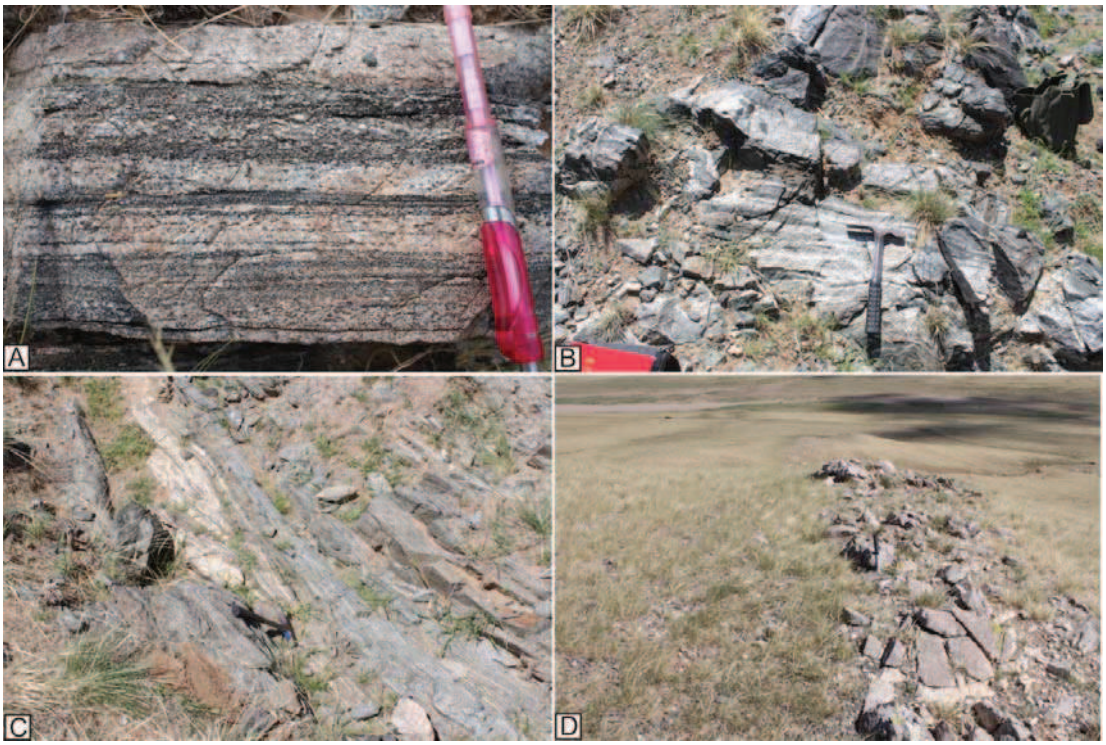

图 3-2-2 温都尔庙图林凯地区角闪岩类和花岗岩类野外特征图片

A、B：角闪岩类岩石由角闪岩和斜长岩条带组成，条带宽度不等；C：角闪岩类内部发生揉皱和韧性变形；D：局部可见花岗岩切穿角闪岩类岩石，花岗岩块状结构

在南部，温都尔庙混杂岩在乌花敖包-图林凯一带沿东西向分布，主要由绢云石英片岩，绿泥绿帘片岩和钠长绿泥绿帘片岩组成。不同尺度的砂岩、灰岩、基性岩块体、含铁石英岩块零散分布在绿片岩基质中（图 3-2-3A）。绿泥绢云石英片岩是最常见的岩石类型，石英含量较高，具有多次揉皱的片理。野外观察，这些石英岩、石英片岩呈条带或条纹状，厚度在 2-50cm 不等，与绿泥石英岩、方解绿泥片岩、大理岩等互层分布（图 3-2-3B）。显微镜下条带状石英集合体与绢云母、绿泥石呈细条状或丝缕状相间分布。

中部混杂带出露不佳，主要由绿泥绿帘片岩、绢云石英片岩和绿泥片岩组成，多被后期中生代喷发玄武岩和沉积岩覆盖。野外调查发现岩块出露种类和数量较少，其显著特征为存在大小不等的含铁石英岩块体，它们呈囊状、透镜体或薄层夹于其中（图 3-2-3C）。

北部混杂带乌兰沟一带出露较好，常见的岩石类型有绿帘绿泥片岩、绿帘绿泥阳起片岩、阳起斜长片岩、绿泥绿帘石英片岩等（图 3-2-3D）。它们遭受较强的变形和变质作用，一般不保留原始的结构构造，镜下显示鳞片变晶结构和显微

纤状变晶结构。混杂块体种类丰富，主要包括枕状玄武岩、火山岩、大理岩、变质砂岩、硅质岩、辉长岩和蓝闪片岩（图 3-2-3 E)。其中野外可见两种类型的玄武岩，一种为压扁的椭球状气孔玄武岩，遭受明显的绿片岩相变质作用，岩枕构造发育，常呈扁平状，上圆下平，底面可见凹坑，塑性变形明显。气孔发育，呈环状与枕面平行（图 3-2-3F)，局部可见 1-2mm 的玻璃质淬火边。岩枕直径 30-50cm，岩枕正面向上，一般倾向北。该类玄武岩为碱性玄武岩，具有板内玄武岩的地球化石特征（黄金香等，2006)。另一种玄武岩未遭受变形，具有气孔状结构或块状结构，其气孔大小 0.2-1cm 不等，常填充白色石英。Miao(2007）曾报道研究区未变形玄武岩含有 ca.260Ma 的锆石。未变形玄武岩不属于混杂岩组份。

混杂岩经历了绿片岩相和蓝片岩相变质作用，发生强烈变形或糜棱岩化。绿片岩相矿物包括：阳起石+ 绿泥石+绿帘石+方解石+钠长石组合和绢云母+绿泥石+钠长石+石英组合；蓝片岩组矿物包括：蓝闪石、硬柱石、金云母、黑硬绿泥石、文石等（Yan and Tang, 1989)。蓝闪片岩具有 Ar/Ar 年龄在 ca.426-453Ma 左右（Tang and Zhang, 1991； Jong, 2006）

根据野外观察和室内分析，我们同意 Wang 和 Liu (1986)的观点，即这套具有混杂堆积特征的岩石组合原岩为富含铁和锰的硅质岩、沉积火山碎屑岩、玄武岩、细碧岩等，具有大洋洋壳岩石组合的特征。其中南带岩石以绿泥绢云石英片岩为主，可能代表洋壳碎片和深海泥砂质岩石组成的混杂体，含有少量细碧质或玄武质的洋壳物质，导致在石英片岩层中含有少量绿泥绿帘片岩。中部的含铁石英岩原岩应以大洋硅质化学沉积为主，富含铁和锰元素，混入少部分火山灰的变质产物。

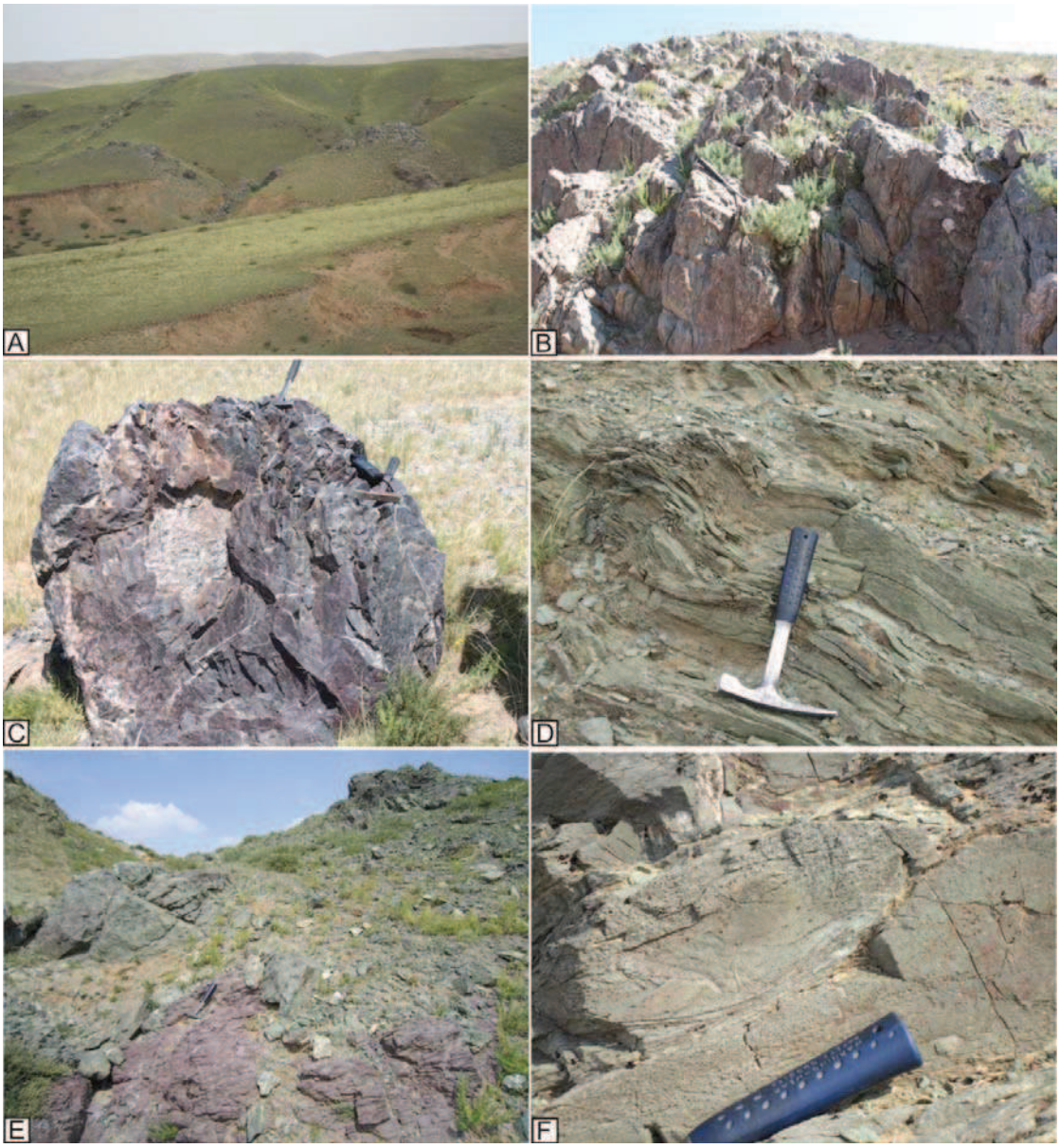

图 3-2-3 温都尔庙地区混杂岩带露头特征图片

A：温都尔庙南部乌花敖包地区混杂岩混杂特征宏观图片，零星分布灰岩和火山岩块体；B：混杂带南部基质包括绢云石英片岩和方解绿泥片岩、大理岩等，互层相间分布；C：温都尔庙地区中部混杂岩带所含囊状含铁石英岩体；D：温都尔庙乌兰沟地区绿泥片岩基质；E：乌兰沟地区绿泥片岩基质中含紫红色硅质岩块体；F：乌兰沟地区压扁拉长得玄武岩块体，气孔呈环状沿枕面分布；

3.2.1.3 沉积盖层 (The Overlying Sedimentary Succession)

研究区南北两侧分布有上石炭统阿木山组，不整合覆盖在上述地层单元之上，主要由陆源碎屑岩和含化石碳酸盐岩组成，指示海陆交互沉积环境。阿木山组下部由含砾粗砂岩，中粗粒硬砂岩、厚层块状灰岩和生物碎屑灰岩组成，中部为深灰、浅灰色薄-厚层灰岩、块状生物碎屑灰岩，夹硬砂质长石砂岩和砂砾岩，

顶部为厚层生物碎屑灰岩及微晶灰岩，灰岩中含大量蜓类、珊瑚类、腕足类和苔藓虫等化石，属于 *Triticites* 带（内蒙古区域地质志，1991），时代为晚石炭纪。本次调查发现，阿木山组灰岩主要为块状结构，未发现明显的韧性变形，与下伏地层变形特点明显不同，它可以界定温都尔庙区混杂岩带韧性变形的时代上限。

3.2.2 温都尔庙地区变形分析 (The Structural and kinematic analysis)

前人对温都尔庙地区进行了详细的变形和变质研究（胡骁等 1990），但是主要集中温都尔庙群的局部地区的变形分析。本次研究通过综合考察温都尔庙地区构造岩石地层，结合运动学分析，认为温都尔庙群经历多期变形，宏观上为一背形的构造格架（见下文）。

3.2.2.1 宏观构造 (The macroscopical structure)

温都尔庙地区作为俯冲混杂岩的典型地区，岩层发生多期次褶皱叠加变形，各种面理线理发育。根据野外片理和线理测量，温都尔庙地区混杂岩构造格架表现为一个 NE-SW 向的复背形（图 3-2-1B）。背形的南翼以向南陡倾的石英片岩片理为特征，近直立（图 3-2-1C）；中部表现为一系列直立褶皱，枢纽近 E-W 向，波长近百米；在北部乌兰沟一带，片理向 N 或 NW 陡倾，组成复背形的北翼。在混杂带南部，图林凯角闪岩类岩浆岩与绿片岩相混杂岩以断层接触，角闪岩类岩石经历复杂韧性变形，露头级别的鞘褶皱和揉皱较发育，但是褶皱形态不规则（图 3-2-5A 和 B）。晚石炭纪阿木山组灰岩于南北两侧覆盖复背形翼部。根据面线组构在不同区段发育程度和组合形式，结合显微镜下定向薄片中的微构造特征，将混杂带划分出三期变形序列(期次)，从老到新依次为：D_1 期形成区域片理；D_2 期以非对称褶皱为特征；D_3 期发育直立褶皱，形成区域构造格架。

D_1 期变形与绿片岩变质作用同时，形成区域性片理 S_1。在南部乌花敖包-图林凯一带，S_1 片理近 E-W 向，近于直立（图 3-2-1C）。L_1 矿物伸展线理近垂直，表现为定向拉长的石英、长石、方解石颗粒，以及绿泥石集合体（图 3-2-5C）。以 S_1 期绿片岩片理作为参考面，在局部可见厘米或米级不对称弯曲 F_2，改造了绿片岩片理 S_1。F_2 褶皱轴近水平。D_3 期变形在露头不可见，通过区域对比可知，南部单元总体向南陡倾构成复背形的南翼。

中部混杂岩 S_1 面理以互层的绿片岩和石英片岩为标志，同样这些地层卷入一系列 E-W 轴向直立褶皱 F_2，褶皱波长近百米，镜下可见这些 S_1 片理发生厘米或毫米级弯曲，代表 D_2 期变形，绿泥绢云片岩和含铁石英岩块体中广泛发育 N-S 或 NW-SE 向伸展线理 L_1。绿泥绢云片岩中以定向拉长的重结晶绿泥石和石英集合体为标志。中部露头褶皱劈理较发育，常常切割 S_1 片理。D_3 期直立褶皱在露头不可见，但是沿剖面统计 S_1 面理，有规律地倾向 NW（N）或 SE（S）（图 3-2-1D），说明 D_3 期变形的存在。

北部在乌兰沟一带混杂岩出露较好（图 3-2-4），我们沿沟从南向北进行了考察。在乌兰沟南侧入口处，绿泥绢云片岩中 S_1 片理 N-S 走向，向 W 缓倾，L_1 线理

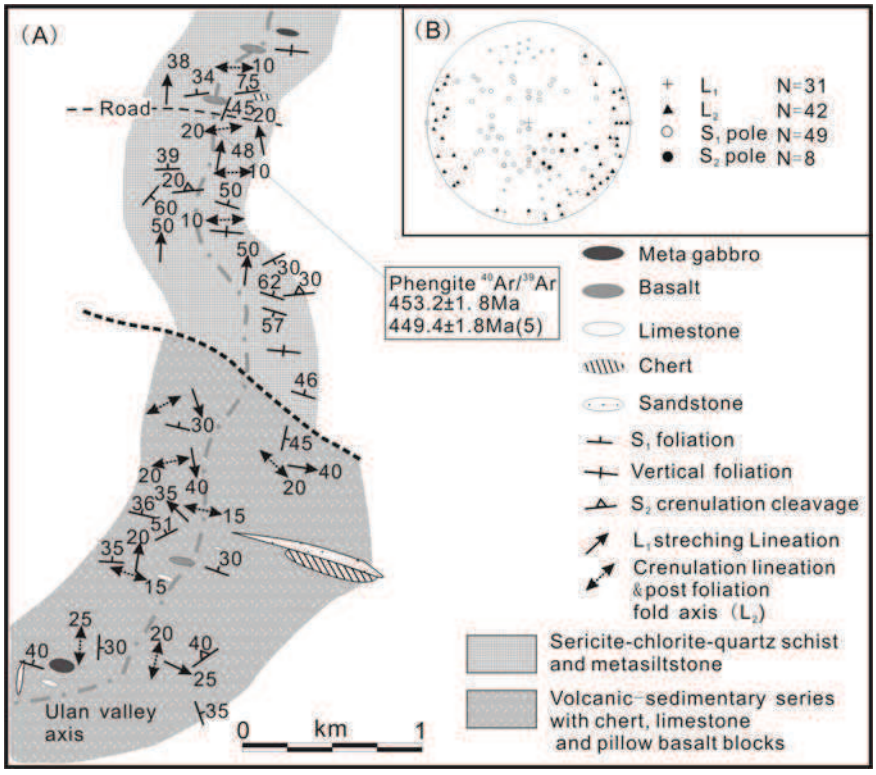

图 3-2-4 乌兰沟地区混杂岩构造特征简图

近 E-W 向。但是继续向北，S_1 面理倾向 NW 或 N。矿物伸展线理 L_1 也转变为 NW-SE 向（图 3-2-5D）。D_2 期是以 D_1 期片理基础发生的再褶皱，表现为褶劈理 S_2 和一系列的非对称小褶皱 F_2，它们强烈改造了 S1 和 L1 线理（图 3-2-5E-H）。这些不对称褶皱轴 L2 近水平，近 E-W 向。值得注意的是 D2 期褶皱有时为倒转褶皱，主体倾向 NW，有的以缓倾角向南倒倾（图 3-2-5E），且褶皱的两翼不对称，北缓南陡。这些褶劈理和不对称轴面面理 S2 可能与 D3 期变形有关，形成复背形的北翼。D3

期褶皱枢纽总体呈北 ENE 和 WSW 方向倾伏，近于水平，推断挤压应力主要为近南-北向。通过填图及构造分析发现，区域性片理的规律性弯曲显示了第三期褶皱的存在，组成温都尔庙地区区域格架。

3.2.2.2 显微组构特征 (The microscopical structure)

平行 XZ 面切割制作薄片，可以观察到明显的岩石显微特征。在显微镜下 σ、δ 型旋转碎斑发育，石英片岩中石英的拔丝构造等显著。L_1 线理以定向拉长的硅酸盐矿物几何体和重结晶的碳酸盐集合体，集合体周围多为不透明难溶物质（图 3-2-6）。在南部 L_1 线理近垂直，镜下可见压力影、σ 旋转碎斑子等，指示其南侧向上剪切的运动学特征（图 3-2-6A-C），消除 D_3 期变形的影响，它代表了顶部 NW 向剪切运动特征。中部绿泥石英片岩中，围绕旋转残斑发育的绿泥石形成压力影，以及长石 σ 残斑指示上部 NW 向的剪切运动特征（图 3-2-6D）。D_2 期是以 D_1 期片理基础发生的再褶皱，大量发育 S_2 褶劈理斜切 S_1 面理，它们强烈改造了 S_1 和 L_1 线理。镜下鉴定，褶劈理表现为斜列的不透明物质，呈条带状分布（图 3-2-6E）。D_3 期变形在镜下并未造成明显的岩石成份分异，表现为 S_3 褶皱劈理以高角度斜切 S_1 面理（图 3-2-6F）。北部绿片岩中的旋转残斑、云母鱼和剪切条带等构造特征明显。在一些以石英、长石为旋转碎斑的变沉积岩中，σ 残斑同样指示其顶部向 NW 剪切运动（图 3-2-6G 和 H）。

3.2.2.3 小结

温都尔庙混杂岩基质以绿片岩为主，含有不同岩性岩块，如枕状熔岩、大理岩和蓝片岩等，其原岩为火山岩和火山沉积岩为主，可能源于俯冲带残余洋壳物质。该混杂岩带主要经历了 3 期变形，D_1 期变形形成广泛分布的 S_1 绿片岩片理，和近 NW-SE 走向的矿物拉伸线理，通过镜下分析 σ 旋转碎斑和压力影的变形特征，消除 D_3 期变形的影响，D_1 期片理倾向 SE，运动学标志显示其遭受了上部向 NW 的剪切作用，与由 SE 向 NW 的逆冲剪切运动有关，由此我们推断可能与俯冲带 SE 向俯冲过程造成的。以 S_1 片理为参考面，D_2 期面理表现为非对称褶皱 F_2 和褶皱劈理 S_2。该期片理在不同区域发育程度不同，但是无论在露头还是镜下，都表现为斜切或置换 S_1 片理。D_3 期变形奠定了现今的构造格架，即形成轴向近 E-W 的复背形。在南部图林凯-乌花敖包一带，片理向南陡倾；在中部表现为一系列

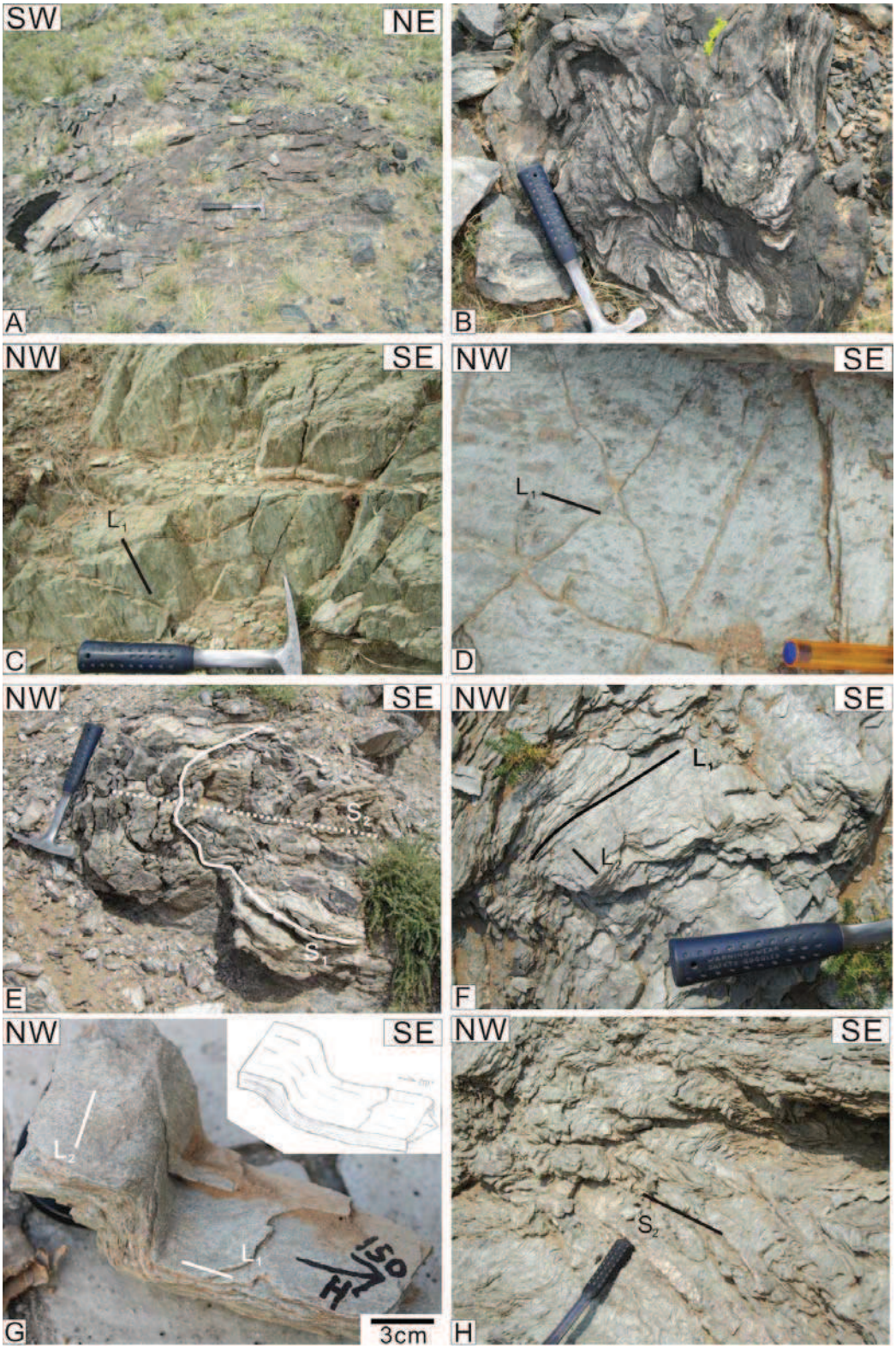

图 3-2-5 温都尔庙地区岩石变形特征露头图片

A：图林凯地区角闪岩内部发育的 A 型鞘褶皱，图为 YZ 切面；B：图林凯斜长岩和角闪岩发生无规则韧性变形；C：温都尔庙混杂岩南部矿物拉伸线理近垂直，以定向拉长的绿泥石集合体为标志；D：乌兰沟混杂岩近 NW 向矿物拉伸线理，以绿帘石矿物定向排列为标志；E：乌兰沟混杂岩绢云石英片岩发生褶皱，轴面 SE 倾向；F、G：乌兰沟混杂岩绢云绿泥片岩中矿物拉伸线理被 D_2 期褶皱改造；H：乌兰沟混杂岩绿泥绢云片岩受到褶皱改造

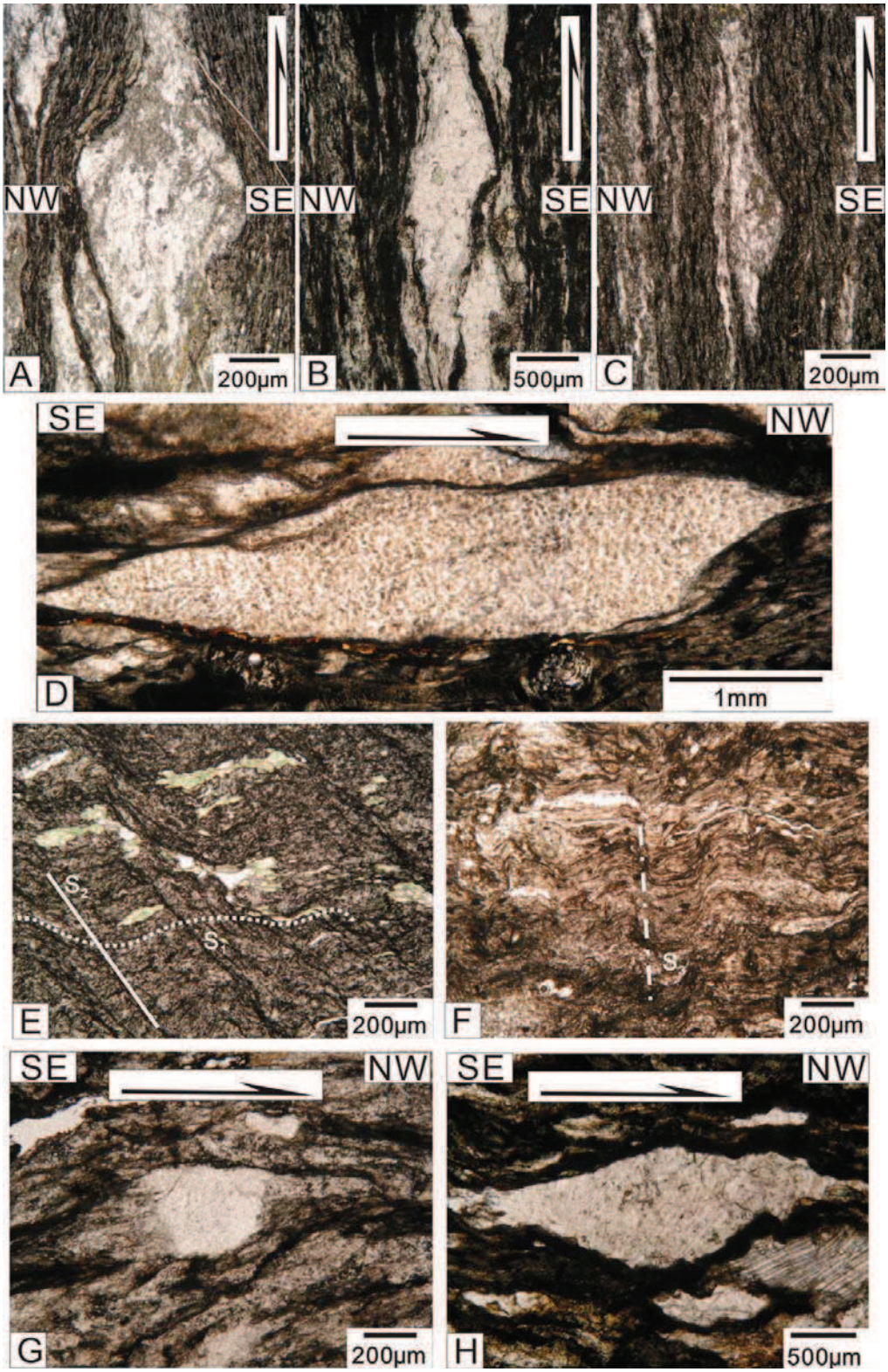

图 3-2-6 温都尔庙地区混杂岩显微构造变形特征图片

A 和 C：σ 形长石残斑指示南侧向上的剪切运动方向；B：石英绿泥片岩中 σ 形方解石残斑指示南侧向上的剪切运动；D：温都尔庙混杂岩中部绢云石英片岩中石英残斑指示顶部向 NW 的剪切方向；E：乌兰沟地区褶皱片理 S_2 与绿片岩片理 S_1 角度切割；F：温都尔庙混杂岩中部褶皱劈理 S_3 垂直切割 S_1 片理；G 和 H：σ 形长石和碳酸盐残斑指示顶部 NW 的剪切运动方向

开阔直立褶皱，在北部乌兰沟一带表现为不同角度片理北倾。上石炭统灰岩则不整合覆盖在这些混杂岩之上，没有显示明显的韧性变形特点。需要注意的是，温都尔庙地区混杂岩的两期褶皱 D_2 和 D_3 无论在大范围内，还是在露头上，都明显地表现为共轴叠加关系或两期褶皱的枢纽以小角度斜交。D_3 褶皱作用并未使 D_2 期褶皱的枢纽发生波状弯曲。在图林凯岛弧区则主要以角闪岩类岩浆岩为特征，这些岩石经历了韧性变形，形成一系列的不规则的褶皱，可能与岛弧深部岩浆作用有关。

第三节 小结 (Summary)

根据我们的野外调查和岩性对比，红旗牧场研究区和温都尔庙研究区均可划分出三个次级构造岩石单元，即白乃庙岛弧带、红旗牧场-温都尔庙混杂岩带以及后期的不整合覆盖其上沉积地层。这些次级岩石构造单元在区域上可进行对比。岛弧带主要由钙碱性玄武质、安山质火山岩以及火山岩碎屑岩组成，包括同期发育的侵入岩，如巴特敖包花岗岩类和图林凯地区角闪岩类岩石。岛弧火山岩在红旗牧场和白乃庙地区分布以包尔汗图群和白乃庙群为代表(唐克东等,1991; Zhang et al., 2012)。在岛弧带的北侧发育混杂岩带，混杂带基质主要为一套绿片岩相变质岩，通过矿物组合特征，推测其原岩为基性火山岩、沉火山碎屑岩（或浊积岩），与俯冲带洋壳残余相关。混杂带中岩块大小不同，种类各异，一般包括蛇纹岩化橄榄岩、枕状玄武岩、大理岩（灰岩）、硅质岩（变质石英岩）、杂砂岩等。值得注意的是，在温都尔庙地区枕状玄武岩为碱性玄武岩，具有板内玄武岩地球化学特征（黄金香等，2006），而非通常认为的俯冲成因的岛弧玄武岩（Xiao et al., 2003）。在红旗牧场混杂带所含岩块中发现角闪岩，代表中-高温变质作用，而温都尔庙地区则存在蓝片岩块体，指示高压变质作用的存在。这些构造岩石单元被下泥盆统查干哈布组和上石炭统阿木山组不整合覆盖。野外调查显示，这些沉积岩主要由陆源碎屑岩和化石碳酸盐岩组成，发育大量原生沉积构造。沉积岩组分和沉积特征指示滨浅海相或海陆交互相沉积环境，说明在泥盆纪之前大洋相关的沉积环境已不存在。

混杂带岩石显示强烈的韧性变形特征。本次研究根据片理、拉伸线理、小褶皱、断层等的组合特征和切割关系，将混杂带从深层次韧性变形到浅表层次脆-韧性变

形划分为三期变形序列(期次)。D_1期主要表现为形成区域性绿片岩片理、矿物拉伸线理、和层内褶皱。D_2期变形可以认为D_1期变形的继续，绿片岩片理发生弯曲，形成不同尺度不同类型的非对称褶皱，以程度不同的褶皱劈理切割绿片岩片理为特征。D_3期脆-韧变形为特征，发育不同尺度的直立褶皱，构成区域构造格架。消除D_3期变形的影响，D_1期片理主体呈 NE-SW 走向，广泛发育 NW-SE 向矿物拉伸线理，沿着 XZ 面制作定向薄片、σ 旋转残斑、云母鱼和剪切条带等微观组构显示顶部 NW 向剪切运动学特征。该运动学特征与 SE 向洋壳俯冲过程相关。红旗牧场地区 D_3期形成的开阔直立褶皱枢纽呈 SE-NW 走向，而在温都尔庙地区枢纽总体呈 E-W 或 NNW 向。红旗牧场地区 D_3期变形卷入下泥盆纪统地层，说明该期变形不早于早泥盆纪，而前两期韧性变形则不晚于早泥盆纪。

第四章 晚古生代构造特征 (The Late Paleozoic tectonics)

研究区晚古生代地层主要分布于索伦敖包至西拉木伦河的广阔区域，大致近东西向分布。出露的地层主要为上石炭统本巴图组、阿木山组和二叠系大石寨组、哲思组。上石炭统地层主要为一套浅海相碎屑岩系和碳酸盐岩，二叠系地层包括一套浅海相喷发中酸性火山岩和其上的一套浅海相砂岩、页岩和碳酸盐组合。值得注意的是这些地层中夹杂有超镁铁质、镁铁质块体，如：索伦山地区包括数百个蛇绿岩块，呈扁豆状和透镜状的块体或狭长的断片产出在中上石炭统和下二叠统地层中（邵济安等，1991）。满都拉地区，超基性—基性岩块呈构造侵位（苏新旭等，2000）或飞来峰（陶继雄等，2004）形式产于石炭系本巴图组中。为了详细研究晚古生代沉积地层及变形特征，本文选择达茂旗满都拉地区进行重点分析。

第一节 满都拉地区构造单元划分 (the litho-tectonic framwork in the Mandula area)

满都拉地区位于达茂旗北部，处于西伯利亚板块和华北板块会聚地带，是著名的“索伦科尔缝合带”（Solonker Suture）的所在地，前人（如 Xiao et al., 2003； Jian et al., 2010）曾提出该带由蛇绿混杂岩、深海放射虫硅质岩等组成，是西伯利亚板块和华北板块晚古生代-早中生代的缝合带。本文对“混杂岩”分布地区的晚石炭世-早二叠世地层进行了系统观察，根据岩性特征将满都拉地区岩石地层划分为四个岩石构造单元，从底至顶依次为大石寨组火山岩单元、浊积岩单元、滑塌堆积单元和哲斯组沉积单元（图 4-1-1）。Jian et al.(2010)所指“灰岩块混杂岩 (limestone block mélange)”和“泥质杂基混杂岩(argillaceous matrix mélange)分别厘定为滑塌堆积单元和浊积岩单元。从南向北依次描述如下：

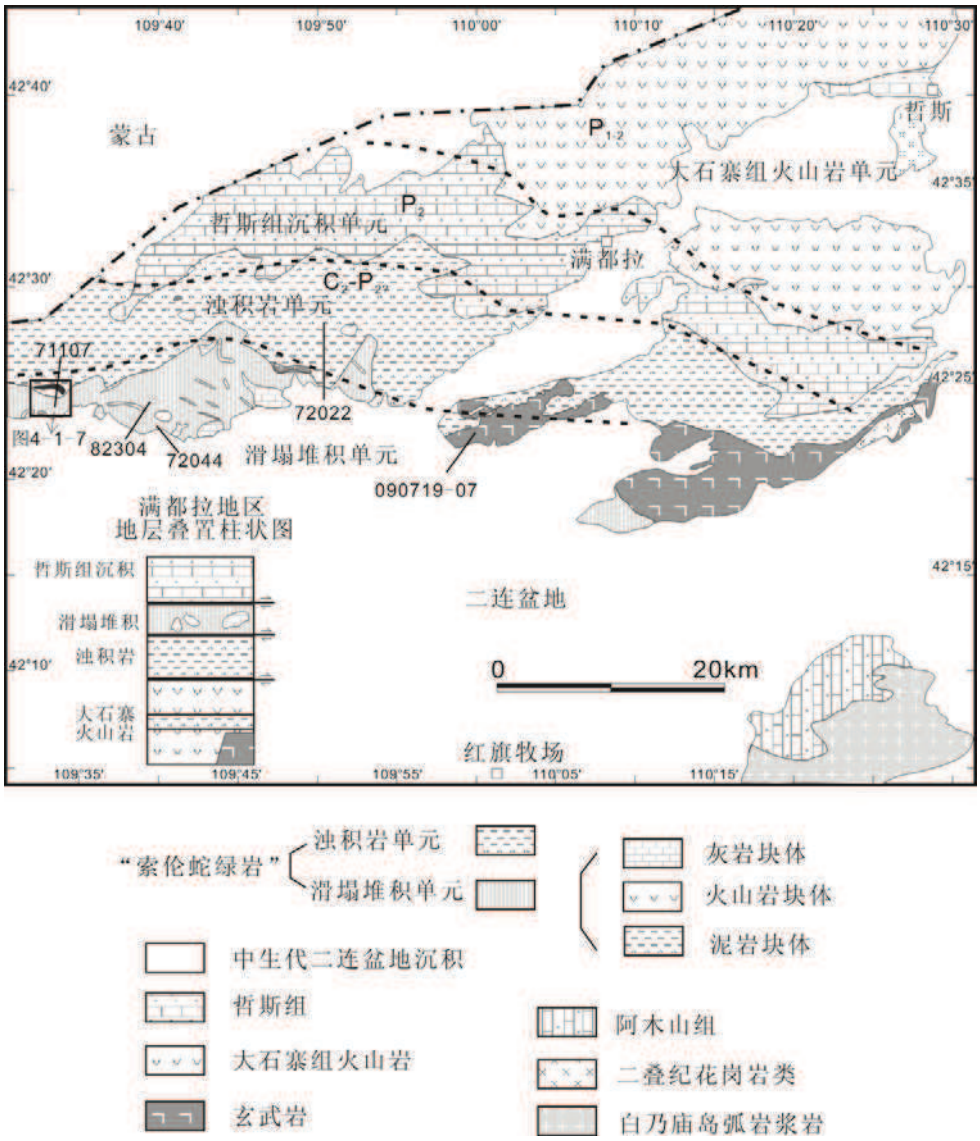

图 4-1-1 满都拉地区区域构造地质图及测年样品位置 （据满都拉地区 1/25 万区调，2003）

4.1.1 滑塌堆积单元 (the Olistostrome Unit)

4.1.1.1 沉积特征 (The sedimentary features)

滑塌堆积单元出露在最南部，东西长近 50km，南北宽 1-8km 不等，南部被中生代二连盆地沉积物覆盖，北部过渡为浊积岩沉积单元。前人将该地层单元置为本巴图组，时代归为晚石炭纪（满都拉地区 1/25 万区调，2003）。

野外调查表明本巴图组主要由生物礁灰岩和陆源碎屑沉积组成。砂岩中混杂有石英砂岩，结晶灰岩、硅质泥岩块(图 4-1-2 A-F)等，并有巨大的火山岩块体，块体的长轴方向与整个岩带的展布方向很不协调。块体大小悬殊，大的数米，小到几厘米，碎屑胶结，分选性和磨圆度差，以角砾状为主，部分浑圆状，成分复

杂。灰岩块体主要包括生物礁灰岩有的灰岩块体延伸上千米，呈山丘状，灰岩地层保持良好，但是侧向不连续（图 4-1-2A）。值得注意的是，这些灰岩块体无论从岩相上，还是化石组合上，都和南部红旗牧场地区出露的晚石炭纪生物礁灰岩相似，因此这些灰岩块体可能来源于南部红旗牧场地区。局部可见硅质泥岩块体，这些块体与浊积岩沉积单元中硅质泥岩相似，它们呈透镜状散布在杂砂质基质中(图 4-1-2B)，块体中含放射虫化石(王惠等，2005)。总体上这些块体的数量和规模具有从南向北逐渐减少的趋势，而泥质岩块体向北逐渐增多。在北部局部可见火山岩块体（图 4-1-2C）。基质主要为砂岩和泥质，呈半连续或完全混杂。它们也有规律的变化，在最南端，基质主要由灰色、灰白色和粉红色调的硬砂岩组成，地层呈半连续状，有时候可见其原始层序（图 4-1-2D）。逐渐向北，基质逐渐变为灰黑色砂岩和泥岩的混合物，其原始层序不可见。

这套岩石组合总体上缺乏成层性，仅局部显示层状构造特征。在生物灰岩中和一些砂板岩层中，成层性明显，具有较好的韵律性，但是与周围地质体为断层接触关系。这套岩石组合由不同岩性、不同时代的岩石构成，镶嵌在杂砂质成份中。它是结晶灰岩、生物礁灰岩以及砂岩沉积在强烈、连续的构造运动中，在海底斜坡或地震浊流等背景下经短距离搬运、沉积方形成。

为了系统说明滑塌堆积的沉积特征和层序序列，我们分别沿着滑塌堆积纵向和横向精确测绘了剖面（图 4-1-3），描述如下：

纵剖面层序特征：（GPS：N42° 25’ 23″； E109° 46’25″）

——未见顶——

48 黄绿色杂岩，泥质成分较高，约 40%，其它主要为长石和石英颗粒，分选和磨圆较差

47 基质为灰白色-黄绿色长石石英粗砂岩，含灰岩山丘（块体）

46 灰色石英粗砂岩，夹块状结构硅质泥岩块体和灰岩块体，块体表面发育明显的擦痕构造，擦痕总体呈 N-S 向

45 黄绿色泥质粉砂岩， 夹薄层砂岩和硅质泥岩块体，块体常呈透镜状顺层产出

44 灰白色石英粗砂岩，破碎严重，成层性较差，夹灰岩透镜体

43 灰白色石英粗砂岩，含灰岩砾石和灰岩透镜体，灰岩主要为化石灰岩 含蜓和腕足类

42 灰岩山丘，局部可见灰岩层

41 片理化泥质粉砂岩，含较多杂砂岩块布丁块体，顺层分布，灰岩砾石较少

40 薄层状硅质泥岩和泥质粉砂岩互层，含灰岩块体，呈山丘状。灰岩包括中薄层生屑灰岩，成层性较好；垮塌角砾状灰岩裂隙发育并被后期方解石脉填充，上部被灰岩山丘覆盖，灰岩底部发育大量摩擦镜面

39 底部为薄层状硅质泥岩，夹薄层砂岩，砂岩层呈塑性变形，被拉长扯断，呈透镜状顺层分布，中上部为灰白色石英粗砂岩

38 青灰-褐红色薄层状泥质粉砂岩，含灰岩砾石透镜体和紫红色长石粗砂岩块体，灰岩砾石顺层产出

37 褐黄色薄层状硅质泥岩

图 4-1-2 满都拉地区滑塌堆积野外沉积特征图片

A：滑塌堆积中的灰岩块体呈山丘状分布，侧向不连续；B：硅质泥岩块体夹杂在砂岩基质中；C：在滑塌堆积北部出现少量酸性火山岩块体；D：滑塌堆积南部紫红-灰白色砂岩层序被错断，地层呈半连续状；

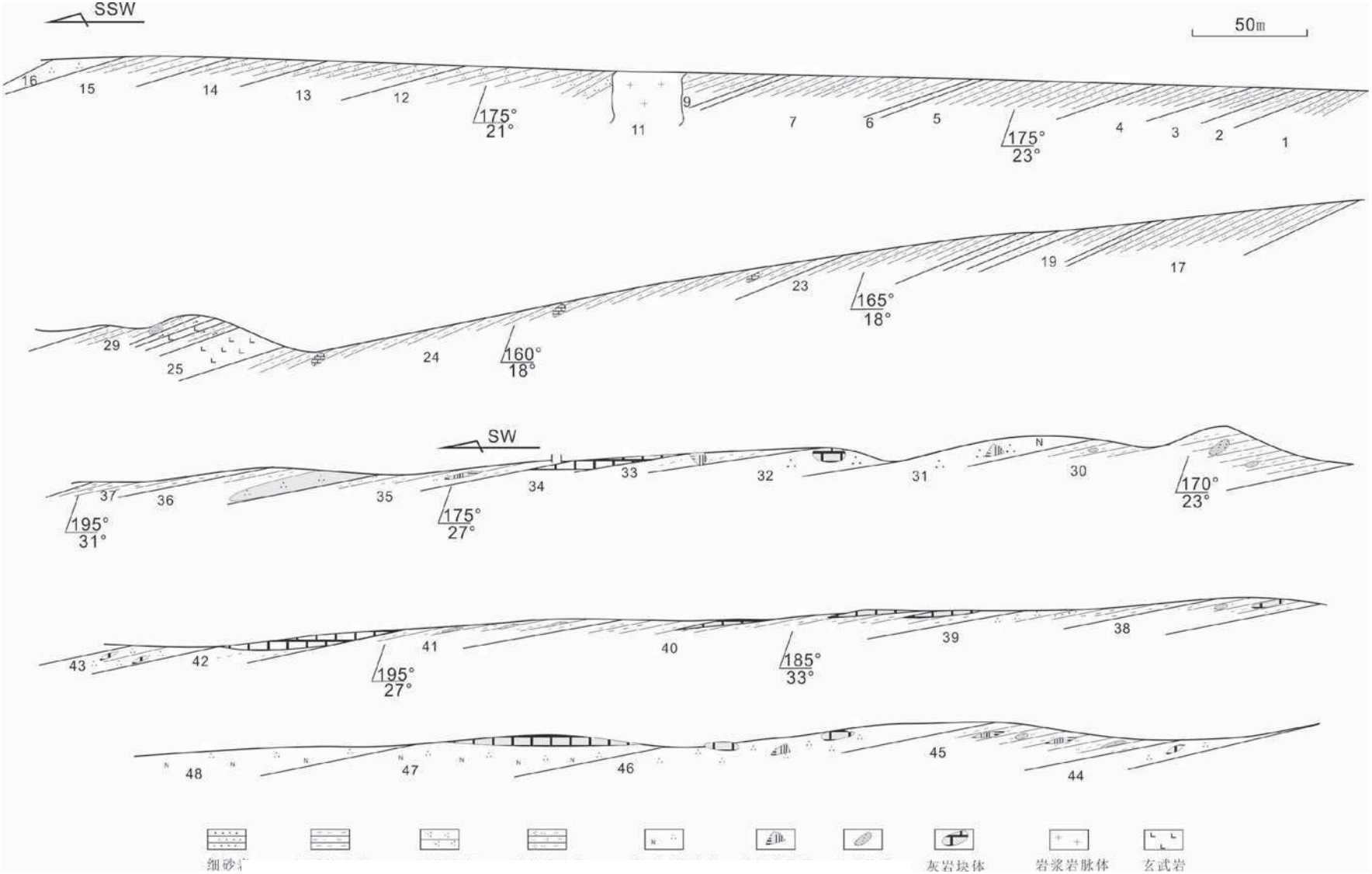

图 4-1-3 满都拉地区滑塌堆积与浊积岩沉积层序特征实测剖面图

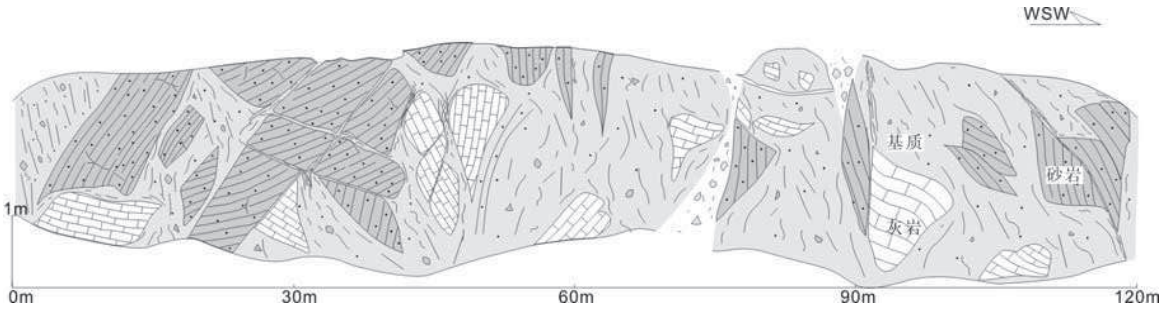

图 4-1-4 满都拉地区滑塌堆积横切面沉积特征实测剖面

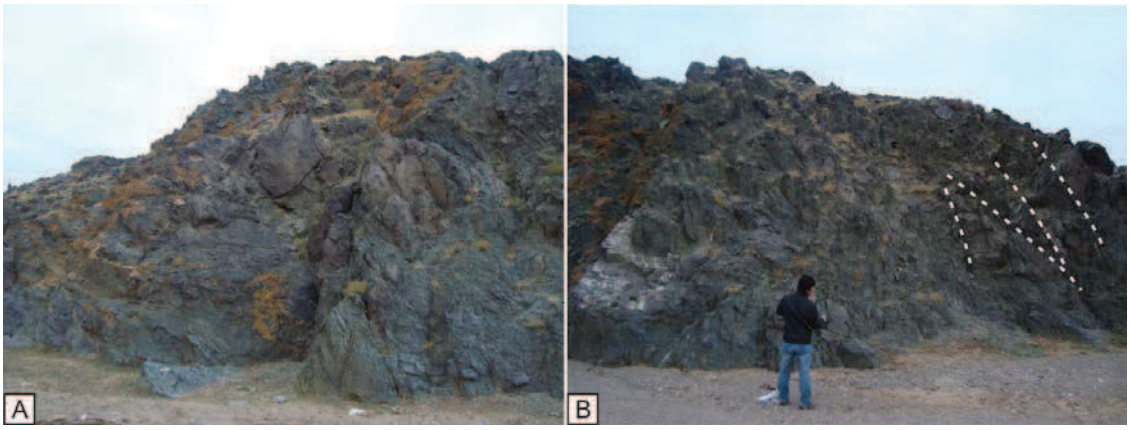

图 4-1-5 满都拉地区滑塌堆积横切面露头特征图片

A：土黄色灰岩块体（图片中部）内嵌于青灰色基质中，灰岩被搓断呈纺锤状、透镜状；B 左下角灰白色为灰岩块体。右上角砂岩块体呈叠瓦状排列

36 中-薄层状石英粗砂岩夹薄层状粉砂岩；石英粗砂岩呈层状或透镜状，成层性较好但是不连续；薄层状硅质泥岩，厚度在 3-5cm，成层性较好

35 紫红色薄层状粉砂岩与石英粉砂岩互层，单层厚度在 2-3cm 之间，夹少量硅质泥岩透镜体

34 大量灰岩块体呈山丘漂浮在砂岩之上，灰岩原始层理保存完好

33 基质为泥质粉砂岩，中间夹硅质泥岩块体

32 灰白色石英杂砂岩，含灰岩透镜体，直径可达数米

31 灰白色长石石英粗砂岩，含石英砂岩和硅化泥岩透镜体

——未见底——

横剖面混杂特征：

滑塌堆积中层 38-40 混杂特征发育较好，出露良好（GPS：N42° 24’ 27″；E109° 44’ 52″）。我们通过野外观察、测绳标记、照片辅助等方法，沿着东西向精确绘制了混杂堆积横切面（图 4-1-4）。剖面中，混杂块体由砂岩和灰岩组成，含量约 40%左右。砂岩和灰岩块体呈叠瓦状分布在砂泥岩基质中（图 4-1-5），块

体边界模糊，与基质常常呈过渡关系。有的砂岩块体呈直立状夹杂在基质中，走向近 N-S（图 4-1-4），可能与滑塌过程中的剪切运动相关。灰岩块体主要为青灰色结晶灰岩，未见化石，它们遭受了强烈的破碎和塑性变形，呈纺锤状、透镜状或无规则状，在基质中杂乱分布。滑塌基质主要由青灰色泥质岩和砂质混杂体组成，成层性很差，发生塑性变形，局部可见揉皱和片理化。

4.1.1.2 软变形特征 (The slumping structure)

在滑塌沉积单元中，岩石混杂无序（图 4-1-6A），但是同沉积软变形构造保存良好。在南部，基质砂岩层呈半连续状，有的砂岩层被扯断，并被泥质填充，形状类似涨缩构造。向北，露头上可见许多无规则褶皱，有时可见褶皱翼部倒转，褶皱轴部加厚，枢纽发生弯曲，但是不发育轴面劈理（图 4-1-6B），这与后期发育的褶皱构造明显不同，后期构造过程中形成的褶皱多发育轴面劈理（见下文）。砂岩透镜体定向排列，长轴总体呈 NW 向。滑塌堆积单元北部，常常发育大量的挤压构造，泥岩中含 σ 变形砾石，显示其向北移动的运动学特征(图 4-1-6C)，有些泥岩发生强烈的韧性揉皱(图 4-1-6D)。露头上可见巨大的灰岩块体漂浮在下伏砂泥岩之上，下部砂泥岩发生变形，灰岩底部常发育摩擦面。

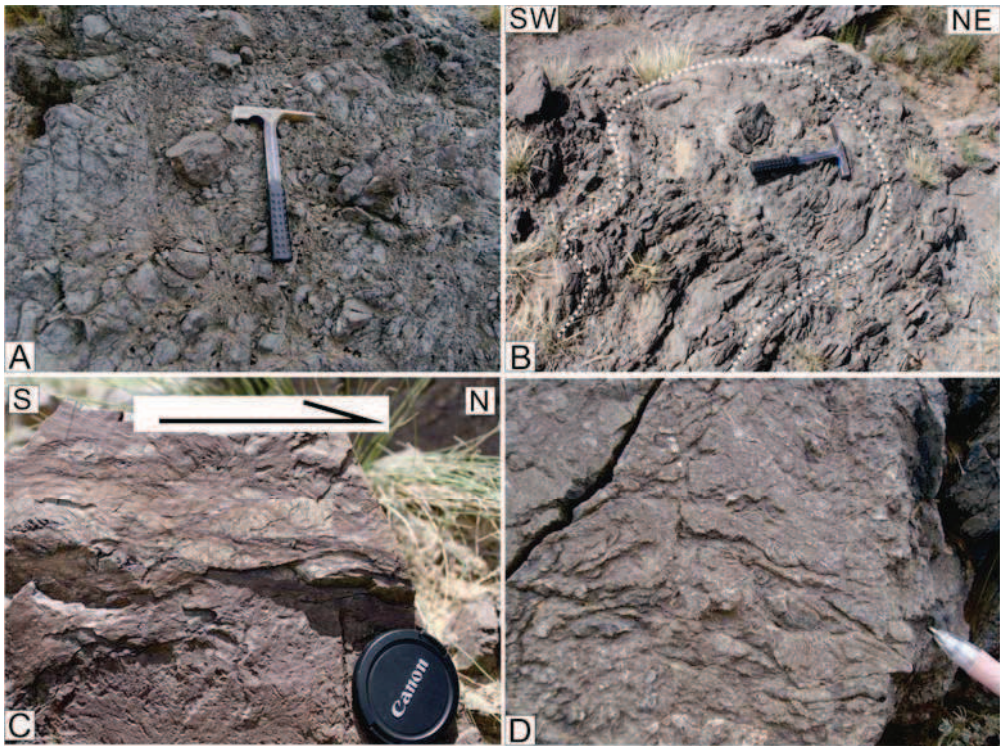

图 4-1-6 满都拉地区滑塌堆积变形特征图片

A：滑塌堆积北部青灰色砂泥质基质，基质内部无序；B：滑塌基质发育的无规则褶皱；C：硅质泥岩中含 σ 变形砾石，显示其向北运移动的特征；D：泥岩因挤压而发生强烈的塑性揉皱

4.1.1.3 小结 (Summary)

满都拉地区滑塌堆积由块体和基质两部分组成。块体包括砂岩、灰岩、火山岩和硅质泥岩等。滑塌堆积的块体具有一定的变化规律，灰岩块体从南向北，在数量和块体规模上，逐渐减少和变小；而硅质泥岩块体和酸性火山岩块体则逐渐增多。砂岩块体在南部规模一般较大，呈山丘状，内部层序保存较好，但是向北出现普遍的岩层拉断现象，北部以青灰色的砂质和泥质混杂体为主，与滑塌基质相近。

沉积软变形主要包括一些小断层、揉皱和塑性变形构造。断层主要见于本单元的南部，常常将原来的有序地层错断，切割成菱形块体。揉皱在粉砂质、硅泥质混杂体中较普遍，以非共轴褶皱，顶部增厚为特征；在灰岩块体可见 σ 状块体，一般呈 S-N 向，规模较大的块体底部常发育摩擦镜面，硅泥质块体中发育近 S-N 向擦痕。这些特征均指示近南北向的滑塌运动。

灰岩块体的生物化石组合特征和南侧红旗牧场地区上石炭统阿木山组的生物化石灰岩、礁灰岩相似，因此可以推断南侧阿木山组沉积物为可能的物源区之一。由于所含灰岩年代为晚石炭世，滑塌堆积的形成年代应该晚于晚石炭世，其详细年代学分析见下文。

满都拉地区滑塌堆积分布范围较大，但是厚度很薄，野外可见有序地层产状舒缓，有时甚至可以直接见到无序块体与其下有序地层接触。值得注意的是，在滑塌堆积中基质和块体没有发生变质作用，这不同于造山带相关的混杂岩堆积。滑塌堆积常见于斜坡环境，与浊积岩沉积关系密切。综合分析各岩石构造单元的特征和相互关系，滑塌堆积形成于大陆斜坡环境，与二叠纪的裂谷活动有关（见下文）。

4.1.1.4 质疑“索伦蛇绿岩”(A doubt to the “Solonker” Suture)

本次研究重点关注了前人提出的“蛇绿岩块体” （邵济安，1991；陶继雄等，2004；王惠等，2005；Xiao et al., 2003；Jian et al., 2010），我们的野外观察和室内分析发现，这些“蛇绿岩块”实际上是由滑塌堆积块体和后期侵入脉体组成。如在满都拉地区某哨所附近，前人认为属于蛇绿混杂岩带，包含有基性块体、硅质岩和灰岩块体。我们的野外观察发现，这些块体散布在一套有序

的沉积地层之上，具体块体描述如下：

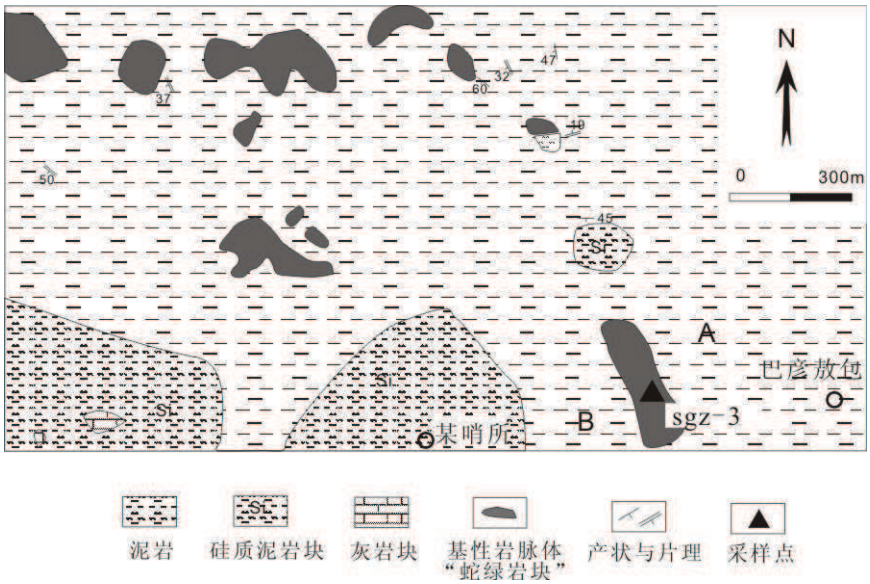

图 4-1-7 满都拉地区某边防哨所附近地质简图

“镁铁质块体”（GPS：E 109°32' 00"；N 42°26' 54"）：镁铁质岩块形态各异，大小不等，多数地段其长轴平行构造带的走向。由于构造挤压及风化作用，多已分解为硅质网状物，原岩组构难以识别。我们针对前人标记的蛇绿岩块体（满都拉地区 1/25 万区调）进行调查，发现所谓的“镁铁质块体”实际上为酸性火山岩层和辉长质侵入体。酸性火山岩呈层状或透镜状夹在浊积岩单元中，由于遭受了强烈的构造改造作用，发生褶皱，长轴近于 SW-NE 向，与区域构造线平行，岩石遭受后期蚀变作用，表面呈土黄色，类似于硅质交代的基性岩块体（图 4-1-8A），但是镜下鉴定为石英安山岩（图 4-1-8B）。另外一种类型的镁铁质岩为辉长岩。他们呈层状夹在周围的有序地层中（围岩常为浊积岩沉积），野外产状可见切割围岩（图 4-1-8C）。镜下鉴定这类岩石主要由粗粒辉石和长石组成，长石发生绢云母化蚀变，辉石蛇纹石化蚀变（图 4-1-8D）。我们获得少量的锆石进行分析，其年代为 253±1Ma（见下文 sgz-3），年轻于围岩地层，和野外切割关系一致。因此我们认为该辉长岩体为后期侵入体，不应该归为“蛇绿岩”的范畴。

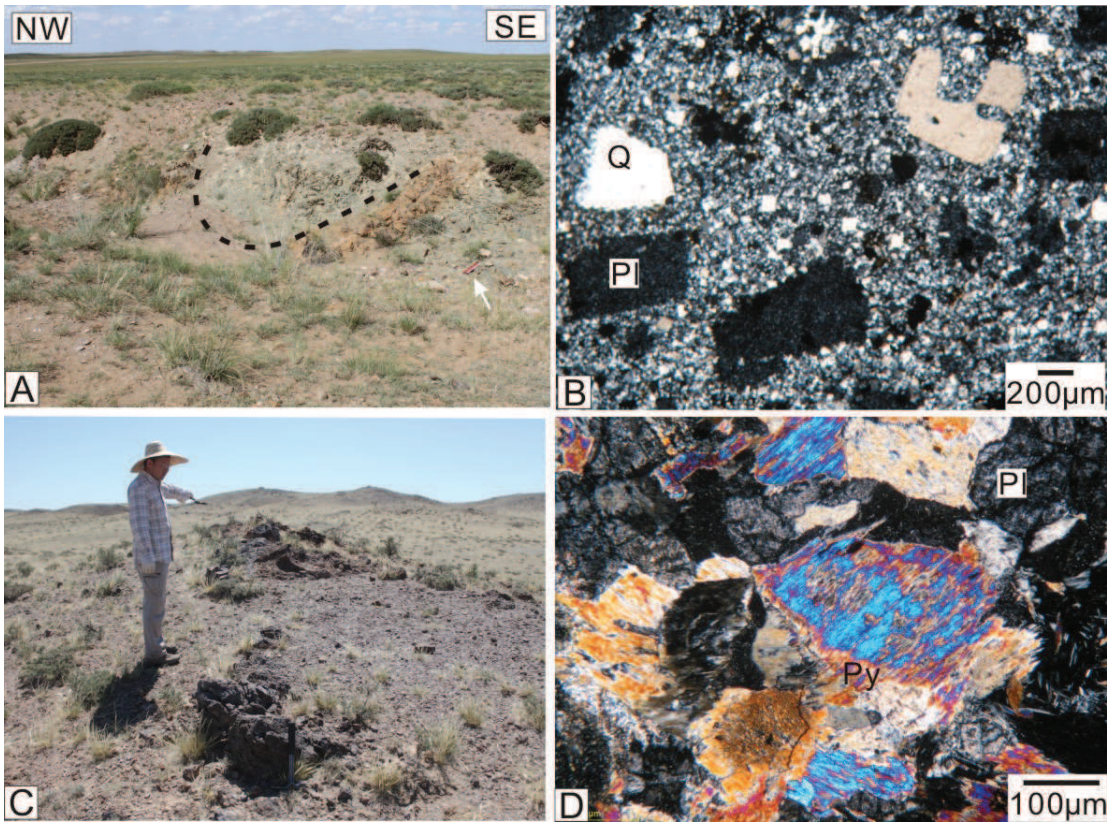

图 4-1-8 满都拉地区“蛇绿岩”露头特征和镜下鉴定图片

A：“超镁铁”岩块体实际为石英安山岩夹层，与浊积岩一起经历褶皱变形；B：镜下鉴定风化的蛇绿岩块体为石英安山质火山岩；C：露头显示辉长质岩浆岩侵入浊积岩沉积地层中；D：辉长岩的镜下鉴定图片，部分辉石和长石发生蚀变

火山岩块体或透镜体（GPS：E 109°30' 59"；N 42°27' 45"）：主要为酸性火山岩块体，多数分布在研究区北部，与大石寨组的火山岩相关。它们有的呈层状夹杂浊积岩中，有的呈块体镶嵌在滑塌堆积基质中。因此火山岩块体与区域上火山岩活动和滑塌堆积有关。

灰岩块体（GPS：E 109°33' 25"；N 42°24' 33"）：灰岩块体一般呈透镜状混杂在滑塌堆积基质中。有的则呈山丘状，漂浮在底部砂岩或滑塌堆积之上，具有良好的内部层序，但是这些灰岩山丘侧向不连续，因此同样属于滑塌堆积的块体。因此前人认为的灰岩块体是混杂岩的组成部分是不合适的。

硅质泥岩（GPS：E 109°33' 26"；N 42°24' 49"）：根据我们的野外观察和镜下鉴定，前人认为的含放射虫硅质岩实际上是硅质泥岩，主要分布于浊积岩单元，在滑塌堆积单元北部与浊积岩单元过渡带也含有硅质泥岩块体，属于滑塌过程中卷入的浊积岩泥岩。

综上分析，我们认为满都拉地区的蛇绿混杂岩带是值得怀疑的。“混杂带”

实际上是滑塌堆积和一些侵入体。它们经历了后期的褶皱作用，地层发生弯曲变形（见下文）。但是总体上浊积岩沉积是一套有序地层，而滑塌堆积单元的基质具有从有序-半无序-无序过渡的特征，为沉积成因。而且这些岩石与常见的混杂带截然不同，它们没有经历中、高级别的变质作用。块体的形成和分布主要与滑塌过程和火山活动有关，后期又被辉长质脉体侵入。因此满都拉地区是否存在蛇绿混杂岩带值得重新认识和评估。

4.1.2 浊积岩单元 (The Turbidite Unit)

4.1.2.1 浊积岩层序特征 (The turbidic sequences)

浊积岩单元出露在混杂单元的北侧，南北宽近 5-15km，出露面积近 150 平方公里，在满都拉地区沿东西向展布。其北部被中二叠统哲斯组覆盖，南侧与滑塌堆积单元接触。野外观察发现浊积岩和滑塌堆积之间没有截然的接触边界，两者逐渐过渡。该单元被置为上石炭统本巴图组（满都拉地区 1/25 万区调，2003），我们的碎屑锆石数据显示年龄可能晚于晚石炭世。

这套碎屑沉积物由含砾石粗砂岩、中至细粒杂砂岩、粉砂岩、粉砂质板岩组成，以发育鲍玛序列为特征，为典型的浊积岩。根据岩性组合和空间分布特点，我们将该单元分为粗浊积岩和细浊积岩两种类型。粗浊积岩的组成成份主要是含砾粗砂岩、中-细粒砂岩，中上部出现细砂-粉砂岩和泥灰岩薄层。沉积组份以陆源碎屑和安山质火山碎屑成分为主。含砾粗砂岩、中细粒砂岩和粉砂岩-泥质粉砂岩浊积岩在剖面上重复有规律地出现。单层粗浊积岩层厚度约 0.5-1m，由下而上，砂质逐渐减少，而泥质和硅质成分增多，颗粒碎屑由粗变细。冲刷构造、粒序层理等在含砾粗砂岩和中粗砂岩中较发育。

为了说明浊积岩的层序特征，本文详细测量了一条粗浊积岩剖面（图 4-1-9），描述如下：

——未见顶——

16 青灰色中薄层状细砂岩 28.5m

15 青灰色粗砂岩夹薄层泥质粉砂岩、泥岩，粗砂岩发育递变层理，泥岩块状结构 9.2m

14 灰白色-紫红色薄层状粗砂岩与薄层粉砂岩薄层，粉砂岩单层厚 2-3cm，粗砂岩发育递变层理 18.4m

13 青灰色细砂岩与泥质粉砂岩互层， 粉砂岩中发育水平层理 16.9m

12 灰白色-紫红色薄层状中-细砂岩，含泥质薄层，发育包卷层理 18.7m

11 灰白色薄层状泥质粉砂岩 11.3m

10 灰白色-紫红色薄层中-细砂岩，发育小型波状层理 15.2m

9 灰白色硅质泥岩，含薄层状粉砂岩层 12.2m

8 灰白色细砂岩，局部含薄层粉砂岩 16.4m

7 青灰色中-粗砂岩，破碎严重，被后期石英脉穿插 14.1m

6 青灰色薄层细砂岩与粉砂岩互层 17.3m

5 青灰色薄层粗砂岩与细砂岩、石英粉砂岩互层，粗砂岩中发育平行层理 20.5m

4 紫红色含砾粗砂岩，砾石成份片岩、砂岩和石英，向上变为薄层粗砂岩 4.2m

3 灰白色厚层含砾粗砂岩，砾石成份以片岩为主，含量约 15%，砾径 2-4mm；向上变为紫红色粗砂岩，砂岩厚约 5m； 共 15.8m

2 紫红色薄层-中层细砂岩，分选磨圆均较好 16.6m

1 多个紫红色-灰白色含砾粗砂岩、粗砂岩向上变细的旋回，顶部为灰色薄层细砂岩-粉砂岩和泥岩互层， 厚 55.7m

——未见底——

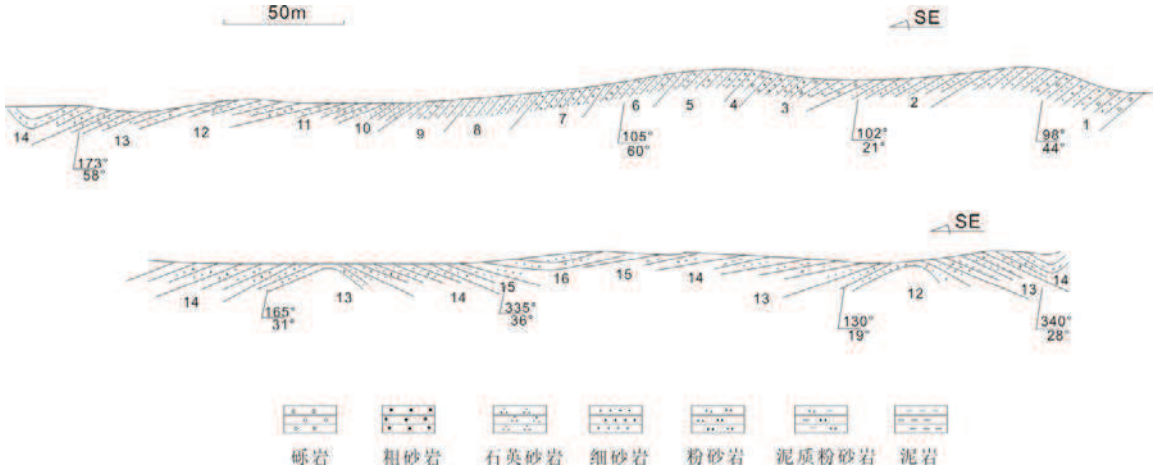

图 4-1-9 满都拉地区浊积岩单元粗浊流沉积层序特征实测剖面

该剖面底部由多个紫红色含砾粗砂岩-砂岩旋回构成，相当于鲍马序列的 Tab， Tad 层组合（图 4-1-10A 和 B）。底部砾石含量约 30%，平均砾径 8cm，分选和磨圆均一般，发育明显的粒序层理（图 4-1-10 C），向上砾石含量较少，粒度变细。每个旋回的底部常常发育底面铸模构造。中部含多层灰白色-紫红色粗砂岩，向上逐渐变细，顶部为韵律状细砂岩、薄层粉砂岩和硅质泥岩构成，多发

育水平纹层和小型波状层理（图 4-1-10 D），以鲍马序列 Tbcd、Tcd 为特征，颗粒粒度分选一般，显示密度逐渐减低，流速逐渐减弱。其中有数层青灰色细砂岩-粉砂岩组合，砂岩呈薄层状块状结构，野外地层连续较好，延伸较远，代表了研究区附近存在多次浊流扇体侧向迁移。该砂岩碎屑成分主要包括长石、石英、火山岩岩屑和泥岩岩屑，杂基含量较高，含较多的泥质和硅质成份，属于硬砂岩质浊积岩。该浊积岩剖面卷入一系列枢纽近 E-W 或 NEE 向褶皱，详细的变形分析见下文。

图 4-1-10 满都拉地区浊积岩单元沉积特征野外图片

A：粗浊积岩沉积 Ta 段，含大量泥质岩、火山岩砾石，分选和磨圆较差；B：粗浊积岩中 Tad 段沉积韵律；C：鲍马序列底部发育明显的粒序层理；D：浊积岩单元偶见发育较完整的鲍马沉积序列，厚度约 0.6m；E：细浊积岩中较为常见的鲍马序列 Tbe；F：细浊积岩粉砂岩段中常发育水平层理和爬升层理（箭头处）

本文沿着滑塌堆积剖面连续测绘了浊积岩剖面（图 4-1-3），描述如下：

——之上为滑塌堆积沉积——（见上文）

32 灰白色石英杂砂岩，含灰岩透镜体，直径可达数米。>20 m

31 灰白色长石石英粗砂岩，含石英砂岩和硅化泥岩透镜体　　19m

30 硅质泥岩夹石英粉砂岩互层，含杂砂岩透镜体 47m

29 底部为紫红色泥质粉砂岩，夹石英粗砂岩块体 26m

28 紫红色薄层石英粉砂岩　1m

27 火山岩夹层 1m

26　黄褐色石英粉砂岩, 发育软变形构造 1m

25 火山岩夹层 2m

24 紫红色粉砂岩、泥质粉砂岩 含灰岩透镜体，直径约 20cm，　该层厚约 27.4m

23　青灰色-紫红色薄层泥质粉砂岩 23.6m

22 紫红色石英粉砂岩夹薄层泥岩　2.5m

21 紫红色石英粉砂岩，向上位泥质粉砂岩　　3.3m

20 底部为石英砂岩，向上变为泥质粉砂岩　　2.1m

19 紫红色泥质粉砂岩 9.8m

18 灰白色薄层石英粗砂岩 2.1m

17 青灰色-紫红色石英粉砂岩，局部夹薄层粗砂岩　35.2m

16 灰-灰白色石英粗砂岩 2m

15　灰色石英粉砂岩　18.9m

14 灰白色薄层状石英粗砂岩　9.4m

13 灰色石英砂岩与泥质粉砂岩互层，砂岩破碎强烈 14.6m

12 灰白色石英粗砂岩夹少量泥质粉砂岩　20.3m

11 白色石英脉体　16.5m

10 青灰色石英细砂岩　2.5m

9 青灰色-粉红色泥质粉砂岩 9.2m

8 青灰色石英粉砂岩　1.3m

7 青灰色泥质粉砂岩 夹薄层细砂岩 21m

6 石英粗砂岩　3.8m

5 石英砂岩、石英细砂岩，上部为红褐色 泥质粉砂岩，破碎强烈 21.5m 4 青灰色石英中砂岩、石英细砂岩 1.3m

3 青灰色-褐红色石英粉砂岩、泥质粉砂岩互层　17.1m

2 青灰色石英砂岩和泥质粉砂岩互层　12.1m

1 青灰色石英粉砂岩、泥质粉砂岩和泥岩互层>5.1m

——未见底——

上述剖面可分三个岩性段。下段底部由灰色中薄层状泥岩、硅质泥岩夹薄层粉砂岩组成,向上变化为青灰色中厚层细砂岩夹紫红色薄层泥岩韵律层，中部出现青灰色厚层石英粉砂岩，夹少量灰白色薄层粗砂岩，具向上逐渐变粗的特点，砂岩中常具有水平层理，该段厚约 130m；中段层以紫红色薄层状韵律层理的粉砂岩为主，泥质粉砂岩和薄层硅质泥岩互层，偶夹薄层石英粗砂岩，砂岩中常具有水平纹层。顶段为韵律状泥质粉砂岩，零星分布椭圆形灰岩块体，逐渐过渡为滑塌堆积。滑塌堆积主要由灰白色杂砂岩中含有大小不等的块体，块体成分以灰岩为主，砂岩和硅质泥岩次之（详见“滑塌堆积单元”）。

4.1.2.2 鲍马序列特征和沉积环境

浊积岩常常发育向上变细的沉积层，组成一个沉积旋回，我们测量大比例尺浊积岩韵律剖面（图 4-1-11），以展示浊积岩沉积特点，由底向顶依次为：

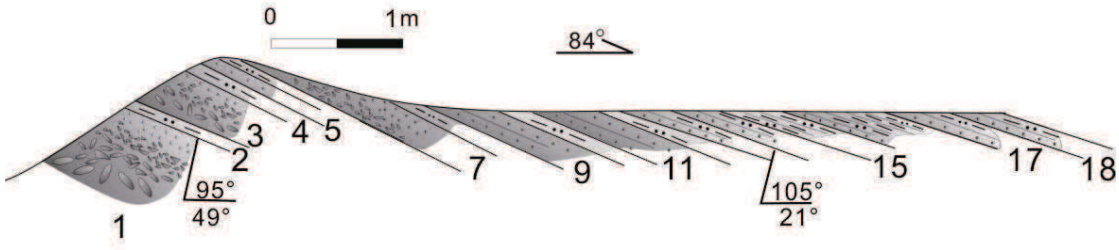

图 4-1-11 塔塔地区浊积岩沉积层序特征实测剖面图

18 灰色薄层细砾岩与薄层泥质粉砂岩层 25cm

17　灰色薄层细砾岩与薄层泥质粉砂岩层 22cm

16　底部为灰色薄层细砾岩，向上变为泥质粉砂岩、泥岩，整个沉积序列厚 55cm

15 灰色薄层状泥质粉砂 30cm

14 紫红色-灰白色薄层细砾岩与 灰色薄层状粉砂岩 35cm

13 灰白色薄层状细砾岩与灰白色薄层状粉砂岩互层 30cm

12 灰白色薄层粉砂岩 10cm

11 紫红色中厚层状砂岩 60cm

10 灰色薄层粉砂岩和粉砂质泥岩 12cm

9 褐红色中厚层状砂岩，夹少量薄层粉砂岩 40cm

8 灰白色薄层泥质粉砂岩 8cm

7 砾岩，砾径约 2-5mm，分选和磨圆一般，砾石成份主要为泥质片岩、粗砂岩和石英等 1m

6 灰白色薄层泥质粉砂岩 5cm

5 灰白色-紫红色细砾岩，向上变为含砾粗砂岩、粗砂岩，顶部为薄层粉砂岩 30cm

4 灰白色-紫红色薄层泥质粉砂岩 8cm

3 青灰色-紫红色含砾粗砂岩，向上变为粗砂岩 0.7m

2 灰色薄层泥质粉砂岩 10cm

1 紫红色含砾粗砂岩，底部含砾石，砾径在 2-25cm，成份以泥质片岩、火山岩和粗砂岩为主，分选较差，磨圆中等，向上粒度变细 1.2m

按照 Walker（1978）的浊流沉积相分类，这套浊积岩可归为四个相：A 相，为灰白、灰绿色厚层粗砂岩为代表，含有分散的砾石，具有正粒序平行层理，单层厚 0.5-1.2m，界面不规则，底部具冲刷面。B 相，由粗-细粒砂岩组成，块状结构或发育平行层理。C 相，典型的浊积岩，由鲍马序列 a,d,e 段组成。a 段是由砂级粒序组成，底部含砾石，有冲刷-填充构造，厚 20-100cm；e、d 段为泥岩和粉砂岩互层，具水平纹层，厚 2-10cm，在露头上紫红色和灰白色韵律式排列。D 相为细砂岩、粉砂岩和粉砂质泥岩组成的韵律层，以鲍马序列 Tbe 和 Tde 段较为常见（图 4-1-10E），该韵律层自下而上由三个单元层组成。砂质层：由中-细砂岩组成，碎屑颗粒下粗上细，岩石和矿物碎屑的分选程度低，磨圆度较差，以泥质胶结为主。少数底部为含砾-中细砂岩，砾石 2-5mm，呈杂乱状排列；底部下伏粉砂泥岩的界线为清晰的突变关系，或呈不规则的冲刷侵蚀接触。上部主要为泥质胶结的细砂岩，具明显的粒序递变性质。细-粉砂质层：具有较好的微细水平层理构造和小型爬升层理（图 4-1-10F）。粉砂-泥质层：主要为块状构造或者发育暗灰色的平行纹理层。

多数研究者认为浊积岩是重力流形成的一套分选较差，具明显韵律的砂质、粉砂质和泥质的浊流沉积，沉积厚度较大。浊积岩不仅可以形成于深海槽或者海沟环境中，而且也可以形成在大陆斜坡下部、广阔的深海盆、弧后盆地或者岛弧

边缘（Partha P. C. Et al., 2002;Belen Alonson &Gemma Ercilla, 2002; Grant W. L., 2007; Jacob A. C. et al., 2009; T.McHargue et al., 2011; 郭谦谦等，2013）。满都拉地区浊积岩单元以连续发育的鲍玛序列为特征。其中粗浊积岩代表了典型的浊积扇体顶部沟道相沉积，以发育 Tab 为特征，粒序层理和冲刷层理较普遍。该砂岩碎屑成分主要包括长石、石英、火山岩岩屑和泥岩岩屑，杂基含量较高，含较多的泥质和硅质成份，属于硬砂岩质浊积岩，具有深水性、浑浊和顺序卸载的沉积特征。细浊积岩为浊积扇远端产物，以鲍马序列 Tbe 和 Tde 段为主。细浊积岩层序在浊积岩沉积中占有较高比例，成为浊积岩单元主体部分。粗碎屑岩中大量的火山岩屑，说明浊流沉积同时区域上存在重要的火山活动，这与碎屑锆石数据相一致（见下文）。本文认为广泛分布的浊积岩沉积和滑塌堆积组合代表深水环境，并且具有一定的斜坡度，结合区域上同时期的岩石地层资料，反映为裂谷背景下的大陆斜坡环境（见下文）。

4.1.3. 哲斯组沉积单元 (The shallow water sediments, the Zhesi Formation)

哲斯组分布在满都拉地区中部，呈东西向展布，覆盖在北侧大石寨组火山岩之上（图 4-1-1）。自上世纪 30 年代哲斯组就受到国内外地质学家的关注，进行了较详细的古生物学和地层学研究，积累了丰富的地质资料（Grabau, 1931； 王惠等， 2002；尚庆华， 2004； 李尚林等, 2004）。哲斯组名称来源于满都拉城东哲斯敖包，主要出露一套含化石碳酸盐岩和细碎屑沉积岩。哲斯组地层分为三个段：一段为陆相灰色砾岩夹含砾不等粒长石岩屑砂岩及中细粒砂岩；二段为海相暗灰色中粒砂岩、钙质砂岩、粉砂质泥岩夹生物碎屑灰岩,局部发育生物丘(礁)；三段为陆相紫灰色复成份砾岩及含砾不等粒长石岩屑砂岩夹粉砂岩（李尚林等，2004，王惠等，2002）。哲斯敖包发育大量的生物礁，含有腕足类、珊瑚类苔藓虫和有孔虫生物化石，包括三个珊瑚组合带、分别为 *Plerophyllum crassoseptatum-tachylasm zhesiense* 组合带，*Pseudow aagenophyllum vesiculosum-Diphycarinophyllum* 组合带和 *Waagenophyllum stereoseptatum-Wentzelella* 组合带，年代为中二叠世晚期（~265Ma）（丁蕴杰等，1985；内蒙古自治区地质矿产局 1996；王惠、高荣宽，1999；刘鹏举和郭伟，1998；王惠等 2002；李尚林等，2004；尚庆华，2004；王平等，2006）。

我们的野外观察发现哲斯组包含数个砾岩-含砾粗砂岩-砂岩旋回组合，之上

发育化石灰岩、生物碎屑灰岩。单个旋回的厚度多为米级，底部砾石含量 20-40%之间，以火山岩、砂岩和泥质砾石为主，有时可见少量灰岩砾（图 4-1-12A）。砾石分选很差，但是磨圆较好，向上顶部粗砂岩分选和磨圆一般，发育块状层理或平行层理，与底部砂岩常呈突变接触（图 4-1-12B）。单个旋回侧向追索延伸较远，有时则尖灭于另外沉积旋回。纵向上，常常数个旋回叠加，构成一套沉积组合，厚度可达十几米至几十米。

哲斯组灰岩主要为含化石灰岩、生屑灰岩、含硅质条带灰岩等。在满都拉城西部主要为生物礁灰岩，地貌上呈孤立的的跺体，杂乱分布在砂岩、砾岩之上。在满都拉城东哲斯敖包附近哲斯组灰岩主要由灰色礁屑砾泥灰岩、细晶生物碎屑灰岩和条带状或团块状硅化生物碎屑灰岩组合（图 4-1-12C），岩层厚 15-30cm 不等，局部可见渣状灰岩，表明存在短暂的暴露。含丰富的化石，主要为海百合、腕足类、珊瑚和腹足类。满都拉城北部，哲斯组灰岩以角砾灰岩为主。逐渐过渡为砂屑灰岩至泥质灰岩，岩石中碎屑成份主要为破碎的生物残骸。

满都拉地区东北一带，哲斯组地层主要由互层的薄层状的石英长石砂岩、钙质粉砂岩与粉砂质泥岩构成，局部夹泥晶灰岩薄层。砂岩顶部常被生物礁灰岩和条带状硅质灰岩覆盖，这些灰岩遭受了褶皱变形（图 4-1-12D）。

满都拉中部的哲斯组主要为紫色变质钙质粉砂岩与变质粉砂质泥岩互层，夹变质细砂岩，泥晶灰岩薄层。满都拉南部哲斯组为灰色变质粉砂岩，变质细砂岩、生物碎屑泥晶灰岩互层，含丰富的动物化石。值得注意的是，前人研究认为哲斯组主要为碎屑岩和碳酸盐岩组成，并且不整合覆盖在大石寨组火山岩之上。但是我们在哲斯组地层中却发现有火山岩夹层（图 4-1-12E），而在大石寨组火山岩和哲斯组砾岩之间，为平行整合关系（图 4-1-12F）。其详细的地质剖面（图 4-1-12）和层序描述如下：

——未见顶——

12 灰白色薄层状石英粉砂岩，中间夹中层状生物碎屑灰岩 >100m

11 灰白色-紫红色厚呈状砂质灰岩和含砾粗砂岩层，砾石含量 10-15%，成分含灰岩砾石，大小 2-5mm，以块状层理和粒序层理为主 28m

10 灰白色薄层状生物碎屑灰岩、生物化石灰岩和钙质细砂岩互层 94m

9 土黄色-灰白色粉砂岩，向上为厚层状生物碎屑灰岩、生物灰岩 286m

8 土黄色火山岩层，厚约 2m，延伸较远，产状稳定 22m

7 灰白色厚层状生物化石灰岩 153m

6 底部为灰白色中薄层状粗砂岩-砂岩，顶部为厚层状细砾岩，砾石大小 1-2cm，分选和磨圆良好，单层厚度大于 1m 总厚度 217m

5 紫红色-灰白色厚层状砾岩-粗砂岩-砂岩旋回，底部砾岩含量约 20%，砂基支撑，砾石成份以火山岩、砂岩为主，含少量灰岩（5%），发育粒序层理，顶部砂岩中常见水平层理 427m

4 喷发火山角砾岩、集块岩，角砾大小约 10-30cm 左右，呈棱角状-次棱角状，杂乱分布，成分以酸性火山岩为主，基质为火山凝灰岩 37m

3 底部为灰色-褐色砾岩层，向上变为细砂岩、粉砂岩和泥岩。底部砾岩分选和磨圆均较差，呈棱角状-次棱角状，大小 2mm-20cm 不等，粉砂岩和泥岩中常含火山岩透镜体，或呈薄层状沿地层逐渐尖灭 223m

2 褐色-灰色厚层状砾岩、含砾粗砂岩和粗砂岩互层，砾石含量约 30%左右，分选较差，磨圆较好，成份复杂，含火山岩、石英、泥岩砾石和灰岩砾石 85m

1 酸性火山岩与灰色薄层状凝灰质细砂岩、长石砂岩互层，火山岩土黄色，风化色灰绿色，块状结构，呈透镜状或薄层状产出，厚度不等，薄层为 20cm 左右，厚者几十米，延伸较远；砂岩成份主要以长石为主，分选较差，杂基含量较高 >50m

——未见底——

综上所述，哲斯组底部为巨厚层火山质砾岩、砂砾岩及少量中粗粒岩屑砂岩组成，砾岩中砾石大小混杂，杂基支撑，呈次棱角－浑圆状，分选极差，成分以火山岩为主，少量碳酸盐岩、脉石英，与下伏大石寨组组成可对比，表明物源来自大石寨组火山岩，底面发育侵蚀构造，常见粒序层理，块状层理、平行层理等沉积构造，具有陆相沉积扇的沉积特点，代表一种快速垂向加积的重力流沉积。中部为细砾岩、含砾粗粒火山岩屑砂岩、中厚层细粒岩屑砂岩、生物碎屑灰岩和化石灰岩，含海百合茎、珊瑚类等化石，发育水平层理，属于滨外浅海相沉积环境，但是局部可见渣状灰岩，表明存在短暂的暴露。需要注意的是与前人发现不同，在碳酸盐岩中含有少量的火山岩夹层，说明周围存在火山岩活动，其喷发环境为滨岸相喷发-沉积环境。结合区域地层和岩浆资料，哲斯组沉积特征指示在中-晚二叠世满都拉裂谷表现为海陆交互沉积环境。

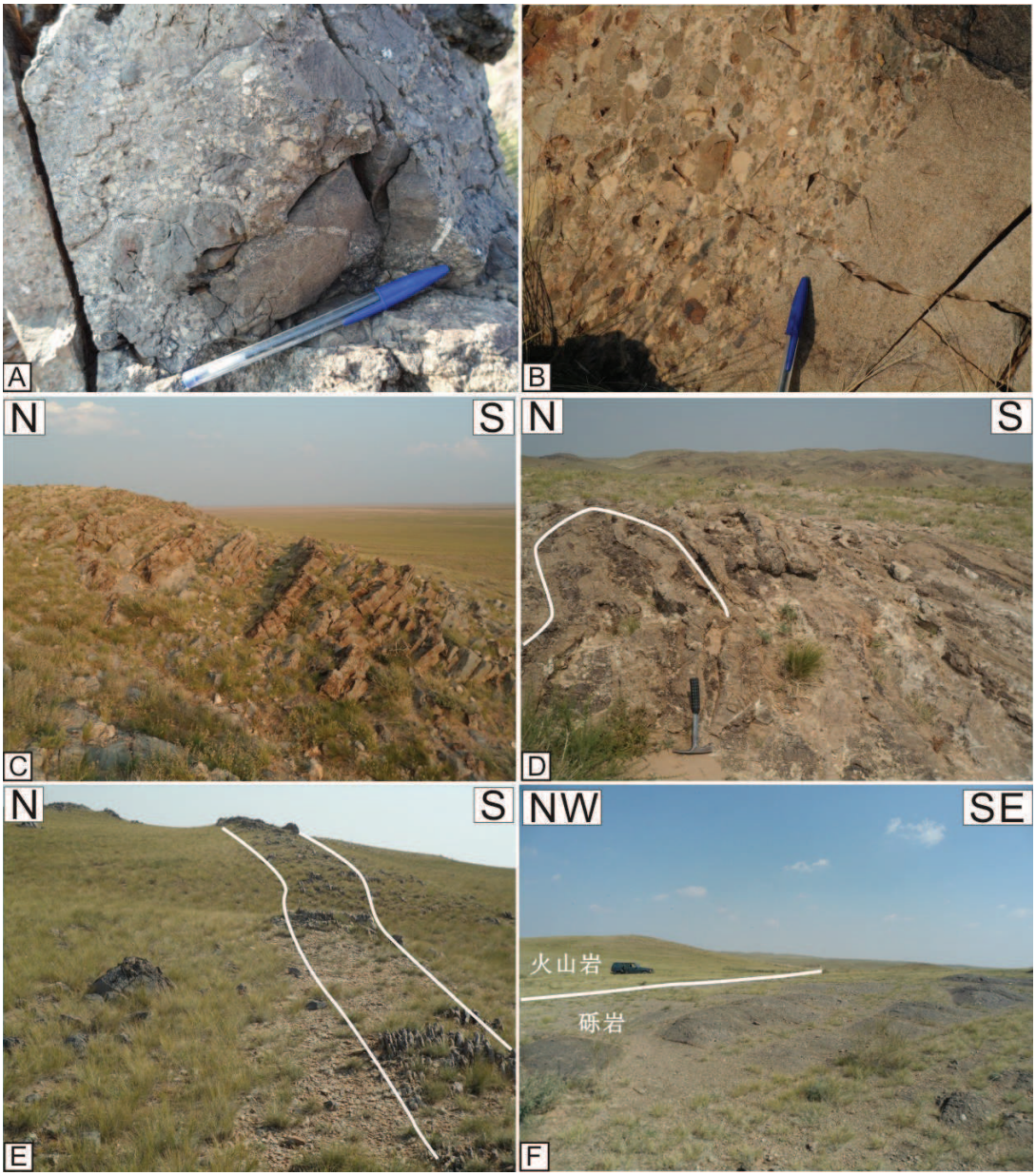

图 4-1-12 满都拉地区哲斯组沉积特征露头图片

A:哲斯组底部砾岩层，砾石含量 20-40%之间，以火山岩、砂岩和泥质砾石为主，砂基支撑，分选差，磨圆一般；B：哲斯组地层由多个砾岩-砂岩旋回组成，旋回之间突变接触。粗砂岩（右下）发育块状层理或平行层理；C：哲斯敖包附近哲斯组发育中-薄层状礁屑砾泥灰岩、生物碎屑灰岩和条带状组合，劈理不发育，灰岩底部未发现断层有关构造，说明为原地地体，层序正常；D：满都拉地区东北一带，砂岩顶部被条带状硅质灰岩覆盖，灰岩遭受了褶皱变形；E：哲斯组地层中含有薄层火山岩层，宽 1m 左右，片理化，火山岩两侧为灰岩；F：哲斯组底部砾岩覆盖在大石寨组火山岩之上，产状平行

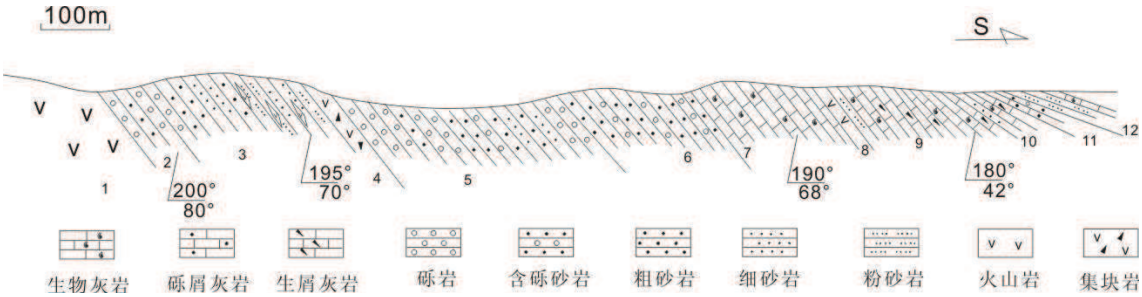

图 4-1-13　满都拉地区哲斯组沉积层序实测剖面

4.1.4 大石寨火山岩单元 (the Permian volvanic rocks, the Dashizhai Formation)

研究区火山岩包括主要包括分布在满都拉城南的基性火山岩以及东、北部的大石寨组中酸性火山岩，本文统称为大石寨组火山岩。

基性火山岩位于满都拉城南 15km 区域，总体呈东西向展布，南部被中生代沉积物覆盖，北部与浊积岩单元断层接触，主要由深灰、灰绿色玄武岩组成，下部为灰绿-灰黑色块状、枕状玄武岩，中部为深灰绿色、紫色气孔杏仁状细碧岩，上部为深灰绿、灰黑色气孔杏仁状、块状玄武岩，厚度大于 2130m（苏新旭等，2000）；该基性火山岩同时伴生一系列辉长岩和闪长岩深成侵入岩系列。在基性岩中常含有细碎屑沉积层（图 4-1-14A），为一套灰、灰紫、灰绿色凝灰质板岩、粉砂质板岩夹变质中细粒岩屑长石杂砂岩、变质泥砾岩以及硅泥岩，总体特征为硅泥质成分较高，沉积物粒度较细，岩层厚度较小，厚度多为厘米级。镜下鉴定表明，这些基性岩具有斑状结构，斑晶含量 10%左右，主要为辉石、斜长石，斑晶多为长柱状、板条状分布于基质中；基质为间粒-间隐结构，斜长石杂乱交错，其间隙常被辉石颗粒或隐晶质物质填充（图 4-1-14B）。气孔或杏仁状玄武岩，斑状结构、基质变余间隐结构，块状或杏仁状构造，斑晶斜长石呈自形柱状，发生蚀变。基质含细小的斜长石微晶，气孔含量约 10-15%，多被石英、钙质或绿泥石填充（图 4-1-14C）。枕状玄武岩，由玄武质枕状体堆积而成，岩枕直径约半米左右，表面发育冷凝边结构。球粒玄武岩（图 4-1-14D），以球颗结构为特征，球颗大小约 0.3-1cm 不等，多呈圆形。我们在基性岩中选取了岩石进行年代学分析，年代为 ca.280-290Ma，与前人结果相似，值得注意的是，其中有 ca.430Ma 的继承锆石（见下文）。

图 4-1-14 满都拉地区南玄武质火山岩露头特征和显微特征图片

A：玄武质熔岩中含薄层状细碎屑沉积层，凝灰质和硅泥质成份含量较高，发育水平纹层；B：玄武质熔岩少斑状结构结构，斑晶辉石、斜长石，基质为间粒-间隐结构，斜长石杂乱交错，其间隙常被辉石（绿泥石化）或隐晶质物质填充；C：杏仁状熔岩，斑状结构，斑晶发生蚀变，杏仁状多被绿泥石或长英质集合体填充（箭头处）；D：球粒玄武岩，球颗结构，圆形球颗大小约 0.3-1cm 不等

大石寨组分布在研究区的北部，总体呈东西向展布，主要由蚀变石英安山岩、气孔安山岩，变英安岩、凝灰岩组成，夹有较厚的灰黄色中粒岩屑砂岩与变质含砾粗粒岩屑砂岩沉积，局部可见火山碎屑岩、火山碎屑沉积岩层。我们在满都拉城东绘制了火山岩-沉积岩剖面（图 4-1-15），描述如下：

——未见顶——

14 底部为青灰色薄层凝灰岩和凝灰质粉砂岩，顶部为沉火山岩碎屑岩 >86m

13 岩性为暗灰色含砾粗粒岩屑砂岩，中细粒岩屑砂岩，夹数层英安岩 98m

12 底部为灰色安山岩，块状构造，斑晶为斜长石和石英，含量 40-50%，大小在 0.2-0.6mm 左右，上部为土黄色酸性火山岩夹细粒岩屑砂岩 226m

11 酸性火山岩层夹少量砂岩夹层 >66m

——第四纪覆盖——

10 灰紫色、灰绿色蚀变安山岩、气孔状蚀变安山岩夹凝灰质细砂岩、粉砂岩层，发生片理

化　92m

9 薄层状凝灰质粉砂岩，含火山岩薄层 顶部为粉红色硅质泥岩　149m

8 底部为土黄色层状火山岩，块状结构，上部为中细粒凝灰质砂岩，顶部被灰岩块体覆盖 >66m

7 底部为凝灰质细砂岩和粉砂岩，顶部多为硅质泥岩沉积，夹少量火山岩夹层，单层厚度 7-10cm 不等　167m

6 灰黄色中粒岩屑砂岩与含砾粗粒岩屑砂岩互层，含少量凝灰岩夹层　63m

5 黄褐色厚层状酸性火山岩，块状结构　98m

4 土黄色火山岩层，单层厚度在 20-50cm 不等，顶部多为硅泥质岩和凝灰岩层 113m

3 黄褐色火山岩层与灰黄色变质中粒岩屑砂岩、粉砂岩互层 102m

2 褐黄色石英安山岩，块状构造，斑状结构，斑晶多为石英和长石，含量约 25%左右，基质为长英质微晶，石英发育溶蚀港湾结构　52m

1 火山角砾岩、集块岩，角砾大小约 20 cm 左右，呈棱角状-次棱角状，成分以酸性火山岩为主，间隙多被细火山碎屑及火山灰填充　>30m

——未见底——

该剖面从北向南发育一系列枢纽近东西向的褶皱中。剖面下部主要由一套石英安山岩、英安岩、凝灰岩和中细粒凝灰质砂岩，碎屑成分以长石和岩屑为主。火山岩具有以爆发火山角砾岩—熔岩—沉积岩的组合特征（图 4-1-16A 和 B），岩层厚度不等。火山角砾岩的角砾成分以安山岩、英安岩为主，角砾含量 30%-50%，基质多为凝灰质成份；其次为火山碎屑岩，碎屑以晶屑、玻屑为主，含量 20%左右（图 4-1-16C），可见少量凝灰质砂岩的角砾。熔岩类主要包括安山岩、石英安山岩和英安岩等。熔岩为致密块状构造或杏仁状构造，斑状结构，斑晶含量 10%-15%，斑晶主要成分为斜长石、石英。基质为交织结构或玻基交织结构，针状或柱状斜长石微晶彼此密集排列，有时略具一定的方向性。剖面中部主要出露熔岩—沉积岩组合或熔岩-碎屑岩-灰岩组合，沉积岩主要由凝灰质砂岩、粉砂岩组成，碎屑以长石和岩屑为主，中薄层状，水平层理较为常见（图 4-1-16D），有时可见生物化石灰岩（图 4-1-16E），呈块状或薄层状覆盖在火山岩熔岩之上。剖面上部出露厚层状的英安质和流纹质火山熔岩，中间夹杂侵入岩体，岩石外貌呈灰色至黄灰色，似斑状结构、块状构造或流纹状构造（图 4-1-16F），斑晶主

要为主要为斜长石，少量石英，呈自形板状，粒度一般小于 1.5mm。层序中含有较多含砾粗粒岩屑砂岩和凝灰质砂岩，同样具有火山岩熔岩-沉积岩组合韵律。

从火山作用相的角度分析，大石寨组火山岩可以划分为溢流相、爆发相、爆发沉积相和次火山岩相。溢流相由安山岩、石英安山岩、英安岩组成（层 2、5、10、12 等），厚度巨大，呈互层或夹层产出，其间发育沉积夹层。火山熔岩常见块状、气孔杏仁状构造。爆发相以火山角砾岩为代表，分布局限（层 1），多呈透镜状或薄的夹层产出，延伸不稳定。爆发沉积相：以凝灰质砂岩、凝灰质粉砂岩为代表岩性（层 4、6、7、9 等），呈夹层透镜状产出。在火山岩喷发间歇期，则主要发育细碎屑砂岩、生物灰岩和生屑灰岩。次火山岩相表现为主要为玢岩、安山质或英安质浅侵岩，多呈脉状产出（层 12）。

大石寨组火山岩主要由数个火山岩碎屑岩—熔岩—沉积岩组成，从下往上火山岩间歇期的碎屑岩和碳酸盐岩的厚度具有增厚的趋势，说明火山活动逐渐减弱，沉积作用逐渐加强。研究区出露的火山岩主要为中酸性为主，代表性的熔岩为石英安山岩、英安岩和流纹岩。值得注意的是，火山岩夹层多为薄层状长石岩屑砂岩和硅质泥岩，砂岩成分成熟度较低，但是碎屑分选和磨圆均较好，发育水平层理，其中含数层生物灰岩和生屑灰岩薄层或透镜体，说明喷发环境为滨岸和滨外环境。 地球化学研究显示大石寨组火山岩具有双峰式火山岩的特征（Zhang et al., 2011）， 因此研究区大石寨组是在二叠纪裂谷背景下发育的滨岸和滨外沉积环境。

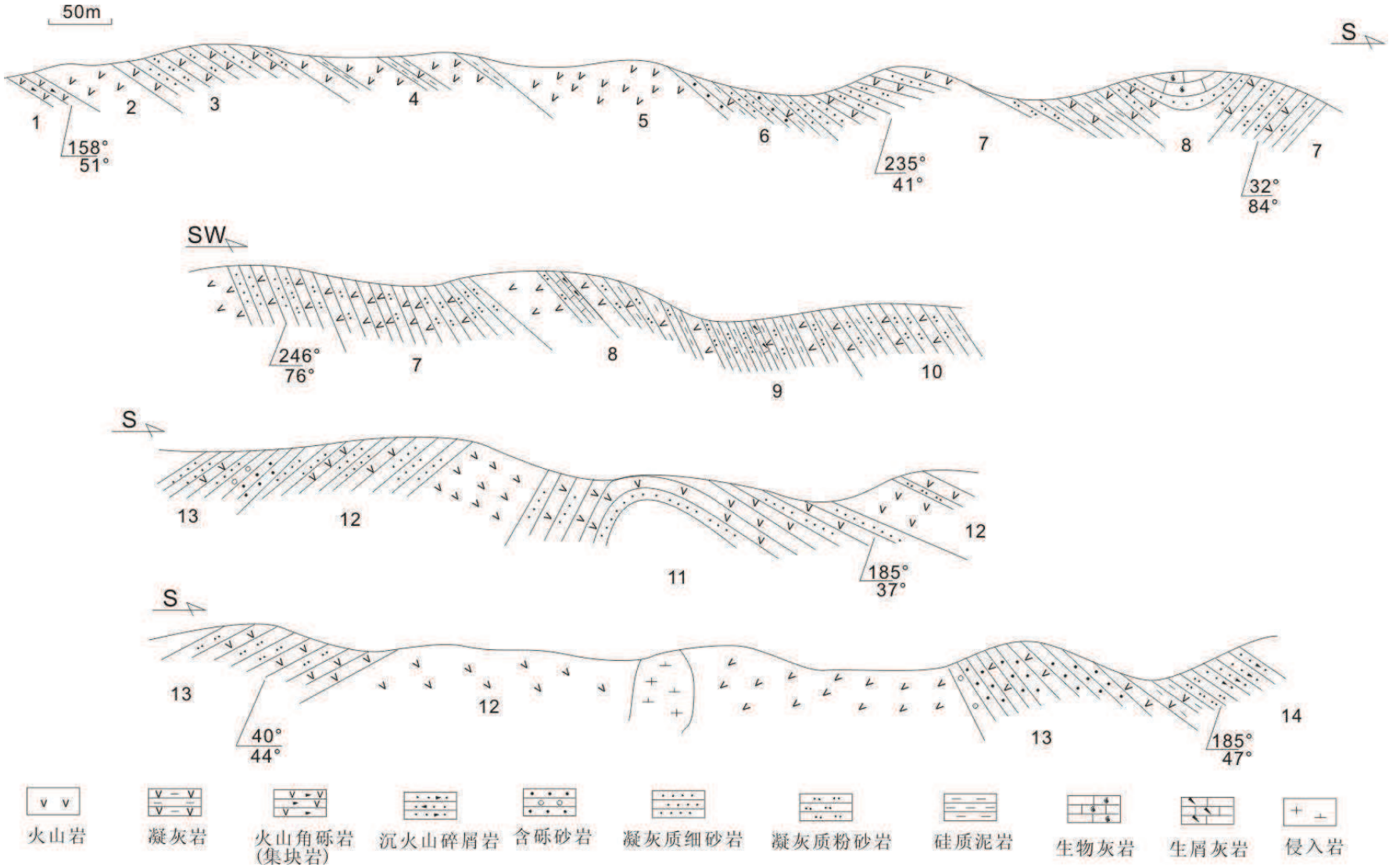

图 4-1-15 满都拉城东大石寨组火山-沉积岩层序特征实测

图 4-1-16　满都拉地区大石寨组露头图片

A：火山熔岩和沉积岩层露头宏观特征，左上为安山质熔岩，右下为薄层状砂岩沉积；B：紫红色砂岩沉积夹灰绿色蚀变安山岩层，劈理发育；C：火山岩碎屑岩，碎屑多为晶屑，基质凝灰质成分为主；D：火山岩中夹薄层状长石岩屑砂岩，常见水平层理，劈理发育；E：火山岩层内夹化石灰岩，化石包括珊瑚类、海百合茎等；F：大石寨组顶部的流纹岩，发育流纹构造

第二节　满都拉地区变形特征分析 (the structural and kinematic analysis in the Mandula area)

满都拉地区位于早古生代混杂带北部，其南部属于华北板块，北部属南蒙古微陆块南缘（Xu et al.,2012）。前文详细叙述了构造岩石单元的特征。我们通过野外考察，分析了满都拉地区的各个岩石构造单元的变形特征（图 4-2-1），

并统计了其面理、线理和劈理分布特征，下面分别进行说明：

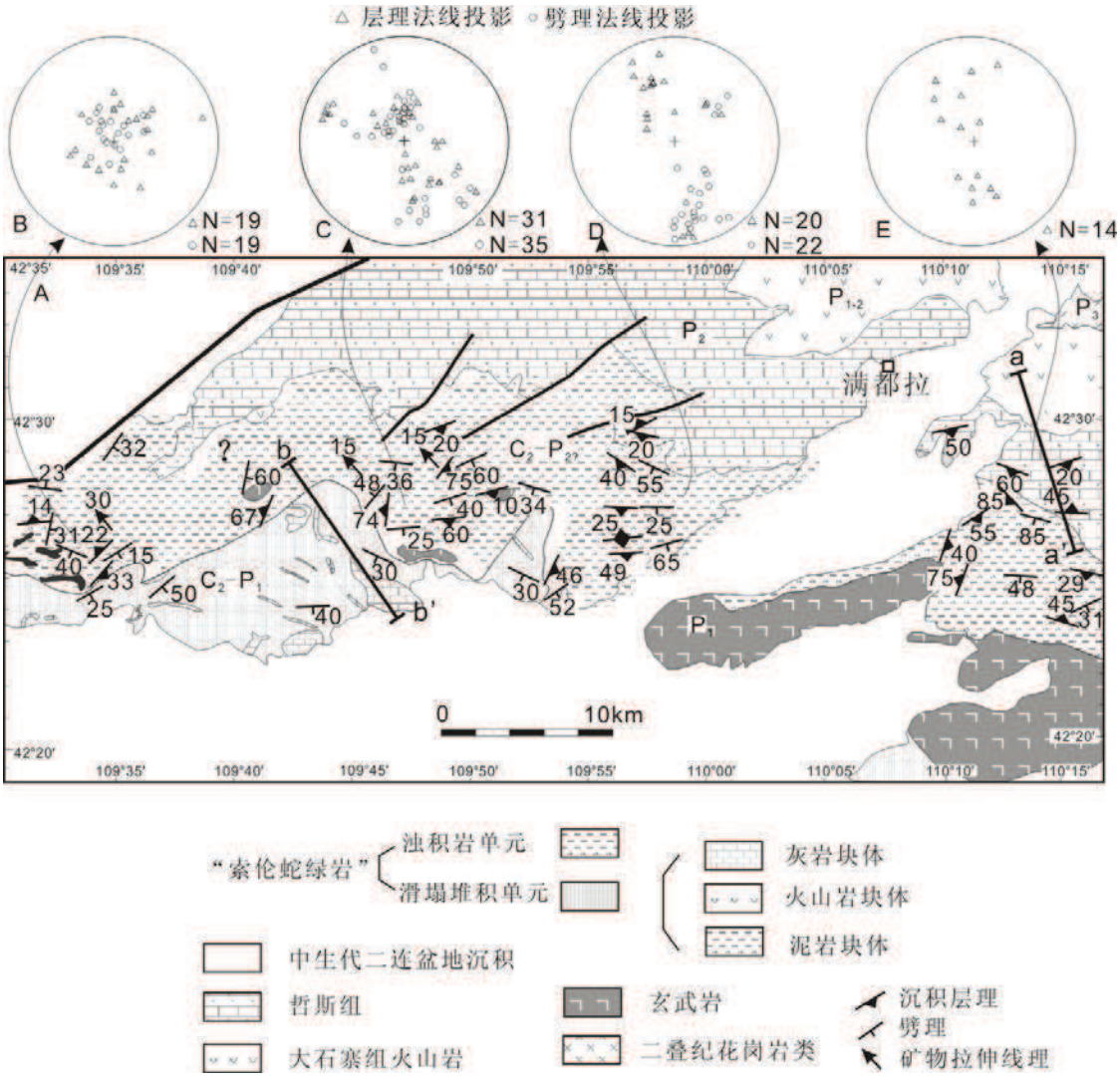

图 4-2-1 满都拉地区构造变形特征简图

4.2.1 浊积岩单元和滑塌堆积单元 (The structure of the olistostrome and turbidite units)

整个满都拉区褶皱变形比较普遍，原生层理 S_0 作为参考面，褶皱表现为歪斜、倒转甚至平卧褶皱，轴面缓倾角，如我们在浊积岩单元中发现薄层火山岩夹层，表现向 N 倒倾的倾卧褶皱，褶皱轴 EW 向，近水平（图 4-2-2A）。轴面劈理极其发育，在转折端可以看到层理与劈理正交或斜交,在两翼轴面与层理近于平行。轴面倾向多为南东倾，倾角 40-50 之间，褶皱与枢纽平行。露头上可见轴面劈理 S_1 与 S_0 呈角度切割关系，交角一般 10-60 度，劈理产状南倾，倾角 10-50 度之间，近东西向延伸（图 4-2-2B）。宏观露头上很难观察到大规模倒转褶皱，

通过原生面理和劈理关系可知，褶皱的两翼不对称，指示褶皱为 NW 向倒倾(图 4-2-2B 和 C)，所以区域上均表现为向北逆冲倒转褶皱作用的特点。该期片理、劈理同时反映了一定程度的逆冲作用。从统计层理和劈理的关系数据看，劈理分布较为分散，走向总体呈近 NE-SW 向分布（图 4-2-1B，C 和 D），可能与近 NW-SE 向挤压缩短作用有关。在褶皱的翼部，劈理和层理近平行（图 4-2-1B），而在核部劈理和层理角度相交（图 4-2-1C 和 D）。由于未发生强烈的变质和构造置换作用，岩层中一些交错层理、平行层理等保存良好。在一些细浊积岩沉积中（Tde），发育良好的层内 A 型褶皱，褶皱轴走向 NW，褶皱表面保存较好的 NW-SE 向拉伸线理（图 4-2-2D）。浊积岩地层中未发现韧性剪切作用形成的糜棱岩的现象，但是在浊积岩 Ta 段，可见一些砾岩层的砾石压扁拉长，其长轴为 NW-SE 向（图 4-2-2E），在镜下这些拉长的砾石形成典型的 σ 碎斑，指示顶部向 NW 向剪切运动（图 4-2-2F）。

滑塌堆积单元覆盖在浊积岩单元之上，同样遭受了近 NW-SE 向的缩短作用，表现为基质内发育的细鳞片状片理和扁平的砾石（图 4-2-2G）。野外见到一些硅化的火山岩块体，性脆而破裂，节理发育，剪切滑动变形迹象明显，块体呈叠瓦状排列（图 4-2-2H），在岩体上到处可见擦痕镜面、擦痕线理，线理近 NW-SE 向。这种强烈挤压或剪切滑动的迹象表明，它们同样经历了比较近 NW-SE 向的挤压作用。

4.2.2 大石寨组火山岩和哲斯组沉积岩 (The structure of the Dashizhai and the Zhesi Formation)

大石寨组火山-碎屑积岩经历了同样的褶皱作用，但是透入性的劈理仅在局部可见，主要集中在沉积岩夹层中，在厚层火山岩中较少见。劈理近直立，分布较为分散，总体走向为近 NNE-SSW（图 4-1-13B 和 D）。区域上这些褶皱以开阔褶皱为主，波长数几百米不等，枢纽近水平，呈 E-W 或 NNE 向。

哲斯组分布在大石寨组南两侧，呈东西向展布。我们的野外观察发现，哲斯组发育了一系列的次级褶皱，褶皱枢纽近水平，倾角 10°左右，背斜倾伏端大多指向南东，向斜扬起端指向北西。褶皱规模大小不等，一般几十米-几百米。哲斯组砾岩和碳酸盐同样卷入轴向近 E-W 的褶皱，但是劈理发育不明显（图 4-2-1E）。

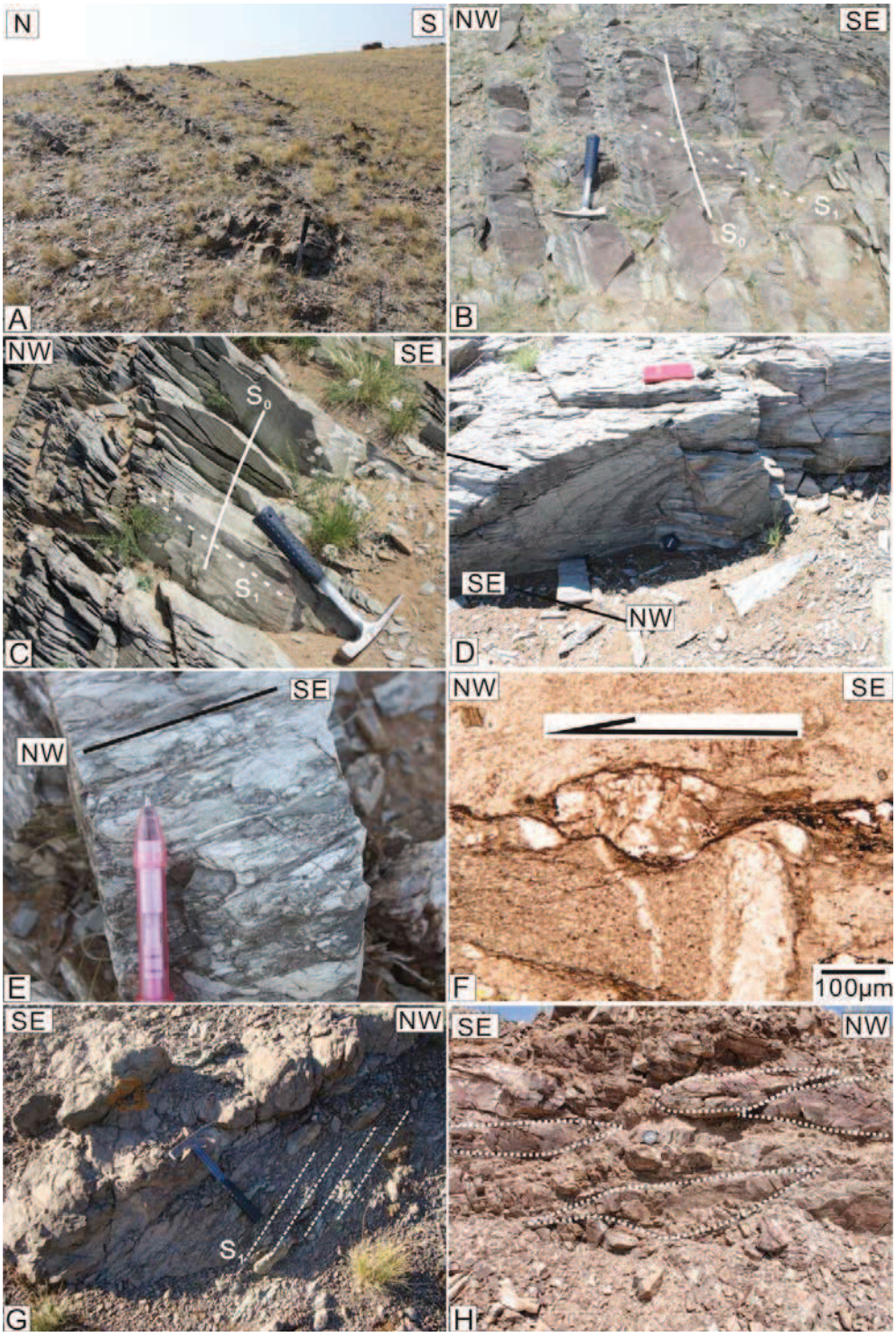

图 4-2-2 满都拉地区岩石地层变形特征露头图片

A：浊积岩单元中火山岩夹层发育倾卧褶皱，轴面近水平，轴向近 E-W；B：粗浊积岩沉积（Tab、Tbd）砂岩层理和劈理大角度相交，指示 NW 倒倾的不对称褶皱作用；C：细浊积岩沉积（Tde）砂岩层理和劈理大角度相交，指示 NW 倒倾的不对称褶皱作用；D：局部可见细浊积岩沉积的层内 A 型褶皱，褶皱表面拉伸线理 NW-SE 向；E 和 F：浊流沉积 Ta 段被定向拉长（E），显微组构显示具有顶部 NW 向的运动性质。G：滑塌堆积粉砂质泥岩基质发育鳞片状劈理；H：一些硅化火山岩块体被扯断，呈叠瓦状排列

通过大石寨组沉积剖面的绘制，识别出三个向斜和二个背斜构造（图4-1-15），褶皱核部分别位于层 7、8、11、13、；其中层 8 向斜核部由大石寨组薄层生物灰岩组成，南翼产状倾向 0-30° 倾角 50-80° 北翼相对倾角较缓，主要由薄层火山岩和凝灰质砂岩层构成。层 11 背斜卷入地层主要为层状火山岩，南翼，倾向 175-200° 之间，倾角较缓，一般在 30-40° 之间。 因此这些褶皱组合表现为轴面略南倾的非对称特点。

第三节 小结 (Summary)

根据岩石的沉积、结构特征，我们将满都拉地区划分为了 4 个次级岩石结构单元，它们分别为滑塌堆积、浊积岩、火山岩单元和哲斯组海陆交互沉积。

滑塌堆积块体包括灰岩、砂岩、火山岩和硅质泥岩，基质由半有序-无序的杂砂岩和泥岩组成。该单元同时保存一些原生的沉积变形构造，如非共轴褶皱，小型错断等，在一些块体中发育韧性拉伸线理，指示近 N-S 向的滑塌运动。由于灰岩中含化石组合与红旗牧场阿木山组生物礁灰岩相似，推测滑塌物源应该来自南部地区。滑塌堆积单元与北侧的浊积岩单元没有截然的分界线，具有逐渐过渡的关系。

满都拉地区浊积岩单元以连续发育的鲍玛序列沉积为特征，其中粗浊积岩以 Tab 段为主，粒序层理和冲刷层理较普遍，代表典型的浊积扇体沟道相沉积。细浊积岩组合中 Tcde、Tde 较为普遍，代表为浊积扇远端产物。根据满都拉地区滑塌堆积和浊积岩的岩石组合特点及分布特征，我们认为它们沉积环境可能大陆斜坡深水环境，由于区域上的火山喷发活动或地震等事件，导致沉积物失稳，形成的一套滑塌沉积。

研究区同时期发育有南部的基性熔岩和北部大石寨组中酸性火山岩。基性熔岩主要由主要由深灰、灰绿色玄武岩组成，夹细碎屑沉积岩层，玄武岩发育球颗构造和枕状构造，具有水下喷发特征。大石寨组主要由火山岩角砾岩、安山质和英安质熔岩、凝灰岩组成，夹有较厚的中粒岩屑砂岩与含砾粗粒岩屑砂岩沉积。大石寨组沉积层序由数个火山爆发—溢流—喷发间歇沉积组成。沉积岩夹层主要为为薄层状长石岩屑砂岩，虽然成分成熟度较低，但是碎屑分选和磨圆均较好，发育水平层理，代表滨外沉积环境，说明火山喷发环境为滨岸相。

野外露头显示哲斯组覆盖在上述单元之上，主要为巨厚层火山质砾岩、砂砾岩、中粗粒岩屑砂岩及化石灰岩组成，包含无数个砾岩-粗砂岩-细砂岩正旋回，每个旋回底部发育粒序层理，块状层理等，显示有冲积扇的沉积特征。生物碎屑灰岩和化石灰岩，含海百合茎、珊瑚类等化石，发育水平层理，属于滨外浅海相沉积环境。因此我们认为哲斯组代表了一套海陆交互沉积。满都拉南部玄武岩、浊积岩沉积特征显示为深水环境，而满都拉北部显示为滨岸相和海陆交互相，暗示中二叠世期间，满都拉地区具有南深北浅的沉积古地理特征。

这些地层单元都卷入一期近 NW-SE 向的褶皱缩短作用。在岩石能干性不同的单元，表现为不同的变形样式。在浊积岩单元主要表现为同斜、倒转和平卧褶皱，轴面缓倾角，轴面劈理很发育，在转折端可以看到层理与劈理大角度相交。根据原生面理和劈理关系可知，褶皱为 NW 向倒倾的非对称褶皱。能干性较强的火山岩层和哲斯组厚层砂岩、砾岩则表现为宽缓的中常褶皱，枢纽近水平，走向变化较大，但是总体呈 E-W 或 ENE-WSW 向，野外产状特征显示为南缓北陡的非对称特征。褶皱中轴面劈理不甚发育，仅在局部薄层沉积岩夹层中可见。这期褶皱作用与区域上一次近 NW-SE 向的挤压运动相关，卷入最新地层为滑塌堆积单元，因此其时代应在滑塌事件之后（详见第六章）。中新生代研究区以差异性升降的断陷盆地和坳陷盆地为主，控制了白垩系、古近系的沉积（Meng，2003）。

第五章 造山带的年代学约束（the Time Constraints）

前文对红旗牧场地区、温都尔庙地区和满都拉地区的地质组成进行了详细的描述，将其划分为多个次级岩石构造单元。有些岩石地层单元前人已经进行了详细的年代学研究，如白乃庙岛弧。对新识别的一些次级单元，除了根据地层切割关系外，缺少精确的年代学约束。有些沉积岩地层，除了年代约束外，其沉积物源以及与区域构造演化的关系，还值得深入探讨。因此本次研究将在岩石构造单元详细划分的基础上，一方面总结前人已有的年代学成果（见附录 1），另一方面进行锆石 U-Pb 年代学测定，对各岩石地层单元的年代和物源进行分析，为构建整个造山带构造演化进程提供年代依据。

第一节 试验方法 (Analytical methods)

5.1.1 样品处理 (Sample experiment process)

锆石分选在河北省廊坊地调院进行，采用常规重液和电磁分选方法，同时结合双目镜下手工挑选。在挑选时要求不区分粒度、颜色和自形程度，尽可能的全部挑出，挑选过程中尽量避免人为筛选。本次试验过程中，玄武质（辉长质）火山岩中锆石样品，单位重量内获得锆石数量较少，碎屑砂岩中锆石含量丰富，每件样品可挑选出 2g 以上锆石。将挑选出来的锆石用树脂固定制成样品靶，贴靶过程中，同样对锆石进行随机挑选，不考虑颗粒大小、颜色及晶形特征，每件碎屑岩样品选取 200 颗以上制靶，火山岩颗粒一般全部贴靶。经过磨制抛光，粘于样品靶面的锆石内部剖面得以完全暴露。对制好的样品靶进行反射光、透射光及阴极发光(CL)照相，以获取锆石的结晶形态及内部结构信息，用以选取合适的区域进行 U-Pb 同位素测定。选取测试点时，综合考虑锆石样品的反射光、透射光和 CL 环带特征，要求避开避开包裹体、裂隙以及核-幔-边交界的位置，以保证年龄结果的准确性。对碎屑岩样品，选择锆石时候，实行随机选择的方式，尽量规避人为筛选。锆石阴极发光(CL)照相在北京大学造山带与地壳演化实验室和北京大学显微镜室完成，设定场发射环境扫描电子显微镜高压(HV)10kv，电流值(SP)5，工作距离 8.0 mm。

5.1.2 LA-ICP-MS 锆石 U-Pb 定年 (LA-ICP-MS dating methods)

激光剥蚀电感藕合等离子质谱(Laser Ablation Induetively Coupled Plasma-Mass spectrometry)，简称 LA-ICP-MS，是近期发展起来的一种原位分析方法，具有成本低，测试速度快等特点，适用于大量样品的分析。本文研究过程中，我们主要采用 LA-ICP-MS 对岩石样品进行锆石 U-Pb 定年分析。实验过程中，使用标准锆石外标校正的方法，以克服激光剥蚀和物质传输过程中出现的质量歧视和同位素分馏效应（Black et al., 2004)。 LA-ICP-MS 锆石 U-Pb 定年分别在中国地质大学(北京)地质过程与矿产资源国家重点实验室完成和北京大学造山带与地壳演化实验室进行。 实验过程中采用 He 气作为载气，Ar 气作为补偿气。每次分析先采集约 20-30s 的气体空白，然后采集 50S 的样品信号。采用 91500 锆石作为 U-Pb 定年校正的外部标准样品，采用青湖样作为内部校正样品，大约每 5 个样品后重复测定标样。91500 锆石 U-Th-Pb 同位素比值的标准值选用 Wiedenbeck 等(1995)数据。样品的同位素比值计算采用 GLITTER(Ver4.0 Macquarie University)程序，实验数据运用 Anderson（2002）方法进行同位素比值的校正，以扣除普通 Pb 对测试结果的影响。对岩浆岩样品一般选取 30 个点进行测试并计算。碎屑岩样品则随机选取大于 65 个颗粒进行统计。实验中采用 8Hz 的激光频率和 32μm 的激光束斑。 $^{206}Pb/^{238}U$ 加权平均值计算使用 ISOPLOT 程序（Ludwig,2003)。单点测定的 U-Th-Pb 同为素比值和年龄误差为 1σ，加权平均年龄结果为 95%的置信度。值得提出的是，尽管选点时已对照锆石透、反射光照片，尽可能避开包裹体和裂隙，仍根据元素信号的波动情况，剔除可能受到干扰的数据。根据 Th/U 比值并结合 CL 图像,对锆石成因进行分析。一般认为典型的变质成因锆石,Th/U 比小于 0.1,而 Th/U 大于 0.3 则指示岩浆成因(Williams et al., 1996)。对获得锆石年龄值，选择谐和度在不低于 90-110%的数据用于结果讨论。在碎屑锆石年龄统计时，若 $^{206}Pb/^{238}U$ 年龄值大于 1.0Ga，以 $^{207}Pb/^{206}Pb$ 年龄作为锆石年龄进行统计，若 $^{206}Pb/^{238}U$ 年龄值小于 1.0Ga，则选取 $^{206}Pb/^{238}U$ 年龄值进行统计。

第二节 测试结果 (Dating results)

5.2.1 混杂带变火山岩块体（the metavocanite blocks in the Hongqi mélange Belt)

火山岩块体 090716-29 采样点位于红旗牧场混杂带内（GPS：N42º59'24″, E109º 55'20″），变质火山岩块呈块状镶嵌在绿片岩基质中。岩块遭受糜棱岩化变形，内部石英被定向拉长，呈拔丝状和条带状分布（图 5-2-1A）。

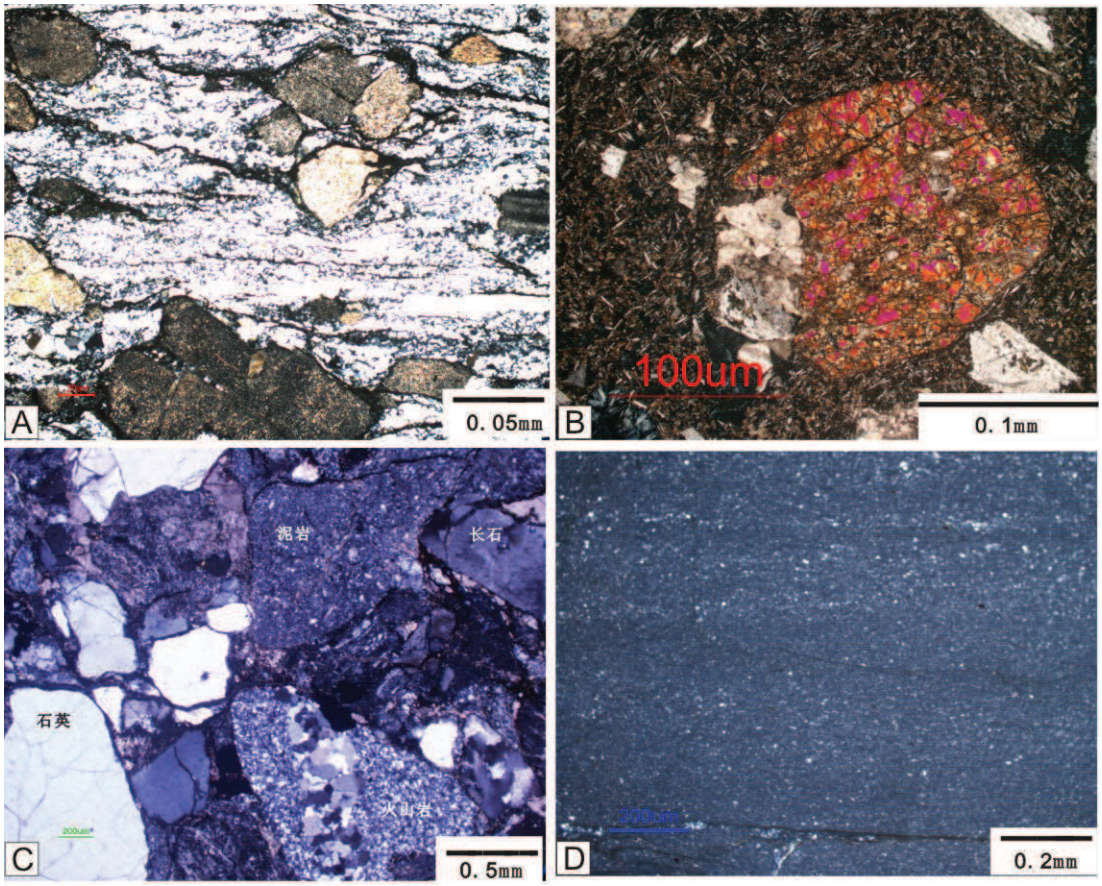

图 5-2-1 测年样品镜下显微特征图片

A：红旗牧场混杂带变质火山岩块体，糜棱结构，长石残斑常常被细小它形重结晶石英集合体环绕。B：满都拉玄武质火山岩，斑状结构；C：满都拉地区粗浊积岩沉积，碎屑成份包含火山岩、泥岩岩屑和石英颗粒等；D：硅质泥岩镜下显微图像，正交镜下

从阴极发光图像上看，该样品的锆石颗粒多为柱状，有的锆石发育明显的韵律环带，显示具有岩浆岩锆石的特征，有的锆石则具有明显的核-边构造，核部多数发光性弱，颜色暗淡，而增生边为宽度不一且发光性强（图 5-2-2 A），这些锆石 Th/U 比值在 0.1 左右，部分小于 0.1，反映受到一定程度的变质改造

(Hoskin and Black, 2000; Corfu et al., 2003)。对样品 090716-29 进行 20 个锆石的分析测试,其中有 6 个数据谐和度较差，偏离谐和线较远，其余数据均在谐和曲线附近。我们选择较集中的年龄簇进行加权计算，$^{206}Pb/^{238}U$ 加权平均年龄为 485±14Ma， MSWD=13（图 5-2-3A），代表火山岩的形成年龄。其它年龄簇落在谐和曲线的内侧，可能与构造扰动造成 Pb 丢失有关，也可能与代表了捕获锆石的年龄。

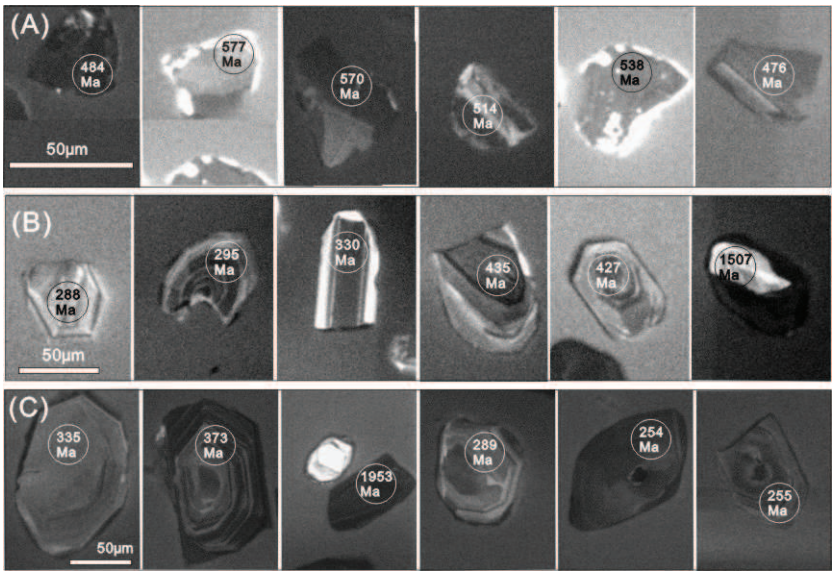

图 5-2-2 岩浆岩测年样品锆石 CL 图形特征

A：红旗牧场变质火山岩样品；B：满都拉地区玄武质熔岩样品；C：满都拉地区蚀变辉长岩侵入体

5.2.2 满都拉玄武岩 (the basalt in the Mandula area)

测年样品 090719-07 采自满都拉城南，经纬度为 N42º22'38″， E109º 58'57″，位于玄武质熔岩内，与 Jian et al.(2010)和 Chen et al.(2012)采样点接近。玄武岩呈灰绿色，块状构造，镜下鉴定为斑状结构，斑晶含量约 15%，主要为斜长石，辉石少量；基质由斜长石微晶组成，间隐结构（图 5-2-1B）。从阴极发光图像上来看，样品的锆石多为较自形的柱状晶体，长宽比在 1-2.5 之间，发育较好的韵律环带，对 30 个锆石的进行单点的 U-Pb 同位素分析，锆石 U 含量范围在 160 到 700ppm 之间，Th 含量在 38 至 250 范围之间，锆石 Th/U 比值多介于 0.3-0.8，显示了基性岩浆岩的特征。有部分锆石内部呈现出明显的核-幔构造，核部颜色暗淡，同样具有环带结构，幔部具有明亮的韵律环带，显示锆石具有不同的成因或不同的期次特征（图 5-2-2B）。30 测试年龄值比较分散，其中最大年龄约为

1800Ma，给出早元古代的年龄，最小年龄组的加权平均值为 289 ± 4 Ma(n=8) MSWD=0.0014（图 5-2-3B），该值与 Jian et al.(2010)和 Chen et al.(2012)接近。但是值得注意的是，样品中还有一些年龄集中分布集中，且谐和度较好，加权平均值 434 ± 4 Ma (n=6)MSWD=0.14,CL 图像显示为继承锆石特征(图 5-2-2B)，说明玄武质岩浆演过程中，受到早古生代物质的混染。

5.2.3 满都拉蚀变辉长岩 (the altered gabbro in the Mandula area)

测年样品 sgz-3 采自满都拉地区哨所一带，经纬度为 N42º24'47″， E109º33'26″。露头呈灰绿-灰黑色，长石斑晶粗大，有的可达 1cm。它们呈层状或透镜状夹在周围的浊积岩沉积层中，野外产状可见切割围岩。镜下鉴定这类岩石主要由粗粒长石和辉石组成，长石发生绢云母化蚀变（图 4-1-15D)。从阴极发光图像上来看，锆石大小变化较大，50-150μm 之间，锆石多为较自形的短柱状晶体，长宽比在 1-2 之间,发育较好的韵律环带或扇状环带,为典型基性岩浆岩锆石(图 5-2-2C)。对 25 个锆石的进行单点的 U-Pb 同位素分析，锆石 U 含量范围在 80 到 700ppm 之间,Th 含量在 30 至 550ppm 范围之间,锆石 Th/U 比值多介于 0.4-1.2，显示了岩浆岩的特征。测试年龄数据多数沿着在谐和线上及附近分布，较大大年龄值在 ca.1850Ma,1600Ma，1000Ma 左右，显示为前寒武纪捕掳晶；较小的年龄簇加权平均值为 257±1Ma（n=6），MSWD=0.3（图 5-2-3C)，代表了辉长岩的侵入年龄。

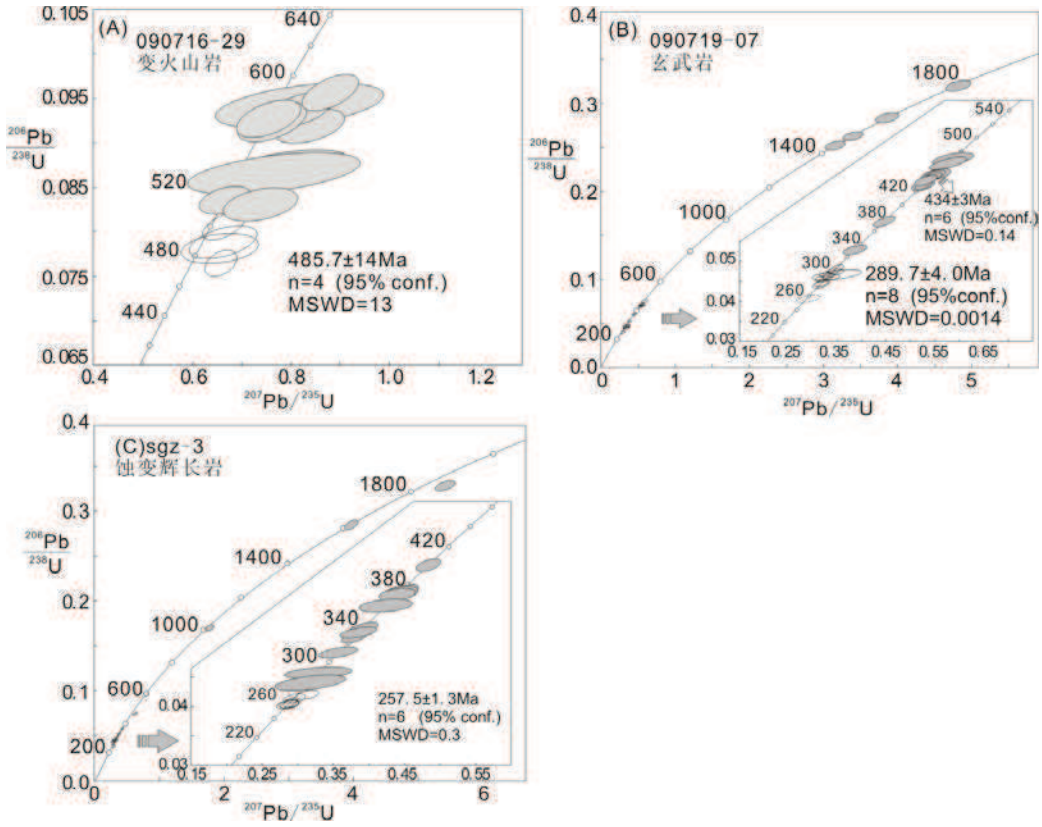

图 5-2-3 岩浆岩样品年代测试数据 U-Pb 谐和图解

5.2.4 滑塌堆积基质 (The matrix of olistostrome in the Mandula area)

样品 82304 采集于滑塌堆积横剖面上(GPS:N42° 24’ 27″; E109° 44’52″),基质主要为青灰色泥质岩和砂质混杂体组成,发生塑性变形,局部可见揉皱和片理化。碎屑锆石大多数为自形或半自形结构,呈现无色或粉色透明状,锆石大小一般 50μm 至 150μm,主要为短柱状,长宽比在 1.5-2 左右。在阴极发光下显现较好的成分环带(图 5-2-4A),多数的测试点得 Th/U 比值在 0.1-0.6 之间,表明锆石为岩浆岩成因,测试数据见附录表。还有一些锆石呈浑圆状,CL 图像无明显环带,表明来源复杂或经过长距离的搬运。本样品一共分析了 65 个数据,其中多数锆石给出了一致或近一致的 U-Pb 年龄,少数年龄谐和度较差(不谐和度大于 10%),未计入统计。锆石 $^{206}Pb/^{238}U$ 年龄主要介于 550-250Ma 之间,在年龄分布图中(图 5-2-5A),锆石年龄构成了 2 个主要的年龄峰值,分别为 263-315Ma 和 411-517Ma。其中较小的年龄颗粒为 250Ma(1 颗),最小年龄值在 ca.245Ma(2 颗)。此外其它锆石给出了少量元古代锆石年龄,800-1100Ma(2 颗),1800-2200Ma(8 颗)和 2300-2500Ma(3 颗)。

样品 72044 采集于滑塌堆积单元最南端(GPS: N42° 23’ 02″;

E109° 40’51″），露头为灰白色杂砂岩，破碎严重，砂岩块体被剪切成多个大小不等地菱形块体。碎屑锆石大多数为自形或半自形结构，呈现无色或粉红色透明状态，锆石大小一般 100μm 至 150μm 左右，主要为短柱状，长宽比在 1.5-2 左右。在阴极发光下多数锆石显现出较弱的环带，表明锆石为岩浆岩成因，少数锆石明亮，并呈混圆状，可能于搬运和沉积过程中的磨蚀有关（图 5-2-4B）。本样品一共分析了 75 个数据（测试数据见附录表），多数的测试点的 Th/U 比值在 0.1-0.6 之间，具有岩浆成因锆石特点。对于该样品中的 71 颗碎屑锆石的 U-Pb 同位素分析结果显示，多数分析点得到比较谐和的锆石 U-Pb 年龄（谐和度小于 10%）。分析结果显示，主要的碎屑锆石 $^{206}Pb/^{238}U$ 年龄介于 400-480Ma 之间，形成一个主要的年龄峰，峰值为 435Ma（图 5-2-5B）。其中有 4 颗碎屑锆石显示年龄为 368Ma，542Ma，669Ma 和 1227Ma。

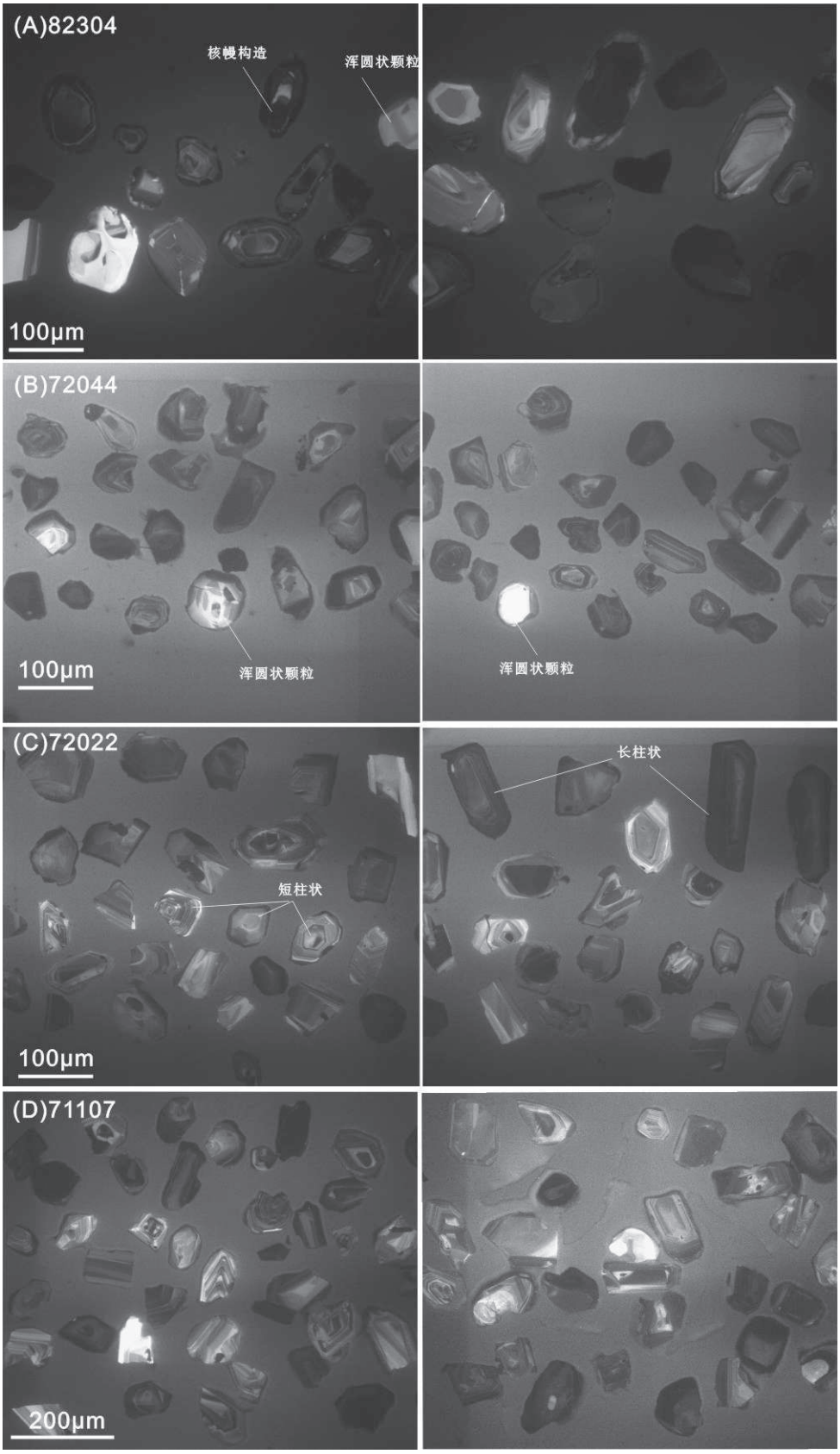

图 5-2-4 碎屑锆石样品锆石颗粒 CL 图像特征图片

A：滑塌堆积基质泥岩碎屑锆石颗粒特征；B：滑塌堆积基质砂岩锆石颗粒特征；C：浊积岩单元砾岩样品碎屑锆石颗粒特征；D：浊积岩单元硅质泥岩锆石颗粒特征

5.2.5 粗浊积岩 (the turbidite sandstones in the Mandula area)

含砾粗砂岩 72022 采集于粗浊积岩单元，经纬度 N42° 27’ 17″；E109° 47’55″。砾石含量 30%左右，一般在 2-10cm 之间，分选很差，磨圆一般，主要成份为火山岩、砂岩和泥岩砾石。镜下鉴定为岩屑石英砂岩，砂状结构，岩屑含量约 40%，岩屑成分为火山岩居多，泥岩次之；其次为单晶石英（30%），磨圆较好（图 5-2-1C）。该样品中获得的锆石为无色或粉色，大致可以分为两类，一类为短柱状，长宽比 1-1.2 左右，锆石大小一般 100-150μm 左右，CL 图像显示明亮的韵律环带，另一类为柱状，长宽比 2 左右，锆石大小一般 150μm 左右，CL 图像的岩浆振荡环带颜色较为暗淡（图 5-2-4C）。本样品中一共分析了 75 颗锆石，除了 3 颗测试年龄值和谐度较差外，其余测试数据都沿着谐和线分布。多数的测试点的 Th/U 比值在 0.1-0.6 之间，为典型的岩浆成因锆石，其中多数短柱状锆石给出-290Ma 的年龄值。 在年龄分布图中（图 5-2-5C），锆石的年龄构成了二个主要的年龄峰值，一个峰在 260-320Ma 之间，峰值为 285Ma。另一峰分布在 420-450 之间，峰值为 431Ma。此外还有一些前寒武纪锆石颗粒，分别为 1175Ma（1 颗），-1800Ma（2 颗），-2500Ma（2 颗）。

5.2.6 硅质泥岩 (the silicified mudstones)

硅质泥岩样品 71107 采集于满都拉西部某边防哨所附近，经纬度 N42° 24’ 54″； E109° 33’22″。由于受到硅化影响，岩石坚硬，在野外呈凸起的山丘，分布在浊积岩单元。前人认为此处为硅质岩，并发现放射虫化石，年代为中二叠纪（王惠等，2005），但是镜下鉴定为泥岩（图 5-2-1D）。经过粉碎挑选后选出的锆石大多数为自形至半自形，锆石大小一般从 50μm 至 150μm 左右，长宽比从 1:1 到 1:2。同时在阴极发光下显现出较为发育的成分环带（图 5-2-4D）。多数的测试点得 Th/U 比值在 0.1-0.6 之间，表明锆石为岩浆岩成因，测试数据见附录表。对样品进行了 73 个点测试，其中 61 个点分布在谐和曲线附近，显示较好的谐和度。在年龄分布图中（图 5-2-5D），这些数据显示有两个主要峰值，一个位于 250-307Ma 之间，峰值为 261Ma，另一个为 3390-460Ma 之间，显示有 2 个次要峰值，分别为 398 和 444Ma。此外还存在 700-1000Ma，1400-2000Ma 以及 2300-2500Ma 的元古代锆石年龄。其中最小年龄值在-255Ma (2 颗)，244Ma（1

颗）左右。

另一个泥岩样品 72034 采集于满都拉城西浊积岩单元中部，属于细浊积岩单元，经纬度为 N42° 27’ 16″； E109° 49’51″。在阴极发光下这些锆石显现出较好的振荡环带，多数的测试点得 Th/U 比值在 0.1-0.6 之间，表明锆石为岩浆岩成因。对该样品进行 30 点的测试，其中 2 个数据不在谐和线附近，其余数据形成明显的两个年龄峰（图 5-2-5E），一个在 260-290Ma 之间，峰值年龄 283Ma，另一个在 430-550Ma 之间，峰值年龄 477Ma。此外还有一颗年龄值为 713Ma。

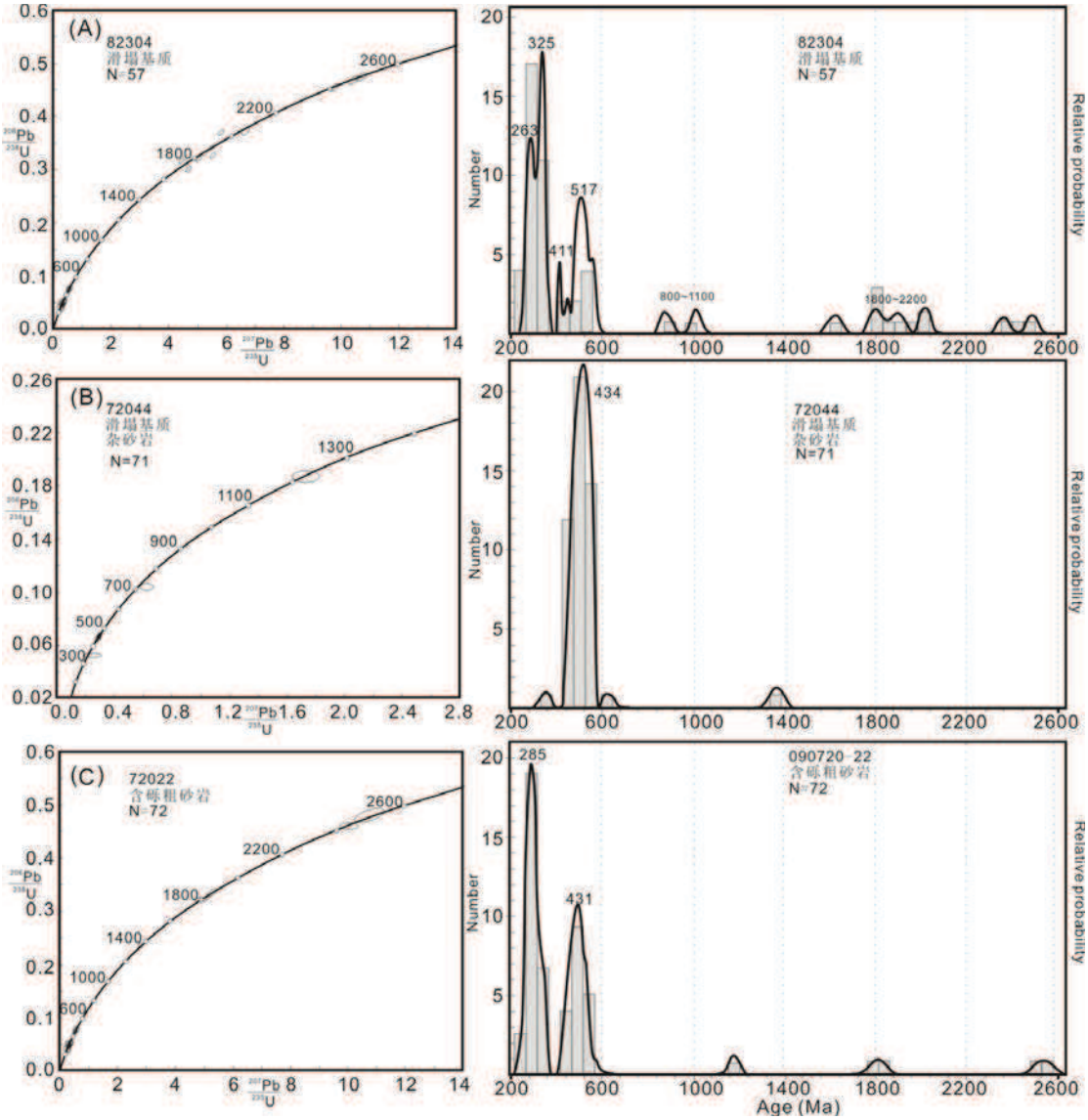

图 5-2-5 满都拉地区碎屑锆石年代学 U-Pb 谐和图解和频率分布图

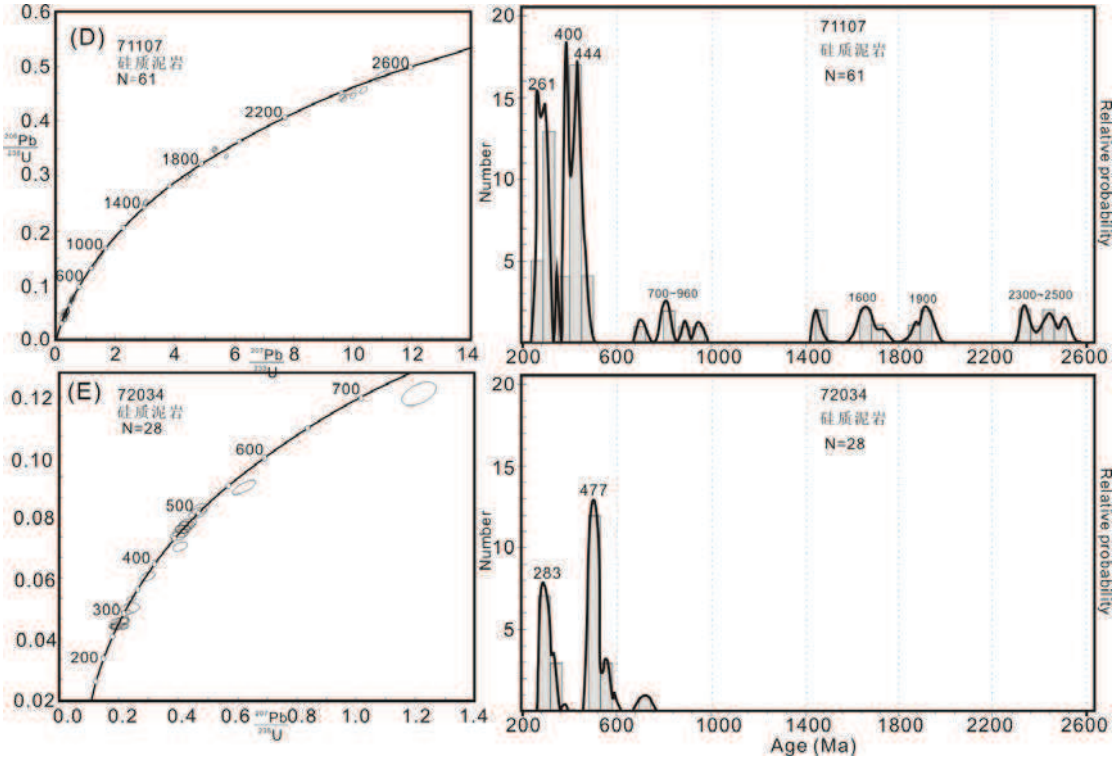

图 5-2-5 满都拉地区碎屑锆石年代学 U-Pb 谐和图解和频率分布图（续）

第三节　年代学意义及小结（the Summary）

在红旗牧场地区混杂岩内，变质火山岩块体 090716-29 显示 $^{06}Pb/^{238}U$ 加权平均年龄 485±14Ma，我们认为它代表了火山岩的形成年龄。该年龄与红旗牧场地区的岛弧岩浆岩年龄相近，根据锆石 U-Pb 年龄和化石证据，后者具有约 430-480Ma 年龄（附录 1），因此该火山岩块体与上覆板块的火山岩活动有关。在古生代洋壳俯冲过程中，上覆板块的部分岛弧火山岩被卷入其中，随着俯冲作用，火山岩块体受到挤压剪切，一些矿物如长石被定向拉长或拉断，形成矿物残斑，长英质物质则遭受定向拉长和重结晶，形成条带结构或拔丝结构。在此过程中，U-Pb 系统可能会受到一些影响，导致一些测试点偏离 U-Pb 谐和曲线，U/Th 比在 0.1 左右（见附录 2）。岩石薄片的矿物组合和变质特征显示没有经历高级别变质作用。

一些地质学者对满都拉地区玄武岩进行了多次年代学研究，研究结果与本次测试结果相近，ca.280Ma。值得注意的是，本次测试发现有大量的继承锆石，它们沿着谐和曲线分布，在 420-500Ma 之间构成一个年龄群，加权平均值为 434Ma，

此外还有数颗元古代的继承锆石。这些早古生代继承锆石与早古生代岩浆岛弧的年代一致。前文研究可知，早古生代岩浆岩为典型安第斯型岛弧，侵位入于元古代基底之上（Xiao et al., 2003; Jian et al., 2010），这些早古生代继承锆石可能来源于此，说明在玄武质岩浆岩形成和运移过程中，在一定程度上受到过元古代基底物质和古生代岛弧岩浆岩物质的混染。这套玄武岩成因意义和所属构造环境存在争论，有的学者认为属于大洋岛弧环境（苏新旭等,2000），有的认为属于 SSZ 环境，代表俯冲开始时拉张环境下的初始岛弧（Jian et al.,2010）；此外还有研究认为这套玄武质岩浆岩代表了类似红海的初始裂谷环境的产物（Chen et al., 2012）。地球化学分析表明（Chen et al., 2012; Jian et al., 2010），该玄武岩稀土元素丰度较低，LREE 轻度亏损、HREE 轻度富集，具有 N-MORB 相似的稀土元素分布特征；初始 143Nd/144Nd 值 0.51262-0.51270 之间，εNd（t）3.4-8.0 左右，这些特征指示岩浆来源于亏损的软流圈地幔。而相对富集 Rb、Ba、Sr 等大离子亲石元素，亏损 Nb、Ta 等高场强元素，这些显示为岛弧岩浆岩的一些特征。初始 87Sr/86Sr 值在 0.70490-0.70537 之间，可能为地壳物质混染所致。洋壳与洋壳俯冲伊始的拉张环境，岩浆快速形成并迅速侵位，由于时间相对较短，所形成的玄武质岩浆岩往往结晶程度较差（Reading et al.,1996; Hawkins, 2003; Stern and Blommer,1992; Stern, 2004），并且不可能存在继承锆石或者受到地壳物质的混染。我们研究发现，这套玄武岩具有典型的斑状结构，斑晶结晶程度较好，并且存在早古生代和元古代继承锆石。这些证据支持初始裂谷环境的模型，即岩浆起源于亏损地幔，同时受到早古生代岛弧岩浆的混染，所以继承了岛弧岩浆的一些地球化学性质；初始 Sr 同位素偏高和存在元古代继承锆石暗示研究区深部存在地壳基底物质。在区域上，晚石炭纪-早二叠纪滨浅海相化石灰岩分布广泛，存在宽广洋壳的可能性较小，因此存在 SSZ 背景下的洋壳俯冲可能性较小。综上分析，我们认为满都拉地区二叠纪初期应该属于初始裂谷环境。在初始裂谷的构造背景下，发育结构和成分成熟度较差的滑塌堆积和浊积岩沉积（见下文）。

满都拉地区哨所一带辉长岩年龄加权平均值为 257Ma，代表结晶辉长岩的结晶年龄。而周围浊积岩地层被认为属于中二叠纪（满都拉地区 1:25 万区调,2003; 王惠等，2005），这与它们的侵入接触关系是一致的。值得注意的是，该辉长岩

样品同样具有 ca.1850Ma,1600Ma，1000Ma 左右的继承锆石，暗示满都拉地区深部可能存在前寒武纪基底。前人认为满都拉地区存在超镁铁质岩块，并将其作为蛇绿岩块体是值得质疑的。

目前沉积物锆石年代学已经广泛应用于研究地层沉积时代、碎屑沉积物源区以及区域构造演化（Fedo et al., 2003；Andersen, 2004；Payne et al., 2006；Moecher and samson, 2006）。地层的沉积时代一定不老于碎屑物质形成的时代，据此碎屑锆石的年龄常常用来制约地层的沉积时代（Nelson, 2001；William,2001； Fedo et al., 2003）。由于不谐和年龄的地质意义很难确定，因此我们将主要根据谐和或者近谐和的年龄数据进行分析和讨论。

满都拉地区滑塌堆积单元中锆石颗粒最小年龄值 ca.245Ma，表明该滑塌事件可能的发生时间不早于 245Ma，其详细的区域构造意见下文（第六章）。在滑塌堆积单元中，测试的样品不同，有各自的峰值特征，但是最主要的碎屑锆石群具有相似的年龄分布特征，如都有 ca.430Ma 的峰值，CL 图像的韵律环带特征显示为岩浆岩锆石(Hancharand Rundnick，1995)，与红旗牧场地区岛弧岩浆岩的年代相似，说明满都拉南部地区早古生代构造地层单元为可能的物源区。这与滑塌堆积中含南部地区的灰岩块体，以及从南向北的滑塌方向相一致。青灰色砂泥岩基质样品中显示有另外谱峰 263Ma 和 325Ma，锆石 CL 图像同样显示韵律环带特征。该年龄峰值与满都拉地区的二叠纪玄武岩和北部大石寨组火山岩活动时代相近，推测与该时期的火山岩活动有关，可能在滑塌过程中卷入下伏浊流沉积物，导致其含有大量晚古生代锆石。研究区附近的岩浆活动，目前发表的年代学数据主要集中在 ca.290Ma, 该样品中含有 ca.325Ma 的年龄峰，说明在晚石炭纪区域上就已存在强烈的岩浆活动，我们在红旗牧场地区发现晚石炭世阿木山组含凝灰岩层相一致。这个晚古生代的锆石年龄谱峰说明研究区岩浆活动从晚石炭纪一直持续到二叠纪末或三叠纪初。

本次研究在浊积岩单元中划分出粗浊积岩和细浊积岩两种沉积类型，但是这些样品中的最主要的碎屑锆石簇具有相似的年龄分布特征（图 5-2-5），分别为 ca.255-300Ma 和 ca.390-460Ma,其峰值年龄集中在约 270-280Ma 之间和 430-440Ma 之间，这些锆石晶形保存较好，反映了这些碎屑锆石遭受了较弱的外动力地质作用改造，碎屑沉积岩源区中绝大多数的物质搬运距离短，碎屑沉积物

以近源为主，CL 图像显示明显的岩浆振荡环带，表明其岩浆岩起源。在区域上，这些年龄峰值与红旗牧场区的早古生代岛弧岩浆岩和满都拉地区的二叠纪火山活动的年代一致。根据野外露头和镜下鉴定，粗浊积岩中含有大量的火山岩砾石，这与碎屑年龄峰的意义相一致，说明物源来自南部的早古生代岛弧地区和附近的二叠纪火山岩。浊积岩单元硅质泥岩中最小年龄值在-250Ma，说明浊流沉积不早于 250Ma，原来认为的中二叠纪沉积岩可能一直延续到晚二叠纪甚至早三叠纪。

值得注意的是，在这些碎屑锆石颗粒当中，存在少数元古代锆石颗粒，它们晶形一般呈浑圆状，说明经历了多次或者长距离搬运。年龄分布显示的群组主要集中在 700-1000Ma、1800-2200Ma 和 2300-2500Ma 之间。近年来，大量来自西伯利亚、华北板块的碎屑锆石 U-Pb 定年结果相继发表，华北板块主要的岩浆岩事件峰期年龄介于 2.9-2.7、2.6-2.5 和 2.35-1.95Ga，变质事件峰期年龄为 2.6-2.4Ga 和 1.9-1.8Ga（Wan et al., 2006; Kroner et al., 2005; Wilde and Zhao, 2005; Zhai and Liu, 2003; Zhao et al., 2000）。在西伯利亚南缘以及南蒙古一带，发育数条新元古代的岩浆弧，其年龄主要集中在 880-860，-800、760-729、700-630 和 536-464Ma（Salnikova et al., 2001; Khain et al., 2003; Wilde et al., 2000, 2003; Kuzmichev et al., 2001, 2005; Rojas-Agramonte, et al., 2010; Demoux, et al., 2009; Wang et al., 2001）。本次研究中元古代碎屑锆石 1800-2200Ma 和 2300-2500Ma 与华北板块的岩浆岩事件峰值一致，表明来源于华北板块，由于锆石颗粒数量较少（约 10%），可能代表多次循环沉积产物。另外还有 700-1000Ma 之间的锆石颗粒（特别是硅质泥岩中），华北板块少见，常见于南蒙古一带，说明研究区北部元古代物质可能提供了少量物源，也暗示研究区附近存在含有 700-1000Ma 左右的岩石构造单元或微陆块。

本次研究发现在碎屑锆石年龄分布中缺乏晚泥盆纪至早石炭纪锆石颗粒，说明研究区存在一个重要的岩浆活动空白期，这个空白期持续时间大概为 80Ma。这与区域上缺少晚泥盆纪和早石炭纪的岩浆活动相对应，其地质意义见第六章。

Chapter 6 The Paleozoic Tectonic evolution in Central Inner Mongolia

Section 6.1 The Litho-geochronological Framwork

We divided the Paleozoic litho-stratigraphy into several litho-tectonic units in the Hongqi area, Ondor Sum area and Mandula area based on the lithological and deformation features. They are the North China Craton, the Bainaimiao Arc Belt, the Hongqi-Ondor Sum Mélange Belt, the Olistostrome Unit, the Turbidite Unit and the volcano-sediemntary Unit from south to north.

Numerous paleontolgical and radioative isotopic data show that the Bainaimiao arc magmatism spaned the whole Ordovician age. The tuffeous sandstones in the Bainaimiao Arc Belt croping out in the Hongqi, Ondor Sum (Tulinkai) area contains the fossils of graptolite, such as *Callograptus sp., Desmograptus sp. Dictyonema sp.,Aspidograptus sp., Dicranograptus? sp.,* designate age of Ordovician (Tang et al., 1992) . The Bater Obo magmatic intrutions with arc signatures in the Hongqi area were dated at ca.440-460Ma (Xu and Tao, 2003; Jian et al., 2008; Li et al., 2010; Appendix 1). The age of rhyolite and dacite in the Bainaimiao area is ca. 474-439Ma (Zhang et al.,2012; Appendix 1). Geochemically, the Bainaimiao arc volcanic rocks display high Sr and low Nd isotopic signature, indicating to some extent contaminated by the crust material, argue that is continental margin arc magmatism (BGMRIM, 1991; Xiao et al.,2003； Jian et al.,2008).

The Hongqi-Ondor Sum mélange developed from the Ordovician to, at least, before the Devonian evidenced by the Devonian red sandstones unconformably covering the mélange belt in the Hongqi area. De Jong et al.(2006) reported that quartz mylonite in the Wulan valley yielded Ar/Ar age of 453Ma and 449Ma. This study shows that the metavolcanite block in the Hongqi mélange belt yields 484 ± 14 Ma. It is worth noting that the Silurian deformed limestone as blocks cropping out in the Hongqi mélange belt, suggesting Devonian the maximum age. All these data argue that the ocean crust subduction was not terminated untill Devonian.

Our study displays that the Basalts in the Mandula area yields concordant age of 289 ± 4Ma, close to others' research results (Jian et al.,2010; Chen et al.,2012). The Basalts contains one remarkable zircon claster with average age of 434 ± 4 Ma. These zircon xenocrysts are interpreted that the basaltic magma were contaminated by the Ordovician arc material. Thus it shows slightly arc magmatic geochemical signature (Jian et al.,2010； Chen et al.,2012).

Zhang et al.(2011) documents the Early Permian mafic and felsic volcanic rocks from the northwestern Inner Mongolia. The geochemical and geochronological research shows that the mafic rocks generate from two mantle source components: the subduction-related metasomatized asthenosphere and lithospheric mantle; whereas the fesic rocks involves partial melts of mixed sources composed of predominante juvenile basaltic underplates and minor ancient crustal materials.

The Zhesi formation geometrically covering the Dashizhai volcanic rocks includes numerous fossils of Brachiopods, bryozoans, corals, sponges with age of middle Pemian. (Grabau, 1931； Mueller et al., 1991； Wang et al.,2002；Leven et al., 2001； wang et al.,2005).

The turbidity current is common in the deep water environment, for example slope environment, oceanic plain (Reading et al., 1996）. The development of turbiditic sediments in the Mandula area suggest the potential deep water setting caused by the Permian rifting.

The olistostrome generally develops in slope environment that has close relationship with turbiditic sediments (Jacobi, 1984； Postma, 1984； Christopher et al., 1987； Liuz, et al., 1998； Direen, et al., 2008). The olistostrome geometrically overlies the turbidite unit. Both of them suggest a deep water setting.

What is the real sedimenting age of the turbidite and the olistotrome in this study, since several relatively younger zircon grains were detected, which are ca.255Ma (2 grains), 250Ma(1 grain) and ca. 245Ma (3 grains). For our current knowledge, there are three possibilities about the origin of these younger grains: 1) they probably come from the regional ca.240-250Ma magmatic plutons. It means these late Permian/early Triassic plutons have exhumated and eroded after their emplacement. However, the

related exhumated structure and geological records are poorly discovered. Furthermore,much more zircon grains should be expected rather than a few, if the ca.240-250Ma plutons were potential sources.Therefore,it seems that this explaination is difficult to realize. 2) These younger grains were contributed by the regional simutaneous volcanic eruption.Jian et al.(2010) discovered ca.252Ma andesite to the north of study area.However,it appears to be doult due to the lack of age peak in those grains. More geological survey are due to answer this question. 3)those younger ages are caused by the loss of Pb,the U-Pb systerm is not completely closed. Whereas the true age close to the peak age,ca.270-280Ma. The third possibility is more logical condering the regional geological record. Also,it is consistent with the fact that the 257Ma gabrroic vein cutting the turbiditic sequences in our field observation. In this study, we assigned the developing age of turbidite and olistostrom as earlier late Permian (Fig.6-1-1).

Section 6.2 Polyphase deformation and time constraints

Four phases deformation were recognized in the three study areas based on the field observation and micro structural analysis. the first two phases developing on the Hongqi-Ondor Sum mélange belt are ductile deformation.

D1 is responsible for the pervasive S1 foliation, NW-SE striking L1 streching lineation and F1 intrafolial folds. These microstructures are coeval with a green schist facies metamorphism. During D2, NW-verging F2 folds associated with a S2 axial planar cleavage deformation S1 and L1. The D2 can be interpreted as the continuationof the same ductile shearing under less penetrative conditions. In both Hongqi and Ondor Sum areas, the D1 kinematic criteria, such as Pressure shadows, Mica fish and sigmoid porphyroclast, indicate a top-to-the-NW sense of shearing. D3 event is defined by SE-NW striking upright folds in the Hongqi area, whereas by SW-NE striking antiform in the Ondor Sum area. At the macroscopic scale, F3 folds deform the S1 foliation, resulting in formation of the general antiformal structural framwork of the mélange belt. The Early Devonian red sandstone unconformably covering the melange unit does not record the D1 and D2 event, and thus provides an

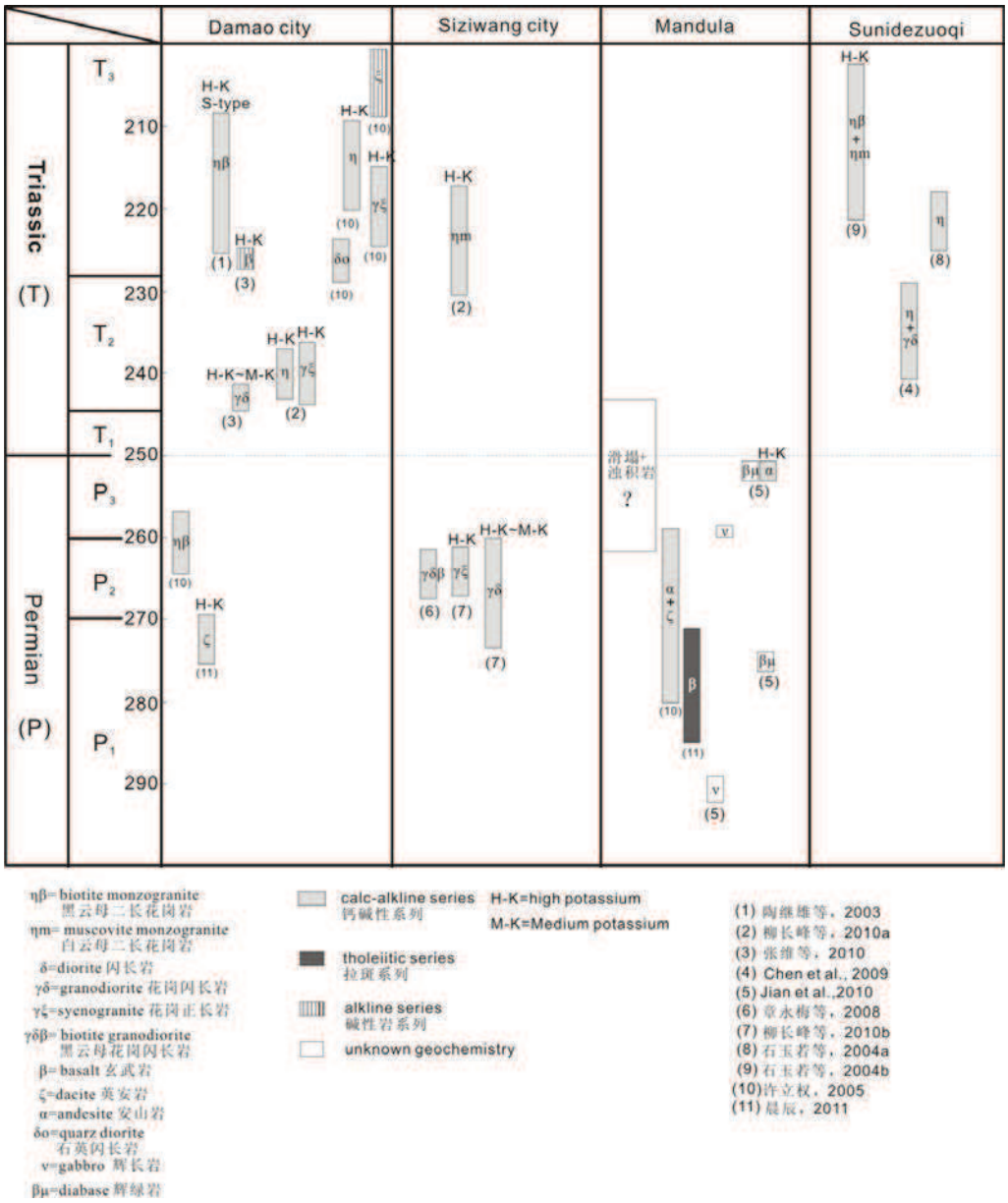

Fig. 6-1-1 The chart of magmatic events in the central Inner Mongolia

upper time limit for the termination of the ductile events. The Km-scale upright folding involves the Devonian and Carboniferous rocks.

D4 phase invoves the Permian stratigraphy that was recognized in the Mandula area. It is represented by a series of isoclinal folds, overturned folds and recumbent folds in the turbidite unit and olistostrome unit with nearly SW-NE or E-W axis. Penetrative cleavage is pervasive in the turbidite unit. However, the deformation is represented by nearly E-W striking open fold without cleavage in the relatively competent volcan-sediments of the Zhesi Formation and Dazhizhai Formation. It is

worth noting that those folded rocks were covered by the southern Mesozoic extensional basin sediments (Meng, 2003). Aslo, the Triassic undeformed plutons were widely spreaded in the study area. Therefore, those folds caused by nearly N-S shortening should happened between the late Permian and early Triassic.

Section 6.3 A possible geodynamic evolutional modle

The Ordovician to Silurian Subduction: An Early Paleozoic SE-dipping Paleo-Asian Ocean subduction zone developed along the northern margin of North China Craton from Hongqi to Ondor Sum area. This oceanic subduction gave rise to the Bainaimiao magmatic arc, and the Hongqi and Ondor Sum mélange units (Fig.6-3-1A). Both the Hongqi area and the Ondor Sum area experienced two ductile deformation phases before the Early Devonian. Although radiometric ages for each phase are not settled, the deformation styles are comparable between the two study areas. Namely, 1) the main event, D_1, is responsible for the development of the S_1 foliation, NW-SE striking stretching lineation (L_1), and intrafolial folds (F_1) with axes parallel to L_1. In Hongqi area, D_1 is coeval with a green schist facies metamorphism whereas, in Ondor Sum area blue schist facies relicts, such as glaucophane, phengite are locally preserved (Tang et al., 1993; De Jong et al., 2006). Our kinematic observations show a top-to-the NW sense of shear in both study areas. F_1 folds correspond to a-type folds formed during the ductile shearing. The D_1 structural elements are subsequently deformed by a D_2 event represented dominantly by numerous NW-verging asymmetric folds associated with an axial-planar crenulation cleavage (S_2). Due to the subsequent deformation (D_3), S_2 dips either to the SE or to the NW in the Ondor Sum area whereas, dips to the NE or the SW in the Hongqi area. However, the fold vergence is consistently to the NW. At Ulan valley, the north dipping schists that constitute the north limb of the antiform show top-to-the NW sense of shearing. Our structural observations and kinematic data do not support a Late Precambrian to Cambrian north dipping subduction giving rise to the Ulan arc (Xiao et al., 2003). Moreover, the alkaline geochemical signature displayed by the deformed pillow basalt of the “Ulan arc” suggests that they originated in a sea-mount

setting (Huang et al., 2006). The blueschist and quartz mylonites with age ranging 426~453 Ma (Tang and Zhang, 1991; De Jong et al., 2006) recorded the Ondor Sum subduction event. In the Hongqi area, the deformed Late Silurian fossiliferous limestone blocks mark the youngest age of the Hongqi mélange.

The Late Silurian Collision: The collision likely occurred in Late Silurian, since the Early Devonian red sandstones unconformably cover the Hongqi mélange. Accretionary tectonics and magmatism must have been stopped at that time. Subsequently, a Late Carboniferous platform limestone developed in a vast area, extending throughout the eastern part of Inner Mongolia (BGMRIM.1991). This formation discordantly overlaid the Hongqi-Ondor Sum mélange and Bainaimiao arc unit. In our study area, the most likely is that a microcontinent, here named the Southern Gobi microcontinent, following Sengor and Natal'in, (1996), entered in the trench and collided with the Andean active margin of the North China craton (Fig.6-3-1B).

The Early Permian Intracontinental rifting: in the Mandula study area, Late Carboniferous to Early Permian series are characterized by a syn-rifting sedimentation coeval with a basaltic and acidic volcanism. The basalts are tholeiitic series, with low TiO_2 and P_2O_5, flat REE, or slightly depleted LREE spectra, enrichment in LILE but strong depletion in Nb and Ta, and initial $^{87}Sr/^{86}Sr$ = 0.7046-0.70537, Nd=3.4-7.8 (Jian et al., 2010; Chen et al., 2012). These features were interpreted as N-MORB with arc signature, indicative of proto-arc in a supra subduction zone setting (Jian et al., 2010). By contrast, Chen et al (2012) argued for a juvenile ocean basin setting with magma genesis of enriched mantle or N-MORB-like depleted asthenospheric mantle contaminated and metasomatised by arc material. The later interpretation is supported by our 437Ma and 1400-1800 Ma zircon xenocrysts in basalt that might be scavenged by the acending magma. The acidic-intermediate volcanic rocks with age of 272Ma (Chen, 2011) display a pronounced A-type affinity and a significant contribution of crustal-derived rocks in their petrogenesis (Chen. 2011). The coeval basaltic and acidic volcanic rocks suggest a bimodal signature, indicative of intracontinental rifting.

Therefore, we propose that an intracontinental rift developed from Late Carboniferous to Early Permian in the Mandula area (Fig.6-3-1C). The rifting gave rise to the N-MORB-like basalt, the turbidite and the olistostrome units that received the rewoked the Early Palezoic deposits (Fig. 6-3-1C, inset). During this period, a narrow sea basin was likely created, but evidence for an oceanic crust is lacking. However, Late Guadalupien (~270Ma) radiolarians are found in mudstone boulders enclosed in the Late Permian conglomerate (Shang, 2004). These mudstones deposited in a deep sea basin and reworked in the Late Permian strata.

The Late Permian-Early Triassic closure of the rift: At that time, the study area experienced a compressional tectonics. The crust of one potential microcontinent, previously heated and thinned during Early Permian rifting, was sliced by NW-directed thrusts along weak crustal shear zones whereas the Early Paleozoic suture zone was inactive. This intracontinental tectonics was responsible for the NW-verging folds in the olistostrome and turbidite units (Fig.6-3-1D). Later the crust thickening results to the development of Triassic high K alkline/Calc-Alkline intrusions (Fig.6-3-1D).

No typical ophiolitic suture zone was left by this intracontinental tectonic activity, but a crustal scar, characterized by NW-thrusting, folding, and emplacement of MORB-type magmatism developed in the Mandula area.

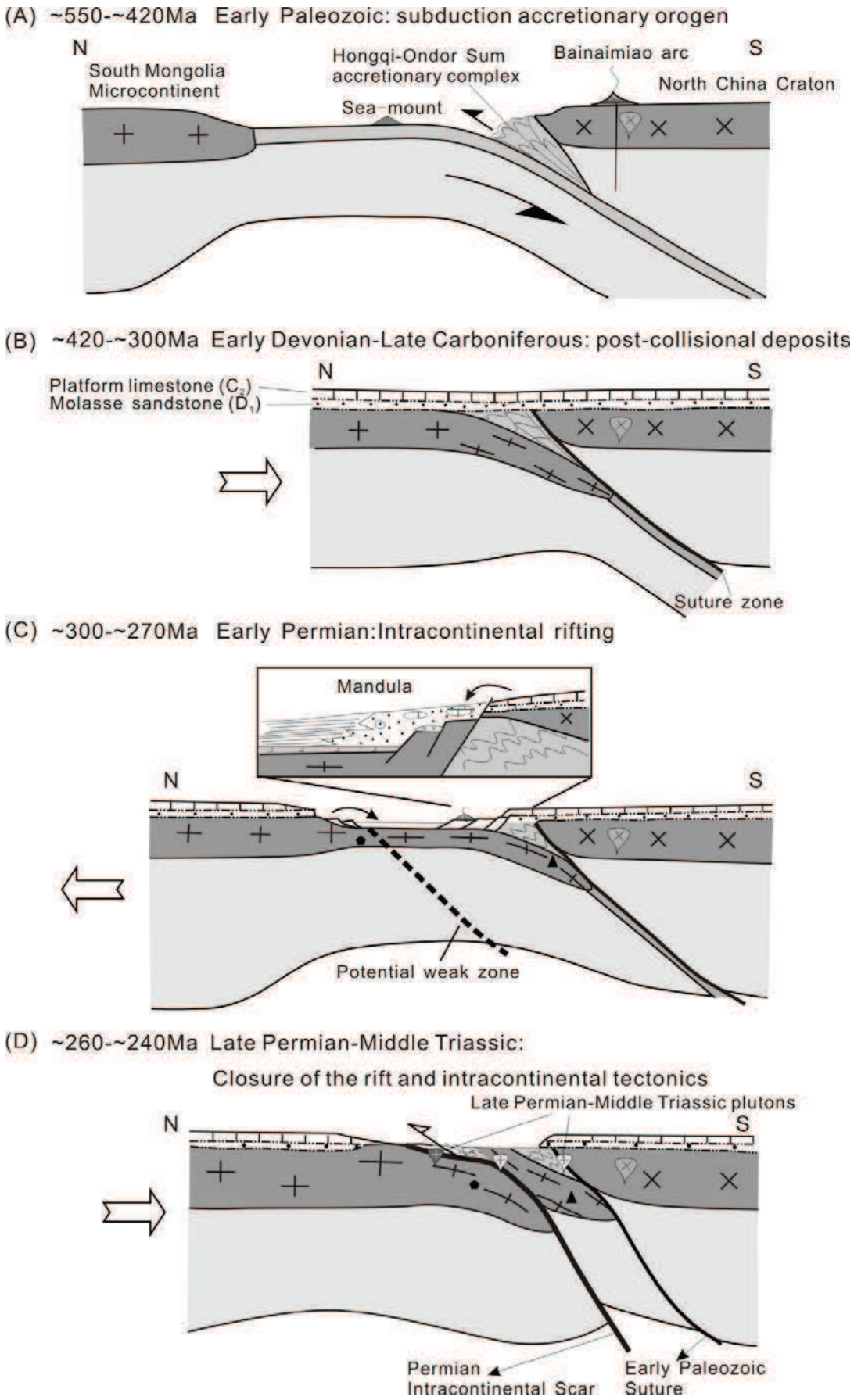

Fig.6-3-1 The Paleozoic tectonic evolutional modle in central Inner Mongolia

Section 6.4 Discussion

6.4.1 The Palezoic tectonic evolution in Inner Mongolia

The Palezoic tectonic evolution of Inner Mongolia has been debated for several decades. Differing model and oppions have been proposed about the orogenic mechanism, the final closure posion and time of Palaeo-Asian ocean (Wang and Liu, 1986； Ruzhentsev et al., 1989； Tang，1991；Hsu et al., 1991; Sengor et al., 1993; Xiao et al., 2003; Xu et al., 2012). Shao (1991) suggested that the final closure position was a broad belt resulted by a “soft” collision between Siberia craton and North China craton During the Carboniferous. This kind of “soft” collsion differing from the typical continent-contient collison can not create strong continental thickening and uplifting. This model well explained the regioanl pervasive late Carboniferous fossiliferous limestones in Inner Mongolia, to some extent presents accretionary orogen features which is no intensive crust uplifting and collsion-related voluminous magmatism. However, this model ignors the regional Devonian sediments unconformably overlying the mélange belt. Xiao et al.(2003) proposed a mutiple suture zone along the Solonker Obo to the XarMoron river synthesizing the stratigraphy correlation, structural analysis, paleontological and geophysical data etc. Even though this is most logical geodynamic model about the tectonic evolution in Inner Mongolia, it can not explain the Devonian and Carboniferous shallow water sediments. Furthermore, the obvious age gap from Devonian to early Carboniferous in our detrital zircon data questions Xiao’s continuous subduction model. Jian et al.(2008, 2010) advocated an apparently perfect model that involves several unverifiable scenario, such as pre-subduction extension, subduction initiation, ridge-trench collision etc., based on the geochemcial and geochronological analysis without any strucrural and regional stratigraphic records.

The geodynamic model proposed here considers the geological facts that: 1) the temporal and spacial relationship of the litho-tectonic units, expecially the Devonian red sandstone uncomformably covering the mélange belt. 2) the Carboniferous fossiliferous limestones indicating a shallow sea environement are common in the

study area. 3) the Permian alkline and bimodal volcanic rocks crop out in/near the study area. 4) the Permian olistostrome and turbditic sediments are coeval with the basalts and volcano-sediments. 5) the Permian stratigraphy experienced near N-S shortening following by the Triassic voluminous high K alkline/ calc-alkline plutons. In this model, a potential microcontinent is induced to terminate the subduction process and contribute the ca.0.6-1.0 Ga detrial zircon grains in the Permian sediments. the key point deffering with precursors' model is the early Permian rifting based on the regional lithological development and geochemcial data. The late Permian folding leads to N-S shortening, crust thickening, finally resulting in Triassic crust melting to produce high-K magmatism.

6.4.2 A doult to the "solonker" ophiolite

The Solonker suture was considered as ophiolitic mélange belt. some geologists aurged that the Mandula area consists of limestone mélange and argillaceous mélange. However, our field observations lead us to divide the "ophiolitic mélange" into olistostrome and turbidite unit. The typcial ophiolitic component are not observed in the study area.

The difference between the olistostrome and the tectonic mélange are widely documented (Hsu, 1974; Potter and Pettijohn, 1977; Wang., 1981; Carine and Michel, 2004). Care must be taken in the outcrops. In the Mandula area, the olistostrome is distinct with tectonic mélange as follows: i) the matrix is mainly composed sandstone and mudstone. Moreover, there is a gradual trend with sandstone decreasing and mudstones increasing northward till the turbidite unit. ii) No typical tectonic shearing deformation and intermediate-high grade metamorphism are observed in the Mandula area. To the south, the head areas of slumps are dominated by demi-continuous bedding while the northern part of the slumps tends to be dominated by compressional structures such as folds and thrusts. The inhomogeneous deformation suggests southern part extension while northern part compression, indicating the northward movement. iii) In the olistostrome unit the blocks include limestone, sandstone, acidic volcanic rocks while in the turbidite unit expose basalt,

volcanic bedding and gabbro intrusion. The typical ophiolitic blocks, such as serpentinite do not exist. The limestone blocks lithologically and paleontologically similar with the southern Amushan Formation (IMBGMR, 2004), suggest the Amushan Formation as a potential source. This is also consistence with uneven slump structure and the kinematic indicator in the siliceous mudstone. Thus the Mandula study area is dominated by olistostrome and volcano-sediments. The reality of the "Solonker" ophiolite should be reassessed.

Chapter 7 Conclusion

This study advances the reseach about the tectonic evolution in Inner Mongolia in the following aspects:

1) Four litho-tectonic units, were recognized in the Honhqi area based on the lithological and structural features. They are, from north to south, the Hongqi mélange belt, the Bainaimiao arc belt, North China Craton and the overlying sedimentary successions, respectively. The Hongqi melange belt consists of mica-chlorite schist, chlorite-quartz schist , calcareous slate and chert etc. with blocks of limestone, sandstone, sepentinite and volcanic rocks. The arc belt is mainly composed of basalt and andesite named The Bulongshan Formation and the Hala Formation. The Early Devonian red sandstone unconformably covering the melang belt and arc belt, suggesting the end of the subduction and collision.

2) Two phases ductile deformation and one phase ductile-brittle deformation were recognized in the Hongqi melange belt. D_1 is characterized by the penetrative S_1 foliation and L_1 stretching lineation coeval with the green schist metamorphism. The kinematic criteria including sigmoidal porphyroclast, pressure shaddow, mica fish and shearing band indicate a top-to-the-NW sense of shearing. D_2 is represented by the asymmertrical fold with axis NE trending. D_3 deformation involving the Devonian sediments shaped the whole framework in the Hongqi area. It formed various sized of axis NW-SE upright fold.

3) Three litho-tectonic units were recored in the Ondor Sum area, which are The Ondor Sum mélang belt, the Bainaimiao arc belt and the overlying sedimentary successions, which can be correlated with the Hongqi area. the blocks of melange belt include basalt, volcanic rock, marble,chert and blueschist. The arc is composed of amphibolites, plagiogranite and gabbro, interpreted as the deep component of the arc basement.

4) The Ondor Sum melange belt experienced three phases deformation: D_1 formed the pervasive S_1 greenschist foliation and NW-SE trending L_1 stretching lineation. The kinematic criteria suggest a top-to-the-NW shearing. Taken the S1

foliation as the reference plane, the D_2 presents the asymmetrical fold F_2 and crenulation cleavage S_2 .D_3 is characterized by the regional antiform structure with aixs nearly E-W.

5) The spacial and temporal distribution of these litho-tectonic units and the structural analysis of the Hongqi-Ondor Sum mélange belt lead us to conclude that ocean crust subducted Southeastward beneath the North China craton during the early Paleozoic. The subduction was terminated at Devonian time by the arrival of a potential microcontinent.

6) The olistostrome unit, turbidite unit, volcano-sediment unit were recognized in the Mandula area. The olistotrome unit includes various sized of blocks of limestone, sandstone and silicified mudstone, within the matrix of graywacke and mudstone. The turbiditic sediments developed typical Bouma sequences. The sedimentary features of volcano-sedimentary rocks indicated erupting in the shallow sea and coastal environment. These litho-tectonic units are caused by the Permian rifting. The well-known “solonker” suture is questionable in the Mandula area. The “solonker” ophiolitic mélange indeed is olistostrome and turbidite with gabbroic intrusions. It generally presents normal sedimentary sequences. The typical ophiolitic component are not existed.

7) The Mandula area suffers D_4 phase deformation caused by a nearly N-S shortening. The turbidite unit displays a series of recumbent fold and tight isoclinal fold with well developed cleavage; Whereas the volcano-sedimentary rocks develop horizontal, E-W or NE-SW trending axis open fold. This nearly N-S shortenting led the rift closure from the late Permian to early Triassic.

8) The detrital zircon analysis shows two age peaks in ca.270-280Ma and ca.440-420Ma. it implies that the Bainaimiao arc belt and the adjacent Permian volcanic activity are the possible source. the ca.700-1000Ma grains that are common in the Mongolia area probably came form the northern potentional microcontinent. The ca.1800Ma, ca.2300-2500 Ma suggested the North China craton was one of the sources.

References

Agard, P., Jolivet, L., Goffé, B., 2001. Tectonometamorphic evolution of the Schistes Lustrés complex: implications for the exhumation of HP and UHP rocks in the Western Alps. Bulletin Societe Geologique France 172 (5), 617-636.

Agard, P., Yamato, P., Jolivet, L. & Burov, E., 2009. Exhumation of oceanic blueschists and eclogites in subduction zones: timing and mechanisms, Earth Science Review, doi:10.1016/j.ears cirev. 2008. 11. 002.

Alexander, Y., 2004. Architecture and mineral deposit settings of the Altaid orogenic collage: a revised model. Journal of Asian Earth Sciences 23, 761-779.

and eclogites in subduction zones: timing and mechanisms. Earth-Science Reviews 92, 53-79.

Andersen, T., 2002. Correction of common lead in U-Pb analyses that do not report ^{204}Pb, Chemical Geology 192, 59-79.

Andersen, T., LaajokiK，S.A., 2004. Age, provenance and tectonostratigraphic status of the Mesoproterozoic Blefjell quartzite， Telemark sector， sonthern Norway， Precambrian Research 135, 217-244.

Arcculus, R. J. 1999. Origins of the continental crust. Journal and Proceedings of the Royal Society of New South Wales, 132, 83–110.

Badarch, G., Cunningham, W.D. & Windley, B.F., 2002. A new terrane subdivision for Mongolia: implications for the Phanerozoic crustal growth of Central Asia. Journal of Asian Earth Sciences 21, 87-104.

Barley, M. E. 1992. A review of Archean volcanic hosted massive sulphide and sulfate mineralization in Western Australia. Economic Geology, 87, 855–872.

Belen, A., Gemma, E., 2002. Small turbidte systems in a complex tectonic settings (SW Medierranean Sea): morphology and growth patterns. Marine adn Petroleum Geology 19 ,1225-1240.

Beltrando, M., Hermann, J., Lister,G., Compagnoni, R. 2007. On the evolution of orogens: Pressure cycles and deformation mode switches. Earth and Planetary Science Letters, 256, 372–388.

Black, L.P., Kamo, S.L., Allen, C.M., Davis, D.W., Aleinikoff, J.N., Valley, J. W., Mundil, R., Campbell, I.H., Korsch, R.J., Williams, I.S., Foudoulis, C., 2004. Improved $^{206}Pb/^{238}U$ microprobe geochronology by the monitoring of a trace-element-related matrix effect; SHRIMP, ID-TIMS, ELA-ICP-MS and oxygen isotope documentation for a series of zircon standards. Chemical Geology 205, 115-140.

Brown, M., 2006. Duality of thermal regimes is the distinctive characteristic of plate tectonics since the Neoarchean. Geology, 34, 961–964.

Brown, M., 2009. Metamorphic patterns in orogenic systems and the geological record. In:Cawood,P. A. & Kroner, A. (eds) Earth Accretionary Systems in Space and Time. Geological Society, London, Special Publications 318, 37–74.

Buchan, C., Pfaender, J., Kroener, A., Brewer, T.S., Tomurtogoo,O., Tomurhuu, D., Cunningham,D.,and Windley,B.F., 2002.Timing of accretion and collisional deformation in the Central Asian orogenic belt: Implications of granite geochronology in the Bayankhongor ophiolite zone: Chemical Geology, 192, 2345-2367

Buslov M.M., Saphonova, I.Y., Watanabe, T., Obut, O.T., Fujiwara, Y., Iwata, K., Semakov, N.N., Sugai, Y., Smirnova, L.V., Kazansky, A.Y., 2001. Evolution of the Paleo-Asian Ocean (Altai−Sayan Region, Central Asia) and collision of possible Gondwana-derived terranes with the southern marginal part of the Siberian continent. Geosciences Journal 5,203-224.

Bureau of Geology and Mineral Resources of Inner Mongolia (BGMRIM), 1991.Regional Geology of NeiMongol (Inner Mongolia) Autonomous Region. Geological Publishing House, Beijing (in Chinese with English summary).

Cawood P., Kroner, A., Collins, W.J., Kusky, T., Mooney, W.D., Windley, B.F., 2009. Accretionary orogens through Earth history, in Cawood P., and Kroner A. (Eds.), Earth Accretionary systems in space and time. Geological Society Special Publication 318, 1-36.

Cawood, P. A., Kroener, A., Windley, B. F., 2003.Accretionary orogens: definition, character,

significance. EGS - AGU - EUG Joint Assembly, The meeting held in Nice, France, 6 - 11 April.

Chao, E.C.T., Back, J.M., Minkin, J.A., Ren, Y., 1992. Host-rock controlled epigenetic, hydrothermal metasomatic origin of the Bayan obo REE-Fe-Nb ore deposit, Inner Mongolia, PRC. Applied Geochemistry 7, 443-458.

Chao, E.C.T., Back, J.M., Minkin, J.A., Tatsumoto, M., Wang, J., Conrad, J.E., Makee, E.H., Hou, Z., Meng, Q., Huang, S., 1997. The sedimentary carbonate-hosted giant Bayan Obo REE-Fe-Nb ore deposit of Inner Mongolia, China: a cornerstone example for giant polymetallic ore deposits of hydrothermal original. USGS Bulletin 2143, 1-65.

Chen B,Jahn BM，Wilde S and Xu B．,2000．Two contrasting Paleozoic magmatic belts in northern Inner Mongolia，China:Petrogenesis and tectonic implications. Tectonophysics 328,157－182.

Chen, B., Jahn, B.M., Tian, W., 2009. Evolution of the Solonker suture zone: constraints from zircon U-Pb ages, Hf isotopic ratios and whole-rock Nd-Sr isotope compositions of subduction and collision-related magmas and forearc sediments. Journal of Asian Earth Sciences 34, 245-257.

Chen, B.,Jahn, B.M.，Wilde, S., Xu, B., 2000．Two contrasting Paleozoic magmatic belts in northern Inner Mongolia，China:Petrogenesis and tectonic implications. Tectonophysics 328, 157-182.

Chen, C., Zhang, Z.C., Guo, Z.J., Li, J.F., Feng, Z.S., Tang, W.H., 2012. Geochronology, geochemistry, and its geological significance of the Permian Mandula mafic rocks in Damaoqi, Inner Mongolia. Science China earth Sciences 55, 39-52.

Chopin, C., 2003. Ultrahigh-pressure metamorphism: tracing continental crust into the mantle. Earth and Planet Science Letters 212, 1-14.

Choulet, F., Chen, Y., Wang, B., Faure, M., Cluzel, D., Charvet, J., Lin, W., Xu, B., 2011. Late Palaeozoic palegeographic reconstruction of western Central Asia based upon paleomagnetic data and its geodynamic implications. Journal of Asian Earth Sciences 42, 867-884.

Choulet, F., Faure, M., Cluzel, D., Chen, Y., Lin, W., Wang, B., 2012.From oblique accretion to transpression in the evolution of the Altaid collage: new insights from West Junggar, northwestern China 21,530-547.

Christopher, J.E., Michael, M.G., Stephen, E.N., 1987. Problems of recognition of olistostromes: An example from the lower Pit Formation, Eastern Klamath Mountains, California. Geology 15, 541-544.

Coleman, R.G., 1989, Continental growth of northwest China. Tectonics 8, 621-635.

Collins,W. J.2002.Hotorogens, tectonic switching, and creation of continental crust. Geology, 30, 535–538.

Corfu, F., Hanchar, J.M., Hoskin, P.W.O., Kinny, P., 2003. Atlas of zircon textures. In: Hanchar, J.M., Hoskin, P.W.O. (Eds.), zircon: Reviews in Mineralogy and Geochemistry 53, 469-500.

Crook, K. A.W. 1974. Kratonisation of west Pacific-type geosynclines. Journal of Geology, 87, 24–36.

David A. F., David R. G., Catherine S., George K., Frank P. B., 2009. Palaeozoic Lachlan orogen, Australia; accretion and construction of continental crust in a marginal ocean setting: isotopic evidence from Cambrian metavolcanic rocks. Geological Society, London, Special Publications 318, 329-349.

De Jong, K., Xiao, W.J., Windley, B.F., Masago, H., Lo, C.H., 2006. Ordovician $^{40}Ar/^{39}Ar$ phengite ages from the blueschist-facies Ondor Sum subduction-accretion complex (Inner Mongolia) and implications for the early Paleozoic history of continental blocks in china and adjacent areas. American journal of Science 306, 799-845. DOI 10.2475/10.2006.02.

Demoux, A., Kroner, A., Liu, D.Y., Badarch, G., 2009. Precambrian crystalline basement in southern Mongoliaas revealed by SHRIMP zircon dating. International Journal of Earth Science 98:1365-1380.

Dewey, J., Mange. M., 1999. Petrography of Ordovician and Silurian sediments in the western Irish Caledonides: Tracers of a short-lived Ordovician continent-arc collision orogeny and the evolution of the Laurentian Appalachian-Caledonian margin, in Continental Tectonics, edited

by M. Niocaill and P. D. Ryan, Geological Society Special Publication 164, 55-107.

Direen, N.G., Jago, J.B., 2008.The Cottons Breccia (Ediacaran) and its tectonostratigraphic context within the Grassy Group, King Island, Australia: A rift-related gravity slump deposit. Precambrian Research 165, 1–14.

Dobretsov, N.L., Berzin, N.A. and Buslov, M.M., 1995. Opening and tectonic evolution of the Paleo-Asian ocean. International Geology Review 35, 335−360.

Ernst, W. G., 2005. Alpine and Pacific styles of Phanerozoic mountain building: Subduction-zone petrogenesis of continental crust. Terra Nova 17, 165–188.

Fedo, C.M., Sircombe, K.N., Rainbird, R.H., 2003. Detrital zircon analysis of the sedimentary record, Review Mineral Geochemistry 53, 277-303.

Grabau, A.W., 1931. The Permian of Mongolia-A Report of the Permian Fauna of the Jisu Honguer Limstone of Mongolia and Its Relations to the Permian of Other Parts of the World. Natural History of Central Asia 4, 1-665.

Grant, W., Lowey., 2007. Lithofacies analysis of the Dezadeash Formation (Jura-Cretaceous), Yukon, Canada: The depositional architecture of a mud/sand-rich turbidite system. Sedimentary Geology 198, 273-291.

Groves,D.I., Bierlein, F. P., 2007. Geodynamic settings of mineral deposit systems. Journal of the Geological Society, London 164, 19–30.

Guillot, S., Hattori, K., Agard, P., Schwartz, S., Vidal, O., 2009. Exhumation processes in oceanic and continental subduction contexts: a review. In: Lallemand, S., Funiciello, F. (Eds.), Subduction Zone Geodynamics. Springer-Verlag Berlin Heidelberg 175-205 p.

Hall, L. M., and Roberts, D., 1988. Timing of Ordovician deformation in the Caledonian-Appalachian orogen, in The Caledonian-Appalachian Orogen, edited by A. L. Harris and D. J. Fettes, Geological Society Special Publication 38, 291-309.

Hanchar, J.M., Rudnick, R.L., 1995．Revealing hidden structures: The application of cathodoluminescence and back- scatter electron imaging to dating zircons from lower crustal xenoliths．Lithos 36, 289-303.

Hatcher, R. D., Jr., 1987.Tectonics of the southern and central Appalachian internides, Annual. Review of Earth Planetary Science 15, 337-362.

Hawkins, J.W., 2003. Geology of supra-subduction zones — implications for the origin of ophiolites. In: Dilek, Y., Newcomb, S. (Eds.), Ophiolite Concept and the Evolution of Geological Thought. Geological Society of America Special Paper 373. Boulder,Colorado, pp. 227–268.

Hoskin, P.W.O., Black, L.P., 2000. Metamorphic zircon formation by solid-state recrystallization of protolith igneous zircons. Journal of Metamorphic Geology 18,423-439.

Hsu, K. J., Wang, Q. Li, J., Hao, J., 1991.Geologic evolution of the Neimonides: A working hypothesis, Eclogae Geol. Helv., 84, 1-31.

Isozaki, Y. 1996. Anatomy and genesis of a subduction related orogen: A new view of geotectonic subdivision and evolution of the Japanese Islands. Island Arc, 5, 289–320.

Jacob A. Covault, Stephen M. Hubbard, Stephan A. Graham, Ralph Hinsch, Hans-Gert Linzer. 2009. Turbidite-reservoir architecture in complex foredeep-margin and wedge-top depocenters, Tertiary Molasse foreland basin system, Austria. Marine and Petroleum Geology 26,379-396.

Jahn, B. M. 2004. The Central Asian Orogenic Belt and growth of the continental crust in the Phanerozoic. In:Malpas, J., Fletcher, C. J. N., Ali, J.R.Aitcheson, J. C. (eds) Aspects of the Tectonic Evolution of China. Geological Society, London, Special Publications, 226, 73–100.

Jahn, B. M.,Wu,F.Y., Chen, B. 2000. Granitoids of the Central Asian orogenic belt and continental growth in the Phanerozoic. Transactions of the Royal Society of Edinburgh, Earth Sciences, 91, 181–193.

Jian, P., Liu, D.Y., et al. 2010. Evolution of a Permian intraoceanic arc–trench system in the Solonker suture zone, Central Asian Orogenic belt, China and Mongolia. Lithos, 118:169-190.

Jian, P., Liu, D.Y., Kroner, A., Windley, B.F., Shi, Y.R., Zhang, F.Q., Shi, G.H., Miao, L.C., Zhang, W., Zhang, Q., Zhang, L.Q., Ren, J.S., 2008. Time scale of an early to mid-Paleozoic

orogenic cycle of the long-lived Central Asian Orogenic belt, Inner Mongolia of China: Implications for continental growth. Lithos, 101:233-259.

Johnson, M.E.，Rong, J.Y.，Wang, C.Y., Wang, P., 2001. Continental island from the Upper Silurian (Ludfordian Stage) of Inner Mongolia: Implications for eustasy and paleogeography. Geology 29, 955-958.

Jolivet, L., Faccenna, C., Goffé, B., Burov, E., Agard, P., 2003. Subduction tectonics and exhumation of high-pressure metamorphic rocks in the Mediterranean orogens. American Journal of Science 303, 353-409.

Khain E.V., Bibikova E.V., Kröner A., Zhuralev D.Z., Sklyarov E.V., Fedotova A.A., Kravchenko-Berezhnoy I.R., 2002.The most ancient ophiolite of the Central Asian fold belt: U-Pb and Pb-Pb zircon ages for the Dunzhugur complex, Eastern Sayan, Siberia, and geodynamic implications, Earth Planetary Science Letter 199, 311-325.

Khain, E.V., Bibikova, E.V., Salnikova, E.B., Kro ¨ner, A., Gibsher, A.S., Didenko, A.N., Degtyarov, K.E., Fedotova, A.A., 2003. The Palaeo-Asian ocean in the Neoproterozoic and early Palaeozoic: new geochronologic data and palaeotectonic reconstructions. Precambrian Research 122, 329– 358.

Kimura, G., Maruyama, S., Isozaki, Y., Terabayashi, M., 1996. Well-preserved underplating structure of the jadeitized Franciscan compex, Pacheco Pass,

Kovalenko, V.I., Yarmolyuk, V.V., Kovach, V.P., Kotov, A.B., Kozakov, I.K., Salnikova, E.B., and Larin, A.M., 2004, Isotope provinces, mechanisms of generation and sources of the continental crust in the Central Asian mobile belt: Geological and isotopic evidence: Journal of Asian Earth Sciences 23, 605-627.

Kroner, A., Hegner, E., Lehmann, B., Heinhorst, J., Wingate, M. T. D., Liu,D.Y., Ermelov,P., 2008. Palaeozoic arc magmatism in the Central Asian Orogenic Belt of Kazakhstan: SHRIMP zircon ages and whole-rock Nd isotopic systematic. Journal of Asian Earth Sciences 32, 118–130.

Kroner,A. Windley, B.F., 2007. Accretionary growth and crust-formation in the central Asian Orogenic Belt and comparison with the Arabian Nubian shield. In: Hatcher, R. D., Jr. Carlson,

crustal processes through time. Geological Society of America, Memoirs 200, 181–210.

Kroner，A., Wilde，S.A., Li，J.H.，Wang，K.Y.，2005. Age and evolution of a late Arehean to Paleoproterozoic upper to lower crustal section in the Wutaishan-Hengshan-FuPing terrain of northern China. Journal of Asian Earth Sciences 24，577-595.

Kuzmichev, A.., Kroner A., Hegner, E., Liu, D.Y., Wan, Y.S., 2005. The Shishkhid ophiolite, northern Mongolia: A key to the reconstruction of a Neoproterozoic island-arc system in central Asia. Precambrian Research 138, 125-150.

Kuzmichev, A.B. Bibikova, E.V., Zhuravlev, D.Z., 2001. Neoproterozoic (800Ma) orogeny in the Tuva-Mongolian Massif (Siberia): island arc-continent collision at the northeast Rodinia margin. Precambrian Research 110, 109-126.

Leven, E. Y., Grunt T. A., Lin,Y. D., 2001. Upper Permian stratigraphy of the Zhesi Honguer area (North China). Stratigraphy and Geological Correlation 9, 441-453.

Li, J.Y., 2006. Permian geodynamic setting of Northeast China and adjacent regions: closure of the Paleo-Asian Ocean and subduction of the Paleo-Pacific Plate. Journal of Asian Earth Sciences 26, 207-224.

Lister, G. S., Forster,M.A., Rawlings, T. J. 2001. Episodicity during orogenesis. In:Miller, J. A.,Holdsworth, R. E., Buick,I.S., Hand,M.(eds) Continental Reactivaton and Reworking. Geological Society, London, Special Publications, 184, 89–113.

Lister, G.S., Forster, M., 1996. Inside the Aegean Metamorphic Core Complexes.

Technical Publication Australian Crustal Research Centre. 45, 110 p.

Ludwig, K. R., 2003. ISOPLOT 3.00: A Geochronological Toolkit for Microsoft Excel. Berkeley: Berkeley Geochronology Center, California.

Luiz, F.G.C., Renoto, O.K., Adriano, R.V., 1998. Slope sedimentary facies associated with Pleistocene and Holocene sea-level changes, Campos Basin, southeast Brazilian Margin. Sedimentary Geology 115, 159-174.

Lustrés complex: implications for the exhumation of HP and UHP rocks in the Western Alps. Bulletin Societe Geologique France 172 (5), 617-636.

Mann, P., 2007. Global catalogue, classification and tectonic origins of restraining and releasing bends on active and ancient strike-slip fault systems. In: Cunningham, W.D., Mann, P. (Eds.), Tectonics of Strike-Slip Restraining and Releasing Bends. Geological Society London Special Publications, 290, pp.13-142.

Maruyama, S. 1997. Pacific-type orogeny revisited: Miyashiro-type orogeny proposed. Island Arc, 6, 91–120.

Matsuda,T. Uyeda, S. 1971. On the Pacific-type orogeny and its model: Extension of the paired belts concept and possible origin of marginal seas. Tectonophysics, 11, 5–27.

Mcculloch, M.T., Bennett, V. C. 1994. Progressive growth of the Earth's continental crust and depleted mantle: Geochemical constraints. Geochimica et Cosmochimica Acta, 58, 4717–4738.

McHargue, T., Pyrcz, M.J., Sullivan, M.D., Clark, J.D., Fildani, A., Romans, B.W., Covault, J.A. , Levy, M., Posamnetier, H.W., Drinkwater, N.J., 2011. Architecture of turbidite channel systems on the continental slope: patterns and Predictions. Marine and Petroleum Geology 28, 728-743.

Meng, Q.R., 2003. What drove late Mesozoic extension of the northern China-Mongolia tract? Tectonophysics 369, 155-174.

Miao, L.C.，Zhang, F.Q.，Fan, W.M., Liu, D.Y., 2007. Phanerozoic evolution of the Inner Mongolia-Daxinganling orogenic belt in North China: Constraints from geochronology of ophiolites and associated formations. In: Zhai MG，Windley BF，Kusky TM and Meng QR(eds). Mesozoic Sub-Continental Lithospheric Thinning under Eastern Asia. Geological Society，London，Special publications，280:223-237

Miyashiro, A., 1973. Metamorphism and Metamorphic Belts. Halstead Press, New York.

Moecher, D.P., Samson, S.D., 2006. Differential zircon fertility of source terranes and natural bias in the detrital zircon record: Implications for sedimentary provenance analysis: Earth and Planetary Science Letters 247, 252-266.

Mossakovsky, A.A., Ruzhentsev, S.V., Samygin, S.G. & Kheraskova, T.N. 1993. Central Asian

fold belt: geodynamic evolution and history of formation. Geotectonics, 6, 3–33.

Mossakovsky, A.A., Ruzhentsev, S.V., Samygin, S.G., Kheraskova, T.N., 1994. Central Asia fold belt: geodynamic evolution and formation history. Geotectonics 27, 445-474.

Mueller, J.F., Rogers, J.J.W., Wang, H.Y., Li, W.G., Chronic, J., Mueller, J.F., 1991. Late Carboniferous to Permian sedimentation in Inner Mongolia, China, and tectonic relationships between North China and Siberia. Journal of Geology 99, 251-263.

Murphy,J.B., Nance, R. D. 1991. Supercontinent model for the contrasting character of Late Proterozoic orogenic belts. Geology, 19, 469–472.

Nelson, D.R.，2001.Anassessment of the determination of depositional ages for Precambrian clastic sedimentary rocks by U- Pb dating of detrital zircon . Sedimentary Geology 141,37-60.

Nie, F., Bjørlykke, A., 1999. Nd and Sr isotope constraints on the age and origin of Proterozoic meta-mafic volcanic rocks in the Bainaimiao-Wenduermiao district, south-central Inner Mongolia, China, Cont. Dyn., 4, 1-14.

Nozaka, T., Liu, Y., 2002. Petrology of the Hegenshan ophiolite and its implication for the tectonic evolution of northern China.Earth and Planetary Science Letters 202, 89-104.

Partha, P. C., Basab, M., Tapan, P., Tanay, D. G., 2002. Statistical appraisal of bed thickness patterns in turbidite successions, Andaman flysch Group, Andaman Islands, India. Journal of Asian Earth Sciences 24, 189-196.

Payne，J.L., Barovieh, K.M., Hand, M., 2006. Provenance of metasedimentary rocks in the northern Gawler Craton, Australia: Implications for Palaeoproterozoic reconstructions，Precambrian Research 148，275-291.

Platt, J.P., 1993.Exhumation of high-pressure rocks: a review of concepts and processes. Terra Nova 5, 119-133.

Platt, J.P., 1993. Exhumation of high-pressure rocks: a review of concepts and processes. Terra Nova 5, 119-133.

Postma, G., 1984. Slumps and their deposits in fan delta front and slope. Geology 12, 27-30.

Jacobi, R.D. 1984, Modern submarine sediment slides, in Raymond, L.A., ed., Mélanges: Their nature, origin, and significance: Geological Society of America Special Paper 198, 81-102.

Reading, H.G., 1996.Sedimentary environments: Processes, Facies and stratigraphy. Third edition, Blackwell Publishing Company.

Ring, U., Brandon, M. T., Lister, G. S. , Wlllett, S. D., (eds) 1999. Exhumation Processes: Normal Faulting, Ductile Flow and Erosion. Geological Society, London, Special Publications 154.

Ring, U., Brandon, M.T., 1994. Kinematic data for the Coast Range fault and implications for exhumation of the Franciscan subduction complex. Geology 22, 735-738.

Ring, U., Laws, S., Bernet, M., 1999. Structural analysis of a complex nappe sequence and late-orogenic basins from the Aegean Island of Samos, Greece. Journal of Structural Geology 21, 1575-1601.

Ring, U., Layer, P.W., 2003. High-pressure metamorphism in the Aegean, eastern

Rojas-Agramonte, Y., Kroner, A., Demoux, A., Xia, X.,Wang,W., Donskaya, T., Liu, D., Sun,M.,2011. Detrital and xenocrystic zircon ages from Neoproterozoic to Paleozoic arc terranes of Mongolia: Significance for the origin of crustal fragments in the Central Asian Orogenic Belt. Gondwana Research 19,751-763.

Royden, L. H. 1993. Evolution of retreating subduction boundaries formed during continental collision. Tectonics, 12, 629–638.

Ruzhentsev, S. V., Pospelov, I. I., Badarch, H. 1989. Geotektonika 6, 13-27.

Salnikova, E.B., Kozakov, I.K., kotov, A.B., kroner, A., Todt, W., Bibikova, E.V., Nutman, A., Yakovleva, S.Z., Kovach, V.P., 2001. Age of Palaeozoic granites and metamorphism in the Tuvino-Mongolian Massif of the central Asian Mobile Blet: loss of a Precambrian microcontinent. Precambrian Research 110, 143-164.

Samson,S.D. , Patchett, P. J. 1991. The Canadian cordillera as a modern analogue of Proterozoic crustal growth. Australian Journal of Earth Sciences, 38, 595–611.

Sengor, A. M. C., Natal'in, B. A., and Burtman, V. S., 1993, Evolution of the Altaid tectonic collage and Paleozoic crustal growth in Eurasia: Nature 364, 299-307.

Sengor, A. M. C., Okurogullari. A. H., 1991.The role of accretionary wedges in the growth of continents: Asiatic examples from Argand to Plate Tectonics Eclogae Geol. Helv., 84, 535-597.

Sengor, A.M.C., Natalin, B.A., 1996. Turkic-type orogeny and its role in the making of the continental crust. Annual Reviews of Earth and Planetary Sciences 24,263-337.

Shao, J., 1989. Continental crust accretion and tectono-magmatic activity at the northern margin of the Sino Korean plate, Journal of Southeast Asian Earth Science 3, 57-62,

Sisson, V. B., Roeske,S., Pavlis, T. L. (eds) 2003. Geology of a Transpressional orogen developed during Ridge–Trench Interaction along the North Pacific Margin. Geological Society of America, Special Papers, 371.

Stanek, K.P., Maresch, W.V., Grafe, F., Grevel, C., Baumann, A., 2006. Structure,

tectonics and metamorphic development of the Sancti Spiritus Dome (eastern

Escambray massif, Central Cuba). Geologica Acta 4, 151-170.

Stern, R. J., Johnson, P. R., Kroner,A.,Yibas,B. 2004. Neoproterozoic ophiolites of the Arabian Nubian Shield. In:Kusky, T. M. (ed.) Precambrian Ophiolites and Related Rocks. Elsevier Developments in Precambrian Geology, 13, 95–128.

Stern, R.J., 2004. Subduction initiation: spontaneous and induced. Earth and Planetary Science Letters 226, 275-292.

Stern, R.J., Bloomer, S.H., 1992. Subduction zone infancy: Examples from the Eocene Izu-Bonin-Mariana and Jurassic California, Geological Society of American Bullutin, 104, 1621-1636.

Tang, K., 1990. Tectonic development of Paleozoic fold belts at the north margin of the Sino-Korean craton. Tectonics 9, 249-260.

Tang, K.D., Yan Z.Y., 1993.Regional metamorphism and tectonic evolution of the Inner

Mongolian suture zone. Journal of Metamorphic Geology 11, 511-522.

Tang, K.D., Zhang, Y.P., 1991. Tectonic evolution of Inner Mongolia. In: Xiao, X.C., Tang, Y.Q. (Eds.), Tectonic Evolution of the Southern Margin of the Paleo-asian Composite Megasuture. Scientific and Tectonical Publishing House, Beijing, pp30-53 (in Chinese with English abstract).

Tatsumi,Y., Eggins, S. 1995. Subduction zone magmatism. Blackwell, Cambridge, MA.

Taylor, S. R. 1967. The origin and growth of continents. Tectonophysics, 4, 17–34.

Taylor,S.R., Mcclennan, S. M. 1985. The Continental Crust: Its Composition and Evolution. Black well Scientific, Oxford.

Walker, R.G., 1978. Deep-water sandstone facies and ancient submarine fans: model for exploration for stratigraphic traps. American Association of Petroleum Geologists Bulletin 62, 932-966.

Wan, Y.S., Wilde, S.A., Liu, D.Y.,Yang, C.X.,Song, B., Yin, X.Y.,2006. Furthern evidence for ~1.85Ga metamorphism in the central zone of the North China Craton:SHRIMP U-Pb dating of zircon from metamorphic rocks in the Lushan area, Henan Province. Gondwana Research 9, 189-197.

Wang, B., Faure, M., Cluzel, D., Shu, L.S., Charvet, J., Meffre, S., Ma, Q., 2006. Late Paleozoic tectonic evolution of the northem West Chinese Tianshan Belt. Geodinamica Acta 19, 237-247.

Wang, Q., Liu, X.Y., 1986. Paleoplate tectonics between Cathaysia and Angaraland in Inner Mongolia of China. Tectonics 5, 1073-1088.

Wang, T., Zheng, Y., Gehrels, G.E., Mu, Z., 2001.Geochronological evidence for existence of South Mongolian microcontinent; a zircon U-Pb age of granitoid gneisses from the Yagan-Onch Hayrhan metamorphic core complex on the Sino-Mongolian border. China Science Bulletin 46, 2005-2008.

Wiedenbeck, M., Alle, P., Corfu, F., Griffin, W. L., Meier, M., Oberli, F., Quadt, A. V., Roddick, J.

C. , Spiegel, W., 1995. Three natural zircon standards for U-Th-Pb, Lu-Hf, trace element and REE analyses. Geostandards and Geoanalytical Research 19, 1-23.

Wilde, S.A., Wu, F.Y., Zhang, X.Z., 2003. Late Pan-African magmatism in northeastern China. SHRIMP U-Pb zircon evidence from granitoids in the jiamusi Massif. Precambrian Research 122, 311-327.

Wilde, S.A., Zhang, X.Z., Wu, F.Y., 2000. Extension of a newly identified 500Ma metamorphic terrane in North East China: further U-Pb SHRIMP dating of the Mashan Complex, Heilongjiang Province, China. Tectonophysics. 328, 115-130.

Wilde，S.A.，Zhao，G.C.，2005.Archean to Paleoproterozoic evolution of the North China Craton. Journal of Asian Earth Sciences 24，519-522.

Williams, I.S., 2001.Response of detrital zircon and monazite，and their U—Pb isotopic systems，to regional metamorphism and host-rock partial melting, Cooma Complex，southeastern Australia. Australia Journal of Earth Science 48, 557-580.

Williams, I.S., Buick, I.S., Cartwright, I., 1996. An extended episode of early Mesoproterozoic metamorphic fluid flow in the Reynolds Range, central Australia. Journal of Metamorphic Geology 14, 29-47.

Wilson, J. T. 1966. Did the Atlantic close and then re-open? Nature, 211, 676–681.

Windley, B. F., 1992. Proterozoic collisional and accretionary orogens. In:Condie, K. C. (ed.) Proterozoic Crustal Evolution. Developments in Precambrian Geology 10, 419–446.

Windley, B. F., Alexeiev, D., Xiao, W., Kroner,A., Badarch, G., 2007. Tectonic models for accretion of the central Asian orogenic belt. Journal of the Geological Society, London 164, 31–47.

Wu, F.Y., Jahn, B.M., Wilde,S., SUN, D.Y. 2000. Phanerozoic crustal growth: U–Pb and Sr–Nd isotopic evidence from the granites in northeastern China. Tectonophysics, 328, 89–113.

Xiao W. J., Windley, B. F. Huang, B. C. Han, C. M. Yuan, C., Chen, H. L., Sun M., Sun S. , Li J. L.,2009. End-Permian to mid-Triassic termination of the accretionary processes of the

southern Altaids: implications for the geodynamic evolution, Phanerozoic continental growth, and metallogeny of Central Asia. International Journal of Earth Science 98, 1189–1217.

Xiao, W., Windley, B.F., Badarch, G., Sun, S., Li, J., Qin, K., Wang, Z., 2004, Palaeozoic accretionary and convergent tectonics of the southern Altaids: implications for the lateral growth of Central Asia. Journal of the Geological Society, London 161, 339-342.

Xiao, W.J., Han, C.M., Sun, M., Lin S.F., Chen, H.L., Li,Z.L., Li,J.L., Sun, S., 2008. Middle Cambrian to Permian subduction-related accretionary orogenesis of Northern Xinjiang, NW China: Implications for the tectonic evolution of central Asia. Journal of Asian Earth Sciences 32, 102–117.

Xiao, W.J., Kusky, T., 2009. Geodynamic processes and metallogenesis of the Central Asian and related orogenic belts: Introduction. Gondwana Research 16, 167-169.

Xiao, W.J., Zhang, L.C., Qin, K. Z., Sun, S., Li, J.L., 2004, Paleozoic accretionary and collisional tectonics of the Eastern Tianshan (China): Implications for the continental growth of central Asia. American Journal of Science 304, 370-395.

Xiao,W.J.,Windley, B.F., Hao, J., Zhai,M., 2003. Accretion leading to collision and the Permian Solonker suture, Inner Mongilia, China: termination of the Central Asian Orogenic Belt. Tectonics 22, 1069. doi:10.1029/2002TC001484.

Yakubchuk, A., 2008. Reciphering the tectonic jigsaw puzzle of northern Eurasia. Journal of Asian Earth Sciences32:82-10.

Yakubchuk, A.S., 2002. The Baikalide-Altaid, Transbaikal-Mongolian and North Pacific orogenic collage: similarity and diversity of structural patterns and metallogenic zoning. In: Blundell, D.J., Neubauer, F., von Quadt, A. (Eds.), The Timing and Location of Major Ore Deposits in an Evolving Orogen, Geological Society of London, vol. 204. Special Publication, pp. 273–297.

Yakubchuk,A., 2004. Architecture and mineral deposit settings of the Altaid orogenic collage: a revised model. Journal of Asian Earth Sciences 23, 761-779.

Yakubchuk,A., Shatov, V.V., Kirwin, D., Edwards, A., Tomurtogoo., Badarch, G.,Buryak,

V.A.,2005. Gold and base metal metallogeny of the Central Asian Super collage. Economic Geology 100th Anniversary Volume, 1035-1068.

Yan, Z.Y., Tang, K.D., Bai, J.W., Mo, Y.C., 1989. High pressure metamorphic rocks and their tectonic environment in northeastern China: Journal of South East Asian Earth Sciences 3, 303-313.

Yarmolyuk, V.V., Kovalenko, V.I., Salnikova, E.B., Kozakov, I.K., Kotov, A.B., Kovach, V.P., Vladykin, N.V., Yakovleva, S.Z., 2005.U-Pb age of syn- and post-metamorphic granitoids of south Mongolia: evidence for the presence of Grenvillides in the Central Asian Fold belt. Doklady Earth Sci 404, 986-990.

Zhai，M.G.，Liu，W.J.，2003.Palaeoproterozoic tectonic history of the North China craton: a review. Preeambrian Research 122，183-199.

Zhang, S.H.，Zhao ,Y.，Song, B.，Yang, Z.，Hu, J.M., Wu, H. , 2007. Carboniferous granitic plutons from the northern margin of the North China block: Implications for a Late Paleozoic active continental margin. Journal of the Geological Society, London 164, 451－463.

Zhang, S.H.，Zhao, Y.，Kroner, A.，Liu, X.M.，Xie, L.W., Chen, F.K., 2009. Early Permian plutons from the northern North China block: Constraints on continental arc evolution and convergent margin magmatism related to the Central Asian Orogenic belt. International Journal of Earth Sciences 121, Doi 10. 1007/s00531－008－0368－2.

Zhang, S.H.，Zhao, Y.，Liu, X.C.，Liu, D.Y.，Chen, F.K.，Xie, L.W., Chen, H.H., 2009a. Late Paleozoic to Early Mesozoic mafic-ultramafic complexes from the northern North China Block:Constraints on the composition and evolution of the lithospheric mantle. Lithos 110, 229－246.

Zhang, S.H.，Zhao, Y.，Song, B.，Hu, J.M.，Liu, S.W.，Yang, Y.H.，Chen, F.K.，Liu, X.M., Liu, J., 2009b. Contrasting Late Carboniferous and Late Permian-Middle Triassic intrusive suites from the northern margin of the North China craton: Geochronology，petro-genesis and tectonic implications. Geological Society of America Bulletin 121, 181-200.

Zhang, W., Jian, P., Kröner, A., Shi, Y.R., 2012. Magmatic and metamorphic development of an

early to mid-Paleozoic continental margin arc in the southernmost Central Asian Orogenic Belt, Inner Mongolia, China.Journal of Asian Earth Sciences, http://dx.doi.org/10.1016/j.jseaes. 2012.05.025.

Zhang, X.H., Gao, Y.L., Wang, Z.J., Liu, H., Ma, Y.G., 2012. Carboniferous appinitic intrusions from the northern North China craton: geochemistry, Petrogenesis and tectonic implications. Journal of the Geological Society 169, 337-351.

Zhang, X.H., Simon, A., Wilde, Zhang, H.F., 2011. Early Permian high-K calc-alkaline volcanic rocks from NW Inner Mongolia, North China: geochemistry, origin and tectonic implications. Journal of the Geological Society, London 168, 525-543.

Zhang, X.H.，Zhang, H.F.，Jiang, N.，Zhai, M.G., Zhang, Y.B., 2010. Early Devonian alkaline intrusive complex from the northern North China Craton:A petrologic monitor of post-collisional tectonics. Journal of the Geological Society, London 167, 10. 1144/0016－76492009－110

Zhang, X.H.，Zhang, H.F.，Tang, Y.J.，Wilde, S.A., Hu, Z.C. , 2008. Geochemistry of Permian bimodal volcanic rocks from Central Inner Mongolia，North China: Implication for Tectonic setting and Phanerozoic continental growth in Central Asian Orogenic Belt. Chemical Geology 249, 261-281.

Zhao, G. C., Sun, M., Wilde, S., 2005. Late Archean to Paleoproterozoic evolution of the North China Craton: key issues revisited. Precambrian Research 136, 177-200.

Zhao，G.C.，Cawood，P.A.，Wilde，S.A.，Sun，M.，Lu，L.，2000. Metamorphism of basement rocks in the Central Zone of the North China craton: implications for Palaeoproterozoic tectonice volution. Precambrian Research 103,55-88.

Zhou, D., Graham S.A., 1996. Songpan-Ganzi complex of west Qinling Shan as Triassic remnant ocean basin fill trapped during the Mesozoic tectonic amalgamation of China, in: Yin A., Harrison T.M.eds., Tectonic evolution of Asia, Cambridge, Cambridge University Press, 281–299.

Zhu, Y.F.，Sun, S.H., Gu, L.B., 2001. Permian volcanism in the Mongolian orogenic zone，

northeast China: Geochemistry，magma sources and petrogenesis. Geological Magazine 138, 101-115.

Zonenshain, L.P., Kuzmin, M.I. & Natapov, L.M. (eds) 1990. Geology of the USSR: a Plate-Tectonic Synthesis. American Geophysical Union, Geodynamic Series, 21.

Reference in Chinese:

鲍庆中，张长捷，吴之理等. 2006. 内蒙古东南部西乌珠穆沁旗地区石炭纪-二叠纪岩石地层和层序地层. 地质通报，25（5）：572-579.

曹从周，杨芳林，田昌裂等. 1986. 内蒙古贺根山地区蛇绿岩及中朝板块和西伯利亚板块之缝合带位置. 中国北方板块构造论文集(第一集). 北京:地质出版社，P64-86.

陈从云. 1993. 白云鄂博群渣尔泰群和化德群的时代隶属. 地质通报 (1).

晨辰. 2011. 内蒙古达茂旗地区早二叠世火山岩的年代学、地球化学及其地质意义. 北京大学硕士论文.

高德臻，蒋干清. 1998. 内蒙古苏尼特左旗二叠系的重新厘定及大地构造演化分析. 中国区域地质，17（4）:401-411.

郭谦谦， 肖文交， 侯泉林， 韩春明， 曲军锋， 田忠华， 宋东方. 2013. 北山造山带古生代浊积岩构造环境探讨及其大地构造意义 . 地质科学， 48（1）：50-70.

洪大卫，黄怀曾，肖宜君等. 1994. 内蒙古中部三叠纪碱性花岗岩及其地球动力学意义. 地质报，68(3):219-230.

洪大卫，王涛， 童英，等. 2003. 华北地台和秦岭-大别-苏鲁造山带的中生代花岗岩与深部地球动力学过程. 地学前缘，10（3）：231-256.

胡骁,许传诗，牛树银等，1990. 华北地台北缘早古生代大陆边缘演化. 北京大学出版社.

黄汲清，1945. 中国主要地质构造单位. 中央地质调查所地质专报.

黄金香，赵志丹，张宏飞等.2006. 内蒙古温都尔庙和巴彦敖包-交其尔蛇绿岩的元素与同位素地球化学：对古亚洲洋东部地幔域特征的限制.岩石学报,22(12),2889-2900.

李春笠. 1980. 中国板块构造的轮廓.中国地质科学院院报，2(1):11-22.

李春昱，汤耀庆.1983.亚洲古板块划分以及有关问题.地质学报 (1).

李福来，曲希玉，刘立等. 2009.内蒙古东北部上二叠统林西组沉积环境.沉积学报， 27（2）：265-272.

李继亮，2004. 增生型造山带的基本特征.地质通报，23（9-10）：947-951.

李建锋，张志诚，韩宝福. 2010.内蒙古达茂旗北部闪长岩锆石 SHRIMP U-Pb、角闪石 $^{40}Ar/^{39}Ar$ 年代学及其地质意义. 岩石矿物学杂志，29（6）：732-740.

李尚林，王训练，徐兴永等. 2004.内蒙古哲斯敖包茅口期生物礁特征.沉积学报，22（3）：434-442.

李述靖,高德臻.1995.内蒙古苏尼特左旗地区若干地质构造新发现及其构造属性的初步探讨.现代地质，9（2）：130-141.

李述靖，张维杰，耿明山. 1998. 蒙古弧地质构造特征及形成演化概述. 北京:地质出版社，145.

李文国.李庆富，姜万德等.1996.内蒙古白治区岩石地层.武汉: 中国地质大学出版社.

梁日暄. 1994.内蒙古中段蛇绿岩特征及地质意义.中国区域地质(1):37-45.

刘长安，单际彩. 1979.试谈蒙古-鄂霍茨克海待古板块构造的基本特征. 长春地质学院院报（2）.

刘敦一，简平，张旗，张福勤，石玉若，施光海，张履桥，陶华. 2003. 内蒙古图林凯蛇绿岩中埃达克岩 SHRIMP 测年:早古生代洋壳消减的证据. 地质学报，77:318－327

柳长峰，杨帅师，武将伟等.2010.内蒙古中部四子王旗地区晚二叠-早三叠世过铝花岗岩定年及成因.地质学报，84（7）：1002-1016.

柳长峰，张浩然，於炀森等.2010a.内蒙古中部四子王旗地区北极各岩体锆石定年及其岩石化学特征.现代地质，24，（1）：112-150.

吕志成，郝立波，段国正，李殿超，潘军．2002．大兴安岭南段早二叠世两类火山岩的的岩石地球化学特征及其构造意义．地球化学，31:338－346

莫宣学，赵志丹，邓晋福等.2007.青藏新生代钾质火山活动的时空迁移及向东部玄武岩省的过渡:壳幔深部物质流的暗示．现代地质．21(2):255-264.

任纪舜，姜春发，张正坤，秦德余．1980.中国大地构造及其演化．地图出版社.

任纪舜，牛宝贵.刘志刚.1999.软碰撞、叠覆造山和多旋回缝合作用.地学前缘，6(3):85-93.

尚恒胜，陶继雄，宝音乌力吉.2003.内蒙古白云鄂博地区早古生代弧-盆体系及其构造意义．地质调查与研究，26（3）：160-168.

尚庆华．2004.北方造山带内蒙古中、东部地区二叠纪放射虫的发现及意义.科学通报，49（24）：2574-2579.

邵济安.1991.中朝板块北缘中段地壳演化.中国北方板块构造丛书.北京大学出版社.

邵济安等.2007.大兴安岭的隆起与地球动力学背景.北京 地质出版社.

沈存利，黄占起，苏宏伟等.2004.内蒙古铜矿床区域成矿特征初步研究.西北地质，（3）：44-50.

施光海，刘敦一，张福勤，简平，苗来成，石玉若，陶华．2003.中国内蒙古锡林郭勒杂岩 SHRIMP 锆石 U-Pb 年代学及意义.科学通报,48(20):2187-2192.

石玉若，刘敦一，张旗，简平，张福勤，苗来成，施光海，张履桥，陶华．2004．内蒙古苏左旗地区闪长-花岗岩类 SHRIMP 年代学．地质学报，78:789－799

石玉若，刘敦一，张旗等.2007.内蒙古中部苏尼特左旗地区三叠纪 A 型花岗岩锆

石 SHRIMP U-Pb 年龄及其区域构造意义.地质通报，26（2）：183-189.

苏新旭，孟二根，张永清. 2000. 内蒙古达茂旗满都拉地区晚古生代板块活动探讨.内蒙古地质 1:17-35.

苏养正.1996.中国东北区二叠纪和早三叠世地层.吉林地质，15（3-4）：55-65.

孙德有，吴福元.张艳斌等. 2004.西拉木伦河-长春-延吉板块缝合带的最后闭合时间-来自吉林大玉山花岗岩体的证据.吉林大学学报(地球科学版),34(2):174-181.

唐克东,1991. 中朝板块北侧褶皱带构造演化及成矿规律. 中国北方板块构造丛书.北京大学出版社.

唐克东、颜竹筠等. 1983. 关于温都尔庙群及其构造意义. 中国北方板块构造文集 1.

陶继雄,白立兵,宝音乌力吉等.2003. 内蒙古满都拉地区二叠纪俯冲造山过程的岩石记录.地质调查与研究，26（4）：241-249.

陶继雄，苏茂荣，宝音乌力吉等. 2004.内蒙古达尔茂明安联合旗满都拉地区索伦山蛇绿混杂岩的特征及构造意义.地质通报，23（12）：1238-1242.

陶继雄，许立权，贺锋等. 2005. 内蒙古巴特敖包地区早古生代洋壳消减的岩石证据. 地质调查与研究:28（1）：1-7.

王成文，金巍，张兴洲. 2008.东北及邻区晚古生代大地构造属性新认识.地层学杂志，32(2):119-136.

王成文，张松梅. 2003.哲斯腕足动物群.北京:地质出版社.

王成源，王平，李文国.2006.内蒙古二叠系哲斯组的牙形刺及其时代.古生物学报，45（2）：195-206.

王国灿 张克信等.1997，东昆仑造山带结构及构造岩片组合. 地球科学， 22（4）:352-356.

王惠，陈志勇，杨万容等. 2002.内蒙古满都拉二叠纪海绵生物丘的发现及意义.

地层学杂志，26（1）：33-38.

王惠，王玉净，陈志勇等. 2005. 内蒙古巴彦敖包二叠纪放射虫化石的发现.地层学杂志,29(4):368-371.

王惠，王玉净，陈志勇等. 2005.内蒙古巴彦敖包二叠纪放射虫化石的发现.地层学杂志，29(4):368-371.

王楫，李双庆，王保良 等. 1992. 狼山-白云鄂博裂谷系. 中国北方板块构造丛书. 北京：北京大学出版社.

王楫，孙玉芳，陆松年，李惠民.1991.白云鄂博群单颗粒锆石 U-Pb 年龄测定结果及地质意义.见：中国北方前寒武纪同位素地质年代学学术讨论会论文摘要汇编。

王平. 2006.内蒙古巴特敖包地区早泥盆世牙形刺.微体古生物学报 23(3):199-234

王荃，刘雪亚，李锦轶.1991.中国华夏与安加拉古陆间的板块构造.北京大学出版社出版.

王玉净，樊志勇. 1997.内蒙古西拉木伦河北部蛇绿岩带中二叠纪放射虫的发现及其地质意义.古生物学报. 36(1):58-67.

肖荣阁，彭润民，王美娟等. 2000. 华北地台北缘西段主要成矿系统分析，地球科学（中国地质大学学报），25（4），362-368.

谢鸣谦.2000.拼贴板块构造及其驱动机理一中国东北及其邻区的大地构造演化.北京:科学出版社.

谢同伦，1980.内蒙古古生代地槽的兴衰。内蒙古地质，(2).

徐备，J.Charvet，张福勤.2001.内蒙古北部苏尼特左旗蓝片岩岩石学和年代学研究.地质科学，36（4）：424-434.

徐备，陈斌. 1997.内蒙古北部华北板块与西伯利亚板块之间中古生代造山带的结构和演化.中国科学（D 辑），27(3):227-232.

徐志琴， 徐惠芬， 张建新． 1994.北祁连走廊南山加里东俯冲杂岩增生地体及其动力学．地质学报，６８（１）：1-15.

徐志琴，侯立玮，王宗秀等，1992，中国松绣-甘孜造山带的造山过程，地质出版社.

许立权，邓晋福，陈志勇等. 2003. 内蒙古达茂旗北部奥陶纪埃达克岩类的识别及其意义.现代地质，17（4）：428-434.

许立权，陶继雄.2003. 内蒙古达茂旗北部奥陶纪花岗岩类特征及其构造意义.华南地质与矿产，23（1）：17-22.

许立权.2005.内蒙古白云鄂博—满都拉地区加里东期—华力西期—印支期岩浆岩特征与大地构造演化探讨. 中国地质大学（北京）博士学位论文.

杨宗让，2002. 川西松潘一 甘孜弧前盆地的形成及演化.沉积与特提斯地质，22（3）：53-59.

张臣、吴泰然.2001.内蒙古苏左旗南部华北板块北缘中新元古代-古生代裂解-汇聚事件的地质记录。岩石学报，17(2):199-205.

张维，简平，刘敦一等.2010.内蒙古中部达茂旗地区三叠纪花岗岩和钾玄岩的地球化学、年代学和 Hf 同位素特征. 地质通报，29（6）：821-832.

张晓晖,翟明国. 2010.华北北部古生代大陆地壳增生过程中的岩浆作用与成矿效应.岩石学报，26(05)：1329-1341.

张晓晖,翟明国.华北北部古生代大陆地壳增生过程中的岩浆作用与成矿效应.岩石学报，2010，026(05)：1329-1341

张玉清,梁丽新,王弢等. 2004.内蒙古达茂旗北瓦窑西别河组、查干哈布组及二者间的不整合.华南地质与矿产, 01:48-55.

张玉清，苏宏伟.2002. 内蒙古宝音图岩群变质基性火山岩锆石 U-Pb 年龄及意义.前寒武纪 研究进展,25(3-4) :199-204.

张玉清. 2002. 内蒙古达茂旗北白云鄂博群阿牙登组藻类化石的发现及其地质

意义. 03(104):10-14.

张玉清.2004.内蒙古白云鄂博北部宝音图岩群变质基性火山岩的年龄、构造背景及地质意义. 地质通报，23（2）：177-183.

张宗清，袁忠信，唐索寒等. 2003.白云鄂博矿床年龄和地球化学.北京：地质出版社.

章永梅，张华锋，周志广等.内蒙古四子王旗大庙花岗岩体的成因与构造意义. 矿物岩石，28（2）：28-38.

赵磊，吴泰然，罗红玲等.2008a. 内蒙古白云鄂博地区呼和恩格尔杂岩体的地球化学特征及其构造意义.高校地质学报.14(1):29—38.

赵磊，吴泰然，罗红玲等.2008b. 内蒙古乌拉特中旗温更辉长岩类的岩石学、地球化学特征及其构造意义.北京大学学报(自然科学版),44(2):201-211.

朱永峰，孙世华，毛骞，赵光.2004.内蒙古锡林格勒杂岩的地球化学研究：从 Rodinia 聚合到古亚洲洋闭合后碰撞造山的历史记录.高校地质学报，10（3）：343-355.

内蒙古区域地质志，1991.内蒙古自治区地质矿产局.

满都拉地区 1/25 万区调，2003.内蒙古区域地质调查院.

艾力格庙 1/20 万区调，1981. 内蒙古区域地质调查院.

白云鄂博地区 1:25 万区调，2002. 内蒙古区域地质调查院

附录一　研究区古生代岩浆岩年代统计

Study area	Setting	Lithology	Age/Ma	Dating method	Geochemisty	Reference	Remarks
Hongqi	Bater Obo arc	diortie (1)	451.5±2.9	zircon SHRIMP	high-K calc-alkaline	Jian et al., 2008	
		quartz diorite (1)	440.3±2.4		high-K calc-alkaline adakite		
		quartz diorite (1)	446±2.2		high-K calc-alkaline		
		hornblendite (2)	446.8±5.8	zircon SHRIMP		Li et al., 2010	
		hornblendite (2)	453±3				
		diortie (2)	459.2±2.4	hornblende 40Ar/39Ar			
		diortie (2)	442.9±4.2	hornblende 40Ar/39Ar			
	Hongqi melange	**acidic volcanite**	**485±14**	**zircon ICP-MS**	**block within melange**	**this study**	
	North China Craton (south of Bayan Obo-Chifeng fault)	rhyolite (3)	270±2	zircon SHRIMP	alkaline	Chen., 2011	εNd(t)=-9.5~-10.3;mantle magma mixed with crust
		dacite (3)	272.5±2.6				
		hornblend pyroxenite (4)	287±13.6	hornblende K-Ar	zoned ulmafic-mafic pluton	Zhao et al., 2008	
Ondor Sum	melange	blueschist	446±15 & 426±15	glaucophane 40Ar/39Ar		Tang and Zhang, 1991	
		quartzite mylonite (5)	453.2 ±1.8 &449.4±1.8	phengite 40Ar/39Ar		De Jong, 2006	
Tulinkai		cumulate gabbro (6)	457±4	zircon SHRIMP		Miao et al., 2007	
		diorite (7)	467±6		adakitic geochemical signature	Liu et al., 2003	
		tonalite (8)	490.1±7.1		MORB with arc signature	Jian et al., 2008	core
			449.8±3.0				overgrowth mantle
		metagabbro (8)	479.6±2.4				
		trondhjemite (8)	471.6±1.7		magmatic zircon/low K boninite		
			439.4 ±3.3		metamorphic zircon		
		quartz diorite (8)	453.7±3.1		magmatic zircon/medium K peraluminous, calc-alkaline, high-Mg		
			438.4±2.2		metamorphic zircon		
		dacite (8)	457±2.6		medium K peraluminous, calc-alkaline, adakite		
		albitite (8)	425.3±2.2		boninite		

附录二　岩浆岩锆石U-Pb数据表

spot	concentritions(ppm)			Th/U	U-Pb isotopic ratios						age						concordance
	Pb Total	Th	U		$^{207}Pb/^{206}Pb$	1σ	$^{207}Pb/^{235}U$	1σ	$^{206}Pb/^{238}U$	1σ	$^{207}Pb/^{206}Pb$	1σ	$^{207}Pb/^{235}U$	1σ	$^{206}Pb/^{238}U$	1σ	
71629-01	59	38	529	0.07	0.1059	0.0033	1.4147	0.0442	0.0969	0.0014	809	121	618	25	567	8	8.99%
71629-02	57	95	499	0.19	0.1270	0.0037	1.5821	0.0468	0.0904	0.0012	752	157	560	30	514	7	8.95%
71629-03	53	39	495	0.08	0.0880	0.0029	1.1695	0.0387	0.0964	0.0014	580	120	574	23	572	8	0.35%
71629-04	191	80	1019	0.08	0.2262	0.0065	3.7293	0.1094	0.1196	0.0016	691	357	604	71	581	10	3.96%
71629-05	75	45	692	0.06	0.1329	0.0040	1.5750	0.0475	0.0860	0.0012	633	179	511	32	484	7	5.58%
71629-06	102	50	1040	0.05	0.0933	0.0028	1.1237	0.0343	0.0874	0.0012	539	121	521	21	517	7	0.77%
71629-07	42	29	374	0.08	0.1025	0.0034	1.3818	0.0457	0.0978	0.0014	600	143	576	27	570	8	1.05%
71629-08	72	52	710	0.07	0.1143	0.0035	1.3358	0.0417	0.0847	0.0012	642	150	517	27	490	7	5.51%
71629-09	39	77	404	0.19	0.0914	0.0029	1.0666	0.0347	0.0846	0.0012	798	110	563	21	507	7	11.05%
71629-10	124	276	1571	0.18	0.0623	0.0019	0.6582	0.0208	0.0766	0.0011	685	44	514	13	476	6	7.98%
71629-11	68	43	490	0.09	0.1701	0.0053	2.3634	0.0743	0.1008	0.0014	791	233	589	47	538	8	9.48%
71629-12	77	27	466	0.06	0.2167	0.0067	3.2237	0.1013	0.1079	0.0015	744	340	577	66	535	9	7.85%
71629-13	56	56	528	0.11	0.0818	0.0027	1.1007	0.0367	0.0976	0.0014	829	94	641	20	589	8	8.83%
71629-14	70	57	814	0.07	0.0700	0.0023	0.7880	0.0262	0.0817	0.0012	595	91	517	16	500	7	3.40%
71629-15	718	36	697	0.05	0.6918	0.0208	31.5738	0.9684	0.3310	0.0046	2385	1868	922	469	435	41	111.95%
71629-16	23	18	213	0.08	0.0888	0.0033	1.1858	0.0439	0.0969	0.0015	721	122	608	25	577	8	5.37%
71629-17	154	13	371	0.03	0.4824	0.0148	11.4598	0.3589	0.1723	0.0024	1400	965	703	214	505	17	39.21%
71629-18	44	77	399	0.19	0.1242	0.0040	1.5163	0.0498	0.0886	0.0012	880	150	582	30	509	7	14.34%
71629-19	424	93	756	0.12	0.5644	0.0175	16.2019	0.5107	0.2082	0.0029	1720	1189	765	285	480	23	59.38%
71629-20	162	105	552	0.19	0.3944	0.0123	7.4780	0.2372	0.1375	0.0019	1311	639	676	145	501	13	34.93%
71907-01	70	85	251	0.34	0.1221	0.0041	4.0433	0.1376	0.2402	0.0034	1782	81	1537	32	1365	18	**30.55%**
71907-02	37	387	417	0.93	0.0559	0.0021	0.5515	0.0207	0.0715	0.0010	448	58	446	14	445	6	0.22%
71907-03	48	23	204	0.11	0.1097	0.0037	3.2979	0.1121	0.2180	0.0031	1742	69	1455	26	1266	16	**37.60%**
71907-04	10	239	239	1.00	0.0603	0.0047	0.2586	0.0201	0.0311	0.0006	616	137	234	16	197	4	**18.78%**
71907-05	12	163	264	0.62	0.0514	0.0028	0.2875	0.0155	0.0406	0.0006	258	96	257	12	256	4	0.39%
71907-06	24	564	327	1.72	0.0774	0.0037	0.5234	0.0247	0.0490	0.0008	1131	67	427	16	309	5	**38.19%**
71907-07	22	105	269	0.39	0.0563	0.0025	0.5773	0.0256	0.0743	0.0011	465	72	463	16	462	7	0.22%

续附录二　岩浆岩锆石U-Pb数据表

spot	concentritions(ppm)			Th/U	U-Pb isotopic ratios						age						concordance
	Pb Total	Th	U		$^{207}Pb/^{206}Pb$	1σ	$^{207}Pb/^{235}U$	1σ	$^{206}Pb/^{238}U$	1σ	$^{207}Pb/^{206}Pb$	1σ	$^{207}Pb/^{235}U$	1σ	$^{206}Pb/^{238}U$	1σ	
71907-08	21	178	232	0.77	0.0564	0.0027	0.5876	0.0287	0.0756	0.0011	467	82	469	18	470	7	-0.21%
71907-09	28	242	321	0.75	0.0557	0.0014	0.5434	0.0135	0.0708	0.0009	440	33	441	9	441	6	0.00%
71907-10	12	100	164	0.61	0.0770	0.0032	0.5797	0.0238	0.0546	0.0008	1121	59	464	15	343	5	35.28%
71907-11	17	204	307	0.66	0.0522	0.0015	0.3367	0.0093	0.0468	0.0006	294	39	295	7	295	4	0.00%
71907-12	15	238	243	0.98	0.0522	0.0026	0.3376	0.0166	0.0469	0.0006	295	88	295	13	295	4	0.00%
71907-13	25	47	79	0.59	0.0939	0.0024	3.3974	0.0875	0.2623	0.0035	1507	29	1504	20	1502	18	0.33%
71907-14	24	253	420	0.60	0.0524	0.0014	0.3471	0.0092	0.0480	0.0006	303	37	303	7	302	4	0.33%
71907-15	14	187	231	0.81	0.0523	0.0017	0.3423	0.0113	0.0475	0.0007	298	50	299	9	299	4	0.00%
71907-16	51	112	699	0.16	0.0554	0.0013	0.5264	0.0121	0.0689	0.0009	428	29	429	8	430	5	-0.23%
71907-17	24	146	290	0.50	0.0550	0.0014	0.5286	0.0137	0.0698	0.0009	411	35	431	9	435	6	-0.92%
71907-18	12	164	210	0.78	0.0522	0.0027	0.3286	0.0171	0.0457	0.0006	293	94	289	13	288	4	0.35%
71907-19	12	181	208	0.87	0.0518	0.0017	0.3171	0.0102	0.0444	0.0006	277	48	280	8	280	4	0.00%
71907-20	42	80	102	0.78	0.1093	0.0025	4.8140	0.1105	0.3194	0.0042	1788	23	1787	19	1787	20	0.06%
71907-21	31	146	382	0.38	0.0556	0.0015	0.5484	0.0146	0.0715	0.0010	438	36	444	10	445	6	-0.22%
71907-22	5	76	91	0.83	0.0542	0.0053	0.3485	0.0339	0.0466	0.0009	380	185	304	26	294	5	3.40%
71907-23	13	146	173	0.84	0.0541	0.0018	0.4462	0.0148	0.0598	0.0008	375	49	375	10	375	5	0.00%
71907-24	33	191	466	0.41	0.0624	0.0020	0.5314	0.0169	0.0618	0.0008	686	45	433	11	387	5	11.89%
71907-25	19	112	239	0.47	0.0554	0.0016	0.5252	0.0155	0.0688	0.0009	428	42	429	10	429	6	0.00%
71907-26	8	112	126	0.89	0.0531	0.0023	0.3850	0.0167	0.0526	0.0008	335	71	331	12	330	5	0.30%
71907-27	13	184	234	0.78	0.0518	0.0018	0.3152	0.0111	0.0441	0.0006	278	55	278	9	278	4	0.00%
71907-28	14	163	247	0.66	0.0521	0.0017	0.3332	0.0108	0.0464	0.0006	290	49	292	8	292	4	0.00%
71907-29	29	52	84	0.62	0.0988	0.0026	3.8582	0.1012	0.2832	0.0038	1602	29	1605	21	1608	19	-0.37%
71907-30	20	38	66	0.57	0.0909	0.0024	3.1544	0.0845	0.2517	0.0034	1445	30	1446	21	1447	18	-0.14%
SGZ3-01	12	113	211	0.54	0.0531	0.0018	0.3908	0.0134	0.0534	0.0007	333	54	335	10	335	4	0.00%
SGZ3-03	29	346	638	0.54	0.0516	0.0017	0.2941	0.0100	0.0413	0.0005	269	54	262	8	261	3	0.38%
SGZ3-04	18	105	222	0.47	0.0614	0.0023	0.6292	0.0233	0.0744	0.0010	652	57	496	15	462	6	7.36%

续附录二　岩浆岩锆石U-Pb数据表

spot	concentritions(ppm)			Th/U	U-Pb isotopic ratios						age						concordance
	Pb Total	Th	U		$^{207}Pb/^{206}Pb$	1σ	$^{207}Pb/^{235}U$	1σ	$^{206}Pb/^{238}U$	1σ	$^{207}Pb/^{206}Pb$	1σ	$^{207}Pb/^{235}U$	1σ	$^{206}Pb/^{238}U$	1σ	
SGZ3-05	23	262	473	0.55	0.0521	0.0055	0.3161	0.0329	0.0440	0.0010	288	193	279	25	278	6	0.36%
SGZ3-06	5	70	84	0.83	0.0519	0.0051	0.3276	0.0323	0.0458	0.0007	279	195	288	25	289	4	-0.35%
SGZ3-07	79	266	406	0.65	0.0755	0.0014	1.7598	0.0347	0.1691	0.0021	1081	20	1031	13	1007	12	7.35%
SGZ3-08	50	687	626	1.10	0.0547	0.0014	0.4836	0.0123	0.0641	0.0008	400	34	401	8	400	5	0.25%
SGZ3-09	13	95	199	0.48	0.0541	0.0022	0.4415	0.0180	0.0592	0.0008	374	68	371	13	371	5	0.00%
SGZ3-10	14	130	330	0.40	0.0513	0.0017	0.2846	0.0097	0.0403	0.0005	253	54	254	8	254	3	0.00%
SGZ3-11	17	130	262	0.50	0.0539	0.0019	0.4427	0.0158	0.0595	0.0008	367	56	372	11	373	5	-0.27%
SGZ3-12	109	308	254	1.21	0.1198	0.0020	5.4291	0.0971	0.3287	0.0042	1953	16	1889	15	1832	20	6.60%
SGZ3-13	8	75	121	0.62	0.0536	0.0033	0.4233	0.0263	0.0573	0.0008	354	116	358	19	359	5	-0.28%
SGZ3-14	3	193	475	0.41	0.0523	0.0069	0.0493	0.0065	0.0069	0.0001	296	264	49	6	44	0.7	11.36%
SGZ3-15	12	85	209	0.41	0.0530	0.0024	0.3840	0.0175	0.0526	0.0007	328	79	330	13	330	4	0.00%
SGZ3-16	34	547	727	0.75	0.0514	0.0012	0.2876	0.0071	0.0406	0.0005	257	33	257	6	257	3	0.00%
SGZ3-17	28	428	646	0.66	0.0638	0.0015	0.3337	0.0083	0.0379	0.0005	734	31	292	6	240	3	21.67%
SGZ3-18	19	181	335	0.54	0.0529	0.0017	0.3780	0.0124	0.0518	0.0007	323	51	326	9	326	4	0.00%
SGZ3-19	8	130	142	0.92	0.0525	0.0028	0.3560	0.0188	0.0492	0.0007	308	95	309	14	309	4	0.00%
SGZ3-20	64	187	177	1.05	0.1010	0.0018	3.9654	0.0745	0.2847	0.0036	1642	18	1627	15	1615	18	1.67%
SGZ3-21	37	291	565	0.52	0.0549	0.0012	0.4524	0.0105	0.0598	0.0008	406	30	379	7	374	5	1.34%
SGZ3-22	26	409	580	0.71	0.0561	0.0027	0.2937	0.0137	0.0380	0.0005	455	111	261	11	240	3	8.75%
SGZ3-23	24	529	482	1.10	0.0513	0.0017	0.2863	0.0096	0.0405	0.0005	254	54	256	8	256	3	0.00%
SGZ3-24	10	187	209	0.90	0.0540	0.0018	0.3124	0.0106	0.0419	0.0006	371	52	276	8	265	3	4.15%
SGZ3-25	19	205	431	0.48	0.0513	0.0013	0.2852	0.0076	0.0403	0.0005	255	37	255	6	255	3	0.00%

附表三　碎屑锆石U-Pb数据表

spot	concentritions(ppm)			Th/U	U-Pb isotopic ratios						age						concordance
	Pb Total	Th	U		$^{207}Pb/^{206}Pb$	1σ	$^{207}Pb/^{235}U$	1σ	$^{206}Pb/^{238}U$	1σ	$^{207}Pb/^{206}Pb$	1σ	$^{207}Pb/^{235}U$	1σ	$^{206}Pb/^{238}U$	1σ	
82304-01	<1.69	61.5	289.66	0.21	0.0548	0.0015	0.4058	0.0108	0.0538	0.0007	403	37	346	8	338	4	2.37%
82304-02	<1.66	30.45	83.08	0.37	0.0509	0.0017	0.2973	0.0095	0.0424	0.0006	236	49	264	7	268	3	-1.49%
82304-03	<1.71	245.63	232.55	1.06	0.0571	0.0011	0.6547	0.0120	0.0832	0.0009	497	22	511	7	515	5	-0.78%
82304-04	<2.04	227.08	330.39	0.69	0.0538	0.0015	0.3830	0.0100	0.0517	0.0006	363	38	329	7	325	4	1.23%
82304-05	<2.07	161.37	375.35	0.43	0.1560	0.0018	9.7380	0.1076	0.4534	0.0046	2412	8	2410	10	2410	20	0.08%
82304-06	<2.01	33.47	86.05	0.39	0.0536	0.0017	0.3069	0.0091	0.0416	0.0005	353	43	272	7	263	3	3.42%
82304-07	<1.98	130.77	288.26	0.45	0.0543	0.0012	0.3428	0.0075	0.0458	0.0005	385	29	299	6	289	3	3.46%
82304-08	<1.74	55.41	375.09	0.15	0.1170	0.0013	5.5156	0.0580	0.3425	0.0034	1910	8	1903	9	1898	16	0.63%
82304-09	<1.95	225.58	473.34	0.48	0.1227	0.0013	5.5048	0.0564	0.3258	0.0032	1996	8	1901	9	1818	16	9.79%
82304-10	<1.81	169.13	428.71	0.39	0.1256	0.0014	6.2587	0.0672	0.3617	0.0036	2038	8	2013	9	1990	17	2.41%
~~82304-11~~	~~<1.86~~	~~75.19~~	~~139.03~~	0.54	~~0.0616~~	~~0.0010~~	~~0.4550~~	~~0.0068~~	~~0.0536~~	~~0.0006~~	~~661~~	~~16~~	~~381~~	~~5~~	~~337~~	~~3~~	~~13.06%~~
82304-12	<1.81	171.95	288.22	0.60	0.1302	0.0015	6.6677	0.0752	0.3720	0.0038	2100	9	2068	10	2039	18	2.99%
82304-13	2.33	198.04	338.35	0.59	0.0614	0.0016	0.3635	0.0090	0.0430	0.0005	452	123	290	13	270	3	7.41%
~~82304-14~~	~~<2.02~~	~~125.6~~	~~189.71~~	0.66	~~0.0795~~	~~0.0011~~	~~0.7118~~	~~0.0091~~	~~0.0650~~	~~0.0007~~	~~1184~~	~~12~~	~~546~~	~~5~~	~~406~~	~~4~~	~~34.48%~~
~~82304-15~~	~~<2.00~~	~~465.89~~	~~717.36~~	0.65	~~0.1121~~	~~0.0014~~	~~4.1671~~	~~0.0489~~	~~0.2699~~	~~0.0028~~	~~1834~~	~~10~~	~~1668~~	~~10~~	~~1540~~	~~14~~	~~19.09%~~
82304-16	<1.78	44.23	121.48	0.36	0.0771	0.0009	1.7732	0.0205	0.1671	0.0017	1073	42	1019	11	994	9	2.52%
~~82304-17~~	~~<2.13~~	~~165.4~~	~~532.9~~	0.31	~~0.1142~~	~~0.0138~~	~~1.2999~~	~~0.1458~~	~~0.0827~~	~~0.0040~~	~~1867~~	~~133~~	~~846~~	~~64~~	~~512~~	~~24~~	~~65.23%~~
82304-18	<2.07	310.28	396.88	0.78	0.0520	0.0010	0.2965	0.0057	0.0414	0.0005	285	25	264	4	262	3	0.76%
~~82304-19~~	~~3.44~~	~~66.08~~	~~102.48~~	0.64	~~0.4612~~	~~0.0132~~	~~12.5298~~	~~0.3003~~	~~0.1973~~	~~0.0042~~	~~4122~~	~~16~~	~~2645~~	~~23~~	~~1161~~	~~23~~	~~255.04%~~
82304-20	<2.01	338.89	494.58	0.69	0.0528	0.0011	0.3067	0.0063	0.0422	0.0005	318	27	272	5	267	3	1.87%
~~82304-21~~	~~<1.94~~	~~465.29~~	~~473.74~~	0.98	~~0.4811~~	~~0.0155~~	~~13.6864~~	~~0.3630~~	~~0.2066~~	~~0.0050~~		~~366~~	~~471~~	~~83~~	~~573~~	~~16~~	~~-17.80%~~
82304-22	<2.08	155.36	588.66	0.26	0.1151	0.0015	5.8618	0.0749	0.3698	0.0039	1882	10	1956	11	2028	18	-7.20%
82304-23	3.43	56.81	144.79	0.39	0.1152	0.0013	5.0557	0.0539	0.3187	0.0032	1883	9	1829	9	1783	15	5.61%
82304-24	<2.14	123.9	279.29	0.44	0.0564	0.0014	0.3934	0.0096	0.0507	0.0006	467	34	337	7	319	4	5.64%
82304-25	<1.87	168.74	323.65	0.52	0.0539	0.0014	0.3381	0.0084	0.0456	0.0005	366	35	296	6	287	3	3.14%
82304-26	<1.95	29.65	72.76	0.41	0.0530	0.0012	0.3175	0.0071	0.0435	0.0005	328	31	280	5	275	3	1.82%
82304-27	<2.16	30.24	62.95	0.48	0.0523	0.0021	0.4768	0.0186	0.0662	0.0009	297	64	396	13	413	5	-4.12%

续附表三　碎屑锆石U-Pb数据表

spot	concentritions(ppm)			Th/U	U-Pb isotopic ratios						age						concordance
	Pb Total	Th	U		$^{207}Pb/^{206}Pb$	1σ	$^{207}Pb/^{235}U$	1σ	$^{206}Pb/^{238}U$	1σ	$^{207}Pb/^{206}Pb$	1σ	$^{207}Pb/^{235}U$	1σ	$^{206}Pb/^{238}U$	1σ	
82304-28	<1.76	101.23	172.38	0.59	0.0523	0.0009	0.3414	0.0055	0.0474	0.0005	299	19	298	4	299	3	-0.33%
82304-29	<2.06	75.73	310.63	0.24	0.0697	0.0013	1.4670	0.0270	0.1528	0.0017	920	20	917	11	917	9	0.00%
82304-30	5.52	112.86	253.01	0.45	0.0555	0.0009	0.6171	0.0095	0.0807	0.0008	433	17	488	6	500	5	-2.40%
82304-31	<2.11	179.79	285.91	0.63	0.0525	0.0010	0.3735	0.0066	0.0517	0.0006	306	22	322	5	325	3	-0.92%
82304-32	<2.14	36.77	114.03	0.32	0.0566	0.0009	0.6454	0.0094	0.0828	0.0009	475	16	506	6	513	5	-1.36%
~~82304-33~~	~~<2.07~~	~~17.15~~	~~27.17~~	0.63	~~0.0912~~	~~0.0019~~	~~0.4793~~	~~0.0095~~	~~0.0382~~	~~0.0004~~	~~1450~~	~~21~~	~~398~~	~~6~~	~~241~~	~~3~~	~~65.15%~~
82304-34	<1.91	134.1	280.3	0.48	0.0524	0.0011	0.3724	0.0073	0.0516	0.0006	304	26	321	5	324	3	-0.93%
82304-36	<1.94	73.58	82.48	0.89	0.1627	0.0017	10.4979	0.1062	0.4687	0.0046	2483	8	2480	9	2478	20	0.20%
82304-37	<1.99	31.45	60.42	0.52	0.0546	0.0012	0.4000	0.0084	0.0532	0.0006	394	27	342	6	334	4	2.40%
82304-38	<2.23	168.34	448.9	0.38	0.0518	0.0009	0.3742	0.0059	0.0525	0.0005	275	19	323	4	330	3	-2.12%
82304-40	<2.13	235.69	226.53	1.04	0.0538	0.0038	0.3341	0.0232	0.0451	0.0008	361	124	293	18	285	5	2.81%
~~82304-41~~	~~1.68~~	~~128.34~~	~~145.78~~	0.88	~~0.1003~~	~~0.0014~~	~~1.8415~~	~~0.0236~~	~~0.1333~~	~~0.0014~~	~~1630~~	~~11~~	~~1060~~	~~8~~	~~807~~	~~8~~	~~31.35%~~
82304-42	5.85	232.32	392.52	0.59	0.0557	0.0013	0.3989	0.0090	0.0520	0.0006	440	30	341	6	327	4	4.28%
82304-43	3.99	141.45	429.2	0.33	0.0514	0.0009	0.2748	0.0044	0.0388	0.0004	260	19	247	3	245	2	0.82%
82304-44	8.43	93.23	568.31	0.16	0.0573	0.0010	0.6119	0.0098	0.0776	0.0008	502	18	485	6	482	5	0.62%
82304-45	3.4	184.27	494.1	0.37	0.1025	0.0012	4.4536	0.0509	0.3155	0.0032	1670	9	1722	9	1767	16	-5.49%
82304-46	<2.18	495.41	814.78	0.61	0.1638	0.0017	10.7015	0.1081	0.4744	0.0047	2495	8	2498	9	2503	20	-0.32%
~~82304-47~~	~~<2.06~~	~~95.74~~	~~366.79~~	0.26	~~0.0622~~	~~0.0011~~	~~0.3570~~	~~0.0061~~	~~0.0417~~	~~0.0005~~	~~682~~	~~19~~	~~310~~	~~5~~	~~263~~	~~3~~	~~17.87%~~
82304-48	<1.17	198.91	361.53	0.55	0.0520	0.0009	0.3557	0.0056	0.0497	0.0005	284	18	309	4	313	3	-1.28%
82304-49	<1.83	151.88	820.07	0.19	0.0525	0.0008	0.3534	0.0053	0.0489	0.0005	306	17	307	4	308	3	-0.32%
82304-50	<1.89	71.29	210.19	0.34	0.0501	0.0018	0.3362	0.0114	0.0487	0.0006	199	55	294	9	307	4	-4.23%
82304-51	<1.82	224.55	212.83	1.06	0.0516	0.0008	0.3614	0.0054	0.0509	0.0005	268	17	313	4	320	3	-2.19%
82304-52	<2.01	102.17	480.64	0.21	0.0515	0.0007	0.2736	0.0035	0.0386	0.0004	261	13	246	3	244	2	0.82%
82304-53	<1.99	136.22	142.72	0.95	0.1153	0.0013	5.2665	0.0560	0.3318	0.0033	1884	9	1863	9	1847	16	2.00%
82304-54	<2.24	56.45	137.93	0.41	0.0564	0.0009	0.5743	0.0083	0.0739	0.0008	470	16	461	5	460	5	0.22%
82304-55	16.81	749.05	2265.39	0.33	0.0521	0.0012	0.3293	0.0071	0.0459	0.0005	289	29	289	5	289	3	0.00%
82304-56	<2.26	250.74	354.09	0.71	0.0515	0.0016	0.3650	0.0108	0.0515	0.0007	263	45	316	8	324	4	-2.47%

续附表三　碎屑锆石U-Pb数据表

spot	concentritions(ppm)			Th/U	U-Pb isotopic ratios						age						concordance
	Pb Total	Th	U		$^{207}Pb/^{206}Pb$	1σ	$^{207}Pb/^{235}U$	1σ	$^{206}Pb/^{238}U$	1σ	$^{207}Pb/^{206}Pb$	1σ	$^{207}Pb/^{235}U$	1σ	$^{206}Pb/^{238}U$	1σ	
82304-57	<2.15	301.61	353.91	0.85	0.1134	0.0013	4.7080	0.0520	0.3015	0.0030	1854	9	1769	9	1699	15	9.12%
82304-58	<2.14	196.14	443.64	0.44	0.0574	0.0008	0.6651	0.0085	0.0841	0.0008	507	13	518	5	521	5	-0.58%
82304-59	<1.94	30.7	76.11	0.40	0.0572	0.0026	0.4304	0.0190	0.0547	0.0008	499	71	363	13	343	5	5.83%
82304-60	<1.96	303.11	612.57	0.49	0.0540	0.0014	0.3711	0.0090	0.0499	0.0006	372	34	320	7	314	3	1.91%
82304-61	<26.61	323.39	466.64	0.69	0.0552	0.0008	0.5068	0.0067	0.0666	0.0007	422	14	416	4	416	4	0.00%
82304-62	39.64	190.12	310.82	0.61	0.0514	0.0009	0.2904	0.0048	0.0410	0.0004	259	20	259	4	259	3	0.00%
82304-63	<1.95	311.35	314.41	0.99	0.0535	0.0014	0.4006	0.0101	0.0544	0.0006	349	36	342	7	342	4	0.00%
82304-64	<2.09	92.62	145.93	0.63	0.0511	0.0010	0.3343	0.0062	0.0475	0.0005	247	23	293	5	299	3	-2.01%
82304-65	<1.98	102.37	227.1	0.45	0.0495	0.0008	0.2694	0.0042	0.0396	0.0004	170	18	242	3	250	3	-3.20%
72044-01	23.50628	102.99	261.33	0.39	0.0558	0.0015	0.5497	0.0146	0.0714	0.0009	446	36	445	10	445	6	0.00%
72044-02	10.22119	84.96	120.18	0.71	0.0560	0.0016	0.5593	0.0157	0.0725	0.0010	451	39	451	10	451	6	0.00%
~~72044-03~~	~~66.53771~~	~~578.15~~	~~820.07~~	~~0.71~~	~~0.0701~~	~~0.0013~~	~~0.6667~~	~~0.0127~~	~~0.0690~~	~~0.0009~~	~~932~~	~~20~~	~~519~~	~~8~~	~~430~~	~~5~~	~~20.70%~~
~~72044-04~~	~~92.5428~~	~~220.38~~	~~492.17~~	~~0.45~~	~~0.1153~~	~~0.0020~~	~~2.7117~~	~~0.0494~~	~~0.1706~~	~~0.0021~~	~~1885~~	~~16~~	~~1332~~	~~14~~	~~1015~~	~~12~~	~~85.71%~~
72044-05	58.51204	443.45	778.23	0.57	0.0567	0.0011	0.5170	0.0106	0.0662	0.0008	479	24	423	7	413	5	2.42%
72044-06	16.48963	95.06	203.71	0.47	0.0561	0.0014	0.5693	0.0142	0.0736	0.0010	456	33	458	9	458	6	0.00%
72044-07	23.35347	135.83	302.67	0.45	0.0543	0.0011	0.5179	0.0110	0.0692	0.0009	383	26	424	7	431	5	-1.62%
72044-08	10.42071	70.99	127.94	0.55	0.0560	0.0014	0.5624	0.0138	0.0729	0.0009	452	32	453	9	453	6	0.00%
72044-09	22.87946	178.01	292.75	0.61	0.0553	0.0011	0.5180	0.0108	0.0680	0.0009	422	25	424	7	424	5	0.00%
72044-10	101.35325	408.51	773.49	0.53	0.0656	0.0013	0.9890	0.0204	0.1093	0.0014	794	23	698	10	669	8	4.33%
72044-11	27.85453	197.08	332.76	0.59	0.0561	0.0011	0.5651	0.0116	0.0731	0.0009	455	24	455	8	455	6	0.00%
72044-12	28.75461	234.22	338.28	0.69	0.0559	0.0014	0.5486	0.0142	0.0712	0.0009	448	35	444	9	443	5	0.23%
72044-13	9.67333	65.7	122.83	0.53	0.0556	0.0016	0.5334	0.0155	0.0696	0.0009	436	41	434	10	434	5	0.00%
72044-14	13.7331	82.2	178.43	0.46	0.0557	0.0014	0.5476	0.0136	0.0713	0.0010	439	32	443	9	444	6	-0.23%
72044-15	12.66209	91.25	161.94	0.56	0.0554	0.0015	0.5288	0.0145	0.0692	0.0009	430	38	431	10	431	5	0.00%
72044-16	41.62314	224.07	521.53	0.43	0.0560	0.0011	0.5590	0.0115	0.0724	0.0009	452	24	451	7	451	5	0.00%
72044-17	12.74856	90.08	161.1	0.56	0.0556	0.0014	0.5343	0.0139	0.0697	0.0009	435	35	435	9	435	5	0.00%
72044-18	56.91866	375.95	580.58	0.65	0.0534	0.0049	0.4322	0.0389	0.0587	0.0009	346	210	365	28	368	5	-0.82%

续附表三　碎屑锆石U-Pb数据表

spot	concentritions(ppm)			Th/U	U-Pb isotopic ratios						age						concordance
	Pb Total	Th	U		$^{207}Pb/^{206}Pb$	1σ	$^{207}Pb/^{235}U$	1σ	$^{206}Pb/^{238}U$	1σ	$^{207}Pb/^{206}Pb$	1σ	$^{207}Pb/^{235}U$	1σ	$^{206}Pb/^{238}U$	1σ	
72044-19	25.55969	247.07	290.26	0.85	0.0559	0.0012	0.5585	0.0119	0.0724	0.0009	450	26	451	8	451	5	0.00%
72044-20	14.02465	82.87	184.37	0.45	0.0556	0.0014	0.5330	0.0133	0.0695	0.0009	436	33	434	9	433	5	0.23%
72044-21	42.30852	203.63	582.97	0.35	0.0552	0.0011	0.5121	0.0101	0.0673	0.0008	420	23	420	7	420	5	0.00%
72044-22	21.27328	120.37	283.46	0.42	0.0553	0.0012	0.5219	0.0112	0.0684	0.0009	425	26	426	7	427	5	-0.23%
72044-23	9.29362	63.74	117.27	0.54	0.0556	0.0015	0.5381	0.0149	0.0702	0.0009	437	38	437	10	437	6	0.00%
72044-24	29.54747	259.23	357.12	0.73	0.0579	0.0028	0.5504	0.0254	0.0689	0.0010	527	108	445	17	430	6	3.49%
~~72044-25~~	~~90.49421~~	~~262.13~~	~~1062.52~~	~~0.25~~	~~0.1065~~	~~0.0019~~	~~1.0094~~	~~0.0187~~	~~0.0688~~	~~0.0009~~	~~1740~~	~~17~~	~~709~~	~~9~~	~~429~~	~~5~~	~~65.27%~~
72044-26	20.92704	95.02	292.93	0.32	0.0551	0.0015	0.5055	0.0135	0.0665	0.0009	416	36	415	9	415	5	0.00%
72044-27	35.48801	175.82	484.23	0.36	0.0552	0.0011	0.5163	0.0106	0.0678	0.0009	422	24	423	7	423	5	0.00%
72044-28	16.71273	144.32	194.29	0.74	0.0558	0.0014	0.5506	0.0137	0.0715	0.0009	446	33	445	9	445	5	0.00%
72044-29	43.24855	261.17	548.08	0.48	0.0588	0.0023	0.5503	0.0202	0.0679	0.0009	559	87	445	13	423	5	5.20%
72044-30	37.8741	205.63	457.46	0.45	0.0563	0.0014	0.5762	0.0147	0.0743	0.0010	462	34	462	9	462	6	0.00%
72044-31	18.4633	192.21	218.97	0.88	0.0549	0.0012	0.5309	0.0122	0.0701	0.0009	408	29	432	8	437	5	-1.14%
72044-32	26.93415	277.74	320.61	0.87	0.0552	0.0011	0.5138	0.0108	0.0675	0.0009	420	25	421	7	421	5	0.00%
72044-33	59.74313	404.74	757.73	0.53	0.0619	0.0012	0.5993	0.0121	0.0703	0.0009	669	23	477	8	438	5	8.90%
72044-34	4.936891	8.72	21.4	0.41	0.0811	0.0025	2.3457	0.0709	0.2097	0.0029	1225	38	1226	22	1227	16	-0.16%
72044-35	21.4458	124.92	278.58	0.45	0.0557	0.0012	0.5434	0.0117	0.0708	0.0009	440	26	441	8	441	5	0.00%
72044-36	26.02418	133.48	354.43	0.38	0.0553	0.0012	0.5210	0.0113	0.0683	0.0009	426	27	426	8	426	5	0.00%
~~72044-37~~	~~89.98313~~	~~92.08~~	~~1240.29~~	~~0.07~~	~~0.0773~~	~~0.0015~~	~~0.7296~~	~~0.0146~~	~~0.0685~~	~~0.0009~~	~~1128~~	~~21~~	~~556~~	~~9~~	~~427~~	~~5~~	~~30.21%~~
72044-38	9.71845	59.23	97.47	0.61	0.0583	0.0042	0.7046	0.0503	0.0877	0.0015	541	128	542	30	542	9	0.00%
72044-39	10.00288	65.78	123.59	0.53	0.0559	0.0015	0.5583	0.0155	0.0724	0.0010	450	38	450	10	450	6	0.00%
72044-40	16.11339	110.37	206.15	0.54	0.0550	0.0013	0.5312	0.0131	0.0701	0.0009	410	32	433	9	437	5	-0.92%
72044-41	22.32418	145.7	287.77	0.51	0.0555	0.0013	0.5336	0.0125	0.0697	0.0009	432	30	434	8	434	5	0.00%
72044-42	7.789798	38.36	99.81	0.38	0.0561	0.0020	0.5651	0.0206	0.0730	0.0010	458	57	455	13	454	6	0.22%
72044-43	36.04132	193.24	491.45	0.39	0.0553	0.0012	0.5238	0.0114	0.0687	0.0009	425	27	428	8	428	5	0.00%
72044-44	30.69257	196.63	388.87	0.51	0.0556	0.0012	0.5412	0.0116	0.0706	0.0009	438	26	439	8	440	5	-0.23%
72044-45	33.31713	297	397.73	0.75	0.0557	0.0012	0.5474	0.0116	0.0712	0.0009	442	26	443	8	443	5	0.00%

续附表三　碎屑锆石U-Pb数据表

spot	concentritions(ppm)			Th/U	U-Pb isotopic ratios						age						concordance
	Pb Total	Th	U		$^{207}Pb/^{206}Pb$	1σ	$^{207}Pb/^{235}U$	1σ	$^{206}Pb/^{238}U$	1σ	$^{207}Pb/^{206}Pb$	1σ	$^{207}Pb/^{235}U$	1σ	$^{206}Pb/^{238}U$	1σ	
72044-46	28.04823	158.48	356.57	0.44	0.0559	0.0012	0.5514	0.0126	0.0716	0.0009	447	29	446	8	446	5	0.00%
72044-47	31.64181	201.98	408.28	0.49	0.0556	0.0013	0.5345	0.0128	0.0698	0.0009	435	31	435	8	435	5	0.00%
72044-48	27.50974	174.91	370.79	0.47	0.0553	0.0012	0.5159	0.0117	0.0677	0.0009	423	28	422	8	422	5	0.00%
72044-49	8.62249	45.18	110.62	0.41	0.0559	0.0016	0.5487	0.0158	0.0712	0.0009	447	41	444	10	444	6	0.00%
72044-50	32.50443	227.99	421	0.54	0.0574	0.0015	0.5396	0.0140	0.0682	0.0009	506	34	438	9	425	5	3.06%
72044-51	31.06866	254.34	399.69	0.64	0.0553	0.0012	0.5164	0.0116	0.0678	0.0009	423	28	423	8	423	5	0.00%
72044-52	24.4506	195	302.85	0.64	0.0557	0.0013	0.5424	0.0127	0.0707	0.0009	440	30	440	8	440	5	0.00%
72044-53	29.54553	188.39	386.71	0.49	0.0555	0.0012	0.5272	0.0118	0.0689	0.0009	432	28	430	8	429	5	0.23%
72044-54	13.58505	85.58	178.25	0.48	0.0555	0.0014	0.5277	0.0134	0.0690	0.0009	431	34	430	9	430	5	0.00%
72044-55	27.08581	182.25	352.09	0.52	0.0556	0.0013	0.5325	0.0123	0.0695	0.0009	435	29	433	8	433	5	0.00%
72044-56	21.9521	192.29	253.99	0.76	0.0552	0.0013	0.5571	0.0129	0.0732	0.0009	421	29	450	8	455	6	-1.10%
72044-57	13.08361	91.02	158.88	0.57	0.0560	0.0014	0.5581	0.0143	0.0723	0.0010	452	34	450	9	450	6	0.00%
72044-58	9.645234	42.98	132.9	0.32	0.0554	0.0016	0.5235	0.0152	0.0686	0.0009	427	41	428	10	428	6	0.00%
72044-59	17.92631	128.91	228.15	0.57	0.0559	0.0018	0.5555	0.0180	0.0721	0.0010	449	47	449	12	448	6	0.22%
72044-60	21.7982	134.08	278.14	0.48	0.0557	0.0013	0.5447	0.0134	0.0709	0.0009	441	32	442	9	442	6	0.00%
72044-61	30.97223	160.57	430.99	0.37	0.0552	0.0012	0.5110	0.0116	0.0672	0.0009	420	29	419	8	419	5	0.00%
72044-62	30.85074	232.01	401.38	0.58	0.0553	0.0013	0.5182	0.0125	0.0680	0.0009	423	32	424	8	424	5	0.00%
72044-63	23.0113	165.91	296.2	0.56	0.0546	0.0013	0.5229	0.0123	0.0694	0.0009	397	30	427	8	433	5	-1.39%
72044-64	23.66429	165.1	312.04	0.53	0.0553	0.0014	0.5179	0.0130	0.0679	0.0009	424	33	424	9	424	5	0.00%
72044-65	18.45633	109.85	244.89	0.45	0.0555	0.0015	0.5299	0.0140	0.0692	0.0009	433	36	432	9	432	5	0.00%
72044-66	12.0335	63.67	162.75	0.39	0.0553	0.0020	0.5201	0.0193	0.0683	0.0009	422	59	425	13	426	6	-0.23%
72044-67	24.76122	179.05	318.55	0.56	0.0556	0.0013	0.5320	0.0130	0.0694	0.0009	435	32	433	9	433	5	0.00%
72044-68	25.22303	239.16	305.05	0.78	0.0556	0.0013	0.5362	0.0129	0.0699	0.0009	438	31	436	9	436	5	0.00%
72044-69	9.312	52.14	121.23	0.43	0.0557	0.0018	0.5438	0.0173	0.0708	0.0010	440	46	441	11	441	6	0.00%
72044-70	28.99812	229.96	348.28	0.66	0.0560	0.0013	0.5598	0.0132	0.0726	0.0009	450	30	451	9	452	6	-0.22%
72044-71	29.12875	139.36	399.33	0.35	0.0543	0.0013	0.5003	0.0124	0.0668	0.0009	384	33	412	8	417	5	-1.20%
72044-72	15.22098	112.4	202.23	0.56	0.0552	0.0015	0.5109	0.0140	0.0671	0.0009	421	38	419	9	419	5	0.00%

续附表三　碎屑锆石U-Pb数据表

spot	concentritions(ppm)			Th/U	U-Pb isotopic ratios						age						concordance
	Pb Total	Th	U		$^{207}Pb/^{206}Pb$	1σ	$^{207}Pb/^{235}U$	1σ	$^{206}Pb/^{238}U$	1σ	$^{207}Pb/^{206}Pb$	1σ	$^{207}Pb/^{235}U$	1σ	$^{206}Pb/^{238}U$	1σ	
72044-73	13.67484	100.38	161.89	0.62	0.0561	0.0014	0.5664	0.0147	0.0733	0.0010	454	34	456	10	456	6	0.00%
72044-74	19.57561	181.67	231.97	0.78	0.0558	0.0017	0.5492	0.0166	0.0714	0.0009	445	44	444	11	444	6	0.00%
72044-75	29.9276	236.37	362.34	0.65	0.0589	0.0015	0.5792	0.0149	0.0713	0.0009	563	34	464	10	444	6	4.50%
72022-1	10.16696	155.61	173.24	0.90	0.0521	0.0025	0.3360	0.0160	0.0468	0.0007	288	82	294	12	295	4	-0.34%
72022-2	30.13202	168.31	386.88	0.44	0.0554	0.0012	0.5250	0.0114	0.0688	0.0009	427	26	428	8	429	5	-0.23%
72022-3	4.869086	58.39	94.41	0.62	0.0516	0.0025	0.3077	0.0150	0.0432	0.0006	270	85	272	12	273	4	-0.37%
72022-4	5.292399	85.12	78.36	1.09	0.0528	0.0022	0.3695	0.0151	0.0507	0.0007	321	67	319	11	319	4	0.00%
72022-5	36.55046	258.45	462.3	0.56	0.0553	0.0011	0.5160	0.0108	0.0677	0.0009	424	25	422	7	422	5	0.00%
72022-6	16.45536	229.45	307.6	0.75	0.0518	0.0015	0.3128	0.0089	0.0438	0.0006	275	42	276	7	276	4	0.00%
72022-7	5.270131	59.21	95.38	0.62	0.0522	0.0023	0.3350	0.0145	0.0466	0.0007	292	72	293	11	293	4	0.00%
72022-8	5.498831	59.76	105.59	0.57	0.0518	0.0023	0.3196	0.0143	0.0447	0.0006	277	76	282	11	282	4	0.00%
72022-9	16.75251	98.28	205.19	0.48	0.0559	0.0014	0.5500	0.0135	0.0714	0.0009	446	32	445	9	445	6	0.00%
72022-10	16.20543	152.5	313.52	0.49	0.0520	0.0013	0.3252	0.0081	0.0454	0.0006	285	34	286	6	286	4	0.00%
72022-11	5.539071	63.87	98.34	0.65	0.0523	0.0021	0.3408	0.0139	0.0473	0.0007	299	67	298	11	298	4	0.00%
72022-12	13.31511	42.07	14.99	2.81	0.1639	0.0036	10.8925	0.2453	0.4818	0.0068	2497	20	2514	21	2535	30	-1.50%
72022-13	10.69781	73.46	128.94	0.57	0.0558	0.0016	0.5474	0.0159	0.0712	0.0010	444	41	443	10	443	6	0.00%
72022-14	10.64774	73.34	132	0.56	0.0555	0.0018	0.5319	0.0172	0.0695	0.0009	433	48	433	11	433	6	0.00%
72022-15	9.22743	170	158.91	1.07	0.0519	0.0018	0.3175	0.0108	0.0444	0.0006	280	52	280	8	280	4	0.00%
72022-16	15.10503	203.39	269.39	0.76	0.0537	0.0015	0.3366	0.0094	0.0455	0.0006	357	39	295	7	287	4	2.79%
72022-17	10.89462	149.17	182.38	0.82	0.0524	0.0016	0.3506	0.0104	0.0485	0.0007	305	43	305	8	305	4	0.00%
72022-18	7.23472	54.67	122.77	0.45	0.0530	0.0018	0.3829	0.0129	0.0524	0.0007	327	51	329	9	329	4	0.00%
72022-19	17.09355	115.18	202.77	0.57	0.0560	0.0013	0.5621	0.0137	0.0727	0.0010	454	31	453	9	453	6	0.00%
72022-20	5.319836	43.24	96.27	0.45	0.0525	0.0025	0.3563	0.0168	0.0493	0.0007	306	81	309	13	310	4	-0.32%
72022-21	13.45192	110.09	246.08	0.45	0.0525	0.0014	0.3535	0.0095	0.0488	0.0007	307	37	307	7	307	4	0.00%
72022-22	8.96672	102.23	169.38	0.60	0.0521	0.0021	0.3253	0.0132	0.0453	0.0006	288	67	286	10	286	4	0.00%
72022-23	8.75665	115.68	167.41	0.69	0.0517	0.0016	0.3124	0.0099	0.0439	0.0006	271	47	276	8	277	4	-0.36%
72022-24	10.31808	66.7	130.12	0.51	0.0556	0.0015	0.5347	0.0147	0.0697	0.0010	437	37	435	10	434	6	0.23%

续附表三　碎屑锆石U-Pb数据表

spot	concentritions(ppm)			Th/U	U-Pb isotopic ratios						age						concordance
	Pb Total	Th	U		$^{207}Pb/^{206}Pb$	1σ	$^{207}Pb/^{235}U$	1σ	$^{206}Pb/^{238}U$	1σ	$^{207}Pb/^{206}Pb$	1σ	$^{207}Pb/^{235}U$	1σ	$^{206}Pb/^{238}U$	1σ	
72022-25	14.78066	73.41	194.62	0.38	0.0555	0.0015	0.5287	0.0145	0.0691	0.0009	431	37	431	10	431	6	0.00%
72022-26	4.295736	49.75	77.28	0.64	0.0522	0.0040	0.3342	0.0254	0.0464	0.0007	295	145	293	19	292	4	0.34%
72022-27	16.34884	130.36	199.94	0.65	0.0555	0.0015	0.5317	0.0144	0.0695	0.0009	431	37	433	10	433	6	0.00%
72022-28	6.103072	179.25	77.01	2.33	0.0522	0.0030	0.3358	0.0189	0.0466	0.0007	296	100	294	14	294	4	0.00%
72022-29	13.78001	122.1	275.98	0.44	0.0519	0.0014	0.3212	0.0088	0.0449	0.0006	281	39	283	7	283	4	0.00%
72022-30	27.74151	246.76	226.15	1.09	0.0593	0.0014	0.7665	0.0182	0.0938	0.0012	578	30	578	10	578	7	0.00%
72022-31	42.74666	105.16	99.78	1.05	0.1097	0.0022	4.8604	0.0999	0.3214	0.0042	1794	20	1795	17	1797	20	-0.17%
72022-32	11.40307	102.95	199.92	0.51	0.0527	0.0019	0.3641	0.0131	0.0501	0.0007	315	56	315	10	315	4	0.00%
72022-33	19.77496	168.02	228.64	0.73	0.0560	0.0014	0.5592	0.0144	0.0724	0.0010	454	34	451	9	450	6	0.22%
~~72022-34~~	~~21.6373~~	~~111.3~~	~~281.47~~	~~0.40~~	~~0.0639~~	~~0.0017~~	~~0.5978~~	~~0.0159~~	~~0.0679~~	~~0.0009~~	~~738~~	~~34~~	~~476~~	~~10~~	~~423~~	~~5~~	~~12.53%~~
72022-35	22.66567	261.07	404.2	0.65	0.0523	0.0014	0.3452	0.0095	0.0479	0.0006	299	39	301	7	301	4	0.00%
~~72022-36~~	~~7.4863~~	~~98.02~~	~~129.97~~	~~0.75~~	~~0.0652~~	~~0.0027~~	~~0.4312~~	~~0.0181~~	~~0.0480~~	~~0.0007~~	~~780~~	~~64~~	~~364~~	~~13~~	~~302~~	~~4~~	~~20.53%~~
72022-37	54.45785	130.59	78.37	1.67	0.1607	0.0032	10.1959	0.2092	0.4602	0.0060	2463	18	2453	19	2441	26	0.90%
72022-38	4.396843	57.65	81.73	0.71	0.0520	0.0022	0.3209	0.0132	0.0448	0.0007	285	67	283	10	282	4	0.35%
72022-39	15.68126	86.81	204.88	0.42	0.0556	0.0014	0.5319	0.0140	0.0695	0.0009	434	35	433	9	433	6	0.00%
72022-40	11.14117	116.78	219.85	0.53	0.0518	0.0015	0.3217	0.0091	0.0451	0.0006	275	40	283	7	284	4	-0.35%
72022-41	15.43269	140.35	303.63	0.46	0.0519	0.0015	0.3269	0.0096	0.0457	0.0006	282	43	287	7	288	4	-0.35%
72022-42	7.19251	137.29	122.6	1.12	0.0545	0.0029	0.3354	0.0178	0.0446	0.0007	392	93	294	14	281	4	4.63%
72022-43	13.69003	224.56	242.84	0.92	0.0519	0.0015	0.3241	0.0096	0.0453	0.0006	280	43	285	7	286	4	-0.35%
~~72022-44~~	~~15.34948~~	~~215.76~~	~~236.54~~	~~0.91~~	~~0.0964~~	~~0.0025~~	~~0.6401~~	~~0.0168~~	~~0.0482~~	~~0.0007~~	~~1555~~	~~29~~	~~502~~	~~10~~	~~303~~	~~4~~	~~65.68%~~
72022-45	5.57895	54.58	73.14	0.75	0.0551	0.0033	0.4888	0.0296	0.0643	0.0010	417	109	404	20	402	6	0.50%
72022-46	21.42303	151.07	417.24	0.36	0.0523	0.0013	0.3432	0.0088	0.0476	0.0006	296	35	300	7	300	4	0.00%
72022-47	22.92695	137.88	286.8	0.48	0.0553	0.0013	0.5494	0.0135	0.0721	0.0010	425	32	445	9	448	6	-0.67%
72022-48	17.44147	296.92	308.57	0.96	0.0520	0.0016	0.3245	0.0102	0.0453	0.0006	284	47	285	8	286	4	-0.35%
72022-49	16.79414	164	327.06	0.50	0.0521	0.0015	0.3301	0.0095	0.0459	0.0006	292	42	290	7	289	4	0.35%
72022-50	19.11007	119.27	242.19	0.49	0.0558	0.0015	0.5466	0.0145	0.0710	0.0010	445	35	443	10	442	6	0.23%
72022-51	6.063	95.1	112.04	0.85	0.0518	0.0034	0.3144	0.0205	0.0440	0.0007	278	123	278	16	278	4	0.00%

续附表三　碎屑锆石U-Pb数据表

spot	concentritions(ppm)			Th/U	U-Pb isotopic ratios						age						concordance
	Pb Total	Th	U		$^{207}Pb/^{206}Pb$	1σ	$^{207}Pb/^{235}U$	1σ	$^{206}Pb/^{238}U$	1σ	$^{207}Pb/^{206}Pb$	1σ	$^{207}Pb/^{235}U$	1σ	$^{206}Pb/^{238}U$	1σ	
72022-52	13.028	72.11	181.21	0.40	0.0547	0.0019	0.4858	0.0173	0.0644	0.0009	400	55	402	12	402	5	0.00%
72022-53	9.44076	129.42	151.8	0.85	0.0529	0.0020	0.3776	0.0141	0.0518	0.0007	325	59	325	10	325	4	0.00%
72022-54	26.17765	75.41	110.9	0.68	0.0791	0.0019	2.1764	0.0539	0.1996	0.0027	1175	29	1174	17	1173	14	0.17%
72022-55	9.19404	118.03	171.39	0.69	0.0521	0.0018	0.3303	0.0116	0.0460	0.0007	289	54	290	9	290	4	0.00%
72022-56	7.26121	80.04	123.91	0.65	0.0528	0.0025	0.3720	0.0178	0.0511	0.0007	318	83	321	13	322	4	-0.31%
72022-57	4.907452	57.89	88.94	0.65	0.0521	0.0029	0.3400	0.0185	0.0473	0.0007	291	96	297	14	298	4	-0.34%
72022-58	16.35711	138.49	198.62	0.70	0.0558	0.0016	0.5454	0.0155	0.0709	0.0010	444	39	442	10	442	6	0.00%
72022-59	28.99811	165.57	385.31	0.43	0.0549	0.0013	0.5192	0.0126	0.0686	0.0009	407	31	425	8	428	5	-0.70%
72022-60	6.89213	61.35	130.68	0.47	0.0523	0.0023	0.3440	0.0152	0.0477	0.0007	300	75	300	11	300	4	0.00%
72022-61	17.86902	127.83	229.22	0.56	0.0555	0.0016	0.5328	0.0154	0.0696	0.0009	434	40	434	10	434	6	0.00%
72022-62	14.64755	183.39	285.61	0.64	0.0519	0.0015	0.3210	0.0096	0.0449	0.0006	281	43	283	7	283	4	0.00%
72022-63	6.62968	129.47	117.99	1.10	0.0519	0.0023	0.3157	0.0138	0.0441	0.0007	281	72	279	11	278	4	0.36%
72022-64	9.97965	117.78	183.72	0.64	0.0523	0.0022	0.3436	0.0143	0.0476	0.0007	300	69	300	11	300	4	0.00%
72022-65	14.88876	88.61	196.73	0.45	0.0555	0.0018	0.5297	0.0170	0.0693	0.0010	430	47	432	11	432	6	0.00%
72022-66	14.49165	115.12	186.69	0.62	0.0554	0.0018	0.5227	0.0172	0.0684	0.0009	430	49	427	11	426	6	0.23%
72022-67	13.06896	70.84	167.77	0.42	0.0559	0.0021	0.5535	0.0209	0.0718	0.0010	448	59	447	14	447	6	0.00%
72022-68	3.778538	44.38	72.09	0.62	0.0522	0.0042	0.3353	0.0269	0.0466	0.0008	293	150	294	20	294	5	0.00%
72022-69	12.53151	86.29	167.66	0.51	0.0553	0.0018	0.5165	0.0170	0.0678	0.0009	424	49	423	11	423	6	0.00%
72022-70	14.60655	100.78	194.72	0.52	0.0553	0.0023	0.5108	0.0211	0.0671	0.0009	423	68	419	14	418	6	0.24%
72022-71	13.63989	141.33	266.26	0.53	0.0521	0.0023	0.3314	0.0148	0.0461	0.0006	291	76	291	11	291	4	0.00%
72022-72	35.38381	309.28	412.51	0.75	0.0561	0.0015	0.5671	0.0152	0.0733	0.0010	456	36	456	10	456	6	0.00%
72022-73	19.98899	192.1	390.02	0.49	0.0519	0.0014	0.3351	0.0094	0.0468	0.0006	283	39	293	7	295	4	-0.68%
72022-74	19.94131	228.34	404.72	0.56	0.0518	0.0016	0.3154	0.0098	0.0442	0.0006	277	46	278	8	279	4	-0.36%
72022-75	30.83377	45.1	79.12	0.57	0.1143	0.0029	5.3022	0.1368	0.3365	0.0045	1869	27	1869	22	1870	22	-0.05%
71107-01	<5.27	108.64	124.96	0.87	0.0553	0.0011	0.5486	0.0110	0.0719	0.0008	426	25	444	7	448	5	-0.89%
71107-02	45.84	583.18	760.05	0.77	0.0555	0.0010	0.5356	0.0098	0.0700	0.0008	433	21	436	6	436	5	0.00%
71107-03	<6.86	500.82	664.35	0.75	0.0540	0.0011	0.3092	0.0061	0.0416	0.0005	369	25	274	5	263	3	4.18%

续附表三　碎屑锆石U-Pb数据表

spot	concentritions(ppm)			Th/U	U-Pb isotopic ratios						age						concordance
	Pb Total	Th	U		$^{207}Pb/^{206}Pb$	1σ	$^{207}Pb/^{235}U$	1σ	$^{206}Pb/^{238}U$	1σ	$^{207}Pb/^{206}Pb$	1σ	$^{207}Pb/^{235}U$	1σ	$^{206}Pb/^{238}U$	1σ	
71107-04	<4.46	44.42	145.29	0.31	0.0576	0.0008	0.5096	0.0073	0.0642	0.0007	513	15	418	5	401	4	4.24%
71107-05	<3.96	110.34	371.86	0.30	0.0523	0.0008	0.3030	0.0044	0.0420	0.0005	300	16	269	3	265	3	1.51%
71107-06	<5.70	72.78	227.6	0.32	0.0569	0.0010	0.4927	0.0081	0.0628	0.0007	487	18	407	6	393	4	3.56%
71107-07	<7.29	164.97	206.86	0.80	0.0552	0.0011	0.3213	0.0064	0.0422	0.0005	421	25	283	5	267	3	5.99%
71107-08	68.84	218.42	998.01	0.22	0.0532	0.0016	0.2953	0.0086	0.0403	0.0005	337	43	263	7	254	3	3.54%
~~71107-09~~	~~<13.08~~	~~267.06~~	~~467.58~~	0.57	~~0.0840~~	~~0.0012~~	~~0.7515~~	~~0.0105~~	~~0.0649~~	~~0.0007~~	~~1292~~	~~13~~	~~569~~	~~6~~	~~405~~	~~4~~	~~40.49%~~
71107-10	<4.26	73.03	151.39	0.48	0.0552	0.0012	0.4818	0.0103	0.0633	0.0007	422	27	399	7	395	4	1.01%
71107-11	8.94	129.11	444.19	0.29	0.0548	0.0009	0.4705	0.0077	0.0622	0.0007	406	18	392	5	389	4	0.77%
~~71107-12~~	~~<15.64~~	~~160.83~~	~~222.16~~	0.72	~~0.1121~~	~~0.0017~~	~~4.3162~~	~~0.0656~~	~~0.2793~~	~~0.0033~~	~~1834~~	~~13~~	~~1696~~	~~13~~	~~1588~~	~~17~~	~~15.49%~~
~~71107-13~~	~~<4.64~~	~~77.61~~	~~129.07~~	0.60	~~0.1115~~	~~0.0012~~	~~4.4422~~	~~0.0476~~	~~0.2890~~	~~0.0030~~	~~1824~~	~~9~~	~~1720~~	~~9~~	~~1636~~	~~15~~	~~11.49%~~
~~71107-14~~	~~<12.72~~	~~111.73~~	~~249.13~~	0.45	~~0.1097~~	~~0.0014~~	~~4.2388~~	~~0.0561~~	~~0.2804~~	~~0.0032~~	~~1794~~	~~11~~	~~1682~~	~~11~~	~~1593~~	~~16~~	~~12.62%~~
71107-15	9.95	105.12	144.9	0.73	0.0499	0.0011	0.2766	0.0059	0.0402	0.0005	191	29	248	5	254	3	-2.36%
71107-16	<4.51	85.58	104.01	0.82	0.0565	0.0009	0.4964	0.0080	0.0637	0.0007	473	18	409	5	398	4	2.76%
71107-17	<5.33	87.53	208.72	0.42	0.0610	0.0012	0.5333	0.0106	0.0634	0.0008	641	23	434	7	396	5	9.60%
71107-18	<4.87	105.45	199.75	0.53	0.0555	0.0015	0.2907	0.0076	0.0380	0.0005	432	37	259	6	240	3	7.92%
~~71107-19~~	~~<4.46~~	~~118.54~~	~~193.59~~	0.61	~~0.0797~~	~~0.0015~~	~~0.4778~~	~~0.0088~~	~~0.0435~~	~~0.0005~~	~~807~~	~~109~~	~~334~~	~~14~~	~~270~~	~~4~~	~~23.70%~~
71107-20	8.05	42.1	329.46	0.13	0.0565	0.0010	0.4996	0.0084	0.0641	0.0007	472	19	411	6	401	4	2.49%
~~71107-21~~	~~<3.73~~	~~194.66~~	~~272.79~~	0.71	~~0.1163~~	~~0.0013~~	~~4.7586~~	~~0.0560~~	~~0.2968~~	~~0.0032~~	~~1901~~	~~9~~	~~1778~~	~~10~~	~~1675~~	~~16~~	~~13.49%~~
71107-22	14.59	32.2	516.26	0.06	0.0521	0.0009	0.2901	0.0049	0.0404	0.0005	292	20	259	4	255	3	1.57%
71107-23	<3.75	68.1	103.58	0.66	0.0530	0.0010	0.3065	0.0056	0.0420	0.0005	329	22	271	4	265	3	2.26%
~~71107-24~~	~~28.67~~	~~360.67~~	~~592.43~~	0.61	~~0.1100~~	~~0.0011~~	~~4.3560~~	~~0.0467~~	~~0.2872~~	~~0.0030~~	~~1800~~	~~9~~	~~1704~~	~~9~~	~~1628~~	~~15~~	~~10.57%~~
71107-25	<3.55	86.59	100.56	0.86	0.0616	0.0009	0.6144	0.0091	0.0724	0.0008	659	15	486	6	451	5	7.76%
71107-26	4.64	213.94	482.02	0.44	0.0591	0.0009	0.5827	0.0087	0.0715	0.0008	572	16	466	6	445	5	4.72%
71107-27	<5.02	154.78	267.63	0.58	0.0638	0.0008	1.0186	0.0125	0.1158	0.0012	700	39	704	7	705	7	-0.14%
71107-28	<3.89	94.14	179.7	0.52	0.0545	0.0008	0.4704	0.0070	0.0627	0.0007	390	16	391	5	392	4	-0.26%
71107-29	<3.58	278.22	327.11	0.85	0.0705	0.0008	1.4400	0.0167	0.1481	0.0016	944	11	906	7	891	9	1.68%
71107-30	10.32	171.06	436.9	0.39	0.0540	0.0010	0.3405	0.0063	0.0457	0.0005	372	22	298	5	288	3	3.47%

续附表三　碎屑锆石U-Pb数据表

spot	concentritions(ppm)			Th/U	U-Pb isotopic ratios						age						concordance
	Pb Total	Th	U		$^{207}Pb/^{206}Pb$	1σ	$^{207}Pb/^{235}U$	1σ	$^{206}Pb/^{238}U$	1σ	$^{207}Pb/^{206}Pb$	1σ	$^{207}Pb/^{235}U$	1σ	$^{206}Pb/^{238}U$	1σ	
71107-31	<4.49	114.93	172.88	0.66	0.0645	0.0010	0.6384	0.0103	0.0718	0.0008	643	81	479	13	445	5	7.64%
71107-32	<4.38	79.7	190.65	0.42	0.0882	0.0010	3.0433	0.0341	0.2503	0.0027	1387	10	1419	9	1440	14	-3.68%
~~71107-33~~	~~<7.49~~	~~97.7~~	~~169.9~~	0.58	~~0.0676~~	~~0.0009~~	~~0.7674~~	~~0.0101~~	~~0.0824~~	~~0.0009~~	~~855~~	~~12~~	~~578~~	~~6~~	~~511~~	~~5~~	~~13.11%~~
71107-34	<4.19	38.95	129.07	0.30	0.0530	0.0008	0.3566	0.0054	0.0488	0.0005	330	17	310	4	307	3	0.98%
71107-35	<3.56	216.64	282.05	0.77	0.1273	0.0013	5.9142	0.0643	0.3372	0.0036	2033	32	1948	12	1869	18	8.77%
~~71107-36~~	~~<4.02~~	~~104.07~~	~~200.53~~	0.52	~~0.0785~~	~~0.0009~~	~~0.7348~~	~~0.0089~~	~~0.0679~~	~~0.0007~~	~~1004~~	~~56~~	~~524~~	~~10~~	~~420~~	~~5~~	~~24.76%~~
71107-37	<3.63	116.63	269.61	0.43	0.1637	0.0017	9.7470	0.1074	0.4320	0.0047	2494	8	2411	10	2315	21	7.73%
71107-38	18.45	314.89	261.48	1.20	0.1596	0.0017	10.0570	0.1084	0.4571	0.0049	2452	8	2440	10	2427	22	1.03%
71107-39	<5.02	166.41	177.02	0.94	0.0609	0.0010	0.6318	0.0099	0.0753	0.0008	634	16	497	6	468	5	6.20%
71107-40	<4.17	70.33	102.41	0.69	0.0594	0.0008	0.6136	0.0082	0.0749	0.0008	583	13	486	5	466	5	4.29%
71107-41	<3.37	161.71	275.42	0.59	0.1685	0.0017	10.5753	0.1104	0.4553	0.0048	2543	8	2487	10	2419	21	5.13%
71107-42	6.09	111.95	217.39	0.51	0.0571	0.0007	0.5535	0.0066	0.0703	0.0008	495	12	447	4	438	5	2.05%
~~71107-43~~	~~<4.56~~	~~205.13~~	~~429.16~~	0.48	~~0.1245~~	~~0.0014~~	~~5.2712~~	~~0.0627~~	~~0.3072~~	~~0.0034~~	~~2021~~	~~9~~	~~1864~~	~~10~~	~~1727~~	~~17~~	~~17.02%~~
71107-44	<3.66	111.84	238.39	0.47	0.1340	0.0018	1.5096	0.0198	0.0817	0.0009	580	126	480	21	460	6	4.35%
71107-45	48.2	131.47	362.64	0.36	0.0547	0.0008	0.5400	0.0080	0.0716	0.0008	401	16	438	5	446	5	-1.79%
71107-46	<6.01	83.42	315.5	0.26	0.0722	0.0009	1.3349	0.0172	0.1341	0.0015	992	12	861	7	811	8	6.17%
71107-47	<4.00	188.42	412	0.46	0.1124	0.0012	5.4037	0.0607	0.3489	0.0038	1838	9	1885	10	1929	18	-4.72%
71107-48	<4.17	136.31	252.04	0.54	0.1679	0.0018	10.2526	0.1157	0.4430	0.0049	2521	30	2448	13	2360	22	6.82%
71107-49	<3.59	138.52	231.83	0.60	0.1599	0.0016	9.6742	0.1029	0.4390	0.0047	2440	28	2395	11	2342	21	4.18%
71107-50	26.76	275.9	465.77	0.59	0.0599	0.0009	0.6209	0.0089	0.0752	0.0008	599	14	490	6	468	5	4.70%
71107-51	14.88	140.11	235.14	0.60	0.0893	0.0010	3.0927	0.0351	0.2513	0.0027	1410	10	1431	9	1445	14	-2.42%
71107-52	<3.48	123.98	388.02	0.32	0.0517	0.0014	0.3450	0.0094	0.0484	0.0006	274	39	301	7	305	4	-1.31%
71107-53	<4.00	92.53	136.63	0.68	0.1644	0.0017	10.9186	0.1176	0.4817	0.0052	2502	8	2516	10	2535	23	-1.30%
71107-54	<3.60	30.09	127.4	0.24	0.0731	0.0010	1.6040	0.0215	0.1592	0.0018	1016	12	972	8	952	10	2.10%
71107-55	<4.26	75.47	39.43	1.91	0.0550	0.0011	0.3514	0.0068	0.0464	0.0005	411	23	306	5	292	3	4.79%
71107-56	19.82	87.8	210.25	0.42	0.0582	0.0009	0.5265	0.0079	0.0656	0.0007	538	16	429	5	410	4	4.63%
71107-57	<3.73	152.21	216.53	0.70	0.0564	0.0010	0.5140	0.0091	0.0662	0.0008	467	20	421	6	413	5	1.94%

续附表三　碎屑锆石U-Pb数据表

spot	concentritions(ppm)			Th/U	U-Pb isotopic ratios						age						concordance
	Pb Total	Th	U		$^{207}Pb/^{206}Pb$	1σ	$^{207}Pb/^{235}U$	1σ	$^{206}Pb/^{238}U$	1σ	$^{207}Pb/^{206}Pb$	1σ	$^{207}Pb/^{235}U$	1σ	$^{206}Pb/^{238}U$	1σ	
71107-58	3.82	129.15	297.46	0.43	0.0571	0.0009	0.4475	0.0073	0.0568	0.0006	497	18	376	5	356	4	5.62%
71107-59	<4.16	198.19	245.14	0.81	0.0530	0.0009	0.3126	0.0051	0.0428	0.0005	330	18	276	4	270	3	2.22%
~~71107-60~~	~~7.11~~	~~139.9~~	~~432.58~~	0.32	~~0.0633~~	~~0.0012~~	~~0.3773~~	~~0.0068~~	~~0.0433~~	~~0.0005~~	~~718~~	~~20~~	~~325~~	~~5~~	~~273~~	~~3~~	~~19.05%~~
71107-61	<9.28	75.09	104.68	0.72	0.0761	0.0010	1.3719	0.0183	0.1307	0.0015	986	58	842	14	788	9	6.85%
71107-62	<4.05	167.38	231.78	0.72	0.1103	0.0012	4.4585	0.0523	0.2933	0.0032	1804	10	1723	10	1658	16	8.81%
71107-63	21.59	428.2	344.74	1.24	0.1092	0.0011	4.5236	0.0490	0.3004	0.0032	1787	9	1735	9	1693	16	5.55%
71107-64	<3.82	53.69	127.04	0.42	0.0540	0.0010	0.3434	0.0061	0.0461	0.0005	372	21	300	5	291	3	3.09%
71107-65	<3.70	63.25	276.66	0.23	0.0575	0.0009	0.5499	0.0089	0.0694	0.0008	512	17	445	6	432	5	3.01%
71107-66	<18.83	79.79	283.46	0.28	0.0570	0.0009	0.5518	0.0090	0.0703	0.0008	490	18	446	6	438	5	1.83%
71107-67	<4.18	154.01	230.73	0.67	0.0593	0.0013	0.4132	0.0088	0.0506	0.0006	329	88	317	10	315	4	0.63%
~~71107-68~~	~~<4.01~~	~~68.06~~	~~110.13~~	0.62	~~0.2696~~	~~0.0029~~	~~2.2611~~	~~0.0252~~	~~0.0609~~	~~0.0007~~	~~1688~~	~~154~~	~~522~~	~~32~~	~~296~~	~~5~~	~~76.35%~~
71107-69	<3.50	113.95	185.83	0.61	0.0586	0.0008	0.5486	0.0077	0.0679	0.0008	473	65	431	9	423	5	1.89%
71107-70	54.42	552.78	768.02	0.72	0.0568	0.0010	0.3865	0.0069	0.0494	0.0006	483	20	332	5	311	4	6.75%
71107-71	<4.13	121.89	97.88	1.25	0.0523	0.0009	0.3272	0.0055	0.0454	0.0005	297	19	287	4	286	3	0.35%
71107-72	<3.88	185.9	255.42	0.73	0.0550	0.0009	0.3656	0.0060	0.0483	0.0006	411	18	316	4	304	3	3.95%
71107-73	<4.48	144.51	258.4	0.56	0.1110	0.0012	5.3600	0.0598	0.3503	0.0038	1816	9	1878	10	1936	18	-6.20%
72034-01	38.8628	246.18	422.44	0.58	0.0568	0.0015	0.6082	0.0162	0.0777	0.0010	482	36	482	10	483	6	-0.21%
72034-02	59.09421	512.29	684.46	0.75	0.0594	0.0016	0.5688	0.0153	0.0694	0.0009	583	36	457	10	433	6	5.54%
72034-03	38.26282	239.44	444.65	0.54	0.0561	0.0015	0.5689	0.0150	0.0736	0.0010	457	35	457	10	458	6	-0.22%
72034-04	11.7161	135.69	217.96	0.62	0.0520	0.0018	0.3229	0.0111	0.0451	0.0006	284	52	284	8	284	4	0.00%
72034-05	7.24545	71.28	145.94	0.49	0.0516	0.0027	0.3070	0.0158	0.0431	0.0007	269	87	272	12	272	5	0.00%
72034-06	15.83081	168.07	297.64	0.56	0.0555	0.0026	0.3442	0.0157	0.0450	0.0007	432	76	300	12	284	4	5.63%
72034-07	34.25829	199.29	410.87	0.49	0.0561	0.0016	0.5605	0.0162	0.0726	0.0010	454	40	452	11	452	6	0.00%
~~72034-08~~	~~21.30381~~	~~232.59~~	~~331.38~~	~~0.70~~	~~0.0576~~	~~0.0057~~	~~0.3256~~	~~0.0320~~	~~0.0410~~	~~0.0007~~	~~514~~	~~227~~	~~286~~	~~24~~	~~259~~	~~4~~	~~10.42%~~
72034-09	10.17139	110.82	190.79	0.58	0.0521	0.0020	0.3259	0.0122	0.0454	0.0007	289	59	286	9	286	4	0.00%
72034-10	11.29783	134.79	190.73	0.71	0.0525	0.0022	0.3543	0.0148	0.0490	0.0007	307	69	308	11	308	4	0.00%
~~72034-11~~	~~15.53747~~	~~217.76~~	~~264.62~~	~~0.82~~	~~0.0592~~	~~0.0026~~	~~0.3796~~	~~0.0165~~	~~0.0465~~	~~0.0007~~	~~574~~	~~69~~	~~327~~	~~12~~	~~293~~	~~4~~	~~11.60%~~

续附表三　碎屑锆石U-Pb数据表

spot	concentritions(ppm)			Th/U	U-Pb isotopic ratios						age						concordance
	Pb Total	Th	U		$^{207}Pb/^{206}Pb$	1σ	$^{207}Pb/^{235}U$	1σ	$^{206}Pb/^{238}U$	1σ	$^{207}Pb/^{206}Pb$	1σ	$^{207}Pb/^{235}U$	1σ	$^{206}Pb/^{238}U$	1σ	
72034-12	29.21611	153.37	337.82	0.45	0.0565	0.0016	0.5902	0.0164	0.0758	0.0010	471	38	471	10	471	6	0.00%
72034-13	36.63876	196.39	438.05	0.45	0.0561	0.0015	0.5701	0.0153	0.0737	0.0010	456	36	458	10	459	6	-0.22%
72034-14	30.16251	154.91	354.3	0.44	0.0564	0.0017	0.5851	0.0182	0.0753	0.0010	468	45	468	12	468	6	0.00%
72034-15	10.55615	222.41	182.56	1.22	0.0516	0.0032	0.3039	0.0188	0.0428	0.0007	266	113	269	15	270	4	-0.37%
72034-16	12.73173	112.28	217.49	0.52	0.0546	0.0037	0.3743	0.0245	0.0497	0.0008	396	155	323	18	313	5	3.19%
72034-17	32.38267	199.68	355.83	0.56	0.0583	0.0018	0.6320	0.0200	0.0786	0.0011	543	45	497	12	488	6	1.84%
72034-18	32.83848	196.14	366.71	0.53	0.0567	0.0016	0.6008	0.0168	0.0769	0.0010	478	38	478	11	478	6	0.00%
72034-19	49.91039	259.36	532.81	0.49	0.0569	0.0015	0.6555	0.0175	0.0836	0.0011	486	36	512	11	518	7	-1.16%
72034-20	14.60028	237.82	197.68	1.20	0.0533	0.0025	0.4013	0.0186	0.0546	0.0008	343	78	343	13	343	5	0.00%
72034-21	44.51957	163.02	632.71	0.26	0.0552	0.0025	0.4621	0.0200	0.0607	0.0008	420	104	386	14	380	5	1.58%
72034-22	24.93251	137.73	246.41	0.56	0.0625	0.0022	0.7556	0.0265	0.0878	0.0012	690	51	571	15	542	7	5.35%
72034-23	36.71995	169.22	408.43	0.41	0.0574	0.0018	0.6430	0.0198	0.0814	0.0011	505	44	504	12	504	6	0.00%
72034-24	12.39827	67.75	140.73	0.48	0.0568	0.0024	0.6091	0.0261	0.0778	0.0011	485	69	483	16	483	7	0.00%
72034-25	25.26045	132.29	308.15	0.43	0.0561	0.0018	0.5640	0.0186	0.0730	0.0010	454	48	454	12	454	6	0.00%
72034-26	28.97477	183.33	331.01	0.55	0.0565	0.0019	0.5905	0.0196	0.0759	0.0010	471	49	471	12	471	6	0.00%
72034-27	108.03649	197.71	872.33	0.23	0.0709	0.0019	1.1433	0.0304	0.1170	0.0016	955	33	774	14	713	9	8.56%
72034-28	27.76825	174.23	311.02	0.56	0.0567	0.0018	0.6029	0.0188	0.0771	0.0011	480	45	479	12	479	6	0.00%
72034-29	19.49923	237.61	375.7	0.63	0.0563	0.0023	0.3450	0.0138	0.0444	0.0006	465	64	301	10	280	4	7.50%
72034-30	12.11221	249.38	203	1.23	0.0567	0.0032	0.3363	0.0188	0.0430	0.0007	479	95	294	14	272	4	8.09%

Journal of Asian Earth Sciences 66 (2013) 123–139

Contents lists available at SciVerse ScienceDirect

Journal of Asian Earth Sciences

journal homepage: www.elsevier.com/locate/jseaes

Structural and kinematic analysis of the Early Paleozoic Ondor Sum-Hongqi mélange belt, eastern part of the Altaids (CAOB) in Inner Mongolia, China

Guanzhong Shi [a,b], Michel Faure [b], Bei Xu [a,*], Pan Zhao [a,b], Yan Chen [b]

[a] Key Laboratory of Orogenic Belts and Crustal Evolution, Ministry of Education, Peking University, Beijing 100871, China
[b] Institut des Sciences de la Terre d'Orléans, UMR Université d'Orléans-INSU/CNRS 7327, 1A rue de la Férollerie, 45071 Orléans, Cedex 2, France

ARTICLE INFO

Article history:
Received 16 August 2012
Received in revised form 18 December 2012
Accepted 23 December 2012
Available online 19 January 2013

Keywords:
Accretionary orogen
Altaids (CAOB)
Inner Mongolia
Early Paleozoic collision

ABSTRACT

We present a structural and kinematic study of an Early Paleozoic subduction mélange and a magmatic arc that form the main elements of the Southern Orogen Belt of Inner Mongolia, which lies in the eastearn part of the Altaids or Central Asia Orogenic Belt. The structural analysis of the mélange conducted in the Hongqi and Ondor Sum areas (western Inner Mongolia) shows two phrases of ductile deformation. The D_1 event is responsible for the pervasive S_1 foliation, NW–SE striking L_1 stretching lineation and F_1 intrafolial folds. These microstructures are coeval with a greenschist facies metamorphism. During D_2, NW-verging F_2 folds associated with a S_2 axial planar cleavage deformed S_1 and L_1. The D_1 kinematic criteria indicate a top-to-the-NW sense of shear. D_1 and D_2 developed before the unconformable deposition of the Early Devonian shallow water sandstone. A lithosphere scale geodynamic model involving an Early Paleozoic southeast-directed subduction beneath the North China Craton and late Silurian collision of the North China Craton with an hypothetical microcontinent is proposed to account for the microstructural evolution.

1. Introduction

Accretionary orogens, formed at active plate margins, play a major role in continental growth either vertically by transfer of mantle material within the crust in magmatic arcs or horizontally by accretion of oceanic material (i.e. magmatic island arcs, sea-mounts, oceanic crust and its sedimentary cover) against the continental margin (e.g. Condie, 2007; Cawood et al., 2009). Accretionary orogens are widespread in Central and East Asia. The Paleozoic accretionary orogens, recognized from the Urals Mts to Inner Mongolia in NE China, are called Altaids (Altaid Tectonic Collage, Sengor et al., 1993; Sengor and Natal'in, 1996) or Central Asia Orogenic Belt (CAOB, Jahn, 2004; Xiao et al., 2003, 2008; Windley et al., 2007). The Altaids/CAOB represents the consumption and remnant of the Paleo-Asian Ocean, currently preserved as ophiolite and serpentinite mélanges. This belt occupies an area of more than 5000 km long and 300 km wide. The end of the oceanic subduction and accretionary process is a critical point in the evolution of any accretionary orogen. Several possibilities have been suggested. Strike-slip tectonics along plate margins may lead to oblique subduction and collage (e.g. Sengor et al., 1993; Choulet et al., 2012). Another possibility is that the stopping of oceanic subduction is due to the entrance of a buoyant feature such as a magmatic arc or a microcontinent in the subduction channel (Condie, 2007; Cawood et al., 2009).

The eastern segment of the Altaids/CAOB is mainly exposed in Inner Mongolia. The Solonker (also called Solon Obo) suture is considered as the major structure that delineates the location of the Paleo-Asian Ocean (Xiao et al., 2003; Windley et al., 2007; Chen et al., 2009; Jian et al., 2010). Xiao et al. (2003) considered that during the Late Precambrian to Cambrian a north-directed subduction gave rise to the Ulan arc, and during the Early Paleozoic, a south-directed oceanic subduction below the North China Craton was coeval with a north-directed oceanic subduction below the southern Mongolian margin. Finally, in Late Permian to Early Triassic, the two opposite subduction systems came into contact to give rise to the Solonker suture. However, the Paleozoic tectonic evolution of this area is also interpreted as the result of two opposite subductions and collisions during the Middle Paleozoic (Xu and Chen, 1993, 1997; Xu et al., 2001, 2012).

The Southern Orogenic Belt (SOB) is equivalent to the Manchurides (Hsü et al., 1991; Sengor and Natal'in, 1996). Xu et al. (2012) argued that during the Early Paleozoic, a south-directed oceanic subduction took place below the North China Craton, and that the subduction system ended around 420–380 Ma. Recently, paired metamorphic belts were reported in the Bainaimiao and the Ondor Sum areas, and the age of 411 ± 8 Ma for undeformed pegmatite dike was regarded as upper limit of the collision (Zhang et al., 2012). Despite the existence of several geodynamic scenar-

* Corresponding author.
E-mail address: bxu@pku.edu.cn (B. Xu).

1367-9120/$ - see front matter © 2013 Elsevier Ltd. All rights reserved.
http://dx.doi.org/10.1016/j.jseaes.2012.12.034

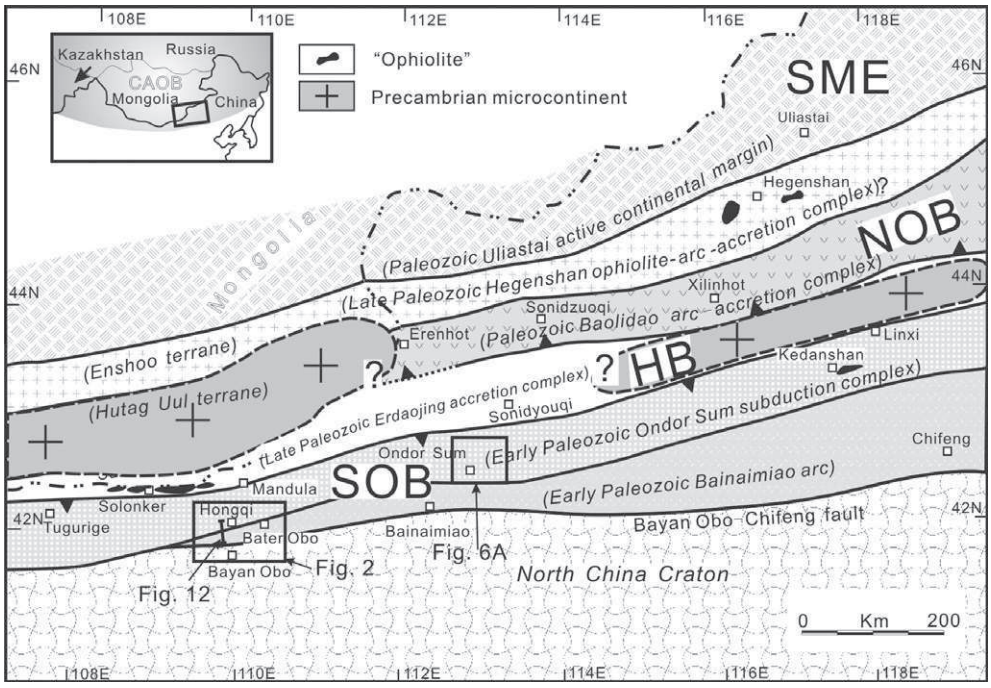

Fig. 1. Tectonic sketch map of central Inner Mongolia modified from Badarch et al. (2002), Xiao et al. (2003) and Xu et al. (2012). The late Mesozoic–Cenozoic formations are omitted for clarity. SME = Southern Margin of Ergun block; NOB = Northern Orogenic Belt; HB = Hunshandake block; SOB = Southern Orogenic Belt; NCC = North China Craton. The double spot dash line representing the Solonker Suture and the names in brackets and italics are from Xiao et al. (2003).

ios, the structural and kinematic features of the south-directed subduction are poorly constrained. This paper deals with the western part of the Southern Orogenic Belt that extends from Hongqi to Ondor Sum, in the west, and east, respectively (Fig. 1). In the following, two main questions will be addressed, namely: (i) what is the bulk geometry and kinematics deduced from microtectonic analysis of the rocks involved in the main tectonic events? (ii) what are the timing and relationships between these deformation events?

2. Regional geological framework

The CAOB of Inner Mongolia is subdivided into several, roughly *W–E* striking, litho-tectonic units namely, from south to north, the North China Craton, the Southern orogenic Belt (SOB), several microcontinents, including the Hunshandake block (HB), and the Hutag Uul block, the Northern orogenic Belt (NOB), and the Southern Margin of the Ergun block (SME) (Fig. 1; Xu et al., 2012).

2.1. The North China Craton (NCC)

The NCC is mainly composed of Archean trondhjemitic–tonalitic–granodiorite gneiss with mafic igneous rocks. Although the detailed tectonic evolution, timing and polarity of subduction remain disputed, it is now well accepted that the NCC was mainly built up during the Paleoproterozoic (ca. 2 Ga) by the collision of several Archean blocks (e.g. Zhao et al., 2005; Kusky and Li, 2003; Faure et al., 2007; Zhai et al., 2010; Trap et al., 2012, and enclosed references). Undeformed Mesoproterozoic to Early Paleozoic, ca.10 km thick, sedimentary deposits intercalated with volcanic rocks unconformably cover the Paleoproterozoic belts (Zhang et al., 1999). All these rocks are in turn unconformably overlain by unmetamorphosed and weakly deformed Carboniferous–Permian strata. (BGMRIM, 1991; Hsü et al., 1991; Zhao et al., 2005; Kusky et al., 2007; Faure et al., 2007; Trap et al., 2007). Late Palaeozoic granite and granodiorite intrude into the Precambrian basement of the NCC (BGMRIM, 1991). The east-west striking Baiyan Obo-Chifeng fault is considered as the northern boundary between the NCC and the Bainaimiao arc that belong to the SOB (Shao, 1991; Tang, 1990; Tang and Yan, 1993; Xiao et al., 2003).

2.2. The South Orogenic Belt (SOB)

The SOB extends at least for more than 700 km from the Tugurige area in the west via Ondor Sum to the Chifeng area in the east (Fig. 1). It is composed of the Ondor Sum mélange unit and the Bainaimiao arc unit (Xiao et al., 2003; Jian et al., 2008; Xu et al., 2012). The Ondor Sum mélange unit consists mainly of blocks of pillow basalts, gabbro, diabase, tuff, metasandstone, chert, pelagic sediments including iron–manganese formation, and rare limestone enclosed into a pelite–siltite matrix (Wang and Liu, 1986; Shao, 1991; Tang, 1990; Xiao et al., 2003). The Bainaimiao arc unit extends along an *E–W* trend from the Bater Obo in the west to the Chifeng in the east. It contains mainly andesite, basalt, a small amount of felsic lava, and volcanic–sedimentary rocks. Several granodiorite and granite plutons also crop out (Xiao et al., 2003). Three magmatic phases have been identified from ca.500 Ma to ca.415 Ma (Jian et al., 2008). Based on the high initial strontium isotope ratio ($^{87}Sr/^{86}Sr = 0.7146$) of granites and the εNd value of 2.4 ± 1.7 of granodiorite (Nie and Bjørlykke, 1999), Xiao et al. (2003) suggested that the Bainaimiao arc was formed by mixing between mantle-derived and crust-derived magmas emplaced in an active continental margin of Cordilleran-type.

2.3. The microcontinents

In southwestern Mongolia several microcontinents have been defined, namely the Hutag Uul block (Badarch et al., 2002), Totoshan Ulanul block (Yarmolyuk et al., 2005), and Tsagan Khairkhan block (Demoux et al., 2009). They are dominated by quartz-rich

micaschist, meta-volcanic rocks, meta-sandstones and marble (BGMRIM, 1980). The Totoshan Ulanul Block contains metamorphic rocks dated at 952 ± 8 Ma (single zircon U/Pb; Yarmolyuk et al., 2005; Demoux et al., 2009). The Tsagan Khairkhan block yields ages of 916 ± 16 Ma (Wang et al., 2001). In central Inner Mongolia, the existence of the Hunshandake Block was deduced from scattered outcrops of metamorphic rocks (BGMRIM, 1991) and the presence of Precambrian detrital zircon grains in mélange matrix (Xu et al., 2012). In our study area, Precambrian rocks are not exposed, however on the basis of microstructural analyses, we shall argue that the Hongqi mélange is underlain by a microcontinent (cf. below). The correlation of this hypothetical microcontinent with the previous ones will be discussed in section 6.

3. The Hongqi area

3.1. The litho-tectonic units

The Hongqi study area is located in the north of Bayan Obo at the western end of the South Orogen of Inner Mongolia. Four litho-tectonic units are recognized from northwest to southeast, namely the Hongqi mélange, the Bainaimiao arc, an overlying sedimentary succession ranging from the Early Devonian to the Late Carboniferous, and the North China craton (Fig. 2).

3.1.1. The Hongqi mélange unit

To the north, the mélange rocks are hidden below the Mesozoic sedimentary rocks of the Erlian basin (Meng, 2003). To the south of the mélange unit, Permian magmatic rocks crop out. The entire mélange unit is cut into two parts by the Suji fault (Fig. 3A). The western part of the mélange is predominantly composed of fine grain quartzite, micaschist, sericite slate, siltstone, iron-bearing chert and metapelite with rare blocks of limestone. Coherent sedimentary strata of alternating beds of fine quartzite and metapelite are locally well preserved, suggesting a turbiditic origin for these rocks. The eastern part of the mélange exhibits a typical block-in-matrix structure. It mainly consists of tuffaceous siltstone, sericite chlorite schist, chlorite quartz schist, calc-slate, chert and a small amount of greywacke. Blocks include amphibolite, pillow basalt, volcanic rocks, limestone and chert (Fig. 4A). These blocks display variable size ranging from tens of centimeters to several hundreds of meters. Mafic-ultramafic rocks, such as serpentinite, serpentinized peridotite and metagrabbro, are reported in the southern part of the mélange (Jia et al., 2003). In the middle part of this unit, due to mining exploration work, amphibolite rocks are digged out below a greenschist cover.

Intense ductile shearing and mylonitization characterize all the rock types. To the south of the mélange, the available geological map shows Silurian strata composed of fossiliferous limestone

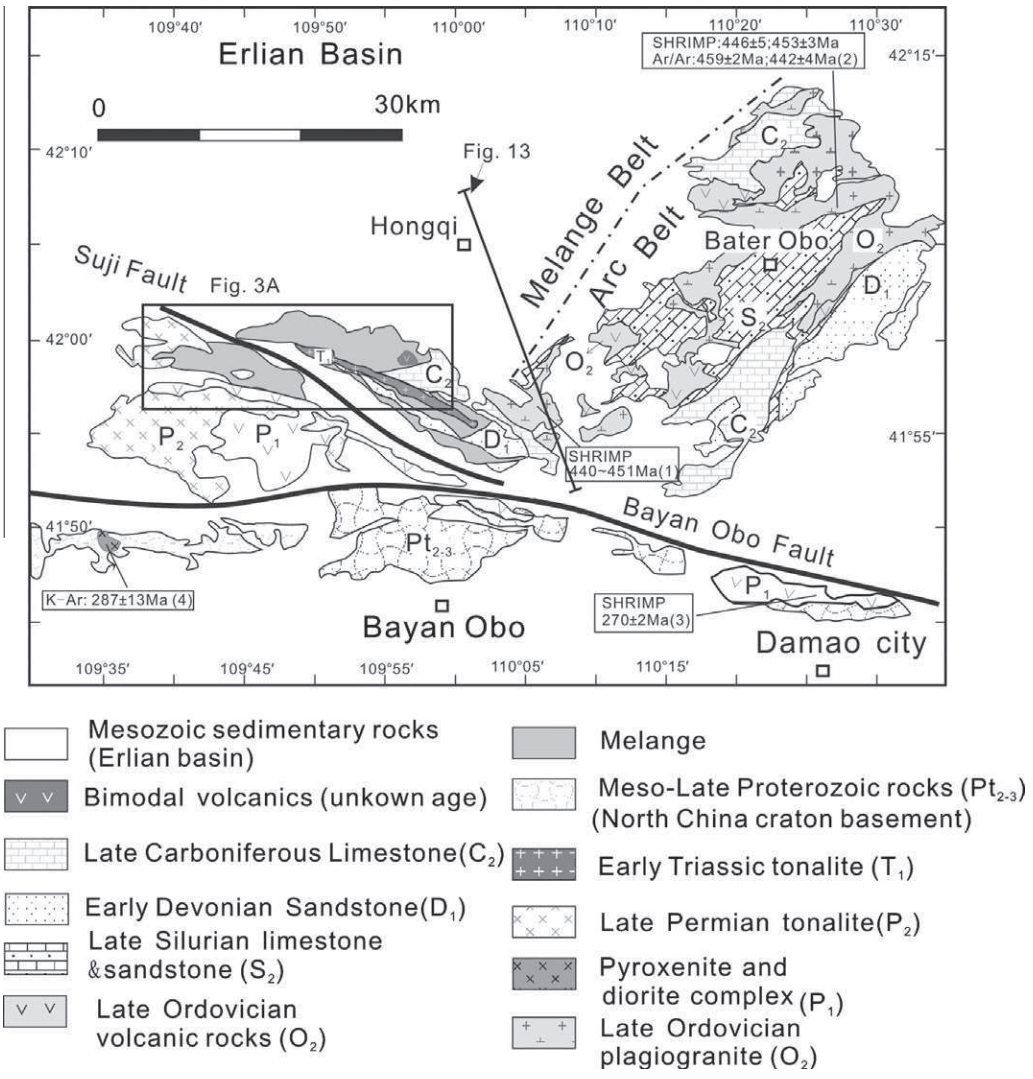

Fig. 2. Geological map of the Hongqi area in Inner Mongolia showing litho-tectonic units distribution. Modified after IMBGMR (2002, 2008).

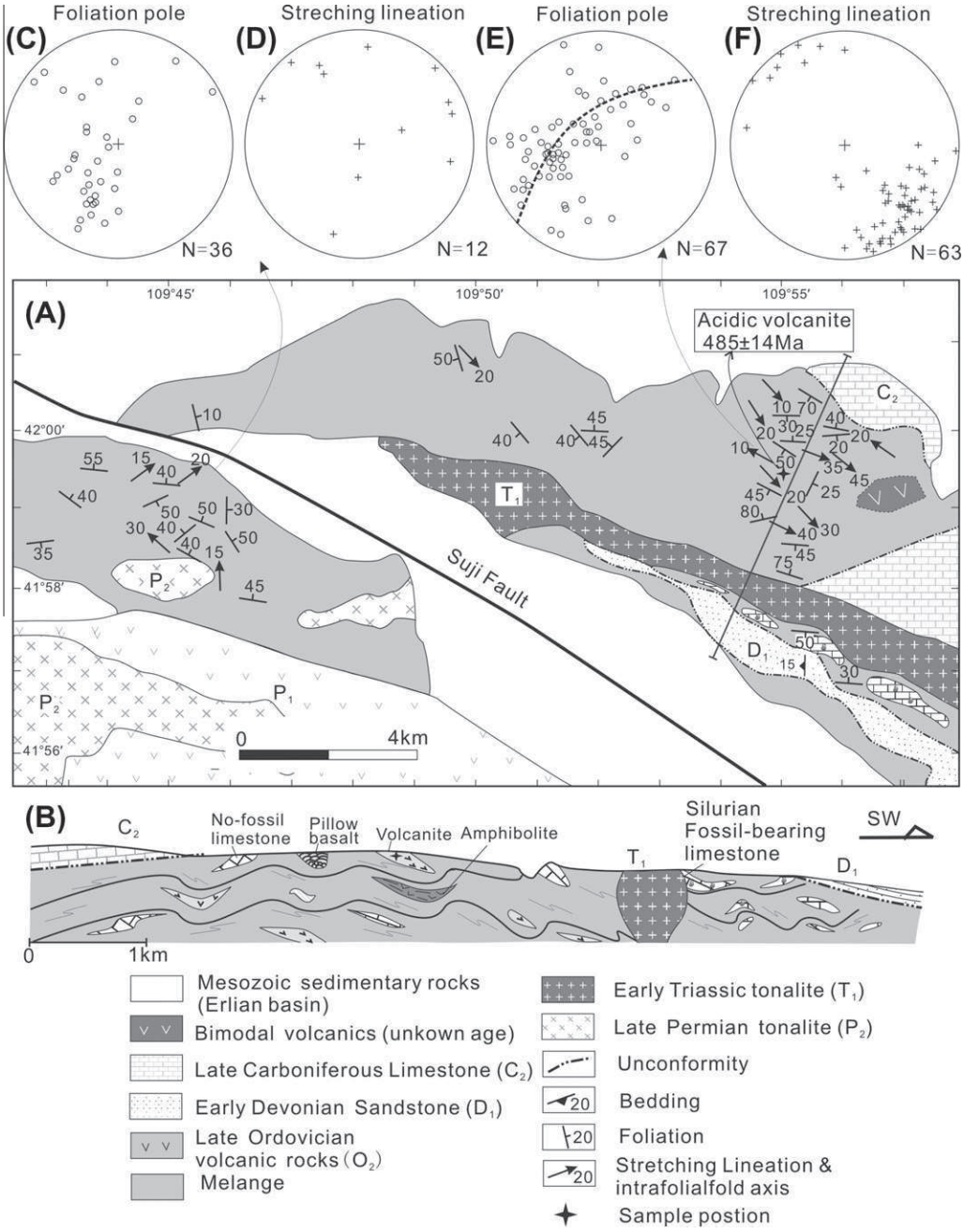

Fig. 3. Geological map (A), cross section (B), and structural elements of the Hongqi mélange (C–F; lower hemisphere projection). Modified after IMBGMR (2002, 2008).

and sandstone. However, our field observation indicates that these rocks are foliated, recrystallized, and contain elongated crinoids (Fig. 4B and C). Additionally, those limestones are laterally discontinuous in the regional scale. Therefore, we consider these rocks as blocks within the Hongqi mélange.

The whole mélange unit is dominated by a greenschist-facies metamorphism with a common mineral assemblage of chlorite, muscovite, biotite, plagioclase and quartz in the metapelite. The amphibolite blocks contain metamorphic minerals such as hornblend, plagioclase, epidote and quartz, indicating an amphibolite facies metamorphism. In the western part of the mélange, biotite and andalusite grains, oblique to the regional foliation, are related to a contact metamorphism probably due to plutonic intrusions emplaced after the main deformation. Graptolite fossils assigned to *Callograptus* sp., *Desmograptus* sp., and *Dictyonema* sp., found in the tuffaceous rocks, suggest an Early to Middle Ordovician age (BGMRIM, 1991). An acidic metavolcanite block is dated at 485 ± 14 Ma by ICP-MS on zircon (see Section 5).

3.1.2. The Bainaimiao arc

Eastward of the mélange, in the Bater Obo area, crops out the Bainaimiao arc. It is composed of basalt, basaltic andesite, andesite, interbedded with up to 10–20 m of tuffaceous siltstone as well as agglomerate, pyroclastite and volcanic breccia. The basalts contain three types of aphanitic, porphyritic and vesicular structure. The basalts with typical porphyritic textures contain olivine (3–5%), pyroxene (10–15%) and feldspar (25–30%) phenocrysts embedded in a fine-grained groundmass of glass, plagioclase and pyroxene microcline. Secondary chloritic and sericitic alterations and fine carbonate veins are common in the volcanic rocks. Numerous granite, plagiogranite, granodiorite, quartz diorite and diorite plutons with calc-alkaline geochemical signatures are exposed (Xu and

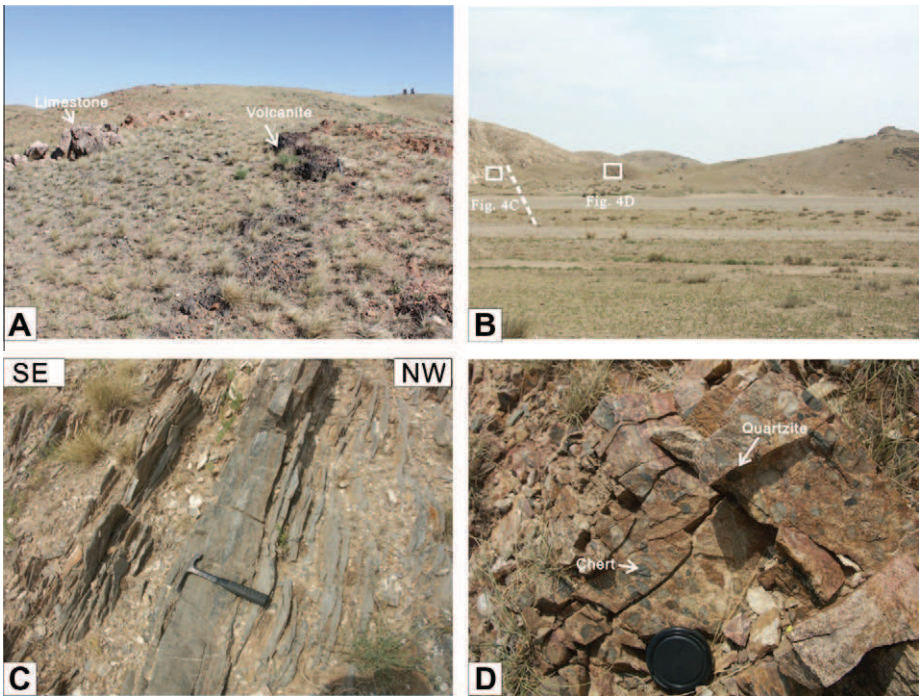

Fig. 4. Field pictures in the Hongqi mélange unit. (A) Blocks of limestone and volcanite embeded in the matrix; (B) Early Devonian basal conglomerates cropping out close to the mélange; (C) Foliated limestone containing elongated Silurian fossils included as block in the Hongqi mélange; (D) Undeformed Early Devonian basal conglomerates including rounded pebbles of volcanic rocks, greenschist, chert and quartzite. (For interpretation of the references to color in this figure legend, the reader is referred to the web version of this article.)

Tao, 2003). Jian et al. (2008) suggested that the quartz diorites are high-K calc-alkaline rocks with adakitic feature, indicating an island arc setting. The age of those plutons with arc signature is about 440–460 Ma (Jian et al., 2008; Li et al., 2010; Fig. 2).

3.1.3. The overlying sedimentary succession

The Early Devonian and Late Carboniferous rocks unconformably overly the volcanic, sedimentary and plutonic rocks mentioned in the previous section. The Lower Devonian Chaganhabu Formation (IMBGMR, 2002), exposed in the southern part of the Hongqi mélange and the Bainaimiao arc, can be subdivided into two units. The lower unit, with a thickness of ca.975 m, consists of basal red conglomerate, siltstone, gray arkose, upperwardly reef limestone and red quartzose arkose and micrite. The upper unit is composed of turbiditic deposits with a thickness of ca.1500 m (Zhang et al., 2004). The association of various fossils, such as corals, brachiopods, bryozoan and conodonts in the limestones indicate an Early Devonian age. The conglomerate and terrigeneous rocks unconformably cover the Upper Silurian series with an angular unconformably (IMBGMR, 2002; Zhang et al., 2004). Our observation of the basal conglomerates of the lower Devonian sequence reveals pebbles of volcanic rock, metamorphic rock, quartzite and chert (Fig. 4B–D). The unconformable contact of this sequence above the underlying deformed limestone rocks can be observed as well. The Uppermost Carboniferous strata consist of fossiliferous limestone and clastic rocks that unconformably cover the lower Devovian (IMBGMR, 2002). This Early Devonian to Late Carboniferous sedimentary succession did not experienced a ductile or syn-metamorphic deformation, but only folding and brittle faulting.

3.1.4. The North China Craton basement

The southernmost unit of the study area is occupied by Meso-to Late Proterozoic volcanic–sedimentary series (Bayan Obo group; Fig. 2). These unmetamorphosed sedimentary rocks represent the NCC basement in the study area.

3.2. The bulk architecture of the Hongqi area

A general cross section of the Hongqi area is drawn along a SW–NE strike (Fig. 3B). The regional framework is represented by an antiform composed of several SE–NW striking folds with hectometer-wavelength. In the center of the antiform, a bimodal volcanic rock with associated gabbro and Early Triassic tonalitic pluton superimpose on the Hongqi mélange unit. The mélange is unconformably covered to the south by the Early Devonian red sandstone, and to the north by Late Carboniferous limestone. The Early Devonian rocks, gently dipping to the west, do not display any metamorphism or ductile deformation. The structural characteristics of the mélange are described in detail below.

3.3. Microstructural analysis of the Hongqi mélange

From our field observations, three deformation events namely: D_1, D_2 and D_3, with the first two of ductile and syn-metamorphic style, and the third one of gentle folding, are recognized.

The D_1 event is responsible for the formation of the main foliation (S_1), stretching lineation (L_1) and intrafolial fold (F_1). In the field, S_1 is defined by the alternation of chlorite quartz schists and sericite chlorite schists. The L_1 lineation is marked by elongated clasts, quartz ribbons, aggregates of chlorite and mica (Fig. 5A). Intrafolial F_1 folds with axes plunging to the SE are also developed within the S_1 foliation (Fig. 5B). In places, the S_1 foliation is approximately parallel to the sedimentary bedding, which is well preserved in the metapelite and meta-quartzstone. Pinch-and-swell and boudinaged structures are also observed in quartz schists indicating a layer-parallel shearing (Fig. 5C). At the microscopic scale, pressure solution seams of dark insoluble material and aligned recrystallized phyllosilicates represent S_1 (Fig. 6A). The S_1 foliation mostly dips to the NE or SW due to D_3 folding. The well foliated and lineated blocks wrapped around by S_1 matrix foliation display SE–NW directed elongation. The L_1 lineation in amphibolite blocks is represented by oriented hornblende and

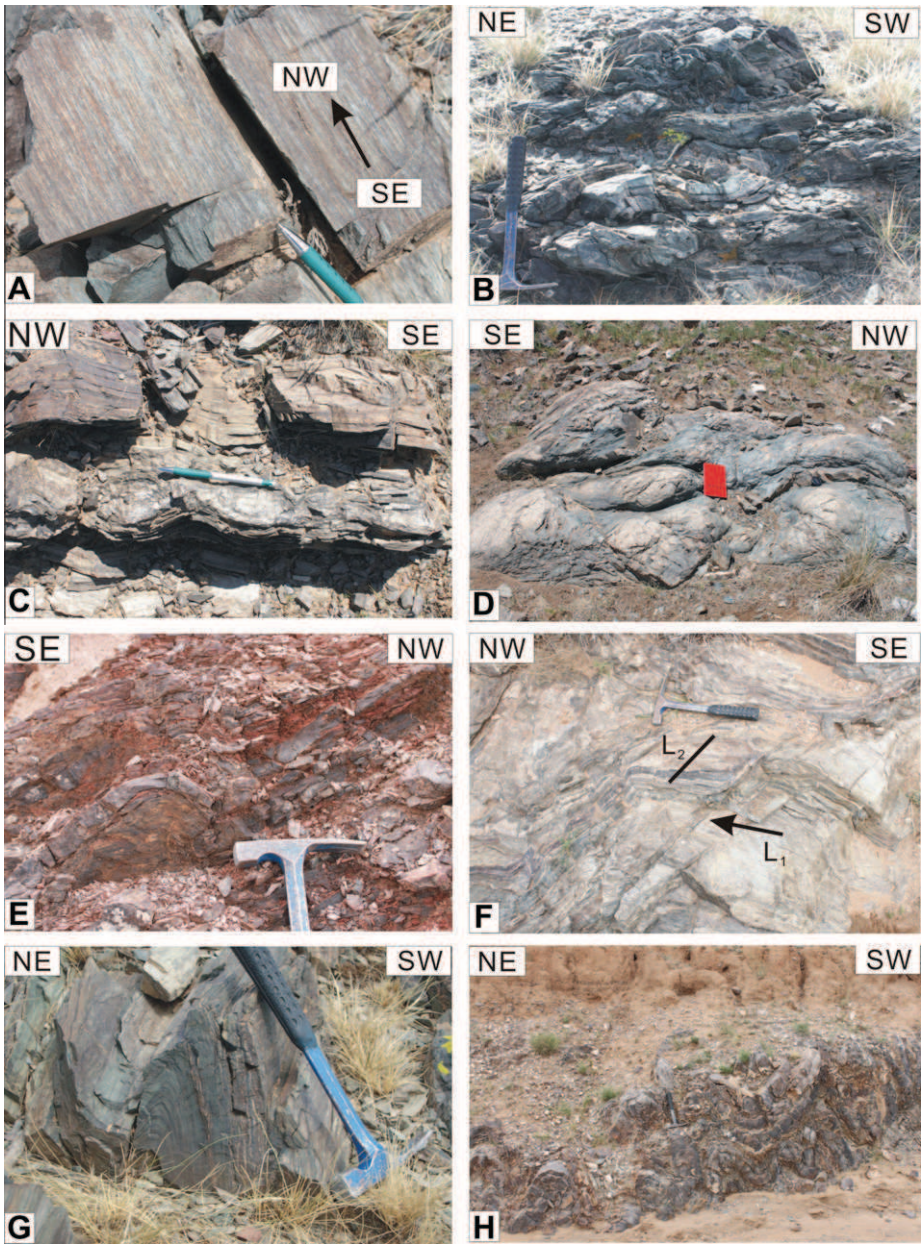

Fig. 5. Field pictures in the Hongqi mélange unit. (A) Stretching lineation in chlorite quartz schist; (B) Intrafolial fold (F_1) with SE–NW striking axis; (C) Pinch-and-swell structure within quartz schists; (D) Flattened and elongated pillow lavas block in the mélange; (E) asymmetrical fold (F_2) with SE-dipping long limb indicating northwest vergence; (F) Asymmetric kink bands F_2 refolded L_1 stretching lineation; (G) Northeast striking upright fold (F_3) developed in quartz chlorite schist; (H) Upright fold formed in quartz-rich layer.

recrystallized quartz and plagioclase aggregates (Fig. 6B). Pillow lava blocks, up to 30–50 cm in diameter, are also elongated in the NW–SE direction (Fig. 5D). Sandstone blocks exhibit commonly elongated chert pebbles along the NW–SE direction. Limestone blocks display aligned and elongated crinoids along the NW–SE stretching direction of L_1.

The D_2 event is associated with the development of NW-verging asymmetrical folds (F_2) that deform S_1 and L_1. The most striking structure is meter-scale asymmetrical fold F_2. F_2 fold with NE–SW trending subhorizontal axes (L_2) exhibits a NW vergence (Fig. 5E). Asymmetric kink bands, bending the S_1 foliation and L_1 mineral lineation, are well developed in quartz sericitic schists (Fig. 5F).

The D_3 event is represented by NW–SE trending upright folds (F_3) responsible for the bulk architecture of the area. Although the eastern and western parts of the mélange unit on each side of the Suji fault should have experienced similar structural histories, the structures of the western part are, to some degree, disturbed by the activity of the brittle Suji fault as well as the post-tectonic intrusions (Fig. 3C and D). In contrast, the three deformation events are well recognized in the eastern part (Fig. 3A, E and F).

The D_3 event is defined by SE–NW striking upright folds. Similar folds are widespread in the layers where incompetent material dominates such as chlorite schists (Fig. 5G), whereas parallel folds with SE–NW trending axes develops in the quartz sandstone layers (Fig. 5H). At the macroscopic scale, F_3 folds deform the S_1 foliation, giving rise to the general antiformal structural framework of the Hongqi mélange (Fig. 3B and E).

Thin sections, made parallel to L_1 and perpendicular to S_1, exhibit numerous kinematic indicators. In amphibolite blocks, the

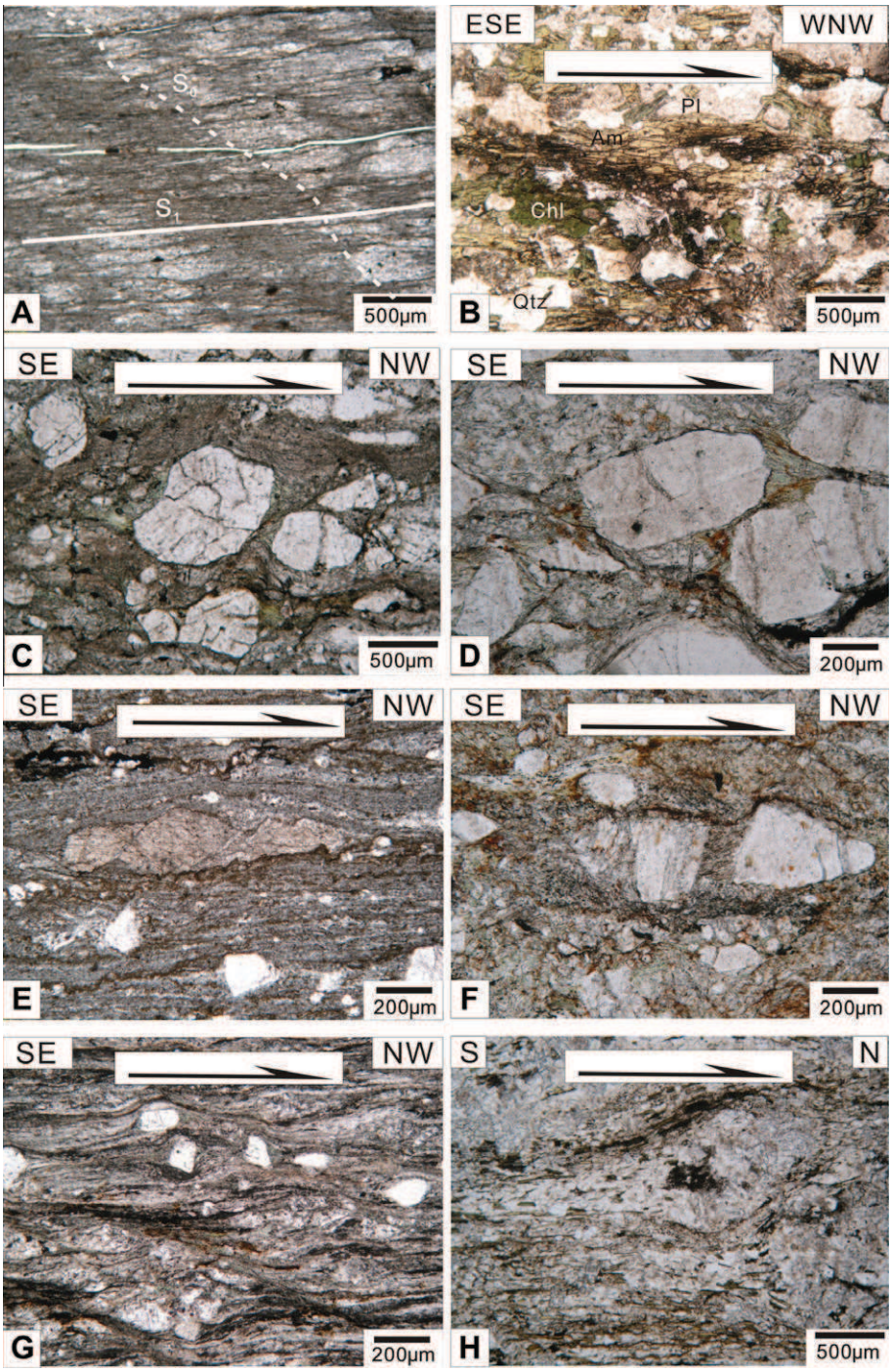

Fig. 6. Microscope scale kinematic indicators in the Hongqi mélange. (A–G) thin sections are cut perpendicular to the main S_1 foliation, and parallel to the L_1 stretching lineation. (A) Geometric relationship between bedding (S_0) and foliation (S_1) in the hinge of an intrafolial fold in metapelite; (B) oriented alignment of amphibole and anhedral quartz indicating top-to-the WNW shearing; Am = Amphiolite, Pl = Plagioclase, Qtz = Quartz, Chl = Chlorite; (C) (D) asymmetrical chlorite fibers developed as pressure shadows constitutes oriented chlorite fibers around the end of a feldspar clast, showing a northwestward shearing; (E) oblique fractured carbonate grains showing a top-to-northwest NW shearing; (F) Boudinage of feldspar clast with recrystallized chlorite fibers in the interspace, suggesting SE–NW stretching direction; (G) Mica bands defined by curved recrystallized mica aggregates and insoluble material, showing northwest ward shearing; (H) Sigmoidal clast indicating top-to-N shearing.

recrystallized amphibole and quartz aggregates indicate a top-to-WNW shearing (Fig. 6B). In mylonitic volcanic–sedimentary rocks, asymmetric pressure shadows defined by chlorite fibers around feldspar porphyroclasts indicate a top-to-the-NW sense of shear (Fig. 6C and D). Quartz oblique grain shape fabric showing a top-to-the NW shearing is also recognized (Fig. 6E). Boudins formed by pull-apart clasts with chlorite aggregates filling in the cracks suggest a top-to-the-NW sense of shear (Fig. 6F). Mica fishs, and shear bands developed in the metapelites also have the same sense of shear (Fig. 6G). Sigma-type porphyroclast systems in the metapelite in the western part of the mélange exhibit a top-to-the-N thrusting (Fig. 6H). Thus the kinematic criteria of the mélange unit show a consistent top-to-the-NW sense of shear.

In summary, the Hongqi mélange of block-in-matrix structure experienced three phases of deformation. The D_1 phase is dominated by a consistent top-to-the-NW sense of shear coeval with

the mélange formation. The NW-verging asymmetric folds developed during the D_2 event can be interpreted as the continuation of the same ductile shearing under less penetrative conditions. The last D_3 deformation forms upright folds, which control the general structural framework of the mélange unit. The Early Devonian red sandstone unconformably covering this mélange unit does not record the D_1 and D_2 events, and thus provides an upper time limit for the termination of the ductile events. The km-scale upright folding involves the Devonian and Carboniferous rocks.

4. The Ondor Sum area (Fig. 7)

4.1. The litho-tectonic units

In the Ondor Sum area, two litho-tectonic units are recognized from north to south. The geometrically lowermost unit corresponds to the Ondor Sum mélange, it is bounded to the south by an amphibolite-granite unit, called "Tulinkai ophiolite" (Jian et al., 2010).

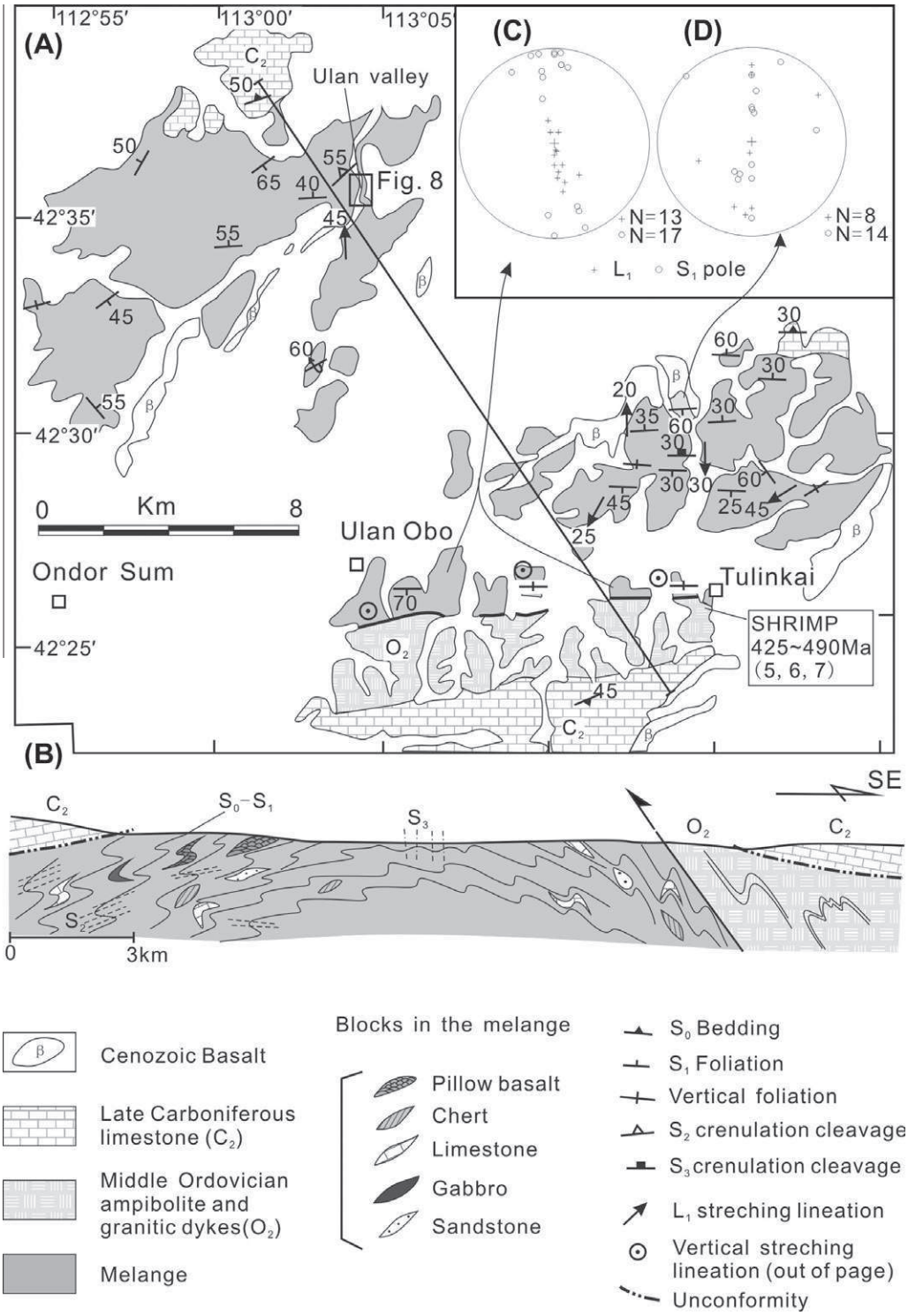

Fig. 7. Sketch map (A), cross section (B), and structural elements of Ondor Sum area (C, D; lower hemisphere projection). modified after IMBGMR (1976). The Cenozoic trap basalts must not be confused with the basaltic blocks included in the mélange.

4.1.1. The Ondor Sum mélange unit

The Ondor Sum mélange crops out in three places: the southern one (or Ulan Obo-Tulinkai area), the middle and the northern Ulan valley areas (Fig. 7A). The Ondor Sum mélange is mainly composed of sericite quartz schists, chlorite–epidote schists and albite-chlorite–epidote schists. Various decimeter to several meter sized lenses of sandstone, limestone, mafic rocks and iron-bearing quartzite are scattered into a greenish matrix. These green and red blocks dispersed in a sandy–silty matrix define a typical colored mélange formation (Fig. 8A and B). Two types of basalts are recognized near the Ulan valley. One is represented by flattened vesicular basalt. As described by Xiao et al. (2003), the pillow lavas are up to 30–50 cm in diameter, elongated, facing upward, and dipping to the north. The other type of basalt is undeformed, with a vesicular or massive texture filled by centimeter sized white quartz. These deformed pillow basalts are blocks within the mélange and were geochemically interpreted as originated from a intraplate basalt (Huang et al., 2006). They must not be confused

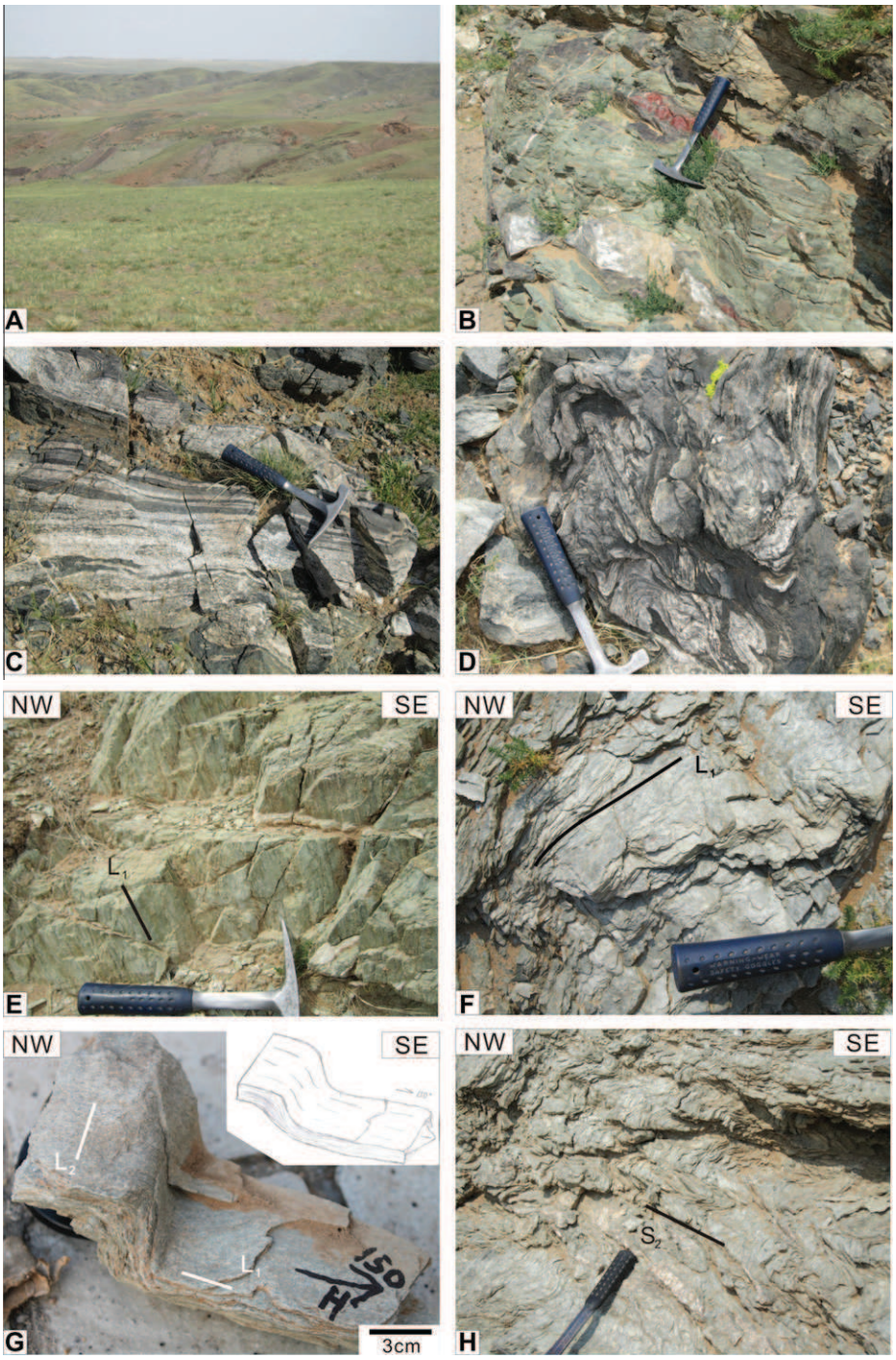

Fig. 8. Field pictures in the Ondor Sum area. (A) Typical field aspect of the Ondor Sum colored mélange due to various blocks of pillow basalts, chert, limestone, sandstone enclosed in a greenschist sandy–silty matrix; (B) Colored conglomerate with red chert, white limestone, green lava or volcanic–sedimentary material in the Ulan Valley; (C, D) Amphibolite and gneissic granite dykes in the Tulinkai and Ulan Obo areas; C: amphibolite-acidic gneiss metre-sized alternation; D: folded amphibolite cross cut by a granitic dyke; (E) Vertical foliation (S_1) and mineral lineation (L_1) in green chlorite–epidote schist in the southern part of the Ondor Sum mélange unit. (F) Mineral and stretching lineation (L_1) folded around an F_2 fold, Ulan valley; (G) L_1 stretching lineation deformed by an SE-verging F_2 fold axis (L_2: F_2 fold axis), Ulan valley; (H) Microfold associated with a crenulation cleavage (S_2) in Ulan valley. (For interpretation of the references to color in this figure legend, the reader is referred to the web version of this article.)

with undeformed basalts that occupy the top of some hills. Some of these undeformed basalts yield a radiometric age of c.260 Ma (Miao et al., 2007); Cenozoic basalts are also likely (IMBGMR, 1976).

In the Ondor Sum mélange, the rocks are pervasively deformed, mylonitized and metamorphosed into greenschist or blueschist facies. Petrological study of metamorphic assemblages led previous authors to deduce P–T conditions of the blueschist facies rocks at 7–8 Kb and 380–400 °C, respectively (Yan et al.,1989; Tang, 1992). Glaucophane from blueschists yields $^{40}Ar/^{39}Ar$ ages of 446 ± 15 Ma and 426 ± 15 Ma (Xiao et al., 2003; and references therein). Phengite from quartzite mylonites at Ondor Sum has $^{40}Ar/^{39}Ar$ plateau age of 449–453 Ma (De Jong et al., 2006). In agreement with Xiao et al. (2003), we consider that this rock assemblage, derived of Fe and Mn siliceous sediments, volcaniclastic sediments, basalts and spilites, indicates an ocean floor origin.

4.1.2. The Tulinkai unit

The Tulinkai unit spreads in the *E–W* direction from Tulinkai to Ulan Obo (Fig. 7A). In the literature, the Tulinkai unit is described as an "ophiolitic suite" (Hu et al., 1990; Jian et al., 2010). Our field observations indicate that the dominant rock is coarse to medium grained, well foliated amphibolite, diorite and gabbro. Granitic layers are also widespread. Some appear as dykes cross cutting the foliation and others show foliation parallel veins (Fig. 8C and D). Large volumes of diorite and granodiorite with mafic boudins are exposed further south of the "ophiolitic" rocks. Cumulate gabbros from Tulinkai have a zircon SHRIMP age of 457 ± 4 Ma, and a diorite intrusion with an adakitic geochemical signature has a zircon age of 467 ± 6 Ma (Liu et al., 2003; Miao et al., 2007). These rocks have been interpreted as supra-subduction zone type ophiolite (Liu et al., 2003; Jian et al., 2008). However, from our field observation, usual ophiolitic component, such as serpentinized peridotite, pillow basalts and siliceous sediments, are not observed. Therefore, in the following section, we shall argue that these rocks might belong to the deep part of a magmatic arc.

4.2. The bulk architecture

Based on field structural measurements, the bulk architecture of the Ondor Sum area is dominated by a NE–SW trending antiform (Fig. 7B). The general structure results of a polyphase deformation evolution. The southern limb of the antiform is dominated by a steeply south dipping or vertical foliation (Fig. 7C). In the middle part, the main foliation is involved in a series of nearly *E–W* trending upright folds (Fig. 7D). The Ulan valley, dominated by northwest dipping foliation, corresponds to the northern limb of the antiform. To the south of the Ondor Sum mélange, the Tulinkai unit is fault-contact with the mélange unit. A top-to-the-north thrusting is documented (IMBGMR, 1976). The light colored gneiss-amphibolite alternation of the Tulinkai unit is ductilely deformed. Amphibolitic and granitic dykes commonly form meter-scale isoclinal folds with approximately NW-dipping axes. The northward and southward dip of the Carboniferous limestone bedding, in the northern and southern limbs of the Ondor Sum antiform indicate that the last deformation event took place after the Carboniferous. However, the synmetamorphic deformations are clearly older than the deposition of the Carboniferous series.

4.3. Microstructural analysis

Like the Hongqi area, three deformation events are also identified in the Ondor Sum area. They are named here D_1, D_2 and D_3,

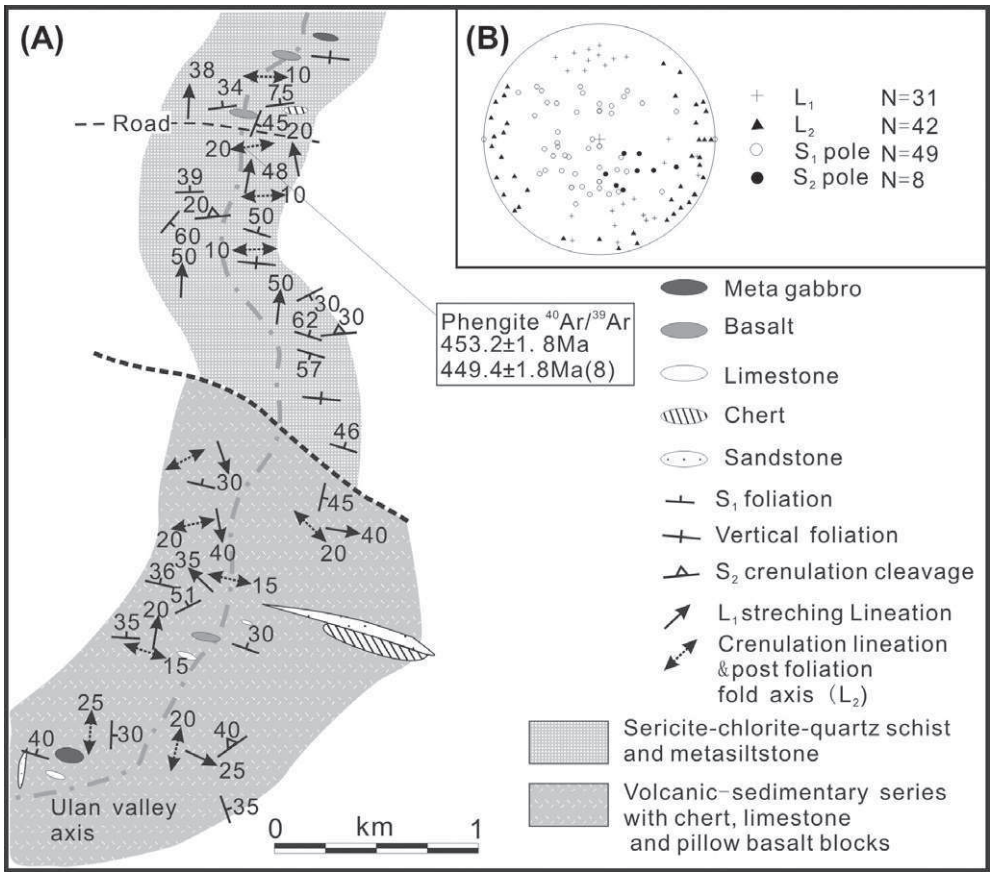

Fig. 9. Structural map of the microtectonic data observed in the Ulan valley (modified after Xiao et al., 2003).

nominally like in the Hongqi area but with a slightly different meaning for D_3.

In the southern limb of the mélange unit, the approximately *E–W* trending S_1 is subvertical or dipping at a high angle to the south. The L_1 subvertical lineation is represented by elongated quartz, feldspar or calcite clasts, and chlorite fibers on the S_1 surface (Fig. 8E). In thin section, the lineation is marked by oriented phyllosilicates and recrystallized carbonate clasts within insoluble material. For this part, a subhorizontal crenulation lineation is weakly developed. But centimeter- to meter-scale asymmetric

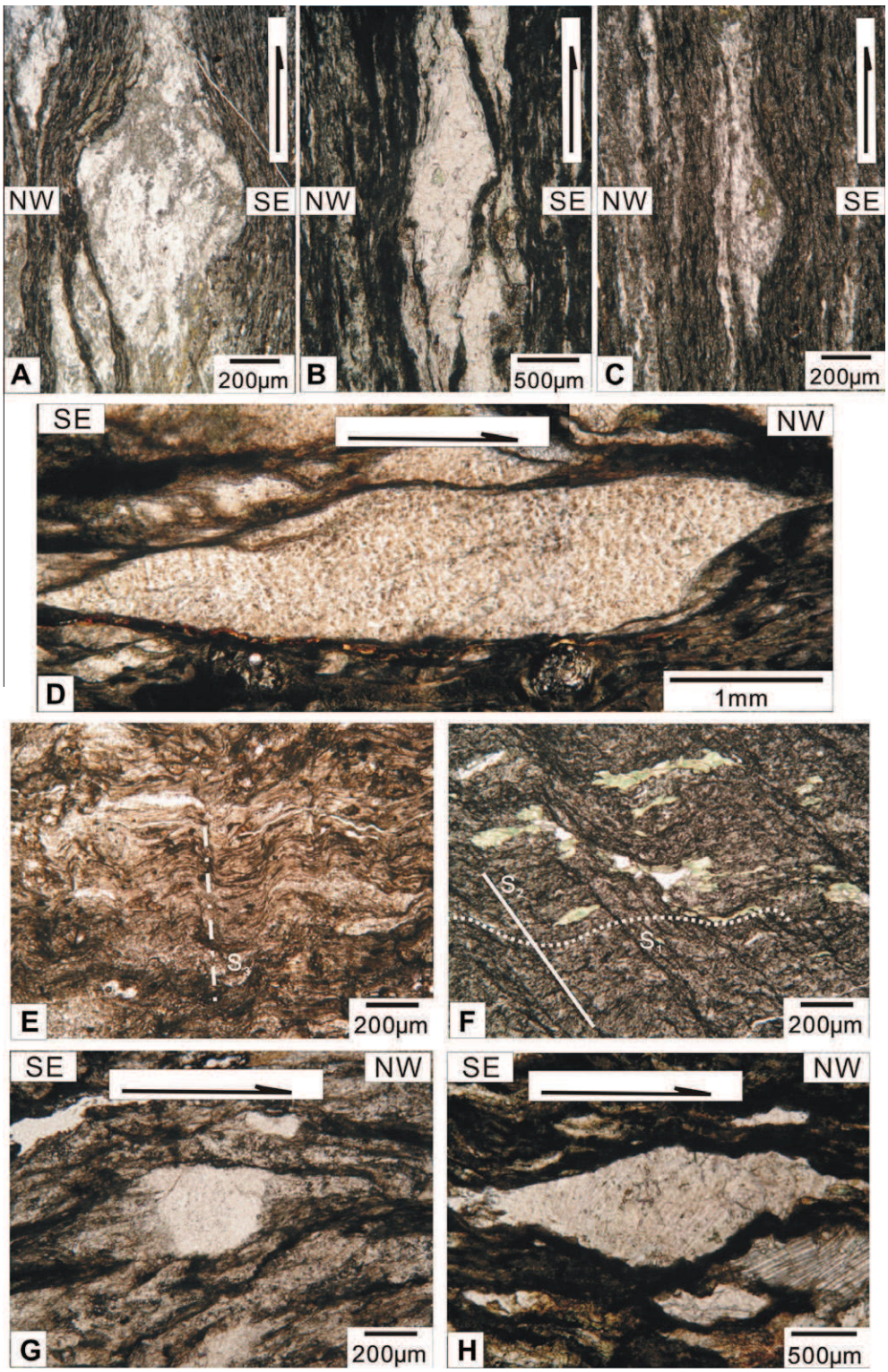

Fig. 10. Microscope scale kinematic indicators in the Ondor Sum mélange. All cross sections are cut perpendicular to the main S_1 foliation, and parallel to the L_1 stretching lineation. (A–C) Sigmoidal feldspar and carbonate porphyroclast showing top-to-the-NW shearing, southern limb of Ondor Sum mélange; (D) Sigmoidal feldspar porphyroclast showing a top-to-the-NW sense of shear in the middle part of the Ondor Sum mélange; (E) subvertical S_3 cleavage cutting the S_1 foliation; (F) Crenulation cleavage oblique to the main foliation S_1. Syn-S_1 chlorite is deformed by D_2 folding; (G) Asymmetric pressure shadow around quartz aggregates showing a top-to-the NW sense of shear, Ulan valley; (H) Carbonate sigmoidal porphyroclast showing a top-to-the-NW sense of shear, Ulan valley;

folds are observed in the chlorite quartz schistose layers. Shear criteria, such as pressure shadows, sigma type porphyroclast systems and shear bands indicate a SE (or S) moving upward sense of shear (Fig. 10A–C). Thus, when the foliation is rotated to horizontal, the kinematic indicators are top-to-the-NW (or N) sense of shear.

In the central part of the Ondor Sum area, a series of *E–W* striking centimeter- to millimeter-scale upright folds deforming S_1 are identified. Both the chlorite and sericite schist matrix and the blocks exhibit a N–S to NW–SE stretching lineation (L_1) marked by elongated recrystallized quartz and chlorite aggregates. Along the lineation, pressure shadows and sigma-type porphyroclasts indicate a top-to-the-NW sense of shear when S_1 lies subhorizontal or gently tilted (Fig. 10D). S_2 is characterized by centimeter wavelength crenulations. At the microscope scale, a S_3 subvertical cleavage cuts at a high angle the S_1 foliation (Fig. 10E).

The Ulan valley has been studied in detail since it is well exposed (Wang and Liu, 1986; Xiao et al., 2003; Fig. 9A). At the southern entrance of the Ulan valley, S_1, generally N–S striking, contains a nearly *E–W* striking L_1 mineral lineation. However, when moving northward, S_1 turns to an *E–W* strike and dips to north or northwest. A conspicuous NW–SE trending stretching and mineral lineation is preserved on the gently dipping foliation (Figs. 8F and 9B). Crenulation wrinkles and asymmetric microfolds (F_2) that intensively deform the S_1 foliation and L_1 lineation are commonly developed (Figs. 8G and H). F_2 folds are scattered with subhorizontal axes (Fig. 9B). An axial planar crenulation cleavage (S_2) marked by the opaque material is well developed (Fig. 10F). S_2 cleavage is tilted to the northwest due to the D_3 antiformal upright folding. Locally, the intense F_2 folding gives rise to well developed inverted limbs with some F_2 folds apparently overturned to the SE (Fig. 8H). In thin sections cut parallel to the L_1 lineation, asymmetric pressure shadows and sigmoidal porphyroclasts indicate a top-to-the-NW sense of shear (Fig. 10G and H).

In conclusion, the Ondor Sum mélange unit is a terrigenous volcaniclastic block-in-matrix series with blocks of oceanic origin. It experienced three deformation phases: D_1 was responsible for the S_1 foliation and L_1 stretching lineation coeval with a greenschist facies metamorphism. Taking S_1 as a reference surface, two subsequent deformation events, D_2 and D_3 are recognized. The D_2 event associated with the F_2 asymmetric folds can be interpreted as the continuation of the top-to-the-NW shearing, that occurred by shortening at a low angle or subparallel to S_1. After the deposition of the Late Carboniferous limestone, the D_3 event gave rise to the general antiform to form the regional structural framework.

5. Geochronological constraints

New zircon dating is obtained by ICP-MS U-Pb analyses method. Cathodoluminescence (CL) images were performed by CAMECA SX-50 microprobe at Peking University in order to document zircon internal structures. Zircon laser ablation ICP-MS U-Pb analyses

Table 1
Summary of geochronological data for the Hongqi–Ondor Sum area. The number in the parentheses corresponds to those in Figs. 2, 7 and 9 respectively.

Study area	Setting	Lithology	Age/Ma	Dating method	Geochemisty	Reference	Remarks
Hongqi	Bainaimiao arc	Diortie (1)	451.5 ± 2.9	Zircon	High-K calc-alkaline	Jian et al. (2008)	
		Quartz diorite (1)	440.3 ± 2.4	SHRIMP	High-K calc-alkaline adakite		
		Quartz diorite (1)	446 ± 2.2		High-K calc-alkaline		
		Hornblendite (2)	446.8 ± 5.8	Zircon		Li et al. (2010)	
		Hornblendite (2)	453 ± 3	SHRIMP			
		Diortie (2)	459.2 ± 2.4	Hornblende $^{40}Ar/^{39}Ar$			
		Diortie (2)	442.9 ± 4.2	Hornblende $^{40}Ar/^{39}Ar$			
	Hongqi melange	Acidic volcanite	485 ± 14	Zircon ICP-MS	Block within melange	This study	
	North China Craton (south of Bayan Obo-Chifeng fault)	Rhyolite (3)		Zircon SHRIMP	Alkaline	Chen (2011)	$\varepsilon Nd(t) = -9.5$ to -10.3; mantle magma mixed with crust
		Hornblend pyroxenite (4)	287 ± 13.6	Hornblende K–Ar	Zoned ulmafic-mafic pluton	Zhao et al. (2008)	
Tulinkai		Cumulate gabbro (5)	457 ± 4	Zircon SHRIMP		Miao et al. (2007)	
		Diorite (6)	467 ± 6		Adakitic geochemical signature	Liu et al. (2003)	
		Tonalite (7)	490.1 ± 7.1		MORB with arc signature	Jian et al. (2008)	Core
			449.8 ± 3.0				Overgrowth mantle
		Metagabbro (7)	479.6 ± 2.4				
		Trondhjemite (7)	471.6 ± 1.7		Magmatic zircon/low K boninite		
			439.4 ± 3.3		Metamorphic zircon		
		Quartz diorite (7)	453.7 ± 3.1		Magmatic zircon/medium K peraluminous, calc-alkaline, high-Mg		
			438.4 ± 2.2		Metamorphic zircon		
		Dacite (7)	457 ± 2.6		Medium K peraluminous, calc-alkaline, adakite		
		Albitite (7)	425.3 ± 2.2		Boninite		
Ondor Sum	Melange	Blueschist	446 ± 15 & 426 ± 15	Glaucophane $^{40}Ar/^{39}Ar$		Tang, (1992); Zhang and Liou, (1987)	
		Quartzite mylonite (8)	453.2 ± 1.8 &449.4 ± 1.8	Phengite $^{40}Ar/^{39}Ar$		De Jong et al. (2006)	

were conducted on an Agilent 7500a ICP-MS equipped with a 193 nm laser in China University of Geosciences, Beijing. Laser spot size was set to ~36 μm for analyses, laser energy density at 8.5 J/cm^2 and repetition rate at 10 Hz. Isotopic ratios and element concentrations of zircons were calculated using GLITTER (ver. 4.4, Macquarie University). Concordia ages and diagrams were obtained using Isoplot/Ex (3.0, Ludwig, 2003). The common lead was corrected using LA-ICP-MS Common Lead Correction (ver. 3.15), following the method of Andersen (2002). The summarized age data and our new measured isotopic data are given in Tables 1 and 2.

An acidic volcanite block (Sample 090716-29; located at 42°59′24″N, 109°55′20″E) embedded in the Hongqi mélange was dated. In thin section, the sample shows a mylonitic texture, with feldspar clasts surrounded by elongated recrystallized subgrain quartz aggregates. Most of the zircon grains from the acidic volcanite (090716-29) are weakly luminescent, and surrounded by a thin bright luminescent rim (Fig. 11A). Some analyzed spots have low Th/U ratios, generally close to 0.1. A few U-Pb isotopic compositions are discordant (Table 2), probably due to Pb loss during shearing in the mélange. 14 of 20 analyzed spots plot slightly on the right side of the Concordia curve, and define three populations around ca. 560–590 Ma, ca. 510–540 Ma, and 485 ± 14 Ma (n = 4; Fig. 11B).

Our analysis paid much attention to detect youngest ages of the volcanite, thus spots focus on zircon rim. The low Th/U (<0.1) ratio, a common geochemical feature of high-grade metamorphic zircons (Williams et al., 1996), are present in both younger and older populations (Table 2). It is worth noting that no distinct high-grade metamorphic minerals are observed in thin section. Globally, the mélange unit experienced a green schist facies metamorphism. Therefore, we consider that these zircons are magmatic ones possibly slightly suffering metamorphism. The youngest population at 485 ± 14 Ma represents the age of the acidic volcanism.

6. Discussion

6.1. Deformation comparison between the Hongqi and Ondor Sum areas

During our field work, we did not find HP rocks, all the microstructures described in this paper are coeval with a greenschist facies metamorphism. The three phases of deformation of the Ondor Sum mélange can be roughly compared with those of the Hongqi mélange as follows: (1) the main event, D_1, is responsible for the development of the S_1 foliation, NW–SE striking stretching lineation (L_1), and intrafolial folds (F_1) with axes parallel to L_1. In the Hongqi area, D_1 is coeval with a green schist facies metamorphism whereas, in the Ondor Sum area blue schist facies relicts, such as glaucophane, phengite are locally preserved (Tang and Yan, 1993; De Jong et al., 2006). Our kinematic observations show a top-to-the-NW sense of shear in both study areas. F_1 folds corresponding to a-type folds formed during the ductile shearing in the Hongqi area. The D_1 structural elements are subsequently deformed by the D_2 event represented dominantly by numerous NW-verging asymmetric folds associated with an axial-planar crenulation cleavage (S_2). Due to the subsequent deformation (D_3), S_2 dips to either the SE or the NW in the Ondor Sum area whereas, dips to the NE or the SW in the Hongqi area. The blueschist and quartz mylonites with age ranging from 453 to 426 Ma (Tang and Yan, 1993; De Jong et al., 2006) recorded the Ondor Sum subduction event. In the Hongqi area, the deformed Late Silurian fossiliferous limestone blocks mark the youngest age of the Hongqi mélange.

6.2. Crustal scale structure framework

A N–S oriented interpretative crustal scale cross section is proposed on the basis of structural, lithological and geochronological

Table 2
ICP-MS U-Pb data for the magmatic zircons.

Spot	Concentritions (ppm)			Th/U	U-Pb isotopic ratios						Age				Conc. (%)
	Pb Total	Th	U		$^{207}Pb/^{206}Pb$	1σ	$^{207}Pb/^{235}U$	1σ	$^{206}Pb/^{238}U$	1σ	$^{207}Pb/^{206}Pb$	1σ	$^{207}Pb/^{235}U$	1σ	$^{206}Pb/^{238}U$	1σ	
71629–01	59	38	529	0.07	0.1059	0.0033	1.4147	0.0442	0.0969	0.0014	809	121	618	25	567	8	8.99
71629–02	57	95	499	0.19	0.1270	0.0037	1.5821	0.0468	0.0904	0.0012	752	157	560	30	514	7	8.95
71629–03	53	39	495	0.08	0.0880	0.0029	1.1695	0.0387	0.0964	0.0014	580	120	574	23	572	8	0.35
71629–04	191	80	1019	0.08	0.2262	0.0065	3.7293	0.1094	0.1196	0.0016	691	357	604	71	581	10	3.96
71629–05	75	45	692	0.06	0.1329	0.0040	1.5750	0.0475	0.0860	0.0012	633	179	511	32	484	7	5.58
71629–06	102	50	1040	0.05	0.0933	0.0028	1.1237	0.0343	0.0874	0.0012	539	121	521	21	517	7	0.77
71629–07	42	29	374	0.08	0.1025	0.0034	1.3818	0.0457	0.0978	0.0014	600	143	576	27	570	8	1.05
71629–08	72	52	710	0.07	0.1143	0.0035	1.3358	0.0417	0.0847	0.0012	642	150	517	27	490	7	5.51
71629–09	39	77	404	0.19	0.0914	0.0029	1.0666	0.0347	0.0846	0.0012	798	110	563	21	507	7	11.05
71629–10	124	276	1571	0.18	0.0623	0.0019	0.6582	0.0208	0.0766	0.0011	685	44	514	13	476	6	7.98
71629–11	68	43	490	0.09	0.1701	0.0053	2.3634	0.0743	0.1008	0.0014	791	233	589	47	538	8	9.48
71629–12	77	27	466	0.06	0.2167	0.0067	3.2237	0.1013	0.1079	0.0015	744	340	577	66	535	9	7.85
71629–13	56	56	528	0.11	0.0818	0.0027	1.1007	0.0367	0.0976	0.0014	829	94	641	20	589	8	8.83
71629–14	70	57	814	0.07	0.0700	0.0023	0.7880	0.0262	0.0817	0.0012	595	91	517	16	500	7	3.40
71629–15	718	36	697	0.05	0.6918	0.0208	31.5738	0.9684	0.3310	0.0046	2385		922	469	435	41	111.95
71629–16	23	18	213	0.08	0.0888	0.0033	1.1858	0.0439	0.0969	0.0015	721	122	608	25	577	8	5.37
71629–17	154	13	371	0.03	0.4824	0.0148	11.4598	0.3589	0.1723	0.0024	1400	965	703	214	505	17	39.21
71629–18	44	77	399	0.19	0.1242	0.0040	1.5163	0.0498	0.0886	0.0012	880	150	582	30	509	7	14.34
71629–19	424	93	756	0.12	0.5644	0.0175	16.2019	0.5107	0.2082	0.0029	1720	1189	765	285	480	23	59.38
71629–20	162	105	552	0.19	0.3944	0.0123	7.4780	0.2372	0.1375	0.0019	1311	639	676	145	501	13	34.93

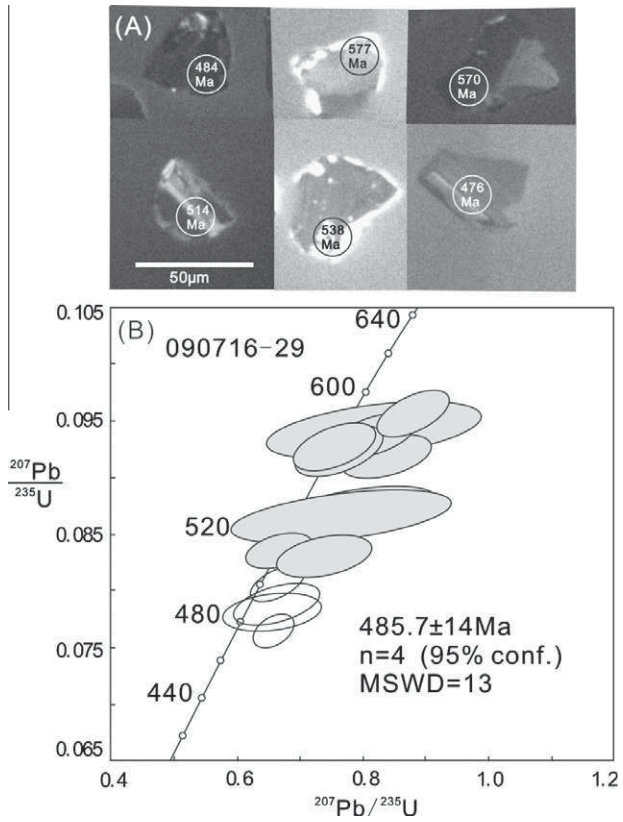

Fig. 11. (A) Representative CL image of dated zircons. (B) U-Pb Concordia diagrams for sample 090716-29 of acidic volcanite (The data ellipses are defined by standard errors (1 sigma) in $^{206}Pb/^{238}U$, $^{207}Pb/^{235}U$ and $^{207}Pb/^{206}Pb$. Gray ellipses represent inherited zircons. The data with age concordance >10% are not projected in the concordia diagram.

data presented above (Fig. 12). The Early Paleozoic Hongqi mélange belt, is unconformably overlain by the Early Devonian red sandstone and Late Carboniferous limestone.

The mélange belt displays a top-to-the-NW thrusting, indicating a southeastern oceanic subduction. The volcanic rocks exposed in the Bater Obo area are comparable with the rocks in the Bainaimiao area. The mafic plutonic rocks exposed in the Tulinkai unit might represent the deep plutonic part of the Bainaimiao arc. The age of the volcanite block dated in the Hongqi mélange, similar to those of the Bainaimiao arc suggest that the magmatic blocks in the mélange might derive from the arc rocks of the upper plate.

At depth, a possible crustal basement is inferred here on the basis of the following points. Firstly, in order to terminate the oceanic subduction before Early Devonian, some buoyant material, such as huge seamount, large oceanic plateau, or microcontinent, underneath the Hongqi mélange, is needed. The collision of this feature will allow the oceanic subduction and the coeval arc magmatism to stop. Secondly, Precambrian crystalline basement rocks are recognized, in the Hutag Uul terrane (Badarch et al., 2002), Totoshan Ulanul block (Yarmolyuk et al., 2005; Demoux et al., 2009), Tsagan Khairkhan massif (Wang et al., 2001) and Hunshandake microcontinent (Xu et al., 2012). Precambrian middle to high grade metamorphic paragneiss are also recognized in the north of the Ondor Sum, near Sunityouqi (Fig. 1; BGMRIM, 1991; Hsü et al., 1991; Li and Gao, 1995; Zhang et al., 1999) or in the Xilingele (or Xinlin Gol) complex near Xilinhot (Zhu et al., 2004). Though an oblique subduction of the underlying plate, accommodated by strike-slip faulting can be proposed to terminate a subduction (Choulet et al., 2012), in the study area, no strike-slip fault of Early Paleozoic age, and associated ductile deformation are observed. Therefore, we argue that the structural features presented above, and particularly the syn-metamorphic ductile shearing can be explained by the subduction of a microcontinent below the North China block.

6.3. A possible geodynamic evolution model

On the basis of our geological data presented in the previous sections, a possible Early Paleozoic geodynamic scenario for the evolution of the eastern part of the CAOB in Inner Mongolia is proposed here.

6.3.1. The Ordovician to Silurian Subduction

An Early Paleozoic SE-dipping Paleo-Asian Ocean subduction zone developed along the northern margin of North China Craton from the Hongqi to the Ondor Sum area. It is supported by the consistent top-to-the-NW sense of shear indicators. This oceanic subduction gave rise to the Bainaimiao magmatic arc, and the Hongqi and Ondor Sum mélange units (Fig. 13A). Both the Hongqi and the Ondor Sum areas experienced two ductile deformation phases before the Early Devonian. Moreover, the north dipping schists at the

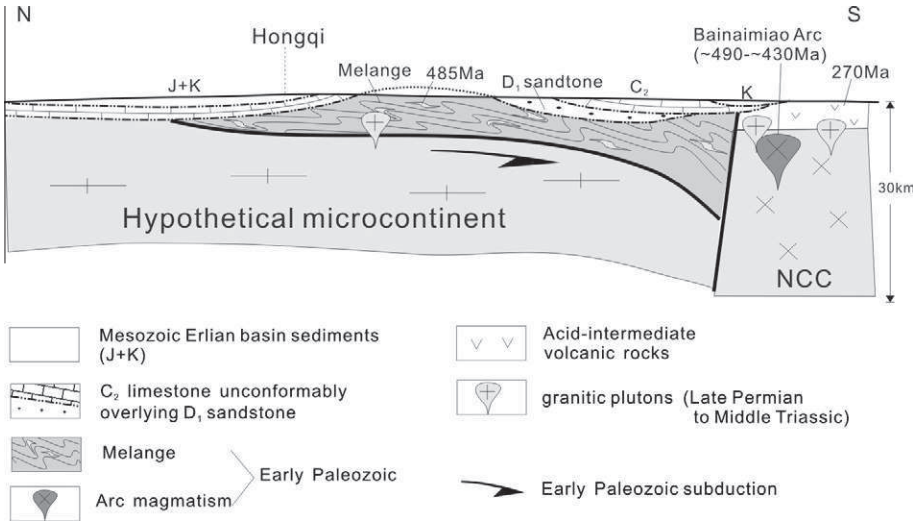

Fig. 12. Interpretative crustal scale cross section of the Southern Orogen of Inner Mongolia, showing the Early Paleozoic accretion–collision belt. The position of this cross section is shown in Figs. 1 and 2.

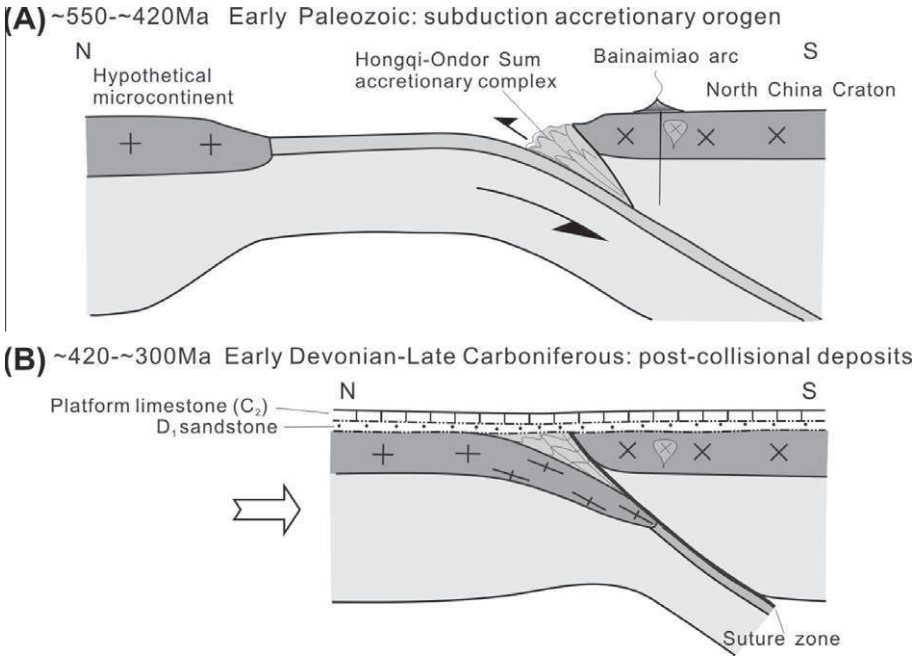

Fig. 13. Tentative Paleozoic geodynamic evolution model of the southern belt of Inner Mongolia (see text for detail).

Ulan valley, which constitute the northern limb of the antiform, show a top-to-the NW sense of shear that is unconsistent with a Precambrian northward subduction.

6.3.2. The late Silurian collision

The collision likely occurred in Late Silurian, since the Early Devonian red sandstones unconformably cover the Hongqi mélange. Moreover, the basal conglomerates of the Early Devonian sediments contain pebbles of the underlying litho-tectonic units. Accretionary tectonics and magmatism must have been stopped at that time. This scenario is supported by the undeformed pegmatite of 411 ± 8 Ma that cuts the low P/T metamorphic complex in the Bainaimiao area (Zhang et al., 2012), and the ca. 417 Ma tonalite interpreted as due to collision magmatism near the Hongqi area (Jian et al., 2008). Subsequently, a Late Carboniferous platform limestone developed in a vast area, extending throughout the eastern part of Inner Mongolia (BGMRIM, 1991). In our study area, the most likely is that a microcontinent, entered in the trench and collided with the Andean active margin of the North China Craton (Fig. 13B). This hypothetical microcontinent might be connected with the South Gobi microcontinent (Sengor and Natal'in, 1996) or the Hunshandake block (Xu et al., 2012). But, the size and distribution of this hypothetic microcontinent are not documented yet, and the correlations with other microcontinental blocks between North China Craton and Siberia remains hypothetic.

7. Conclusion

(i) The mélange belt exposed in the Hongqi and Ondor Sum areas, is characterized by two phrases of ductile deformation and a top-to-the-NW sense of shear, suggesting a southeastward subduction during the Early Paleozoic.

(ii) The ductile deformations in the Ondor Sum-Hongqi mélange belt are coeval with greenschist facies metamorphism. The unconformably overlying Early Devonian sedimentary rocks indicate that subduction and collision should terminate before the Early Devonian.

(iii) In the present knowledge, the South-directed of a microcontinent below the North China Craton appears as the most likely geodynamic scenario to account for the structural evolution.

Acknowledgements

This work has been funded by the National Key Basic Research Program of China (2013CB429800) and the National Science Foundation of China (40872145 and 41121062). The China Scholarship Council is acknowledged for providing a Ph.D. scholarship to G.Z. Shi, supporting a joint training Ph.D. program between the Université d'Orléans and Peking University. We gratefully acknowledge constructive reviews from Xiao Wenjiao and Boris A. Natal'in. Flavien Choulet is thanked for useful suggestions to improve a first draft of the manuscript. Tong Qilong, Li Ruibiao, Fang Junqin and Cheng Shengdong are thanked for their help in the field work. This is a contribution to IGCP#592 supported by UNESCO-IUGS.

References

Andersen, T., 2002. Correction of common lead in U-Pb analyses that do not report ^{204}Pb. Chemical Geology 192, 59–79.

Badarch, G., Cunningham, W.D., Windley, B.F., 2002. A new terrane subdivision for Mongolia: implications for the Phanerozoic crustal growth of Central Asia. Journal of Asian Earth Sciences 21, 87–104.

BGMRIM, 1980. Regional Geological Investigation Report of 1:200000 scale Naomugen Quadrangle. Inner Mongolian Bureau of Geology and Mineral Resources.

BGMRIM (Bureau of Geology and Mineral Resources of Inner Mongolia), 1991. Regional Geology of NeiMongol (Inner Mongolia) Autonomous Region. Geological Publishing House, Beijing (in Chinese with English summary).

Cawood, P., Kröner, A., Collins, W.J., Kusky, T., Mooney, W.D., Windley, B.F., 2009. Accretionary orogens through Earth history. In: Cawood, P., Kröner, A. (Eds.), Earth Accretionary Systems in Space and Time, vol. 318. Geological Society Special Publication, pp. 1–36.

Chen, B., Jahn, B.M., Tian, W., 2009. Evolution of the Solonker suture zone: constrains from zircon U-Pb ages, Hf isotopic ratios and whole-rock Nd–Sr isotope compositions of subduction and collision-related magmas and forearc sediments. Journal of Asian Earth Sciences 34, 245–257.

Chen, C., 2011. Geochronology, Geochemistry, and its Geological Significance of the Early Permian Volcanic Rocks in Damaoqi, Inner Mongolia. Master degree thesis, Peking University. 50 pp.

Choulet, F., Faure, M., Cluzel, D., Chen, Y., Wei, L., Wang, B., 2012. From oblique accretion to transpression in the evolution of the Altaid collage. Gondwana Research 21, 530–548.
Condie, K.C., 2007. Accretionary orogens in space and time. In: Hatcher, R.D., Jr., Carlson, M.P., Mc Bride, J.H., Martinez-Catalan, J.R. (Eds.), 4D Framework of the Continental Crust, vol. 200. Geological Society of America Memoir, pp. 154–158.
De Jong, K., Xiao, W.J., Windley, B.F., Masago, H., Lo, C.H., 2006. Ordovician $^{40}Ar/^{39}Ar$ phengite ages from the blueschist-facies Ondor Sum subduction-accretion complex (Inner Mongolia) and implications for the early Paleozoic history of continental blocks in China and adjacent areas. American journal of Science 306, 799–845. http://dx.doi.org/10(2475/10), 2006, 02.
Demoux, A., Kröner, A., Liu, D.Y., 2009. Precambrian crystalline basement in southern Mongolia as revealed by SHRIMP zircon dating. International Journal of Earth Sciences (Geol Rundsch) 98, 1365–1380. http://dx.doi.org/10.1007/s0051-008-0321-4.
Faure, M., Trap, P., Lin, W., Monié, P., Bruguier, O., 2007. Polyorogenic evolution of the Paleoproterozoic Trans-North China Belt, new insights from the in Lüliangshan–Hengshan–Wutaishan and Fuping massifs. Episodes 30, 96–107.
Hsü, K.J., Wang, Q., Li, J., Hao, J., 1991. Geologic evolution of the Neimonides: a working hypothesis. Eclogae Geologicae Helvetiae 84, 1–31.
Hu, X., Xu, C.S., Niu, S.Y., 1990. Evolution of the Early Paleozoic Continental Margin in Northern Margin of the North China Platform. Peking University Publish House, Beijing (in Chinese with English abstract).
Huang, J.X., Zhao, Z.D., Zhang, H.F., Hou, Q.Y., Chen, Y.L., Zhang, B.R., Depaolo, D.J., 2006. Elemental and Sr–Nd–Pb isotopic geochemistry of the Wenduermiao and Bayanaobao-Jiaoqier ophiolites, Inner Mongolia: constraints for the characteristics of the mantle domain of eastern Paleo-Asian Ocean. Acta Petrologica Sinica 22, 2889–2900.
IMBGMR, 1976. Regional Geological Investigation Report of 1:200000 scale Xianghuangqi Quadrangle. Inner Mongolian Bureau of Geology and Mineral Resources.
IMBGMR, 2002. Regional Geological Investigation Report of 1:250000 scale BaiyunObo Quadrangle. Inner Mongolian Bureau of Geology and Mineral Resources.
IMBGMR, 2008. Regional Geological Investigation Report of 1:50000 scale Wulanbulage Quadrangle. Inner Mongolian Bureau of Geology and Mineral Resources.
Jahn, B.M., 2004. The Central Asian Orogenic Belt and growth of the continental crust in the Phanerozoic. In: Malpas, J., Fletcher, C.J.N., Ali, J.R., Aitchinson, J.C. (Eds.), Aspects of the Tectonic Evolution of China. Geological Society, London, pp. 3–100.
Jia, H.Y., Baoyin, W.L.J., Zhang, Y.Q., 2003. Characteristics and tectonic significance of the Wude suture zone in northern Damaoqi, Inner Mongolia. Journal of Chengdu University of Technology (Science & Technology edition) 30, 30–34 (in Chinese with English abstract).
Jian, P., Liu, D.Y., Kröner, A., Windley, B.F., Shi, Y.R., Zhang, F.Q., Shi, G.H., Miao, L.C., Zhang, W., Zhang, Q., Zhang, L.Q., Ren, J.S., 2008. Time scale of an early to mid-Paleozoic orogenic cycle of the long-lived Central Asian Orogenic Belt, Inner Mongolia of China: implications for continental growth. Lithos 101, 233–259.
Jian, P., Liu, D.Y., Kroner, A., Windley, B.F., Shi, Y.R., Zhang, W., Zhang, F.Q., Miao, L.C., Zhang, L.Q., Tomurhuu, D., 2010. Evolution of a Permian intraoceanic arc–trench system in the Solonker suture zone, Central Asian Orogenic Belt, China and Mongolia. Lithos 118, 169–190.
Kusky, T.M., Windley, B., Zhai, M., 2007. Tectonic evolution of the North China Block: from orogen to craton to orogen. In: Zhai, M., Windley, B., Kusky, T., Meng, Q. (Eds.), Mesozoic Sub-Continental Lithospheric Thinning Under Eastern Asia, vol. 280. Geological Society Special Publications, London.
Kusky, T.M., Li, J.H., 2003. Paleoproterozoic tectonic evolution of the North China Craton. Journal of Asian Earth Science 22, 383–397.
Li, J.F., Zhang, Z.C., Han, B.F., 2010. Ar–Ar and zircon SHRIMP geochronology of hornblendite and diorite in northern Darhan Muminggan Joint Banner, Inner Mongolia, and its geological significance. Acta Petrologica et Mineralogica 29, 732–740 (in Chinese with English abstract).
Li, S.J., Gao, D.Z., 1995. New discovery of geological structures in Sonid Zuoqi of Inner Mongolia and discussion on tectonic features. Journal of Graduate School, China University of Geosciences 9, 130–141 (in Chinese with English abstract).
Liu, D.Y., Jian, P., Zhang, Q., Zhang, F.Q., Shi, Y.R., Shi, G.H., Zhang, L.Q., Tao, H., 2003. SHRIMP dating of Adakites in the Tulingkai Ophiolite, Inner Mongolia: evidence for the Early Paleozoic subduction. Acta Geologica Sinica 77, 317–327 (in Chinese with English abstract).
Ludwig, K.R., 2003. User's Manual for Isoplot 3.0: A Geochronological Toolkit for Microsoft Excel Berkeley Geochronology Center, vol.4. Special Publication, pp. 1–71.
Meng, Q.R., 2003. What drove late Mesozoic extension of the northern China – Mongolia tract? Tectonophysics 369, 155–174.
Miao, L.C., Zhang, F.Q., Fan, W.M., Liu, D.Y., 2007. Phanerozoic evolution of the Inner Mongolia–Daxinganling orogenic belt in North China: constraints from geochronology of ophiolites and associated formations. In: Zhai, M.G., Windley, B.F., Kusky, T.M., Meng, Q.R. (Eds.), Mesozoic Sub-Continental Lithospheric Thinning Under Eastern Asia, vol. 280. Geological Society Special Publication, London, pp. 223–237.
Nie, F.J., Bjørlykke, A., 1999. Nd and Sr isotope constraints on the age and origin of Proterozoic meta-mafic volcanic rocks in the Bainaimiao–Wenduermiao district, south-central Inner Mongolia, China. Continental Dynamics 4, 1–14.
Sengor, A.M.C., Natal'in, B.A., Burtman, V.S., 1993. Evolution of the Altaid tectonic collage and Paleozoic crustal growth in Eurasia. Nature 364, 299–307.
Sengor, A.M.C., Natal'in, B.A., 1996. Paleotectonics of Asia: fragments of a synthesism. In: Yin, A., Harrison, T.M. (Eds.), The Tectonic Evolution of Asia. Cambridge University Press, New York, pp. 486–640.
Shao, J.A., 1991. Crustal Evolution in the Middle Part of the Northern Margin of the Sino-Korean Plate. Peking University Publish House, Beijing (in Chinese with English abstract).
Tang, K., 1990. Tectonic development of Paleozoic fold belts at the north margin of the Sino-Korean craton. Tectonics 9, 249–260.
Tang, K.D., 1992. Tectonic evolution and minerogenetic regularities of the fold belt along the northern margin of sino-korean plate. Peking University Publishing House, Beijing (in Chinese with English abstract).
Tang, K.D., Yan, Z.Y., 1993. Regional metamorphism and tectonic evolution of the Inner Mongolian suture zone. Journal of Metamorphic Geology 11, 511–522.
Trap, P., Faure, M., Lin, W., Monié, P., 2007. Late Palaeoproterozoic (1900–1800Ma) nappe stacking and polyphase deformation in the Hengshan–Wutaishan area: implication for the understanding of the Trans-North China Belt, North China Craton. Precambrian Research 156, 85–106.
Trap, P., Faure, M., Lin, W., Le Breton, N., Monié, P., 2012. Paleoproterozoic tectonic evolution of the Trans-North China Orogen: Toward a comprehensive model. Precambrian Research 222–223, 450–473.
Wang, Q., Liu, X.Y., 1986. Paleoplate tectonics between Cathaysia and Angaraland in Inner Mongolia of China. Tectonics 5, 1073–1088.
Wang, T., Zheng, Y.D., Gehrels, G.E., Mu, Z.G., 2001. Geochronological evidence for existence of South Mongolian microcontinent zircon U-Pb age of grantoid gneisses from the Yagan-Onch Hayrhan metamorphic core complex. Chinese Science Bulletin 46, 2005–2008.
Williams, I.S., Buick, I.S., Cartwright, I., 1996. An extended episode of early Mesoproterozoic metamorphic fluid flow in the Reynolds Range, central Australia. Journal of Metamorphic Geology 14, 29–47.
Windley, B.F., Alexeiev, D., Xiao, W.J., Kröner, A., Badarch, G., 2007. Tectonic models for accretion of the Central Asian Orogenic Belt. Journal of the Geological Society, London 164, 31–47.
Xiao, W.J., Windley, B.F., Hao, J., Zhai, M., 2003. Accretion leading to collision and the Permian Solonker suture, Inner Mongilia, China: termination of the Central Asian Orogenic Belt. Tectonics 22, 1069. http://dx.doi.org/10.1029/2002TC001484.
Xiao, W.J., Han, C., Yuan, C., Sun, M., Lin, S., Chen, H., Li, Z., Li, J., Sun, S., 2008. Middle Cambrian to Permian subduction-related accretionary orogenesis of northern Xinjiang, NW China: implications for the tectonic evolution of central Asia. Journal of Asian Earth Sciences 32, 102–117.
Xu, B., Charvet, J., Chen, Y., Zhao, P., Shi, G.Z., 2012. Middle Paleozoic convergent orogenic belts in western Inner Mongolia (China): framework, kinematics, geochronology and implications for tectonic evolution of the Central Asian Orogenic Belt. Gondwana Research. http://dx.doi.org/10.1016/j.gr.2012.05.015.
Xu, B., Chen, B., 1993. The opposite subduction and collision between the Siberian and Sino-Korean plates during the early-middle Paleozoic. Report No: 4 of the IGCP Projrct 283: Geodynamic Evolution of Paleoasian Ocean, Novosibirsk, USSR, pp. 148–150.
Xu, B., Chen, B., 1997. Framework and evolution of the middle Paleozoic orogenic belt between Siberian and North China Plates in northern Inner Mongolia. Science in China (Series D) 40, 463–469.
Xu, B., Charvet, J., Zhang, F.Q., 2001. Primary study on petrology and geochronology of the blueschist in Sonid Zuoqi, northern Inner Mongolia. Chinese Journal of Geology 36, 424–434 (in Chinese with English abstract).
Xu, L.Q., Tao, J.X., 2003. Characteristics and tectonic signification of Ordovician granites in northern Damao, Inner Mongolia. Geology and Mineral Resources of South China 01, 17–22 (in Chinese with English abstract).
Yan, Z.Y., Tang, K.D., Bai, J.W., Mo, Y.C., 1989. High pressure metamorphic rocks and their tectonic environment in northeastern China. Journal of South East Asian Earth Sciences 3, 303–313.
Yarmolyuk, V.V., Kovalenko, V.I., Salnikova, E.B., Kozakov, I.K., Kotov, A.B., Kovach, V.P., Vladykin, N.V., Yakovleva, S.Z., 2005. U–Pb age of syn- and post-metamorphic granitoids of south Mongolia: evidence for the presence of Grenvillides in the Central Asian Foldbelt. Doklady Earth Sciences 404, 986–990.
Zhai, M.G., Li, T.S., Peng, P., Hu, B., Liu, F., Zhang, Y.B., 2010. Precambrian key tectonic events and evolution of the North China Craton. In: Kusky, T.M., Zhai, M.G., Xiao, W.J. (Eds.), The Evolving Continents: Understanding Processes of Continental Growth, vol. 338. Geological Society Special Publication, London, pp. 235–262.
Zhang, H.T., So, C.S., Yun, S.T., 1999. Regional geologic setting and metallogenesis of central Inner Mongolia, China: guides for exploration of mesothermal gold deposits. Ore Geology Reviews 14, 129–146.
Zhang, Z.M., Liou J.G., 1987. The high P/T metamorphic rocks of China, in Terrane Accretion and Orogenic Belts. In: Leitch, E.C., Scheibner, E. (Eds.), Geodynamics Series, vol. 19. AGU, Washington, D.C., pp. 235–247, http://dx.doi.org/10.1029/GD019p0235.
Zhang, Y.Q., Ling, L.X., Wang, T., Xu, L.Q., 2004. Xibiehe Formation, Changanhabu Formation and unconformity between them in Wayao, northern Damao of Inner Mongolia. Geology and Mineral Resources of South China 1, 48–54 (in Chinese with English abstract).
Zhang, W., Jian, P., Kröner, A., Shi, Y.R., 2012. Magmatic and metamorphic development of an early to mid-Paleozoic continental margin arc in the southernmost Central Asian Orogenic Belt, Inner Mongolia, China. Journal of Asian Earth Sciences, http://dx.doi.org/10.1016/j.jseaes.2012.05.025.
Zhao, G.C., Sun, M., Wilde, S., 2005. Late Archean to Paleoproterozoic evolution of the North China Craton: key issues revisited. Precambrian Research 136, 177–200.

Zhao, L., Wu, T.R., Luo, H.L., He, Y.K., Jing, X., 2008. Geochemistry of Huheengeer Complex, Bayan Obo Region, Inner Mongolia and its tectonic implications. Geological Journal of China Universities 14, 29–38 (in Chinese with English abstract).

Zhu, Y.F., Sun, S.H., Mao, Q., Zhao, G., 2004. Geochemistry of the Xilingele Complex, Inner Mongolia: a historic record from Rodinia accretion to continental collision after closure of the Paleo-Asian Ocean. Geological Journal of China Universities 10, 343–355 (in Chinese with English abstract).

Late Paleozoic crustal evolution of the Mandula area, Inner Mongolia and a question to the Solonker suture

Guanzhong SHI [a,b], Bei Xu[a], Michel Faure[b], Pan Zhao[a], Yan Chen[b]

[a]Key Laboratory of Orogenic Belts and Crustal Evolution, Ministry of Education, Peking University, Beijing 100871, China

[b]Institut des Sciences de la Terre d'Orléans, UMR Université d'Orléans-INSU/CNRS 7327, 1A rue de la Férollerie, 45071 Orléans, Cedex 2, France

[*]Corresponding author E-mail address: bxu@pku.edu.cn

Abstract

In Mandula area, the Early Permian formations are represented by turbidite and olistostrome coeval with mafic and intermediate lavas. Various sizes of blocks belong to the olistostrome deposits and volcanic sills in the turbidites. A Permian "Solonker" suture was questioned since typical ultramafic rocks, pillow lavas and deep-sea radiolarian chert are absent. The sedimentary setting is continental slope with a northward deeper trend. The sources of the olistostrome and turbidite are from the southern Early Paleozoic material and contemporaneous Early Permian volcanic magmatism. Intensive NW-directed folds and thrusts deform the turbidite and olistostrome deposits. The chaotic terrigenous sedimentation and the bimodal magmatism are interpreted as formed in a limited intracontinental rift opened and closed during the Permian.

Key words: Central Asia Orogenic Belt, Late Paleozoic rifting, Solonker Suture, Inner Mongolia

1. Introduction

Central Asian Orogenic Belt (CAOB) is the largest accretionary orogen of the earth in Phanerozoic and represents the remnant of the Paleo-Asian Ocean, currently preserved as ophiolite and serpentinite melanges (Sengor et al., 1993; Sengor and Natal'in, 1996; Xiao et al., 2003, 2008; Jahn, 2004; Windley et al., 2007). The eastern segment of the CAOB, also called Manchurides (Sengor and Natal'in, 1996), is mainly exposed in Inner Mongolia. The Solonker (also called Solon Obo) suture is considered by most of geologists as the major structure that delineates the location of the Paleo-Asian Ocean (Xiao et al., 2003; Windly et al., 2007; Chen et al., 2009; Jian et al., 2010). However, the Solonker mélange rocks are questioned since an Early Paleozoic double-direction subduction model was proposed (Xu and Chen, 1993; 1997; Xu and Charvet, 2010, 2011; Xu et al., 2012). Xu et al., (2012) suggested that during early Paleozoic, a south-directed oceanic subduction below the North China

Craton coeval with a north-directed oceanic subduction. Finally, the two opposite subduction systems came into contact with a microcontinent around 420-380Ma. Although it is hotly debated, the detail lithological composition, spatial and temporal distribution and genetics of the disordered rocks along the Solonker zone are few documented.

This paper deals with the western part of the Solonker suture in the Mandula area. The Mandula study area lies within Solonker suture zone. The previous studies in the Mandula area proposed a Permian tectonic mélange for a clastic deposits and disorder deposits, namely "argillaceous mélange" and "limestone mélange" respectively (Jian, 2010). The bearing radiolarian chert is also reported as the blocks within mélange (Wang et al., 2005). In the following, three main questions will be addressed, namely: i) what is the lithological composition and distribution in the Mandula area, ii) what is the bulk geometry and kinematics deduced from microtectonic analysis of the rocks and what is the timing of the deformation, and iii) what is the significance of the "Solonker suture" area in the geodynamic evolution of the eastern part of the CAOB.

2. Regional Geological Framework

The litho-tectonic units namely, from south to north, the North China Craton (NCC), the Southern orogenic Belt(SOB), the Northern orogenic Belt(NOB), the South Mongolia microcontinent (SMM), the Hunshandake block (HB) and the Southern Margin of the Ergun block (SME) (Fig.1; Xu et al., 2012). Here we focus on three main litho-tectonic units correlative to the Mandula area.

2.1 The SOB

The SOB crops out to the south of the Mandula area. It refers to an Early Paleozoic orogenic belt composed of the Ondor Sum subduction complex and the Bainaimiao arc belt (Xiao et al., 2003; Jian et al., 2008; Xu et al, 2012). The Ondor Sum subduction complex in the Hongqi area consists of tuffaceous siltstone, sericite chlorite schist, chlorite quartz schist, calc-slate, chert and a small amount of greywacke. It contains various sizes of blocks of amphibolite, pillow basalt, volcanic rocks, limestone and chert (our other paper). The Bainaimiao arc is dominated by granitic plutons of ca.440-480Ma cropping out to the east of the Hongqi area. The Early Devonian shallow water sandstones and the Early Carboniferous limestone rocks unconformably cover the SOB, suggesting the subduction and collision end before Early Devonian (our other paper).

2.2 The SMM

The SMM lies to the north of the Mandula area, it is considered as a potential microcontinent that collided with the NCC during the Early Paleozoic (Xu et al., 2012). This microcontinent is similar to the Hutag Uul block (Badarch et al., 2002), Totoshan Ulanul block (Demoux, et al., 2009) and Tsagan Khairkhan massif (Wang et al., 2001) in southwestern Mongolia. It is dominated by quartz rich micaschist, meta-volcanic rocks, meta-sandstone and marble (BGMRED, 1991). The Totoshan Ulanul Block contains metamorphic rocks dated at 952±8Ma (single zircon U/Pb;

Yarmolyuk et al. 2005; Demoux, et al., 2009), Tsagan Khairkhan massif with age of 916±16Ma (Wang et al., 2001). The Hunshandake Block was deduced from the scattered outcrops of metamorphic rocks (Xu et al., 2012).

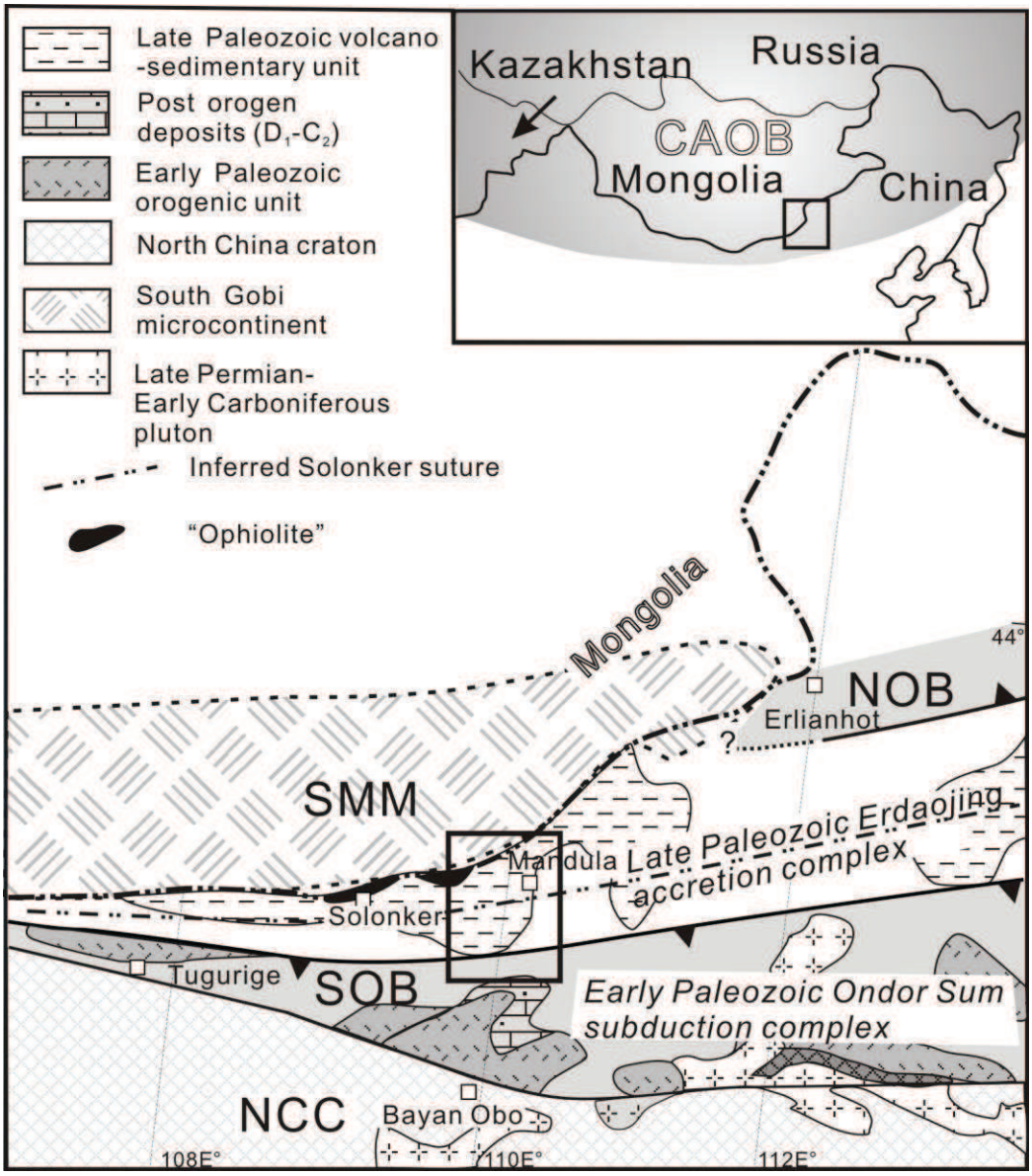

Fig.1 Tectonic sketch map of central Inner Mongolia modified from Xiao et al., (2003) and Xu et al., (2012). The late Mesozoic-Cenozoic formations are omitted for clarity.

2.3 The "Solonker suture"

The Solonker suture is widely regarded as the suture zone between NCC and South Mongolia (Sengor et al., 1993; Sengor and Natal'in, 1996; Xiao et al., 2003; Jian et al., 2010). In the western part (i.e. Solonker area) of the suture, the ophiolite, associated with Lower Permian sedimentary rocks, consists of harzburgite, dunite, gabbro, pillow basalt and chert (Wang and Liu, 1986). Extending to the east, the Erdaojing complex is regarded as an accretionary wedge (Xiao et al., 2003). It consists of two types of mélange, namely a tectonic mélange and an olistostrome (Tang, 1990; Xiao et al., 2003). The tectonic mélange forms the structurally lower unit

of the Erdaojing complex. It is characterized by lenses of mafic-ultramafic rocks within an argillite matrix. The olistostrome is in fault contact with the southern tectonic mélange unit. It consists of coherent turbidites including blocks of ophiolitic rocks, chert, marbles and arc volcanic rocks. A few Tabulata fossils found within a limestone lens indicate a Silurian age (Wang and Liu, 1986; Tang, 1990). In the eastern end of the Solonker suture (out of Fig.1), cumulate gabbro, dykes, pillow spilite, and quartz keratophyre with a whole rock Rb-Sr isochron age of 262Ma have been described to crop out in Lower Permian clastic sediments (Wang and Liu, 1986).

3. **The litho-tectonic units of the Mandula area**

The Mandula area is located to the north of the Bainaimiao arc unit (Fig. 2). To the north, it extends up to the Mongolian border. To the south, it is covered by Mesozoic Erlian basin (Fig. 2). The Mandula area consists of five lithological and tectonic units, namely: olistostrome, turbidites, shallow water sedimentary rocks, Early Permian volcanics and Solonker mafic rocks (Fig. 10).

3.1 The olistostrome unit

Reefal limestone and terrigenous rocks, named the Benbatu formation (IMBGMR, 2004), characterize the olistostrome unit. This unit is also referred to as the "Mandula forearc mélange" (Jian et al., 2010). Indeed, the limestones are olistoliths, rotated in various directions with disorganized bedding, enclosed within a terrigenous matrix. The blocks, with sizes ranging from the centimetre to kilometre scale, consist of biohermal limestone, siliceous mudstone, volcanic rocks and coarse-grained sandstone (Figs. 3A-F). Plurimeter-scale limestone blocks may appear as continuous at outcrop scale, but are discontinuous and scattered at the regional scale (Fig. 3A). Huge limestone hills are commonly floating both on the demi-continuous and mixed matrix showing well-preserved bedding. It is worth to note that the limestone is petrologically and palaeontologically similar to the Late Carboniferous limestone exposed in the southern part of the study area (Amushan Formation), near Hongqi (Fig. 2), indicating a possible source for these olistoliths. In places, siliceous mudstone blocks derived from the underlying mudstone occur in a sandstone matrix (Fig.3B). Some of these siliceous rocks contain radiolarian fossils (Wang et al., 2005). Rare acidic volcanic rocks are also included in the coarse sandstone matrix (Fig.3C). Globally, the amount and size of blocks decrease northwards. Pebbly mudstone becomes dominant northwardly. There is a gradual changing in the matrix: to the southern most and west part of the olistostrome unit, the matrix mostly consisting of grey white and pink argentite displays like pinch-and-swell structure showing demi-continuous of primal bedding (Fig.3D). To the Northeast, the matrix is dominated by dark grey mixture of sandstone and mudstone and the original bedding is absent (Fig.3E).

The synsedimentary deformations are well-preserved locally. In the southern part, it is slump-related demi-continuous sandstone is common. In the centre of the olistostrome unit, the deformation is expressed as small-scale, rounded, overturned folds with a ductile appearance without axial-planar cleavage (Fig.3F). Slump folds

can be distinguished from tectonic folds by a transecting cleavage (i.e. cutting already deformed beds, and non cylindrical geometries, such as thickened hinges and curved axes). The lens of sandstone oriented with ellipsoid surface to the southwest includes in the mixed matrix. In the northern margin of the olistostrome, compressional deformation is common. The mudstone sometimes develops sigmoid structure

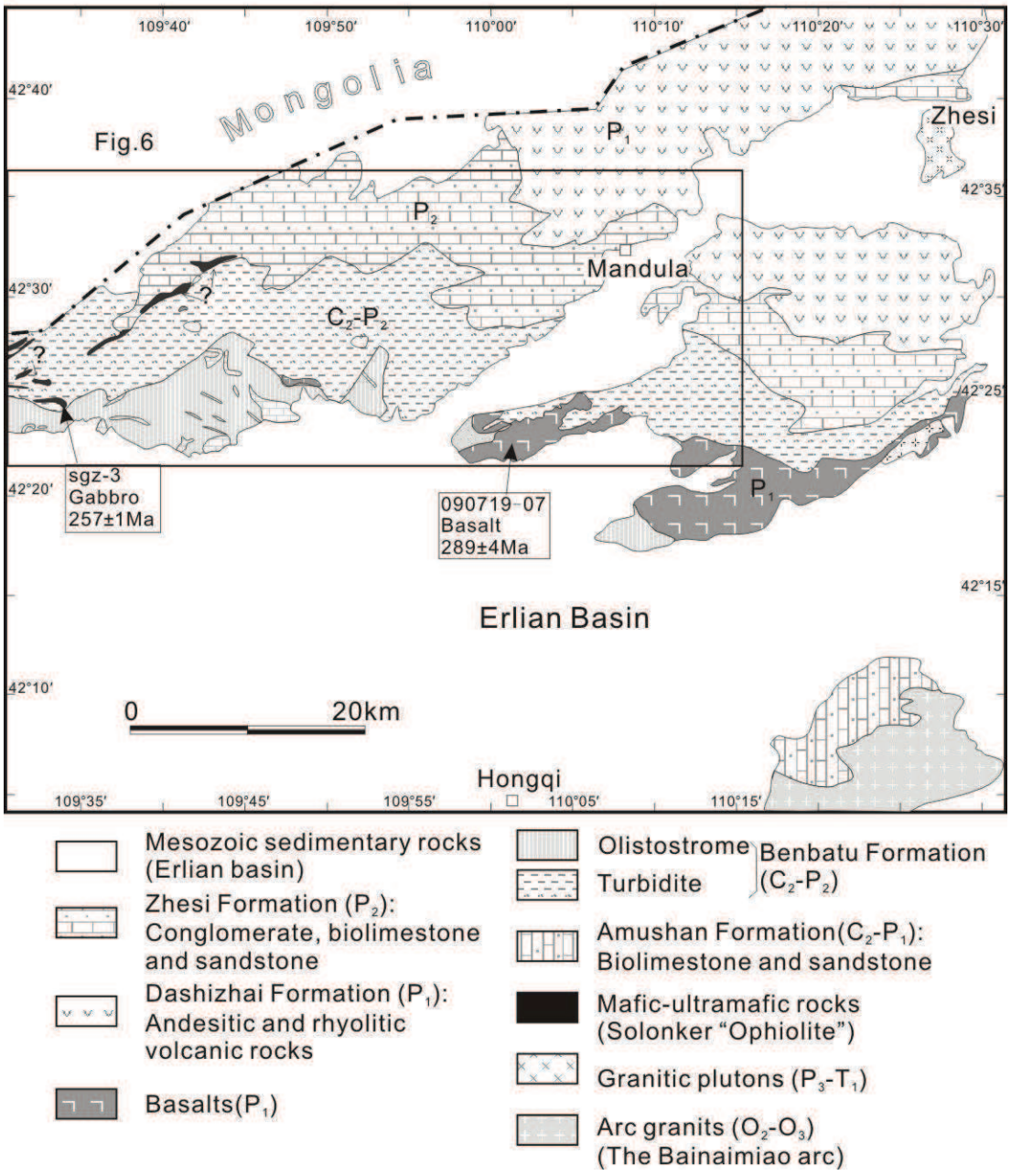

Fig.2 Geological map of the Hongqi-Mandula area in Inner Mongolia showing litho-tectonic units distribution. Modified after IMBGMR, (2002, 2004).

showing northward thrusting (Fig.3G) and sometimes strongly ductile crumpled (Fig.3H). It is worth noting that no metamorphism is observed in the field and thin section which is distinct with typical tectonic mélange. Deformation Small-scale faults with a reverse sense of movement are observed. The slide style exhibits as

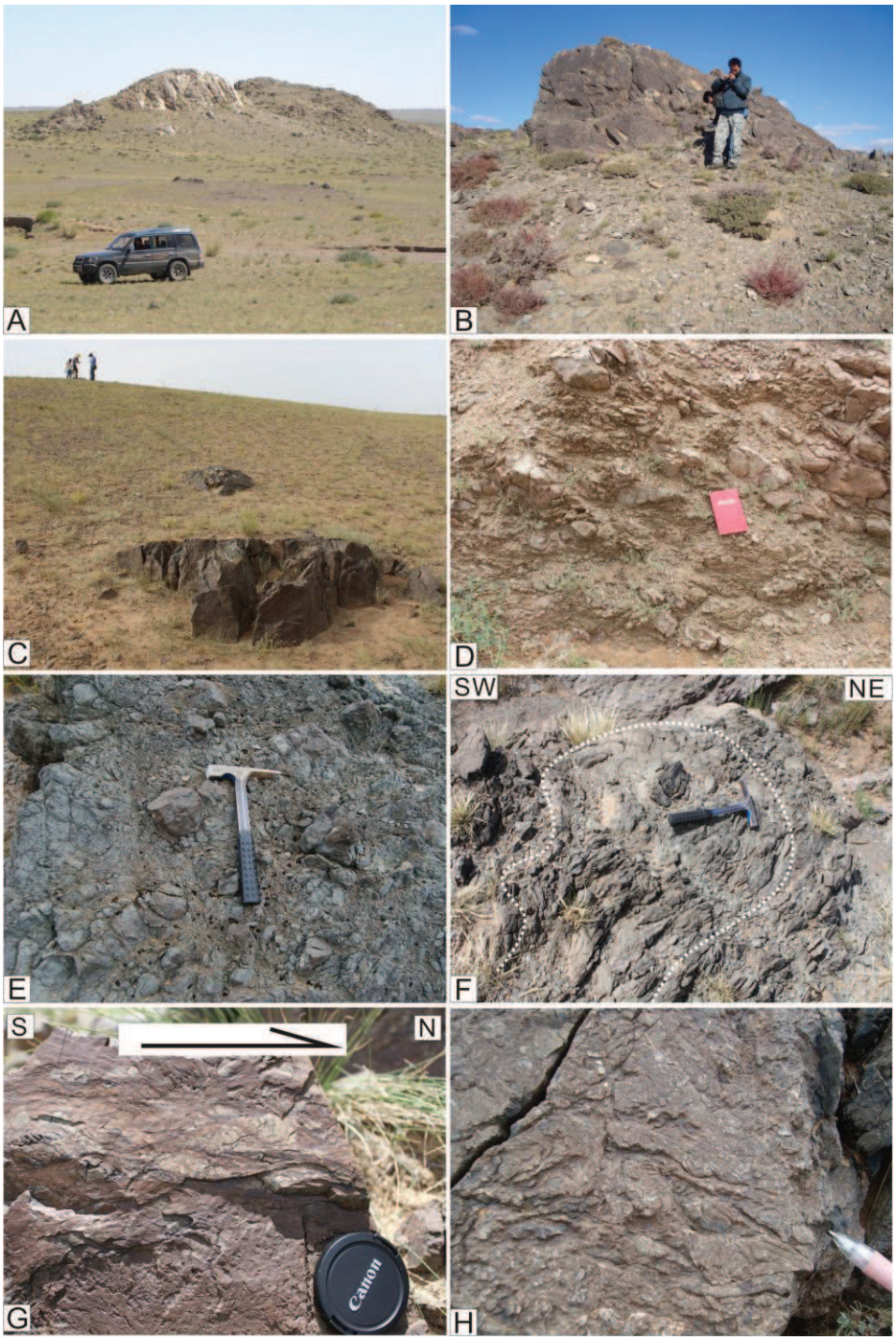

Fig.3 Field pictures of the olistostrome unit. (A) Plurimeter-scale limestone olistolith in olistostrome unit; (B) Mudstone olistolith in the coarse sandstone matrix; (C) acidic volcanic olistolith in the olistostrome unit; (D) Sandstone olistolith in the red pelite/siltstone matrix (ca.20 cm red field book as scale, the same as following); (E) Pebbly limestone in the dark grey mixture of sandstone and mudstone; (F) Inharmonious fold in the olistostrome unit; (G) Sigmoidal indicator in the mudstone lithofacies near the olistostrome margin showing northward slump. (H) Ductile crumple deformation near the margin of the olistostrome unit.

huge limestone mountain covering the underlying disordered slump style deposits or demi-continuous sandstone layers. The sedimentary sequence of Limestone Mountains is well-preserved. Sometimes, a slip surfaces can be observed.

3.2 The turbidite unit

This unit refers to a terrigenous volcanic sedimentary rock association that develops geometrically underlying to the olistostrome unit. Indeed, the turbidite unit and the olistostrome unit are not sharply separated. The appearance of sandstone-mudstone alternation and the disappearance of limestone blocks define a progressive olistostrome-turbidite boundary. Our study allows us to recognize four major lithofacies assemblages in the turbidite unit on the basis of grain size, sedimentary structure and bed thickness.

3.2.1 Mudstone-dominated assemblage

It is composed mainly of massive mudstone, siliceous mudstone and silty mudstone with less very fine grained sandstone laminae (Fig.4A). The siliceous mudstone forms horizontally laminated or massive sequences more than 20m thick. The mudstone-dominated assemblage occurs in the southernmost part of the turbidite unit, interfingering contact or underlying to the olistostrome unit. Sometimes the massive mudstones expose as blocks in the olistostrome.

3.2.2 Medium/thick-bedded sandstone assemblage

It contains two types of sandstone assemblage. One is composed of amalgamation of individual thick bedded sandstone. The stacks of amalgamation of isolated medium-thick bedded sandstone internally have massive or flat laminar structure (Fig.4B). The base sometimes incites into the underlying mudstone assemblage. The other is composed of random stacking of the medium-thick bedded sandstone and rhythmic alternating sandstone and mudstone (Fig.4C and D). It generally shows typical Bouma sequence (generally Tab, Tbc, Tb-e, Tcde division of Bouma, 1962; Fig.4D). The base is generally made up of pebbly sandstone, locally conglomerate. Pebbly sandstone beds are dark grey to light pink, composed of volcanic and sedimentary fragments. The sandstone beds are either internally structureless or exhibit normally graded gradually to parallel lamination, ripple cross lamination. Scour and groove structures are common in the Ta division of sandstone and pebbly sandstone, locally the dewatering structure is well-preserved (Fig.4E). This assemblage is common in the centre part of the turbidite unit. The thickness of the succession is various, commonly 2-5m and is laterally continuous in outcrop.

3.2.3 Thin bedded sandstone assemblage

It is dominated by rhythmic thin bedded fine grained sandstone, siltstone and mudstone (Fig.4F). Grey/light grey siltstone-mudstone form packets, up to 100m thick, with a minor amount of thin bedded sandstone intercalations. The ratio of the sandstone and mudstone ranges from 0.5-2. The Tbc, Tcde division of Bouma sequence (1962) is common. The fine grained sandstone beds display either internally

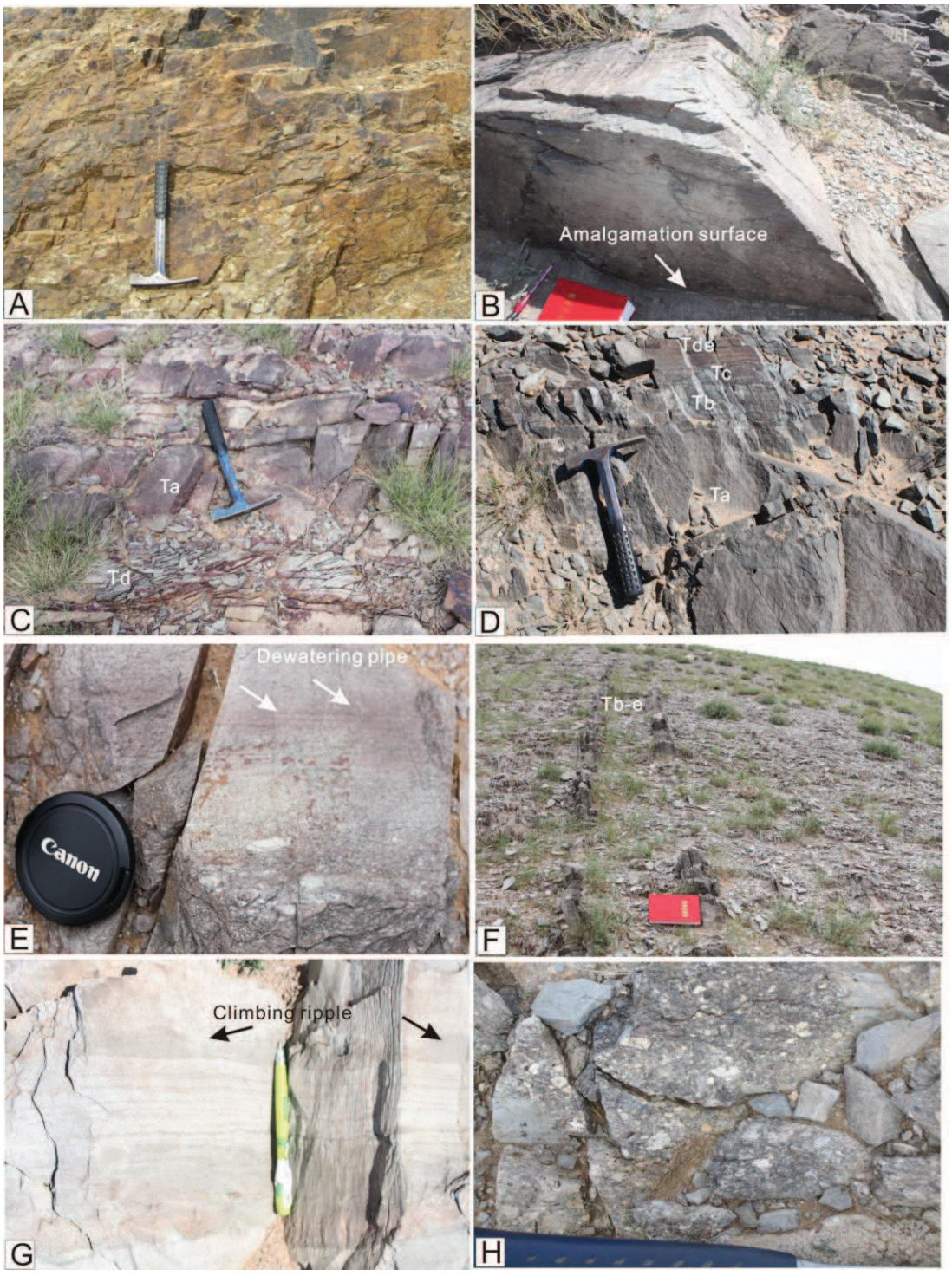

Fig.4 Field pictures of the turbidite unit. (A) Massive mudstone; (B) amalgamated medium-thick bedded sandstone, internally flat laminar structure; (C) Random stacking of the medium-thick bedded sandstone and siltstone; (D) Typical Bouma sequence in the medium/thick-bedded sandstone assemblage; (E) Grade bedding in the Ta division of sandstone and pebbly sandstone, upper develops the dewatering structure; (F) rhythmic thin bedded fine grained sandstone, siltstone and mudstone; (G) Parallel lamination, ripple cross lamination in the Bouma sequence; (H) conglomerate including rip up mudstone fragment and volcanic clasts, massive structure.

structureless or parallel lamination, ripple cross lamination (Fig.4G), rare erosional structures can be recognized. The acidic volcanic bedding is intercalated in this assemblage. The thickness is uniform and typical successions of upward thinning or thickening are not observed. This siltstone-mudstone assemblage is widely exposed to the north and west of the turbidite unit. It may have interfingering contacts with the medium/thick-bedded sandstone assemblage.

3.2.4 Thick bedded conglomerate assemblage

The conglomerate assemblage usually discontinuous laterally occurs in the mudstone and thin bedded sandstone assemblages with a common erosional base. It is made up of conglomerate or multiple stacking of conglomerate, pebbly sandstone and thick bedded sandstone from base to top. The conglomerate contains plenty of rip up mudstone fragment and volcanic clasts. Internally it is massive structure and roughly grading bedding (Fig.4H). There are siltstone-fine sandstone couplet with well developed climbing ripple laminae and slumped turbidites cropping out near the conglomerate package. The thickness of the conglomerate assemblages is various from 20cm to 1m. The thick bedded conglomerate assemblage is sparsely dispersed in the turbidite unit.

3.3 The shallow water sedimentary rocks

The shallow water sedimentary unit was named Zhesi Formation and has been studied in detail in the entire Inner Mongolia region (Grabau, 1931; Wang et al., 2002; Shang, 2004; Li et al., 2004). It crops out in the northern of the Mandula area geometrically covering the volcanic rocks (Dashizhai Formation). The Zhesi Formation is composed of basal conglomerates, middle interval of lenses of fossiliferous limestone and near the top biohermal grading laterally into shales that was interpreted as alluvial to neritic environment (Wang et al., 1999, 2002; IMBGMR, 2004).

3.4 The Solonker mafic rocks

Altered gabbroic, basaltic and acidic volcanic bodies with sizes ranging from 1 to ~100 m, are widespread in the turbidite. These rocks belong to the so-called “Solonker ophiolite” defined along the Chinese-Mongolian border (Sengor and Natal’in, 1996; Xiao et al., 2003; Tao et al., 2004; Jian et al., 2010). Dismembered mafic rocks are shown in the geological map of the study area (IMBGMR, 2004; Fig. 2). However, our observations of the easternmost exposures indicate that these lenses lithologically include three main types: gabbro, basalt and acidic volcanic rocks with the geometry concordant with the turbiditic bedding. The acidic volcanic rocks show yellow colour due to strongly weathering that apparently like the produces of weathered ultra basic rocks (Fig.5A). Indeed, it is andesitic rock in the thin section with age of 282Ma (Fig.5B, see below). The basalt lenses sparsely dispersed in the turbiditic bedding (Fig.5C) exhibit a porphyritic texture with plagioclase phenocrysts (10-15%) in a groundmass of glass and tiny microcline. It is lithologically corresponding to the Early Permian basalt exposed to the south of the Mandula area.

The acidic volcanic and basaltic lenses might be interpreted magmatic sill or volcanic bedding. A red thermal aureole developed in the turbidite around the altered gabbro "blocks" has been observed, indicating an intruding feature. This is also supported by the gabbro age of 257Ma (Fig.5D; see below). Furthermore, it is worth to note that neither serpentinite masses, nor radiolarite have been observed in the study area. Some "serpentinite" rocks shown in the geological map (IMBGMR, 2004; Jian et al., 2010) are indeed strongly weathered yellowish andesite block or aphanitic acidic lava. Thus, more investigation is needed in order to ensure the reality of the Solonker ophiolite.

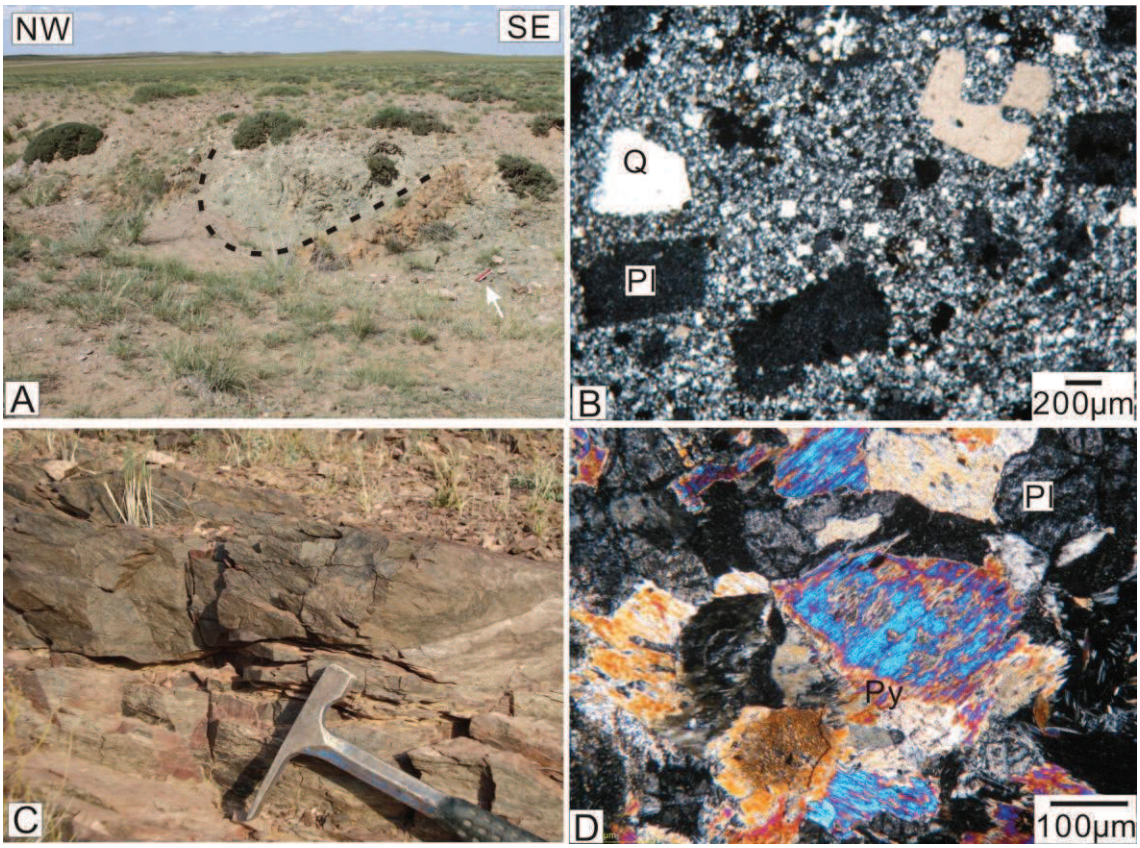

Fig.5 Field pictures and microscope images of the "Solonker ophiolite"; (A) Folded yellowish silicified aphanitic lava within the turbidite unit (42º29′19″, 109 º34′56″); (B) Microscope image of the andesite "block" in turbidite; (C) Greenish basalt lens in the reddish mudstone of the turbidite (hammer ca.30cm length, the some as following); (D) Microscope image of the thin section of gabbro intrusion.

3.5 The Early Permian magmatism

A large mass of intermediate-acidic volcanic rocks (Dashizhai Formation) crops out to the north of the Zhesi Formation. This volcanic unit consists dominantly of andesite, dacite, tuff and volcaniclastic rocks interbeded with rhythmic feldspathic sandstone and muddy limestone lens. The age of the Dashizhai Formation is dated at 276±1 Ma by single zircon apparent age (Xu, 2005).

The basalts exposed in the southernmost part of the Mandula consist of massive basalt, and amygdaloidal spilites as well as gabbroic, dioritic intrusions (IMBGMR,

2004).the massive basalt are dated at 289Ma with Early Paleozoic inherited zircons. It is debated about the origin of those basalts (Jian et al., 2010; Chen et al., 2012), but our inherited zircons supports an origin of N-MORB-like depleted asthenospheric mantle contaminated and metasomatised by arc material (see below).

4. **Structural analyses**

The bulk architecture of the Mandula area results of a multiphase deformation (Fig.6). A pervasive deformation is widespread in the turbidite unit. The primary bedding (S_0) is deformed by regional isoclinal folds with a relatively large scattering of axes from NW to NE. An axial planar cleavage (S_1) is well developed (Figs. 6C, D and E). The bedding-cleavage relationships indicate a northward (NE or NW) vergence (Fig.7A). Acidic volcanic layers in the turbidite also develop north-verging recumbent folds with nearly N90E striking axes. Intrafolial folds are also observed in sandstone-siltstone lithofacies assemblage (Fig. 7 B). In the conglomerate layers of the turbidite, pebbles exhibit a NW-SE striking stretching lineation (Fig. 7C). Both in outcrop and thin section scales, these elongated pebbles and the matrix show

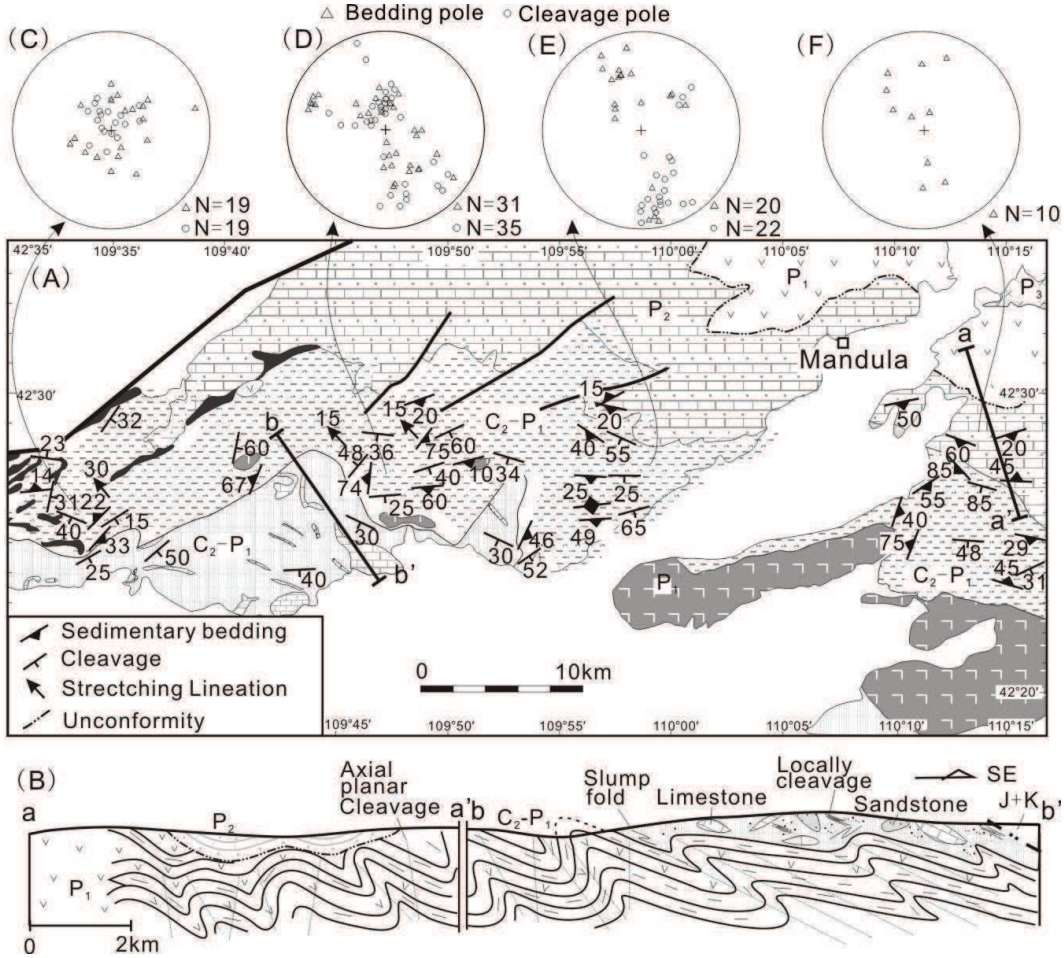

Fig.6 Geological map, structural elements (A) and cross section (B) of the Mandula area; modified after Geological Survey Institute of Inner Mongolia, (2004); C-E showing the projection of cleavage and sedimentary bedding of the turbidite; F showing the projection of sedimentary bedding of the Zhesi Formation.

kinematic indicators such as asymmetric pressure shadows, sigmoidal aggregates, indicate a top-to-the-NW sense of shear (Figs.7C and D). The olistostrome geometrically overlying the turbidite unit is also involving the nearly NW-SE

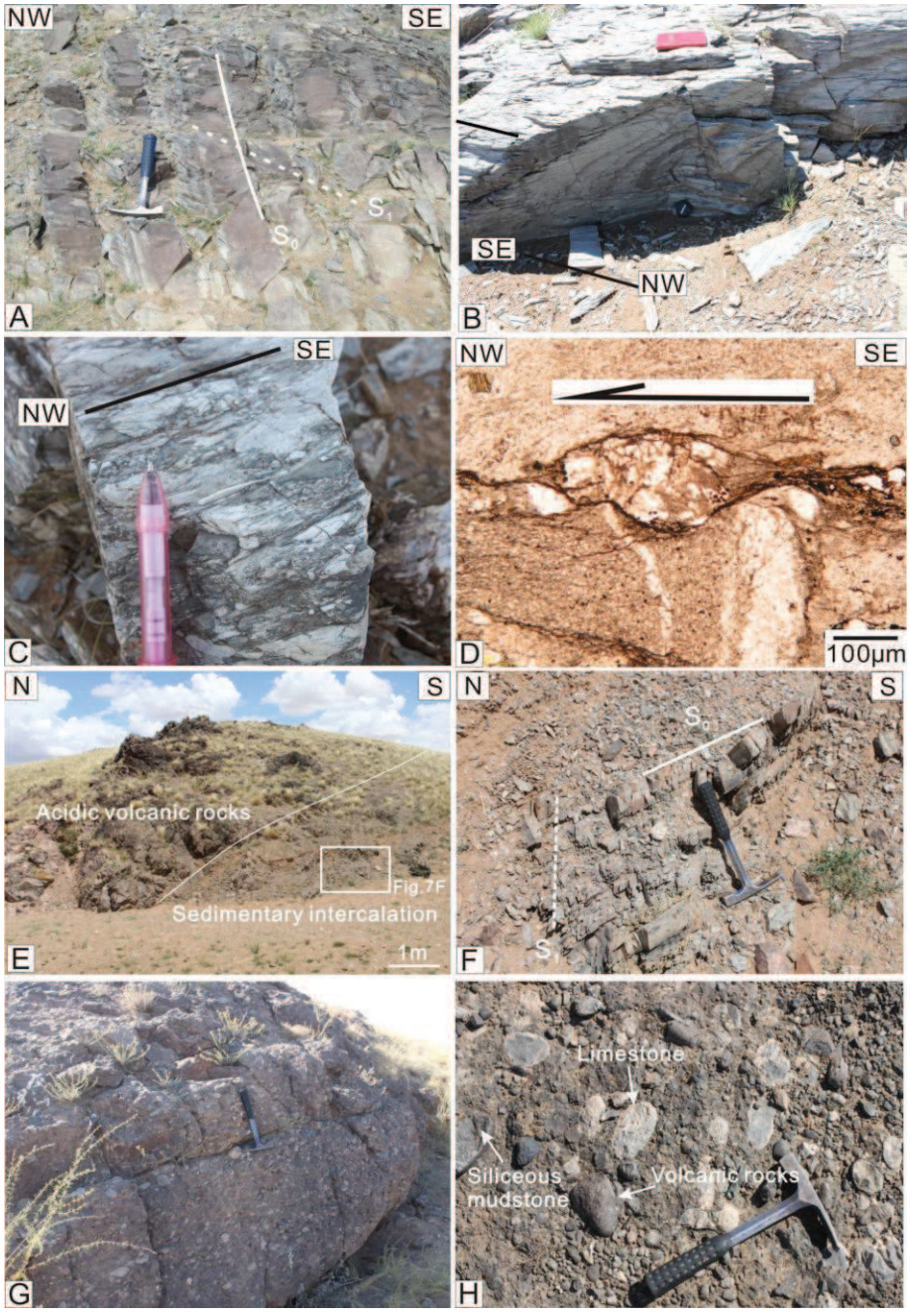

Fig.7 Field pictures of the deformation style. (A) Ta, Tac, Tcd division of Bouma; the bedding (S_0)-cleavage(S_1) angular relationships and upward fining bedding indicate NW ward vergence; (B) intrafolial fold in turbidites composed of dark grey thin bedded sandstone and grey medium bedded siltstone; In the inverted limb, the sandstone shows graded bedding; (C) NW-SE elongated pebble in turbidite (Ta), indicating NW shearing; (D) Pressure shadow at the margins of feldspar clast, showing top-to-the NW sense of shear; (E-F) the volcanic bedding of the Dashizhai Formation steep dipping while sedimentary intercalation with well developed cleavage. (G-H) the Zhesi Formation is gentle dipping with pebbles of limestone, volcanic rock and mudstone of underlying strata.

shortening by locally well developed scaly foliation and flattened boulders. The thick volcanic bedding of the Dashizhai formation develops open fold with nearly E-W axis. Although no cleavage within the volcanic bedding is observed, the sedimentary intercalations within the volcanic rocks develop pervasive N or S dipping cleavage (Figs.7E and F). The structurally overlying Middle Permian Zhesi Formation is characterized by E-W trending, hectomoter to kilometer of wavelength, open folds with axes plunging gently eastward or westward, and devoid of axial planar cleavage (Figs.6F, 7G and H).

5. **Geochronological constraints**

New zircon dating is obtained for magmatic and sedimentary rocks by ICP-MS U-Pb analyses. Cathodoluminescence (CL) images were performed by CAMECA SX-50 microprobe at Peking University in order to document zircon internal structures. Zircon laser ablation ICP-MS U-Pb analyses were conducted on an Agilent 7500a ICP-MS equipped with a 193 nm laser in the China University of Geosciences, Beijing. Laser spot size was set to ~36μm for analyses, laser energy density at 8.5 J/cm^2 and repetition rate at 10 Hz. Isotopic ratios and element concentrations of zircons were calculated using GLITTER (ver. 4.4, Macquarie University). Concordia ages and diagrams were obtained using Isoplot/Ex (3.0, Ludwig, 2003). The common lead was corrected using LA-ICP-MS Common Lead Correction (ver. 3.15), following the method of Andersen (2002). All magmatic sample ages reported below are concordia ages (uncertainties are given at the 95% confidence limit).

5.1 Magmatic rock dating

5.1.1 Basalt (Sample 090719-07; 42º22′38″, 109 º 58′57″)

This sample was taken from the southern part of the Mandula area. In CL images zircons appear heterogeneous. The dominant population consists of short prismatic grains with a broadly spaced zoning. A few grains are prismatic and display rhythmically zoned mantle with an inherited core. All isotopic compositions scatter concordantly along the Concordia curve, and most of the grains are grouped at 289±4 Ma (n=8) and at 437±2Ma (n=6; Fig.8A). Four grains with a more or less rounded shape, with an internally patchy structure yield a Proterozoic age (ca.1.4~1.8Ga). These grains are interpreted as xenocrysts.

5.1.2 Altered gabbro (Sample sgz-3; 42º24′50″, 109 º 33′22″)

In this sample, most of zircon grains display patchy and widely spaced zoning gabbroic zircons (Corfu et al., 2003), but other grains have internally heterogeneous structures. The analyses are either clustered at 257±1Ma (n=6; Fig.8B) or dispersed along the Concordia from ca. 280 to 400Ma, as well as three grains of Proterozoic age. Those relatively old zircons, either internally homogeneous or rhythmically zoned, are regarded as xenocrysts. We consider that the age of 257Ma corresponds to the crystallization age of the gabbro intrusion.

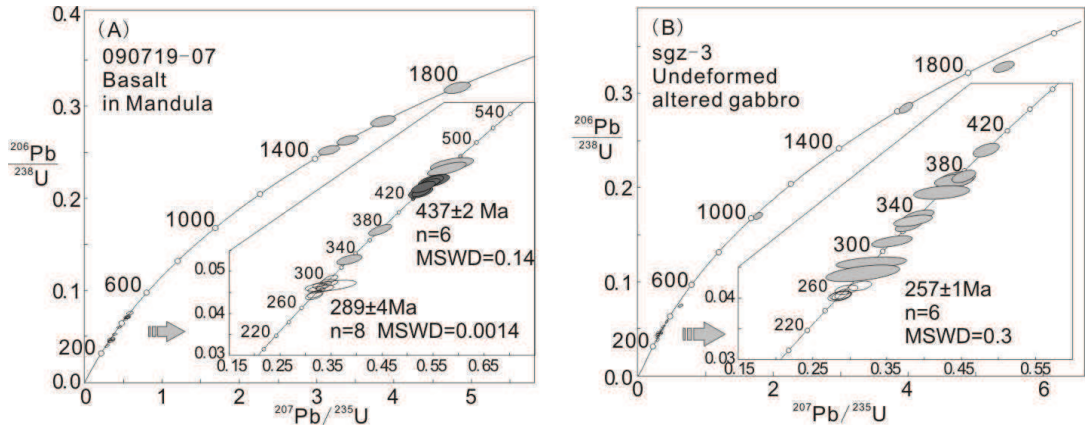

Fig.9 U-Pb Concordia diagrams for samples: (A)Basalt (090719-07); (B) Altered gabbro (sgz-3); The sample location is shown in Fig.2. The data ellipses are defined by standard errors (1 sigma) in $^{206}Pb/^{238}U$, $^{207}Pb/^{235}U$ and $^{207}Pb/^{206}Pb$, and grey areas represent inherited zircons in (A), (B) and (C). The black areas in (A) represent analytical concordia age of the Early Paleozoic inherited zircons.

5.2 Detrital zircon dating

Two sandstone samples, collected in the sandstone-conglomerate lithofacies (090720-22), mudstone lithofacies (090720-34) of turbidite have been processed for detrital zircon dating. The raw data for age spectra are given in Table 2 and illustrated in the statistical diagrams (Fig.9). Zircon grains from all these samples mainly 50-150 μm in size, typically well zoned or patchy zoned with euhedral crystal faces are representative of a first magmatic cycle and short transport history.

Of 75 grains analyzed in sample 090720-22, 2 grains are discordant and disused in the probability density diagram. Most of the zircon grains of the sample define a ~285Ma and a ~431Ma grains populations, with five Proterozoic age grains at ~2500Ma (n=2), ~1800Ma (n=2) and 1200Ma (n=1) (Fig.9A).

30 grains are analyzed in sample 090720-34. The zircon population consists of two main groups at 284 and 478Ma, with four sub-groups at 271 Ma, 310 Ma, 458 Ma, and 512Ma, respectively. The youngest grains are at 258Ma (Fig.9B).

The zircon population at ca. ~280Ma (Early Permian) found in both sample 090720-22 and 090720-34 is similar to the age of the nearby magmatic rocks. Thus these zircon grains are probably derived from the contemporaneous magmatic activity. This interpretation is supported by the euhedral crystal habitus, and the numerous basaltic and acidic volcanic fragments found in sandstone-conglomerate lithofacies. The zircon population of ~430-480Ma is similar to the southern Bainaimiao arc magmatism (Jian et al., 2008; Li et al., 2010). Therefore, the southern Early Paleozoic arc magmatic rocks are the most likely source for this population. It should be underlined that there is an important age gap in the Devonian and Early Carboniferous (Fig.9), suggesting a lack of magmatism in this period around our study area. Therefore, a continuous oceanic subduction coeval with an arc magmatism from Early Paleozoic to Permian (Xiao et al., 2003) is not documented by the age of detrital zircons.

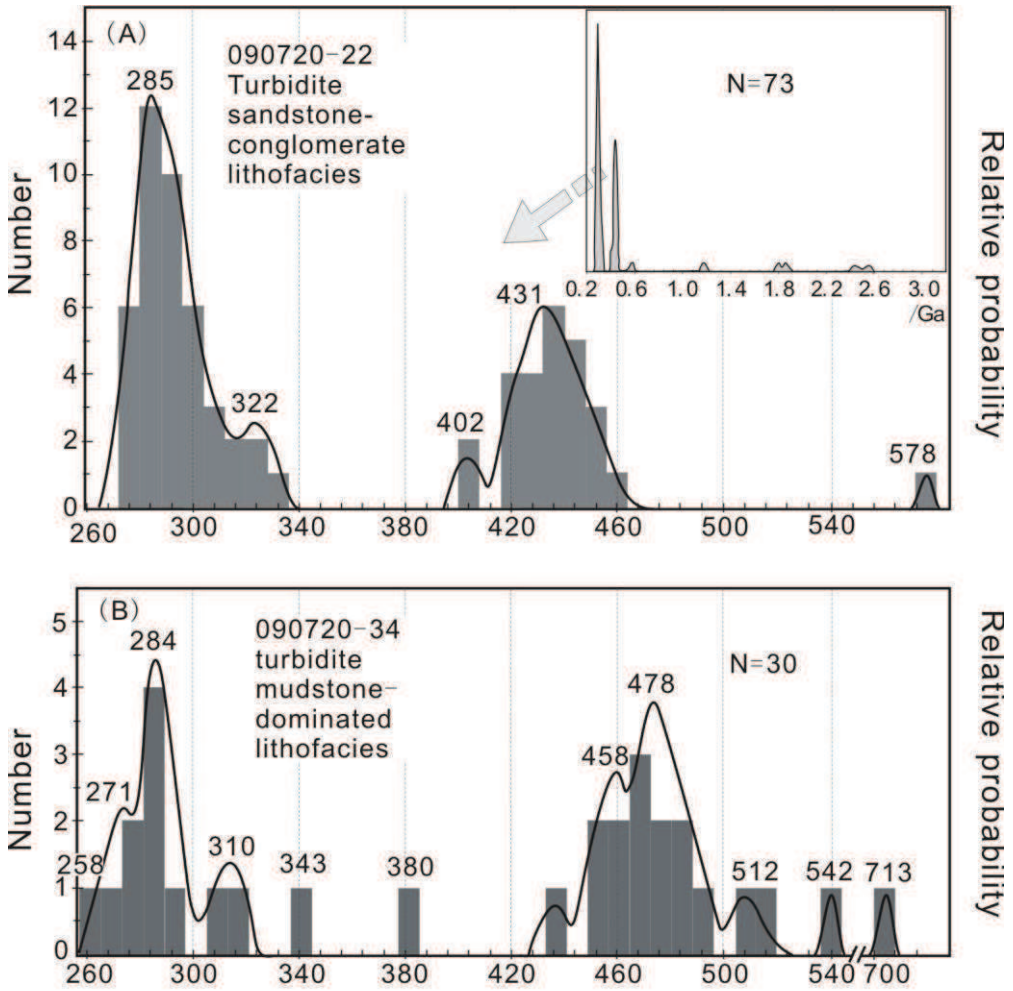

Fig.9 Probability density diagram for the age of detrital zircons from turbidite unit and olistostrome unit; y-axis represents the number of zircon grain and relative probability, x-axis represents the age $^{206}Pb/^{238}U$ of zircon grain ($^{206}Pb/^{207}Pb$ age for zircon older than 1Ga); the minimum width for histogram is 8Myr. The grey column represents the statistical magnitude, and the curve represents relative probability density. N is the total number of analyzed grains. The inset of (A) shows the general age distribution of sample 090720-22.

6. **Discussion**

6.1 The olistostrome or tectonic mélange?

The difference between the olistostrome and the tectonic mélange are widely documented (Hsu, 1974; Potter and Pettijohn, 1977; Wang., 1981; Carine and Michel, 2004). But care must be taken in the outcrops. In the Mandula area, the olistostrome is distinct with tectonic mélange as follows: i) the matrix is mainly composed sandstone and mudstone. Moreover, there is a gradual trend with sandstone decreasing and mudstones increasing northward till the turbidite unit. ii) No typical tectonic shearing deformation and intermediate-high grade metamorphism are observed in the Mandula area. To the south, the head areas of slumps are dominated by demi-continuous bedding while the northern part of the slumps tends to be dominated by compressional structures such as folds and thrusts. The inhomogeneous

deformation suggests southern part extension while northern part compression, indicating the northward movement. iii) In the olistostrome unit the blocks include limestone, sandstone, acidic volcanic rocks while in the turbidite unit expose basalt, volcanic bedding and gabbro intrusion. The typical ophiolitic blocks, such as serpentinite do not exist. The limestone blocks lithologically and paleontologically similar with the southern Amushan Formation (IMBGMR, 2004), suggest the Amushan Formation as a potential source. This is also consistence with uneven slump structure and the kinematic indicator in the siliceous mudstone.

There is also volcanic bedding or block in the turbidite unit. The andesitic rocks are volcanic sills emplaced in the turbidite since it has age 282±3Ma similar to the northern volcanism (Dashizhai Formation). The existence of numerous volcanic clasts in the conglomerate assemblage and volcanic bedding in the turbidite suggests generally coeval volcanism and turbidity deposits. Thus the Mandula study area is dominated by olistostrome and volcano-sediments. The reality of the "Solonker" ophiolite should be reassessed.

6.2 The sedimentary setting

The turbidite can be divided into four main lithofacies assemblage. The thick bedded conglomerate assemblages contain plenty of various sized mudstone rip-up clasts with poorly sorted sandstone matrix. The typical graded structures are not observed, indicating the genesis of debris-flow or inertia debris-flow (Postma et al., 1988) or high-density turbidite. The medium-thick bedded sandstone assemblage shows finer grain-size in contrast to the pebbly sandstone may suggest a bipartite gravity flow (Tinterri et al., 2003), of which pebbly sandstone facies are deposited from the lower current and the medium-thick sandstone from the upper current. The abundant mudstone fragments in the conglomerates and pebbly sandstone facies indicate channel incision into an underlying mudstone lithofacies. The erosional base and lenticular shape of conglomerate lithofacies assemblage suggests depositing as channel fill. The siltstone-fine sandstone couplets with well developed climbing ripple laminae juxtaposed with slumped turbidites are interpreted as channel-margin or levee facies (Walker, 1985).

The medium/thick-bedded sandstone assemblage includes two types. The amalgamation of thick bedded sandstone with flatten bedding can be correlated to high-density turbidites or concentrated-density flow (Lowe, 1982; Mulder and Alexander, 2001). The random stacking of the medium-thick bedded sandstone exhibiting erosive structure, grading bedding and locally dewatering structure represents a high-density turbidite while the presence of many Tbc and Tcde division of rhythmic sandstone and mudstone lithofacies indicates deposition from low-density turbidite current (Lowe, 1982). The thickness of Medium/thick-bedded sandstone assemblage is less systematic changed at mapping scale, suggesting a steady sheet sandstone body.

The thin bedded sandstone assemblage is considered as low-density turbidites and classical turbidite (Lowe, 1982; Walker, 1992) based on the facies characteristics that grading structure, traction-current structure of Bouma sequence (Bouma, 1962).

The mudstone contains turbidite mudstone and hemipelagic mudstone. The lower sandstone/mudstone ratio rhythmic sandstone beds might deposit in distal area relative to the higher sandstone/mudstone ratio rhythmic alternating sandstone beds and the mudstone mainly consists of hemipelagic mudstone.

The mudstone-dominated assemblage generally derived from hemipelagic suspension materials that deposit in a slope or geographic high setting. This environment cannot be affected by turbidity current.

The development of olistostrome and turbidite is common in the slope environment (Jacobi, 1984; Postma, 1984; Christopher et al., 1987; Liuz, et al., 1998; Direen, et al., 2008). In Mandula area the slumped structure and the source of olistostrome unit suggest a northward movement. In the downslope areas, compression is more common with thrusting and bulldozing of basin-floor sediments (Lewis, 1971; Dingle, 1977). To the north of the olistostrome occurs the turbidite which also received the southern materials. The lithofacies assemblage within the turbidite displays a general northward or northwestward gradual low-density turbidite evolutional trend, indicating a geographically northward deeper. The southern Amushan Formation is dominated by bioclastic limestone, reef and sandstone and was interpreted as the continental marginal shallow sea and carbonate platform setting (IMBGMR, 2004). Thus the Mandula area is slope setting that deposits the southern shallow sea sediments and the northern volcanic materials. It is also possible that the turbidite unit is from the olistostrome deposits evolution during slump process (Reading, 1996; Haughton, et al., 2009).

6.3 The geochemical constraint

In the Mandula study area, the turbidity deposits are coeval with a basaltic and acidic volcanism to the south and north respectively. The basalts are tholeiitic series, with low TiO_2 and P_2O_5, flat REE, or slightly depleted LREE spectra, enrichment in LILE but strong depletion in Nb and Ta, and initial $^{87}Sr/^{86}Sr$ = 0.7046-0.70537, εNd=3.4-7.8 (Jian et al., 2010; Chen et al., 2012). These features were interpreted as N-MORB with arc signature, indicative of proto-arc in a supra subduction zone setting (Jian et al., 2010). By contrast, Chen et al (2012) argued for a juvenile ocean basin setting with magma genesis of enriched mantle or N-MORB-like depleted asthenospheric mantle contaminated and metasomatized by arc material. The later interpretation is supported by our 437Ma and 1400-1800 Ma zircon xenocrysts in basalt that might be scavenged by the ascending magma. Also, the coeval basaltic and acidic volcanic rocks suggest a bimodal signature, indicative of intracontinental rifting.

In the Hongqi area, the acidic-intermediate volcanic rocks with age of 272Ma display a pronounced A-type affinity and a significant contribution of crustal-derived rocks in their petrogenesis (Chen, 2011). To the north of the Mandula area, Zhang et al., (2011) reported an Early Permian mafic and felsic volcanic rocks which involved subduction-related metasomatized asthenosphere and lithospheric mantle components and melts of mixed source of predominant juvenile basaltic underplates and minor ancient crustal materials.

Based on geochemical and sedimentary facies data mentioned above, we propose an intracontinental rift developed during the Early Permian in the Mandula area. The rifting is probably controlled by normal faults and forms a northward deeper geography accommodating the turbidite and the olistostrome units.

6.4 The closure of rift

Both the turbidite unit and the olistostrome unit experienced a compressional tectonics resulting in the development of the northwest-directed recumbent and/or isoclinal folds. This NW-SE compression causing the closure of the rift involved the Early Permian litho-tectonic units. The Middle Permian Zhesi Formation (~265Ma) was also subjected to a nearly NW-SE compression event, reflecting a same strain regime to the turbidite during the Middle Permian. An unconformity relationship was reported between the Early Permian volcanic rocks (Dashizhai Formation) and the Middle Permian Zhesi Formation (Wang et al., 1999, 2002). It is worth noting that in the Mandual area, triassic sediments is absent (Mueller et al., 1991; IMBGMR 2004; Shi et al., 2006). But Late Permian to Middle Triassic alkaline and calc-alkaline undeformed granitoids emplaced near the study area (Zhang et al., 2009; Zhang et al., 2010). These undeformed rocks provide an upper limit for the NW-directed deformation. Thus, it is most possible that the closure of the rift happened during late Permian time.

7. Conclusion

i) The Mandula area is composed of olistostrome, turbidite and coeval Early Permian basalts and acidic volcanic rocks. The previous mélange blocks indeed are olistoliths and volcanic sills in the turbidite.

ii) The sedimentary setting is continental slope with a northward deeper trend. The sources of the olistostrome and turbidite are from the southern Early Paleozoic material and contemporaneous Permian volcanic magmatism.

iii) The sedimentary succession in the Mandula area characterized as NW verging isoclinal fold indicating a NW-SE directed shortening.

iv) Integrating the lithofacies assemblage, regional geochemical data and deformation style, we argued that the Mandula area experienced an Early Permian intracontinental rifting and Late Permian closure of the rift.

Acknowledgements

This work has been funded by the National Science Foundation of China (40872145, 41121062). The China Scholarship Council is acknowledged for providing a Ph.D. scholarship to Shi, G.Z., supporting a joint training Ph.D. between the Université d'Orléans and Peking University. Flavien Choulet is thanked for useful suggestions and improving a first draft of the manuscript. Tong Qilong, Li Ruibiao, Fang Junqin and Cheng Shengdong are thanked for their help in the field work. This

is a contribution to IGCP#592 supported by UNESCO-IUGS.

References:

Andersen, T., 2002. Correction of common lead in U-Pb analyses that do not report ^{204}Pb, Chemical Geology 192, 59–79.

Badarch, G., Cunningham, W.D., Windley, B.F., 2002. A new terrane subdivision for Mongolia: implications for the Phanerozoic crustal growth of Central Asia. Journal of Asian Earth Sciences 21, 87–104.

BGMRIM (Bureau of Geology and Mineral Resources of Inner Mongolia), 1991.Regional Geology of NeiMongol (Inner Mongolia) Autonomous Region. Geological Publishing House, Beijing (in Chinese with English summary).

Bouma, A.H., 1962. Sedimentology of some Flysch deposits: A graphic approach to facies interpretation, Elsevier, Amsterdam.

Carine, C., Faure, M., 2004. The Saint-Georges-sur-Loire olistostrome, a key zone to understand the Gondwana-Armorica boundary in the Variscan belt (Southern Brittany, France). Int J Earth Sci (Geol Rundsch) 93: 945–958.DOI 10.1007/s00531-004-0398-3.

Chen, B., Jahn, B.M., Tian, W., 2009. Evolution of the Solonker suture zone: Constrains from zircon U-Pb ages, Hf isotopic ratios and whole-rock Nd-Sr isotope compositions of subduction and collision-related magmas and forearc sediments. Journal of Asian Earth Sciences 34, 245-257.

Chen, C., 2011. geochronology, geochemistry, and its geological significance of the Early Permian volcanic rocks in Damaoqi, Inner Mongolia. Master degree thesis, Peking University. 50pp.

Chen, C., Zhang, Z.C., Guo, Z.J., Li, J.F., Feng, Z.S., Tang, W.H., 2012. Geochronology, geochemistry, and its geological significance of the Permian Mandula mafic rocks in Damaoqi, Inner Mongolia. Science China earth Sciences 55, 39-52.

Christopher, J.E., Michael, M.G., Stephen, E.N., 1987. Problems of recognition of olistostromes: An example from the lower Pit Formation, Eastern Klamath Mountains, California. Geology, v. 15, P.541-544. June 1987.

Corfu, F., Hanchar, J.M., Hoskin, P.W.O., Kinny, P., 2003. Atlas of zircon textures. In: Hanchar, J.M., Hoskin, P.W.O. (Eds.), zircon: Reviews in Mineralogy and Geochemistry 53, 469-500.

Demoux, A., Kröner, A., Liu, D.Y., 2009. Precambrian crystalline basement in southern Mongolia as revealed by SHRIMP zircon dating. Int J Earth Sci (Geol Rundsch) 98, 1365-1380. DOI 10.1007/s0051-008-0321-4.

Dingle R.V., 1977. The anatomy of a large submarine slump on a sheared continental margin (SE Africa). Journal of the geological Society, London 134, 293-310.

Direen, N.G., Jago, J.B., 2008.The Cottons Breccia (Ediacaran) and its tectonostratigraphic context within the Grassy Group, King Island, Australia: A rift-related gravity slump deposit. Precambrian Research 165,1–14.

Grabau, A.W., 1931. The Permian of Mongolia-A Report of the Permian Fauna of the Jisu Honguer Limestone of Mongolia and Its Relations to the Permian of Other Parts of the World. Natural History of Central Asia 4, 1-665.

Haughton, P., Davis, C., Mccaffrey. W., Barker, S., 2009. Hybrid sediment gravity flow deposits – Classification, origin and significance. Marine and Petroleum Geology, 26, 1900-1918.

Hsu, K.J., 1974. Mélange and their distinction from olistostromes: In Dott, R.H. and Shaven R. H.

(eds.), Mordern and Ancient Geosynclinal Sedimentation, Soc. Econ. Palaeont. Min. Special Pub.19, 321-333.

IMBGMR, 2004 .Regional Geological Investigation Report of 1:250000 scale Mandula Quadrangle. Inner Mongolian Bureau of Geology and Mineral Resources.

Jacobi, R.D. 1984, Modern submarine sediment slides, in Raymond, L.A., ed., Mélanges: Their nature, origin, and significance: Geological Society of America Special Paper 198, 81-102.

Jahn, B.M., 2004. The Central Asian Orogenic Belt and growth of the continental crust in the Phanerozoic. In: Malpas, J., Fletcher, C.J.N., Ali, J.R., Aitchinson, J.C., (Eds.), Aspects of the Tectonic Evolution of China. Geological Society, London, 3–100.

Jian, P., Liu, D.Y., Kröner, A., Windley, B. F., Shi, Y.R., Zhang, F.Q., Shi, G.H., Miao, L.C., Zhang, W., Zhang, Q., Zhang, L.Q.,Ren, J.S., 2008. Time scale of an early to mid-Paleozoic orogenic cycle of the long-lived Central Asian Orogenic Belt, Inner Mongolia of China: Implications for continental growth. Lithos 101, 233-259.

Jian, P., Liu, D.Y., Kroner,A., Windley, B.F., Shi, Y.R., Zhang, W., Zhang, F.Q., Miao, L.C., Zhang, L.Q., Tomurhuu, D., 2010. Evolution of a Permian intraoceanic arc–trench system in the Solonker suture zone, Central Asian Orogenic Belt, China and Mongolia. Lithos 118, 169-190.

Lewis, K.B., 1971. Slumping on a continental slope inclined ata 1º-4 º. Sedimentology 16, 97-110.

Li, J.F., Zhang, Z.C., Han, B.F., 2010. Ar-Ar and zircon SHRIMP geochronology of hornblendite and diorite in northern Darhan Muminggan Joint Banner, Inner Mongolia, and its geological significance. Acta Petrologica et Mineralogica 29, 732-740. (In Chinese with English abstract).

Li, S.L., Wang, X.L., Xu, X.Y., Zhang, H.J., Liu, X.D., Li, J.W., 2004. Characteristics of the Maokou'an Reef in the Zhesiaobao, Inner Mongolia. Acta Sedimentologica Sinica 22, 434-442

Lowe, D.R., 1982. Sediment gravity flows: II. Depositional models with special reference to the deposits of high-density turbidity currents. Journal of Sedimentary Petrology 52, 279-297.

Ludwig, K.R., 2003. User's Manual for Isoplot 3.0: A Geochronological Toolkit for Microsoft Excel Berkeley Geochronology Center. Special publication 4, 1–71.

Luiz F.G.C., Renoto, O.K., Adriano, R.V., 1998. Slope sedimentary facies associated with Pleistocene and Holocene sea-level changes, Campos Basin, southeast Brazilian Margin. Sedimentary Geology 115, 159-174.

Mueller, J.F., Rogers, J.W., Jin, Y.G., Wang, H.Y., Li, W.G., Chronic, J., Mueller Jo.F., 1991. Late Carboniferous to Permian sedimentation in Inner Mongolia, China, and tectonic relationships between North China and Siberia. Journal of Geology, 99, 251-263.

Mulder, T., Alexander, J., 2001. The physical character of subaqueous sedimentary density flows and their deposits. Sedimentology 48, 269-299.

Postma, G., 1984. Slumps and their deposits in fan delta front and slope. Geology, v.12, P.27-30.

Postma, G., Nemec, W., Kleinspehn, K.L., 1988. Large floating clasts in turbidite: a mechanism for their emplacement. Sedimentary geology 58, 47-61.

Potter, P.E., Pettjohn, F.J., 1977. Paleocurrents and basin analysis, 2nd ed. Springerverlag, Berlin, Heidelberg, New York.

Reading, H.G., 1996. Sedimentary Environments: processes, Facies and Stratigraphy. Blackwell Publishing Company. Third edition, pp 407-418.

Sengor, A.M.C., Natal'in, B.A., 1996. Paleotectonics of Asia:Fragments of a synthesism. In: Yin, A., Harrison, T.M. (Eds.), The Tectonic Evolution of Asia, Cambridge Univ, New York, pp.486-640.

Sengor, A.M.C., Natal'in, B.A., Burtman, V.S., 1993. Evolution of the Altaid tectonic collage and Paleozoic crustal growth in Eurasia. Nature 364, 299-307.

Shang, Q.H., 2004. Occurrences of Permian Radiolarians in Central and Eastern Neimongol (Inner Mongolia) and their geological significance to the Northern China Orogen. Chinese Science Bulletin 49, 2613-2619.

Shi, G.R., 2006. The marine Permian of East amd Northeast Asia: an overview of biostratigraphy, palaeobiography and palaeogeographical implications. Journal of Asian Earth Science 26, 175-206.

Tang, K., 1990. Tectonic development of Paleozoic fold belts at the north margin of the Sino-Korean craton, Tectonics 9, 249-260.

Tao, J.X., Su, M.R., Baoyin, W.L.J., Bai, L.B.,2004. Characteristics and tectonic significance of the Solon Mountain ophiolitic melange in the Mandula area, Darhan Muminggan, Inner Mongolia. Geological Bulletin of China 23, 1238-1242.

Tinterri, R., Drago, M., Consonni, A., Davoli, G., Mutti, E., 2003. Modeling subaqueous bipartite sediment gravity flows on the basis of outcrop constraints: first results: Marine and Petroleum Geology 20, 911-933.

Walker, R.G., 1985.Mudstones and thin-bedded turbidites associated with the Upper Cretaceous Wheeler Gorge conglomerates, California; a possible channel-levee complex. Journal of Sedimentary Research 55, 279-290.

Walker, R.G., 1992. Turbidites and submarine fans. In: Walker, R.G., James, N.P. (Eds.), Facies Models: Response to Sea Level Change. Geol. Assoc. Can., pp. 239-263.

Wang, C.S., 1981. Olistostrome and melange in the evolution of subduction complexes. Memoir of the geological society of China, 4, 55-65.

Wang, C.Y., Wang, P., Li, W.G., 2006. Conodonts from the permian Jisu Honguer (Zhesi) Formation in Inner Mongolia, China. Acta Palaeontologica Sinica 45, 195-206.

Wang, H., Chen, Z.Y., Yang, W.R., 2002. Discovery of the Permian sponge mounds in Mandula, Inner Mongolia. Journal of stratigraphy 26, 33-38. (In Chinese).

Wang, H., Gao, R.K., 1999. Further Study on Biostratum Division and Correlation of Early Permian Epoch of Mandula Area of Damaoqi, InnerMongolia. Geology of Inner Mongolia 91, 7-20.

Wang, H., Wang, Y.J., Chen, Z.Y., Li, Y.X., Su, M.R., Bai, L.B., 2005. Discovery of the Permian radiolarians from the Bayanaobao area, Inner Mongolia. Journal of stratigraphy 29, 368-372.

Wang, Q., Liu, X.Y., 1986. Paleoplate tectonics between Cathaysia and Angaraland in Inner Mongolia of China. Tectonics 5, 1073-1088.

Wang, T., Zheng,Y.D., Gehrels, G.E., Mu,Z.G., 2001. Geochronological evidence for existence of South Mongolian microcontinent zircon U-Pb age of grantoid gneisses from the Yagan-Onch Hayrhan metamorphic core complex. Chinese Science Bulletin 46, 2005-2008.

Windley, B.F., Alexeiev, D., Xiao, W.J., Kröner, A., Badarch, G., 2007. Tectonic models for accretion of the Central Asian Orogenic Belt. Journal of the Geological Society, London 164, 31-47.

Xiao,W.J., Han, C., Yuan, C., Sun, M., Lin, S., Chen, H., Li, Z., Li, J., Sun, S., 2008. Middle

Cambrian to Permian subduction-related accretionary orogenesis of northern Xinjiang, NW China: implications for the tectonic evolution of central Asia. Journal of Asian Earth Sciences 32, 102-117.

Xiao,W.J.,Windley, B.F., Hao, J., Zhai,M., 2003. Accretion leading to collision and the Permian Solonker suture, Inner Mongilia, China: termination of the Central Asian Orogenic Belt. Tectonics 22, 1069. doi:10.1029/2002TC001484.

Xu, B., Charvet, J., 2010. Mid-Paleozoic opposite Orogenic Belt in Inner Mongolia of China and its significance for Central Asian Orogenic Belt, International Association for Gondwana Research Conference Series 9, Qingdao, China, Abstract Volume, p. 84.

Xu, B., Charvet, J., Zhang, F.Q., 2001. Primary study on petrology and geochronology of the blueschist in Sonid Zuoqi, northern Inner Mongolia. Chinese Journal of Geology 36, 424–434 (in Chinese with English abstract).

Xu, B., Chen, B., 1993. The opposite subduction and collision between the Siberian and Sino-Korean plates during the early-middle Paleozoic. Report No: 4 of the IGCP Projrct 283: Geodynamic Evolution of Paleoasian Ocean, Novosibirsk, USSR, pp.148-150.

Xu, B., Chen, B., 1997. Framework and evolution of the middle Paleozoic orogenic belt between Siberian and North China Plates in northern Inner Mongolia. Science in China (series D) 40, 463-469.

Xu, B.,, Jacques Charvet, Yan Chen , Pan Zhao, Guanzhong Shi, Middle Paleozoic convergent orogenic belts in western Inner Mongolia (China): framework, kinematics, geochronology and implications for tectonic evolution of the Central Asian Orogenic Belt, Gondwana Res. (2012), doi:10.1016/j.gr.2012.05.015

Xu,L.Q., 2005. The Characteristics of Magmatic Rocks and Discussion of Geotectonics Evolution from Caledonian through Hercynian to Indosinian stage in the Baiyun'ebo-Mandula Region, Inner Mongolia. PhD thesis, China university of Geosciences (Beijing), pp. 116.

Yarmolyuk, V.V., Kovalenko, V.I., Salnikova, E.B., Kozakov, I.K., Kotov A.B., Kovach, V.P., Vladykin, N.V., Yakovleva, S.Z., 2005. U–Pb age of syn- and post-metamorphic granitoids of south Mongolia:evidence for the presence of Grenvillides in the Central Asian Foldbelt. Doklady Earth Sci 404:986–990.

Zhang, S.H., Zhao, Y., Song, B., Liu, S.W., Yang, Z.Y., Chen, F.K., Hu, J.M., Liu, X.M., Liu, J., 2009. Contrasting Late Carboniferous and Late Permian–Middle Triassic intrusive suites from the northern margin of the North China craton: geochronology, petrogenesis, and tectonic implications. Geological Society of America Bulletin 121, 181–200.

Zhang, X.H., Wilde, S.A., Zhang, H.F., Zhai, M.G., 2011. Early Permian high-K calc-alkaline volcanic rocks from NW Inner Mongolia, North China: geochemistry, origin and tectonic implications. Journal of the Geological Society, London 168, 525-543.

Zhang, W., Jian, P., Liu, D., Hu, K., 2010. Geochemical study, SHRIMP zircon dating, and Hf isotopic composition of Triassic granodiorite–diorite and shoshonite from the northern Damaoqi area, Inner Mongolia. Geological Bulletin of China 29, 821–832 (in Chinese with English abstract).

[Guanzhong SHI]

[Évolution polycyclique de l'Est de la Central-Asie Orogénique Belt—Microtectonique analyse, géochronologie et tectonique dans le centre d'Inner Mongolie, la Chine] (en français)

Résumé : (1700 caractères max.)

Il est débattue sur le temps closural finale de l'océan paléo-asiatique et la position. Certains géologues ont préconisé la suture "Solonker" marque la zone closural finale du Permien , tandis que d'autres insistent sur le fait Paléozoïque milieu. Nos trois domaines d'étude, le Hongqi , le Ondor Somme et le Mandula ont essentiel et important de résoudre ces controverses.

Les unités litho-tectonique reconnus dans le domaine Hongqi-Ondor Sum sont le mélange Belt de Hongqi-Ondor Sum, la Belt de l'arc Bainaimiao, craton du Nord de Chine et les roches sédimentaires post-orogéniques. Le Mélange Belt de Hongqi-Ondor Sum connu déformation ductile en deux phases et une phase de la déformation ductile-fragile. D1 est responsable de la S1 foliation, linéation minérale L1, et intrafolial pli F1. Les critères cinématique indique un sens cisaillement de top-to-the-NW. D2 est caractérisée par divers taille de plis asymétriques avec axe presque NE correspondant à la poussée NW cisaillement. D3 formé le cadre régional dans le Hongqi et les zones Ondor Sum.

La zone Mandula contient les sédiments olistostrome, les sédiments turbiditiques et roches volcano-sédimentaires. Grains de zircons détritiques dans des échantillons sédimentaires indiquent la zone d'étude Mandula reçu des matériaux d'arc Bainaimiao et matières contemporaines de l'éruption volcanique du Permien. Les sédiments et les roches volcaniques dans la région Mandula soumettent un NW-SE ou près de N-S du raccourcissement.

les données géologiques indiquent qu'une subduction et collsion dans Paléozoïque inférieur, et rifting et fermeture rift dans Palezoic supérieur. Les fragments ophiolitiques "Solonker" sont en effet olistostrome. Composants ophiolitiques typiques ne sont pas observés dans la région Mandula.

Mots clés : Centrale de la Mongolie intérieure; Asie ceinture orogénique centrale; déformation polyphasée; sédimentaire faciès analyse; évolution tectonique

[Polycyclic evolution of the Eastern Central-Asia Orogenic Belt— Microtectonic analysis, geochronology and tectonics in Central Inner Mongolia] (en anglais)

Summary : (1700 caractères max.)

It is hotly debated about the final closural time and position of the Paleo-Asian Ocean. Some geologists advocated the "Solonker" suture marks the final closural zone in Permian, whereas others insist in middle Paleozoic. Our three study areas, the Hongqi, the Ondor Sum and the Mandula is essential and important to solve those controversies.

The litho-tectonic units recognized in the Hongqi-Ondor Sum area include the Hongqi-Ondor Sum mélange belt, the Bainaimiao arc belt, North China Craton and post-orogenic unconformably sedimentary rocks. The Hongqi-Ondor Sum mélange belt experienced two phase ductile deformation and one phase ductile-brittle deformation. D_1 is responsible for the regional greenschist foliation S_1, elongated mineral lineation L_1, and intrafolial fold F_1. The kinematic criteria indicates a top-to-the-NW shearing sense. D_2 is characterized by various sized of unsymmetrical folds with nearly NE axis corresponding to the NW thrust shearing. D_3 formed the regional framework in the Hongqi and the Ondor Sum areas.

The Mandula area contains olistostrome sediments, turbiditic sediments and volcano-sedimentary rocks. Detrital zircon grains in sedimentary samples argue the Mandula study area received the southern Bainaimiao arc materials and coeval Permian volcanic erupting materials nearby. The sediments and volcanic rocks in Mandula area subject a nearly NW-SE or N-S compressional shortening.

The geological data support that an Early Paleozoic subduction and collsioan, Late Palezoic rifting and rift closure model. The so called "Solonker" ophiolitic fragments indeed are olistostrome. Typical ophiolite components are not observed in the Mandula area.

Keywords : Central Inner Mongolia; Central Asian Orogenic Belt; Polyphase deformation; Sedimentary facies analysis; Tectonic evolution

[Guanzhong SHI
Address: Faculty of Earth Resource, China University of Geosciences Wuhan
No.388, Lumo Road, Hongshan District, Wuhan
430074, China **]**

北京大学
PEKING UNIVERSITY

UNIVERSITE D' ORLEANS

OSUC